



Universiteit
Leiden
The Netherlands

Targeting MHC-I related proteins for cancer diagnosis and therapy

Verhaar, E.R.

Citation

Verhaar, E. R. (2024, July 4). *Targeting MHC-I related proteins for cancer diagnosis and therapy*. Retrieved from <https://hdl.handle.net/1887/3766089>

Version: Publisher's Version

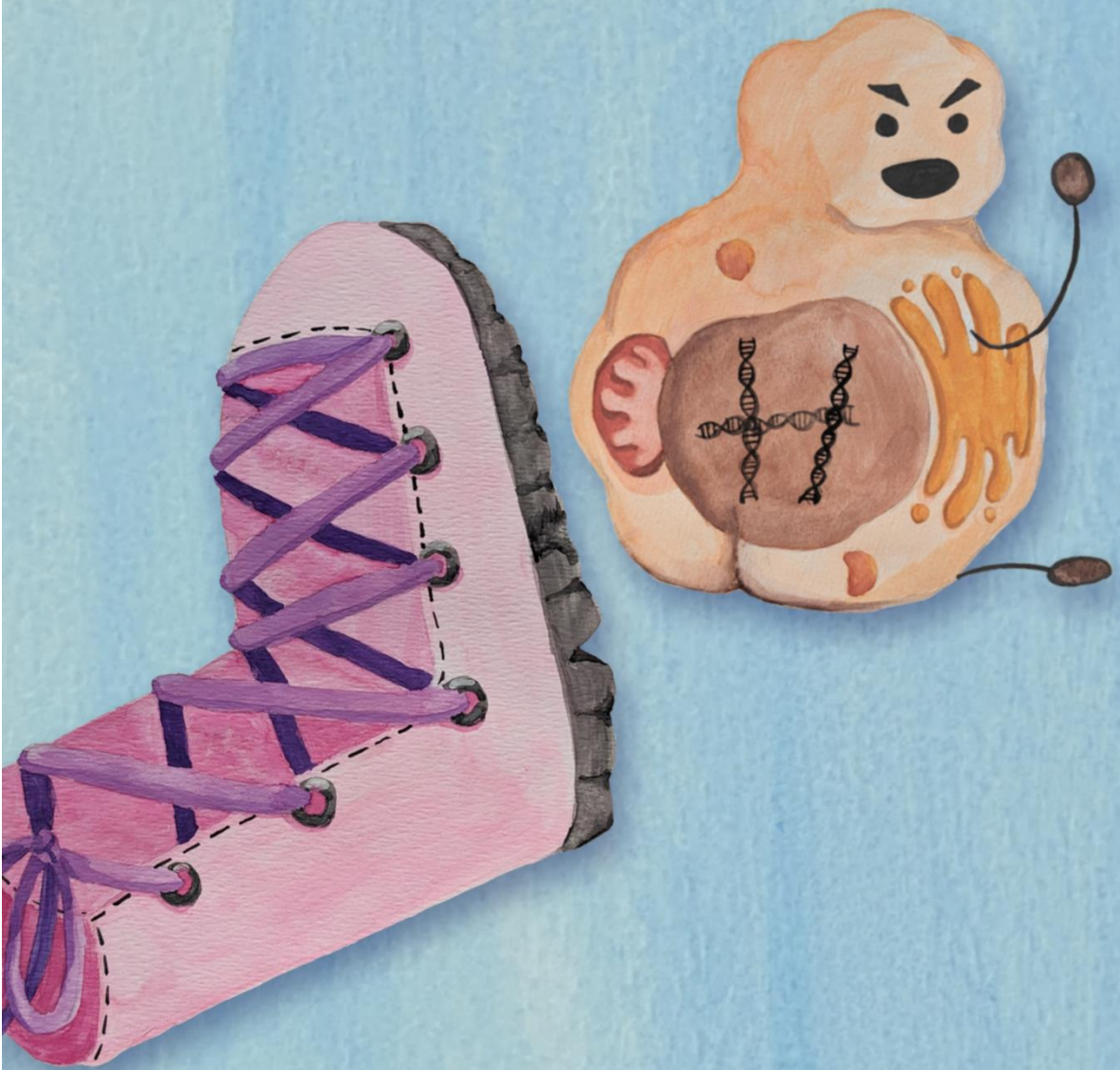
License: [Licence agreement concerning inclusion of doctoral thesis in the Institutional Repository of the University of Leiden](#)

Downloaded from: <https://hdl.handle.net/1887/3766089>

Note: To cite this publication please use the final published version (if applicable).

Targeting MHC-I Related Proteins for Cancer Diagnosis and Therapy

Elisha Verhaar



Targeting MHC-I Related Proteins for Cancer Diagnosis and Therapy

Proefschrift

ter verkrijging van
de graad van doctor aan de Universiteit Leiden,
op gezag van rector magnificus prof.dr.ir. H. Bijl,
volgens besluit van het college voor promoties
ter verdedigen op donderdag 4 juli 2024
klokke 13:45 uur

door

Elisha Robin Verhaar
geboren te Vlissingen
in 1995

Promotors: Prof. Dr. H.L. Ploegh (Boston Children's Hospital)
Prof. Dr. J. Neefjes

Leden promotiecommissie: Prof. Dr. J.G. Borst
Prof. Dr. P. ten Dijke
Dr. G.J. van der Heden van Noort
Prof. Dr. H.S. Overkleeft
Prof. Dr. T. Sixma (Nederlands Kanker Instituut)

ISBN: 978-94-6496-150-8

© 2024 Elisha Verhaar, Leiden, The Netherlands

No part of this book may be reproduced, stored in a retrieval system, or transmitted in any form or by any means without permission of the author or the journals holding the copyrights of the published manuscripts.

Targeting MHC-I Related Proteins for Cancer Diagnosis and Therapy - The work presented in this thesis was performed at Boston Children's Hospital, the Program for Cellular and Molecular Medicine, Boston, United States of America. This research was funded by the National Institute of Health Pioneer Grant (DP1AI150593-05).

Cover design: Elisha Verhaar

Printing: Gildeprint Enschede | www.gildeprint.nl

Aan papa en mama

To David

Table of contents

General introduction		
Chapter 1	Introduction to immuno-oncology	7
Chapter 2	Nanobodies in cancer	29
	Outline of this thesis	55
Part 1: Targeting MICA		
Chapter 3	MICA-specific nanobodies for diagnosis and immunotherapy of MICA ⁺ tumors	59
Chapter 4	MICA-specific nanobody-drug conjugate for <i>in vivo</i> treatment of MICA ⁺ EL-4 tumors (unpublished data)	81
Chapter 5	Nanobody-based CAR NK-92 cells for possible immunotherapy of MICA ⁺ tumors	91
Chapter 6	Nanobody-based CAR T cells for selective cytotoxicity of MICA ⁺ cancer cells <i>in vitro</i> (unpublished data)	121
Part 2: Targeting HLA-E		
Chapter 7	A monoclonal antibody that recognizes a unique 13-residue epitope in the cytoplasmic tail of HLA-E	135
Discussion		
Chapter 8	Summary, general discussion, future perspectives	167
Appendices		
	Nederlandse samenvatting	185
	List of abbreviations	193
	Publications	195
	Curriculum Vitae	197
	Acknowledgements	199
	References	201

Chapter 1:

Introduction to immuno-oncology

Tumor development

The World Health Organization reports approximately 20 million people in the world got diagnosed with cancer in 2022. The most common types of cancer are lung, colon, and prostate cancer for men, and breast, lung, and colon cancer for women. Although ongoing efforts to prevent and treat cancer have improved survival rates, an estimated 9.7 million patients worldwide died from cancer in 2022¹. The most common cause of death is metastatic diseases, which is the spread of cancer from the localized origin to other sites in the body². Metastases and cancer growth are facilitated by cellular changes, as well as by changes in the tumor microenvironment (TME)³⁻⁵.

Some well-studied changes in tumor cells that lead to cancer and metastases are the downregulation of certain tumor suppressor genes (TP53, BRCA1/BRCA2, and PTEN)⁶⁻¹³, or the increase in expression of oncogenes (RAS, MYC, and WNT)¹⁴⁻²⁴. Other cellular changes include downregulation from the cell surface of certain MHC Class I (MHC-I) molecules such as HLA-A, -B, and -C, which renders the tumor cells invisible to CD8⁺ T cells. Such downregulation applies to 40-90% of epithelial cancers and correlates with worse prognosis²⁵⁻³³. Alternatively, upregulation of other MHC-I molecules such as HLA-E and -G can lead to inactivation of immune cells³⁴⁻³⁷. Strategies of immune-evasion deployed by tumor cells will be described in greater detail below.

The tumor microenvironment and the immune system

Besides the tumor itself, the TME consists of stromal cells, the extracellular matrix (ECM), the tumor vasculature, and immune cells (Figure 1). The ECM, comprised of connective tissue-specific molecules like collagen, hyaluronic acid, proteoglycans, and laminins, creates a dense environment that surrounds the tumor cells. This creates a diffusion barrier that inhibits access of drugs, nutrients, and oxygen to the tumor³⁸. Furthermore, the ECM contributes to the epithelial-to-mesenchymal transition (EMT) and subsequent metastases. Epithelial cells are characterized by their apical-basal polarity and contact with adjacent cells through adherens junctions, tight junctions, and desmosomes. In the EMT, an epithelial cell transitions into a mesenchymal cell, characterized by a loss of the apical-basal polarity and separation of neighboring cells by interaction with the ECM. Mesenchymal cells can migrate out from the primary tumor and establish metastases at distant sites³⁹⁻⁴³. The ECM also determines the infiltration of immune cells

such as CD4⁺ or CD8⁺ T cells, natural killer (NK) cells, and antigen presenting cells (APC) like macrophages and dendritic cells (DC)⁴⁴ into the tumor. Such tumor-infiltrating lymphocytes can have either a tumor-promoting or tumor-inhibiting effect, which will be described in greater detail below.

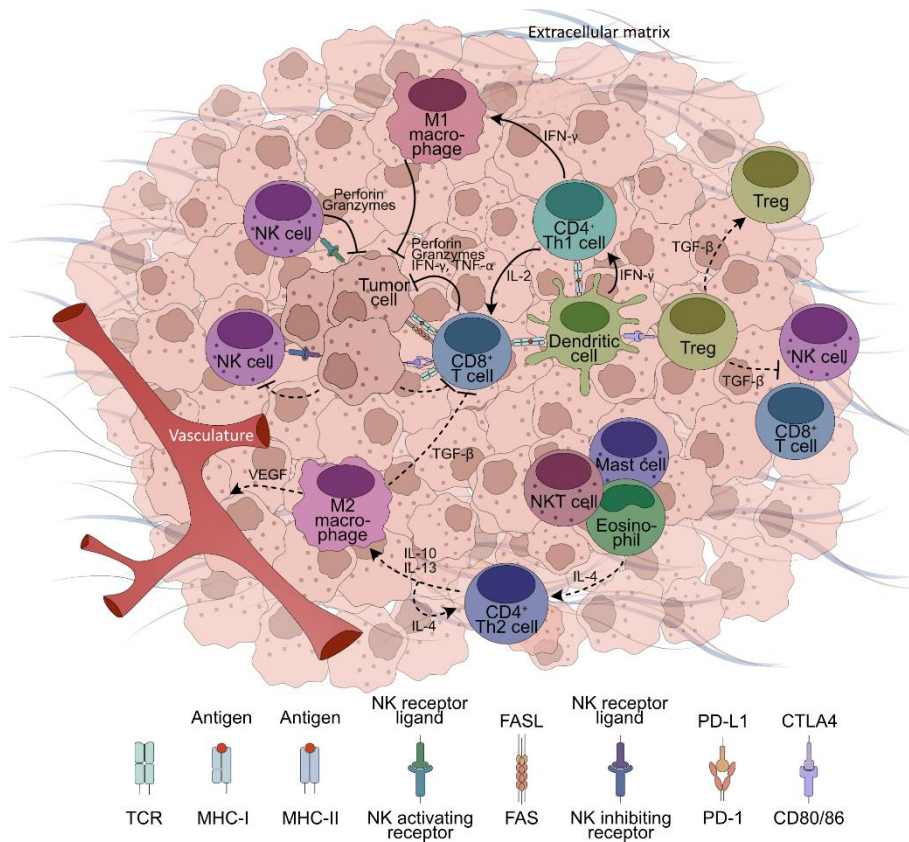


Figure 1. The tumor microenvironment consists of stromal cells, the extracellular matrix, the tumor vasculature, and immune cells. Infiltration of lymphocytes in the tumor can have a tumor-promoting (dashed lines) or tumor-inhibiting (solid lines) effect.

CD4⁺ T cells

APCs present antigens in the form of peptides derived from extracellular proteins on class II MHC (MHC-II) molecules. CD4⁺ T cells engage MHC-II via their T cell receptor (TCR) and the CD4 co-receptor. Naïve CD4⁺ T cells differentiate into T helper cells (Th) under the influence of different chemokines and cytokines. Several types of Th cells exist: Th1, Th2, Th9, Th17,

Th22, follicular helper T cells (Tfh), and regulatory T cells (Treg). Each type of Th cell has a distinct function in pro- or anti-tumor immunity⁴⁵ (Figure 2).

Differentiation of naïve CD4⁺ T cells into Th1 cells is facilitated by the cytokines interferon- γ (IFN- γ), secreted by activated dendritic cells (DC), and interleukin (IL)-12 and IL-18, secreted by activated macrophages. Th1 cells produce IFN- γ , tumor necrosis factor- α (TNF- α), and IL-2, which play a role in tissue-specific destruction during pathogenesis and autoimmune disease, as well as in elimination of cancer cells⁴⁶. Th1 cells activate and regulate the persistence of CD8⁺ cytotoxic T lymphocytes (CTL), maturation and activation of APCs, and induction of immunoglobulin class-switching, mostly to IgG2a, which increases tumor-specific antibody production⁴⁷. Increased levels of Th1 cells in the TME are associated with a positive prognosis and an improved response to immunotherapy in cancer patients⁴⁸⁻⁵¹.

Differentiation of naïve CD4⁺ T cells into Th2 cells is induced by the extracellular pathogen pathway, primarily through the effects of IL-4 secreted by mast cells, eosinophils, and natural killer T cells (NKT cells), or by IL-25 and IL-33 produced by epithelial cells⁵². Th2 cells that have differentiated produce IL-4, which regulates immunoglobulin class switching to IgE in B cells and acts as a positive feedback loop for Th2 activation⁵³. Although the precise role of Th2 cells in tumor proliferation is still unknown, some studies associate large numbers of Th2 cells in tumors with worse prognosis, for instance because Th2 cells drive the polarization of nM ϕ and M1-type macrophages towards M2-type macrophages through secretion of IL-4, IL-10, and IL-13⁵⁴⁻⁵⁶. The properties of macrophages are described in more detail later. Other studies ascribe a more ambivalent role to Th2 cells in the TME⁵⁷, and even show that large numbers of Th2 cells are associated with a positive prognosis in patients with colon cancer⁵⁸, pancreatic cancer^{58,59}, melanoma⁶⁰, breast cancer⁶¹ and lymphoma⁶², possibly due to Th2-driven infiltration of anti-tumor immune cells like eosinophils, M1-type macrophages, and neutrophils^{57,58,62}.

Th9 cells differentiate in response to transforming growth factor- β (TGF- β) and IL-4. Th9 cells produce IL-3, IL-9, IL-10, and IL-21. Although the role for Th9 cells in tumorigenesis is not entirely clear, Th9-driven secretion of IL-9 and IL-21 primarily promotes anti-tumor immunity⁶³⁻⁷⁰. Th17 cells are induced by the synergistic action of IL-6, TGF- β , and IL-21 or IL-23^{71,72}. Th17 cells produce IL-6, IL-17, IL-17A, IL-17F, IL-21, and IL-22. The cytokines secreted by

Th17 cells promote inflammatory reactions of endothelial cells, epithelial cells, and fibroblasts⁷³, which primarily play a role in protection against bacterial and fungal infections but are also believed to take part in development of certain auto-immune diseases like rheumatoid arthritis⁷⁴. Although the role of Th17 cells in cancer immunology is still poorly understood, higher levels of Th17 cells or Th17-associated cytokines in the serum of breast cancer patients are believed to have both a positive^{75,76} and negative^{77,78} effect on tumor prognosis and therapy.

Th22 cells arise through the combined action of IL-6 and TNF- α . Upon activation, Th22 cells secrete TNF- α , IL-13, and IL-22⁷⁹⁻⁸¹. Th22 cells participate in induction of inflammation, mucus production, epithelial cell growth, and wound repair. High levels of IL-22 found in patients with hepatocellular carcinoma and lung cancer are associated with poor prognosis^{82,83}. Furthermore, Th22 cells are suggested have a tumor-promoting effect in colorectal cancer⁸⁴.

Tfh differentiate under the effects of IL-6 and IL-21. Tfh cells are found in the germinal centers and activates B cells to become plasma cells to induce antibody production^{85,86}. Although the role of Tfh cells on cancer progression is still largely unknown, increased numbers of Tfh cells in patients with B cell-associated malignancies are associated with a poor prognosis⁸⁷⁻⁹⁰, whereas in patients with solid tumors the presence of Tfh cells is associated with a more favorable outcome⁹¹⁻⁹⁵.

Treg cells can be produced by the thymus (natural Treg cells), or proliferated from peripheral naïve CD4⁺ T cells under the influence of TGF- β (adaptive Treg cells). Treg cells express CTLA-4 and CD28 on their cell surface, which bind to CD80 and PCD86 on APCs and inhibit T cell activation^{96,97}. Tregs secrete cytokines TGF- β and IL-10. TGF- β not only attracts more Treg cells, it also suppresses the infiltration in tumors of CD8⁺ cytotoxic T cells and natural killer cells (NK), and other inflammatory responses, thus promoting tumor development and progression^{98,99}. In a tumor microenvironment, the Treg cells, tumor cells, and myeloid derived suppressor cells all produce TGF- β , which suppresses the maturation and egress of NK cells from the bone marrow. In addition, TGF- β downregulates the expression of Nkp30 and NKG2D receptors on NK cells, thereby impairing the recognition and activation of NK cells. NK cells and their receptors will be described in greater detail below.

High levels of TGF- β are associated with poor prognosis in lung carcinoma, pancreatic cancer, colorectal cancer, gastric cancer, and hepatocellular carcinoma¹⁰⁰.

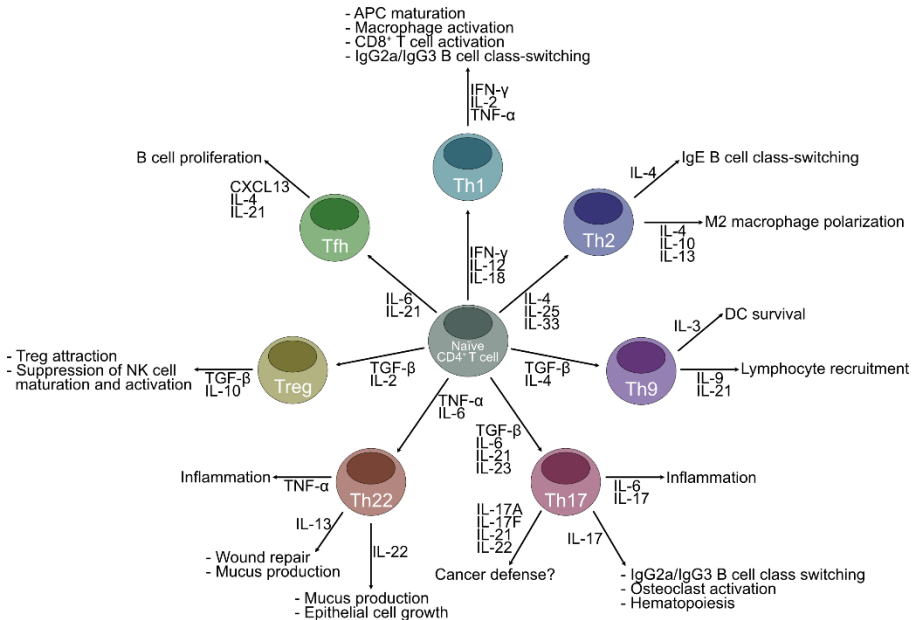


Figure 2. Proliferation and functioning of naïve CD4⁺ T cells. Naïve CD4⁺ T cells differentiate into several different types of Th cells under the influence of different chemokines and cytokines. CD4⁺ T cells can proliferate into Th1, Th2, Th9, Th17, Th22, Treg, and Tfh cells. Each type of Th cell has a distinct function in pro- or anti-tumor immunity.

CD8⁺ T cells

CD8⁺ T cells engage with MHC-I via their T cell receptor (TCR) and CD8 co-receptor. All nucleated cells of vertebrates present antigens derived mostly from intracellular proteins in the form of peptides on MHC-I¹⁰¹. A healthy cell will present peptides derived from normal cellular protein turnover, to which a CD8⁺ T cells will not respond due to the imposition of central and peripheral tolerance¹⁰². However, when a cell presents foreign peptides on MHC-I, for instance due to viral or bacterial infection, or due to malignant transformation, the CTLs will be activated. Most activated CD8⁺ T cells differentiate into effector CTLs, which exert cytotoxicity through secretion of granzymes and perforins, cytokines like IFN- γ and TNF- α , and induction of caspase-mediated apoptosis through Fas/FasL interactions^{103–108}. High levels of CTLs in the TME are associated with better prognosis in cancer patients^{109–112}.

Some cancer cells present tumor-specific antigens, also referred to as neoantigens, on MHC-I. Neoantigens could have oncoviral origins, such as the human papilloma virus-derived HPV E6 and E7 in cervical cancer^{113,114}, mutated versions of proteins like Claudin 18.2 in several epithelial cancers¹¹⁵, Wilms-tumor gene 1 isoforms in leukemia^{116–118}, and BRCA1/BRCA2 in ovarian and breast cancer^{119,120}, or overexpression of tumor-associated antigens such as HER2 in breast cancer^{121,122}, mesothelin in pancreatic cancer¹²³, and CD19 in B cell lymphoma¹²⁴. These neoantigens are recognized by the CD8⁺ T cells, upon which these CTLs will be activated. Somatically acquired mutations in other genes can also specify neoantigens. Such mutations might be unique to a given cancer, and may or may not contribute to the transformation themselves. The various mutant versions of KRAS fall into the former category.

Memory T cells

Although the majority of activated CTLs die once an infection is cleared, a small subset of activated CD8⁺ T cells differentiate into memory CTLs and return to an inactive state. These memory CTLs contribute to the central memory immune response, of which memory B cells and memory helper T cells are also a part. When these memory T cells encounter the same antigen, they are quickly activated and differentiate into effector T cells^{106,125}. Although the mechanism of differentiation into memory T cells is not completely understood, it is hypothesized that they arise from a population of activated T cells that, after pathogen clearance, turn off their effector functions¹²⁶. Tumor-specific CTLs also require activation, presumably under inflammatory conditions, and are likely to behave similarly to their pathogen-specific counterparts. The genes encoding their effector functions are maintained in a state of low methylation, allowing rapid reactivation upon pathogen encounter^{127,128}.

The memory T cell repertoire includes stem cell memory T cells (Tscm), central memory T cells (Tcm), effector memory T cells (Tem), and the more recently discovered tissue-resident memory T cells (Trm). Tcm and Tem cells are characterized by high CCR7 expression and mostly reside in the secondary lymphoid organs. Tem cells are also found in non-lymphoid tissues. CD4⁺ and CD8⁺ Trm cells are not circulating and are found in the peripheral tissues and mucosa. Trm cells are distinguished from other memory T cells by expression of CD69, CD49a, and CD103^{129–131}.

CD103⁺ Trm cells are found in various human cancers, and high levels are associated with better prognosis and improved relapse-free survival in patients with melanoma^{132–134}, lung cancer^{109,135,136}, breast cancer^{137,138}, ovarian cancer¹³⁹, and other solid tumors¹⁴⁰.

Macrophages

Macrophages are innate immune cells of the monocyte lineages. Their main function is the engulfment and digestion of micro-organisms, dead cells, and immune complexes. Macrophages stimulate other immune cells through secretion of chemokines and cytokines¹⁴¹. Macrophages are broadly divided into two distinct subtypes: M1 and M2 macrophages, which are polarized from undifferentiated macrophages (Mφ) through stimulation of different cytokines and other factors^{142–145}.

Polarization of Mφ macrophages into M1 macrophages is facilitated by Th1 cells, and by secretion of signals such as bacterially derived lipopolysaccharides (LPS), IFN-γ and TNF-α. M1 macrophages are associated with an anti-tumor response. They secrete the pro-inflammatory cytokines IL-1β, IL-6, IL-12, IL-23, and TNF-α and chemokines CXCL9, CXCL10, CXCL11, CXCL16, and CCL5^{55,56,142,143,146}. Polarization of Mφ macrophages into M2 macrophages is facilitated by the Th2 cell response through secretion of IL-4, IL-10, IL-13, IL-21, and TGF-β^{54–56,141–143,147–149}. M2 macrophages can be further subdivided into M2a, M2b, M2c, and M2d macrophages, each polarized under the effect of different cytokines and chemokines¹⁴¹. M2 macrophages are often referred to as tumor-associated macrophages (TAMs). Typically, high levels of TAMs in the TME are associated with poor prognosis^{150–153} in part because TAMs negatively influence the infiltration and function of Th1 and Th2 cells through secretion of IL-10 and TGF-β, the latter of which also suppresses CTL function¹⁵⁴. TAMs secrete other tumor-promoting factors, such as vascular endothelial growth factor (VEGF), which contributes to neovascularization and lymphangiogenesis^{154–158}.

Natural killer cells

NK cells are CD3[−] and CD56⁺/CD16⁺ cells that can be divided into two subsets: the naïve CD56^{bright}/CD16^{dim} and the mature CD56^{dim}/CD16^{bright} cells¹⁵⁹. NK cells lack the antigen specificity of B or T cells and instead recognize infected and malignant cells through germline-encoded NK receptors (NKR). According to the 'missing self-hypothesis', coined in 1981, a major function of NK cells is to recognize and eliminate cells that do not express 'self MHC-I'¹⁶⁰.

Because NK cells don't require prior antigen sensitization or presentation by MHC-I for activation, NK cells contribute to a rapid anti-viral and anti-tumor immune response¹⁶¹.

The activities of NK cells are regulated by NK-cell inhibitory or activating receptors on the surface of the NK cells, and NK-cell receptor ligands on the surface of target cells. Activating receptors, which include NKP46, NKP30, NKG2C, NKG2D, and CD16, are upregulated upon stimulation with IL-2, IL-15 or IL-1 β , often released by activated dendritic cells and macrophages¹⁶¹⁻¹⁶³. NK inhibiting receptors, like natural killer group 2 member A (NKG2A) and its splice variant NKG2B, and human killer cell immunoglobulin-like receptor (KIR) are constitutively expressed on NK cells¹⁶⁴. They interact with ligands that are primarily expressed on healthy cells and thus contribute to regulation of autoimmunity¹⁶⁵. For the context of this thesis, the NK cell receptors NKG2D and NKG2A and their ligands will be explained in greater detail in the section "Tumor targets".

Immunotherapy to treat cancer

Treatment of cancer has long been based on surgical removal of the primary tumor and surrounding lymph nodes, localized radiation of the tumor, or administration of chemotherapeutic drugs. Immunotherapy is a concept in tumor treatment that, based on its success, has gained popularity and employs a patient's own immune system to fight or prevent cancer. Examples of immunotherapy are based on modulating the immune system with monoclonal antibodies acting as checkpoint inhibitors or targeting tumor-associated antigens, or adoptive cell transfer (ACT).

Monoclonal antibodies

Monoclonal antibodies (mAbs), typically of the IgG class, are increasingly commonly used for the treatment of cancer. The FDA has approved the use of dozens of mAbs for cancer treatment, among which are mAbs that target tumor-associated antigens such as Herceptin in breast cancer (Trastuzumab¹⁶⁶), CD20 in lymphoma (Rituximab¹⁶⁷), epidermal growth factor receptor (EGFR) in head-and-neck and colorectal cancer (Cetuximab¹⁶⁸), CD56 in several solid tumors (Lorvotuzumab¹⁶⁹) and VEGF-A in several solid tumors (Bevacizumab¹⁷⁰).

Antibody-drug conjugates

mAbs can be employed as the targeting moiety of an antibody-drug conjugate (ADC). The cytotoxic payload of ADCs are often (micro)tubulin inhibitors

like Maytansine, DNA damaging agents like Exatecans, and immune modulators like STING agonists^{171,172}. The mAb targets and binds its antigen and gets internalized through receptor-mediated endocytosis. Inside the cell, the cytotoxic payload is released and exerts its cytotoxic actions¹⁷³.

For the research in this thesis, we employed the cytotoxic activities of Maytansine, fused to a nanobody as targeting moiety. Maytansine and its analogs (Maytansinoids, also referred to as DM1 and DM4), bind to the vinca site of microtubules, causing depolarization of the microtubules and subsequent mitotic arrest^{174–177}. Due to this powerful cytotoxicity, the therapeutic window of Maytansine is small, with adverse effects often experienced on the gastrointestinal system. Conjugated to a monoclonal antibody, however, tissue-specific delivery of Maytansine is possible. This not only significantly improves anti-cancer therapy, it also decreases adverse effects. This has been shown in several clinical trials, for instance where DM1 was fused to Trastuzumab to treat breast cancer¹⁷⁸, and Lorvotuzumab to treat several solid and hematopoietic tumors^{179,180}.

A common effect of ADCs is called “bystander killing”, which occurs when the payload of the ADC is released from the target cell, either after internalization and degradation or by release of the drug in the extracellular space, leading to the uptake and killing of surrounding “bystander cells”, even if they don’t express the target antigen. Because DM1 has a positive charge, it is unable to permeate a cell membrane on its own. This drug is thus suitable for use without risk of the bystander killing effect¹⁸¹.

Immune checkpoint inhibitors

Cancer cells develop defense mechanisms by downregulation of MHC-I, secretion of perforin-degrading enzymes, and overexpression of programmed cell death ligand 1 (PD-L1). PD-L1 is found on healthy cells and interacts with programmed cell death protein 1 (PD-1) found on T cells. The interaction between PD-L1 and PD-1 inactivates the T cells and prevents cytotoxicity, a mechanism employed in healthy tissue to prevent T cell exhaustion and auto-immunity^{182,183}. PD-L1 is frequently overexpressed on cancer cells, rendering them resistant to T cell cytotoxicity^{182,183}. Checkpoint inhibitors are antibodies that target the PD-1 or PDL-1, thereby inhibiting the interaction between them^{184–186}.

CTLA-4 is found on CD8⁺ T cells and T_{reg} cells. It interacts with B7-1 and B7-2 (also known as CD80/86) on the surface of APCs. This interaction inhibits

T cell activation^{96,97}. CTLA-4 targeting antibodies are used to inhibit the T cell inactivation. CTLA-4 inhibitors are sometimes administered together with PD-1 or PDL-1 inhibitors¹⁸⁷.

Adoptive cell transfer and CAR therapy

Adoptive cell transfer is a type of immunotherapy in which a patient receives T cells to fight cancer. As explained in a previous section, the tumor microenvironment can contain tumor infiltrating lymphocytes that recognize and eliminate cancer cells. These tumor infiltrating lymphocytes can be sourced from the tumor after surgical resection, expanded *ex vivo* with the help of IL-2 and CD3, and reintroduced in large numbers into the patient. Treatment with tumor infiltrating lymphocytes has been successful for metastatic melanoma in a phase 3 clinical trial¹⁸⁸. Other clinical trials are on the way for treatment of gastrointestinal cancer (NCT01174121), HPV-associated cancers (NCT01585428), breast cancer (NCT05250336), and other solid tumors (NCT05087745, NCT06047977).

CAR T cell therapy

In another form of adoptive cell transfer, a patient's circulating T cells are engineered with a chimeric antigen receptor (CAR) that targets the tumor cells and exerts cytotoxic activity upon binding. CAR constructs encode a protein that comprises an antigen-binding extracellular domain and intracellular signaling domains, connected to each other via a hinge and a transmembrane domain (Figure 3).

The extracellular antigen-binding targeting portion often consists of a single-chain variable fragment (scFv), composed of the heavy and light chain variable regions of an immunoglobulin, connected by a linker segment¹⁸⁹. scFvs are around one-fifth the size of a conventional immunoglobulin, at 30 kD compared to 150 kD. Their small size imparts excellent solubility while maintaining antigen-recognition. However, the linker that connects the heavy and light chains, as well as the (often) mouse origin of the source immunoglobulin, could be immunogenic and both have been shown to elicit an antibody-response in patients, limiting the anti-tumor response of the infused CAR T cells¹⁹⁰⁻¹⁹⁴. Instead, the more recently discovered heavy-chain only variable fragments (VHH, also referred to as nanobodies) from camelid-derived heavy-chain only antibodies are suggested to be superior as the antigen-binding portion of CARs. Chapter 2 will go into more detail on the properties of nanobodies. Briefly, nanobodies are characterized by their small

size (15kD), solubility, ease of production, and excellent antigen-binding properties compared to full-length immunoglobulins¹⁹⁵. Moreover, nanobodies are poorly immunogenic in humans due to the high homology between camelid and human heavy chain variable region sequences^{196,197}.

The intracellular signaling domains of a CAR harbor an activation domain and one or two co-stimulatory domains. First-generation CARs were engineered with only the cytoplasmic activation domain of CD3 ζ . These CAR T cells were unable to direct lasting T cell responses or sustained cytokine release and were thus considered clinically non-effective¹⁹⁸. Second-generation CARs combine the CD3 ζ domain with additional co-stimulatory domains such as those derived from the cytoplasmic tail of CD28 or 4-1BB, which enhances survival and expansion of T cells *in vivo*^{199,200}. CD28/CD3 ζ -based CAR T cells are believed to elicit superior cytotoxic capacity *in vivo*, whereas 4-1BB/CD3 ζ -based CAR T cells show higher *in vivo* expansion and persistence²⁰¹. The FDA approved six second-generation CAR T cell therapies for hematopoietic cancers such as relapsed or refractory B-cell lymphoma or acute lymphatic leukemia based on CD19 targeting with an scFv (Axicabtagene ciloleucel, brexucabtagene autoleucel, lisocabtagene maraleucel, and tisagenlecleucel), and relapsed or refractory multiple myeloma, based on B-cell maturation antigen (BCMA) targeting with an scFv (idecabtagene vicleucel) or a VHH (ciltacabtagene autoleucel)²⁰².

Third-generation CAR T cells combine the potential of the two costimulatory domains to enhance both the T cell response and the *in vivo* survival and expansion of the CAR T cells. Fourth-generation CAR T cells are enhanced by inclusion of other transgenes, for instance those promoting autologous cytokine secretion or other costimulatory ligands, into the T cell²⁰³.

CAR NK cell therapy

Just like therapies based on T cells, NK cell-based therapies have proven promising in clinical trials treating both hematological and solid cancers²⁰⁴. CAR NK cells can be produced from NK cells derived from the patient's or a donor's peripheral blood, from a placenta or umbilical cord blood, existing immortalized NK cell lines (NK-92 or NK-92MI) or manufactured from induced pluripotent stem cells (iPSC)²⁰⁵⁻²¹⁰. There are a few advantages of treatment with CAR NK cells versus CAR T cells. First, unlike T cells, NK cells do not form the risk of Graft-versus-Host disease (GVHD) in an allogeneic setting. In fact, NK cells are believed to protect against GVHD in T cell-based

cancer treatments^{211–215}. Furthermore, NK cells allow for the inclusion of a wider range of co-stimulatory domains, using not only traditional intracellular domains derived from CAR T therapies based on CD28, 4-1BB, and CD3 ζ , but also NK-specific domains such as CD244 and NK-ARs^{209,216,217}. Moreover, if a tumor were to downregulate the CAR's target in an attempt at immune escape, the NK cells would still be effective against the tumor cells due to the intrinsic cytotoxic capabilities of NK cells. Lastly, a major reported side-effect of CAR T therapy is cytokine release syndrome, which is systemic inflammation caused by a large amount of cytokines released by the CAR T cells. The cytokines released by NK cells (IFN- γ , IL-3, and TNF- α) do not induce such inflammation, and thus do not cause cytokine release syndrome²¹⁷. For these reasons, CAR NK cell therapy is potentially a more effective and a safer alternative to CAR T cell therapy.

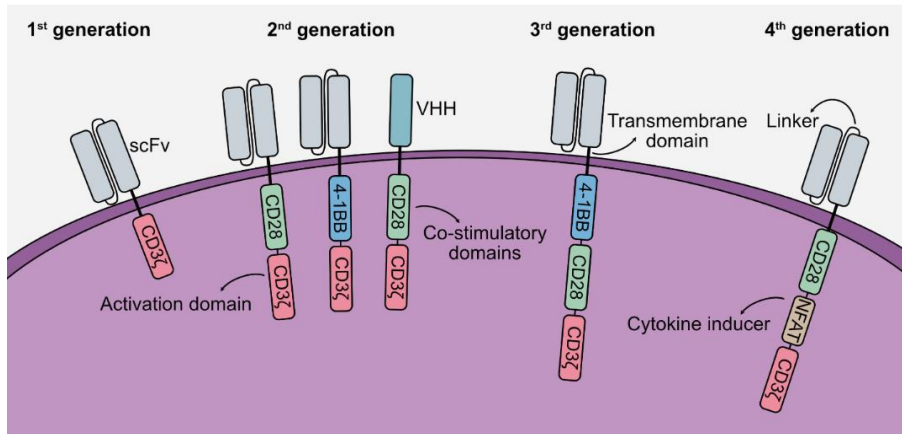


Figure 3. Composition of common CAR constructs. The extracellular antigen-binding targeting portion often consists of an scFv, composed of the heavy and light chain variable regions of an immunoglobulin connected by a linker segment, or a VHH, the variable region of camelid heavy-chain only antibodies. The intracellular signaling domains harbor the cytoplasmic CD3 ζ activation domain (first generation) or a the cytoplasmic CD3 ζ activation domain in combination with a CD28 or 4-1BB co-stimulatory domain (second generation). Third-generation CAR T cells combine the potential of the two costimulatory domains. Fourth-generation CAR T cells are enhanced by inclusion of other transgenes, for instance those promoting autologous cytokine secretion.

Tumor targets

Although often effective in treating tumors and metastases, a huge disadvantage of current (immuno)therapies is the large number of side-effects that patients experience. Most cancer drugs target proteins that are expressed on a wide variety of rapidly dividing cells, which include healthy cells, such as cells of the skin, stomach, gut, and hair. This explains the most frequently reported side-effects of rashes, nausea, diarrhea or constipation, and hair loss. An ongoing quest in clinical research has been the identification of tumor-specific targets to treat and/or prevent cancer. Tumor-associated and tumor-specific antigens, like those mentioned earlier, are important for therapies that involve CARs and antibodies. We propose the targeting of two MHC-I associated proteins: MICA and HLA-E.

MICA

The MHC-I chain-related proteins A and B (MICA and MICB) are encoded within the family of human HLA class I (MHC-I) genes on chromosome 6. MICA/B consists of 3 extracellular, immunoglobulin-like domains (α_1 , α_2 , and α_3). The protein has a molecular mass of 36 kDa, but contains 8 potential N-linked glycosylation sites, some of which are used, resulting in an apparent molecular mass of approximately 56 kDa when the protein is examined by SDS-PAGE. Unlike conventional MHC-I proteins, MICA and MICB do not associate with beta-2-microglobulin and do not present antigen, but rather act as ligands for the NKG2D receptor on NK cells, CD8⁺ T cells, and $\gamma\delta$ T cells²¹⁸. Upon binding, these cells can eradicate MICA/B-positive targets through cytotoxicity and secretion of cytokines^{219–221}.

NKG2D signaling

MICA/B, as well as other proteins such as the UL-16 binding proteins (ULBP) in humans, and members of the H6o, RAE and MULT1 protein families in mice, act as ligands for the NK cell-activating receptor NKG2D. Upon binding to ligands expressed on tumor cells or virus-infected cells, NKG2D pairs with DNAX-activating protein-10 (DAP-10). The complex transmits intracellular signals via the Phosphoinositide 3-kinase (PI3K) and Growth Factor Receptor Bound Protein 2 (GRB2) signaling pathways through tyrosine phosphorylation. This triggers activation of the AKT/MAPK or NF κ B/NFAT pathway, causing NK-mediated cytotoxicity and production of cytokines, chemokines, and granzymes^{220,221} (Figure 4).

The protease Granzyme B (GrzB), together with the glycoprotein perforin, participates in the induction of apoptosis of NK and T cell targets. GrzB has hundreds of substrates, most of them involved in induction of apoptosis, inflammation, and remodeling of the extracellular matrix. In the anti-tumor response, GrzB enters the target cell with the help of perforin, or by endocytosis facilitated by binding to the negatively charged heparan sulphate-containing receptors on the surface of the target cells. Inside the target cell, GrzB cleaves and activates initiator caspases 8 and 10 and executioner caspases 3 and 7, which triggers the apoptosis pathway^{222,223}.

MICA/B as target

The MICA/B proteins are expressed only weakly on healthy cells but are overexpressed on the surface of cells under stress, for instance due to infection or malignant transformation²²⁴. High levels of expression of MICA/B have been seen in both hematopoietic malignancies and in a wide variety of epithelial solid tumors such as colorectal cancer²²⁵, ovarian cancer²²⁶, cervical cancer²²⁷, breast cancer²²⁸, pancreatic cancer²²⁹, melanoma²³⁰, and cholangio-carcinoma²³¹. Surface expression of NKG2D ligands can be regulated transcriptionally, translationally, and post-translationally by the tumor microenvironment. Post-translationally, the surface expression of MICA and MICB on tumor cells can be downregulated through shedding. Shedding is mediated by proteolytic cleavage at the $\alpha 3$ domain involving the disulphide isomerase ERp5 and ADAM-type proteases such as ADAM10 and ADAM17²³²⁻²³⁶. Increased levels of soluble MICA/B in the serum of patients are associated with poor prognosis and worse disease progression^{29,225,237}. Loss of surface-bound MICA renders tumor cells less sensitive to NKG2D-positive NK cells. Furthermore, soluble MICA might occupy the NKG2D receptors on NK and CD8⁺ T cells and thus inhibit the cytotoxic activity on cells that express MICA/B at the surface^{238,239}.

In clinical settings, patients with melanoma who received a GM-CSF secreting cell-based cancer vaccine (GVAX) and anti-CTLA-4 antibodies generated high titer antibodies against MICA²⁴⁰. These antibodies inhibited the immune suppression caused by soluble MICA, and increased innate and adaptive anti-tumor immunity by CD8⁺ T cell and NK cell responses. The increase in anti-MICA antibodies resulted in a decrease in soluble MICA in the patient's circulation²⁴¹. The increase of humoral anti-MICA antibodies and its benefit in cancer therapy suggests a useful role for MICA/B-based vaccination. Indeed, by vaccinating mice with the conserved $\alpha 3$ domain of MICA/B,

proteolytic shedding of MICA/B from the surface of murine-derived B16F10 melanoma cells transfected to express human MICA/B, was prevented both *in vitro* and in a mouse model. Furthermore, mice immunized with the MICA/B $\alpha 3$ domains showed significantly reduced tumor growth of MICA/B⁺ B16F10 melanoma and EL-4 T cell lymphoma tumors.

The vaccine safety and immunogenicity was examined in rhesus macaques which, unlike mice, endogenously express MICA/B proteins homologous to human MICA/B. High serum titers of anti-MICA/B antibodies were found following immunization with macaque MICA/B $\alpha 3$ domains, while no clinical side effects were observed²⁴². The monoclonal antibody “7C6” specifically targets the $\alpha 3$ subunit of the MICA/B protein, thereby inhibiting shedding by the TME through obstructing access of ERp5. Mice treated with monoclonal antibody “7C6” showed significant reduction in tumor growth and metastases formation of MICA⁺ B16F10 tumors²⁴³.

The absence of MICA/B on the surface of healthy cells, and the ability to overcome proteolytic shedding from the tumor cell membrane, makes MICA/B an appealing target for tumor therapy.

HLA-E

MHC-I molecules are found on the surface of all nucleated cells in vertebrates. Assembly of MHC-I with $\beta 2M$ is facilitated in the endoplasmic reticulum (ER), where the complex is loaded with peptides with the help of Tapasin and TAP²⁴⁴. Peptide-bound MHC-I rapidly exits the ER, traverses the secretory pathway, and is expressed at the cell surface^{101,245–250}. MHC-I presents fragments of intracellular proteins in the form of peptides to cytotoxic T cells. As discussed earlier, healthy cells will display peptides from normal cellular proteins on their MHC-I, to which the CTLs will not react due to imposition of central and peripheral tolerance^{102,251}. When cells express foreign proteins on MHC-I, like those found intracellularly after a viral infection or malignant transformation, the cytotoxic T cells will recognize and kill the affected cell^{103,106}. The MHC-I molecule HLA-E presents a unique case, as it is specialized in the presentation of so-called “VL9” peptides (VMAPRT(L/V)(L/V/F)L). These peptides are derived from the signal sequences of other MHC-I products, or of viral type I membrane glycoproteins^{252–260}.

Virus-infected and malignantly transformed cells can escape immune cell recognition by down-regulation of MHC-I, which can be achieved transcriptionally and post-transcriptionally²⁶¹⁻²⁶⁵. Human cytomegalovirus (CMV) expresses the VL9 peptide in the leader sequence of its UL40 protein. This peptide can be loaded onto HLA-E in a TAP-independent manner in the ER^{266,267}. This is sufficient to upregulate the expression of HLA-E on the cell surface, preventing NK cell-mediated cytotoxicity of the infected cells through interaction with NKG2A. Thus, if a virus succeeds in down-regulation of the classical Class I HLA-A, -B and -C products, VL9 peptides would continue to be produced and could serve as peptide cargo for HLA-E, rendering the infected cell resistant to NK and T cell lysis²⁶⁶⁻²⁶⁸.

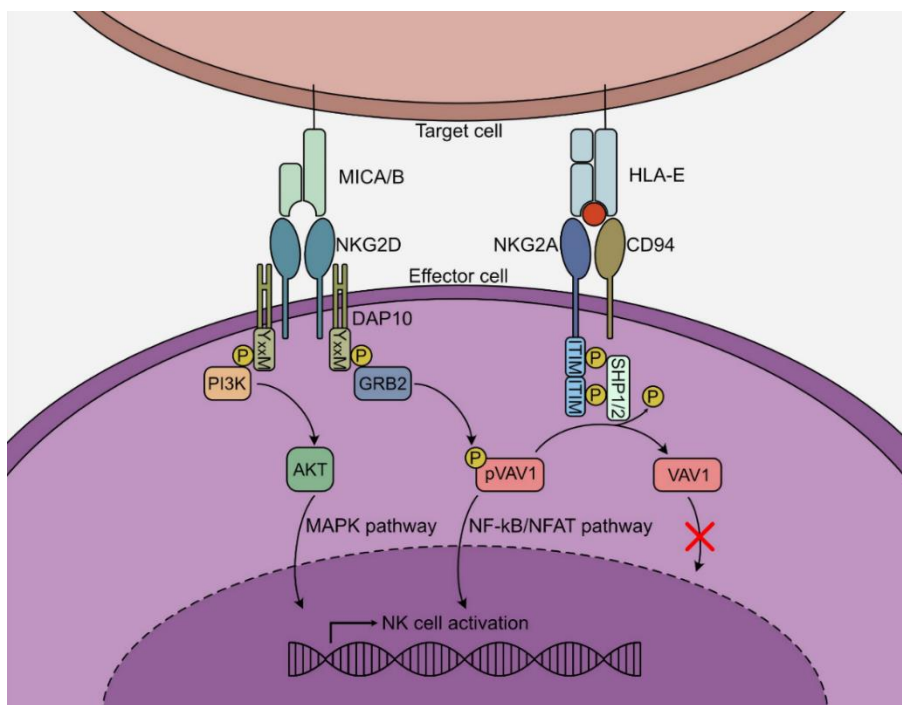


Figure 4. Activating and inhibiting receptors on NK cells. The NK cell-activating receptor NKG2D is activated by MICA/B in humans. Upon binding to its ligand, NKG2D forms a complex with DAP-10, resulting in tyrosine phosphorylation of DAP-10. The complex transmits intracellular signals via the PI₃K and GRB2 signaling pathways, triggering activation of the AKT/MAPK or NFκB/NFAT pathways, causing NK-mediated cytotoxicity and production of cytokines, chemokines, and granzymes. The NK-cell inhibiting receptor NKG2A is activated by the ligand HLA and forms a heterodimer with CD94. The interaction of NKG2A with HLA-E causes phosphorylation of the NKG2A ITIM motifs, which recruits SHP1/2. SHP-1/2 in turn dephosphorylates signaling molecules such as VAV1, blocking downstream NK cell activation signals.

NKG2A signaling

HLA-E serves as a ligand for CD94/NKG2A and NKG2C on NK cells and T cells, and causes inhibition of the cytotoxic activity of such cells^{258,260,269-279}. The interaction of NKG2C The interaction of NKG2A/CD94 with peptide-presenting HLA-E causes phosphorylation of the intracellular immunoreceptor tyrosine-based inhibitory motifs (ITIM) of NKG2A. This recruits the activating Src homology 2 domain-containing protein tyrosine phosphatases SHP-1 and SHP-2. SHP-1/2 dephosphorylates signaling molecules such as VAV1, blocking downstream NK cell activation signals^{278,279} (Figure 4).

The cytoplasmic tail of HLA-E

The ectodomains of the MHC-I products, including that of HLA-E, are highly homologous. There are few locus-specific features present in the ectodomains that would allow an unambiguous assignment of a sequence to the HLA-A, -B or -C locus. In contrast, the cytoplasmic tails of the classical MHC-I products show such locus-specific features, shared among virtually all alleles at that locus (Chapter 7, Figure 1).

The cytoplasmic tail of MHC-I is involved in trafficking peptide-bound MHC-I from the ER to the cell membrane, and in endocytosis²⁸⁰. In the case of HLA-E, surface-disposed HLA-E is unstable and rapidly internalized, causing HLA-E to be enriched in endosomal structures. HLA-E is also retained in an immature state in the ER, as defined by the sensitivity of HLA-E to Endoglycosidase H, and intracellular accumulation seen by immuno-fluorescence²⁸¹.

The cytoplasmic tail plays a role in ER retention. This has been confirmed by swapping the cytoplasmic tail domains of HLA-E and HLA-A3, creating HLA-E(A3) and HLA-A3(E). HeLa cells transfected with these transgenes showed a 1.7-fold increase in expression of HLA-E(A3) compared to HLA-E, and a reduction (0.7-fold) in expression of HLA-A3(E) compared to HLA-A3. Furthermore, the surface half-life of HLA-E(A3) molecules was twice that of HLA-E, confirming that the cytoplasmic tail of HLA-E also plays a role in its endocytosis and relocation of HLA-E to late and recycling endosomes^{281,282}. The rapid turnover of surface-disposed HLA-E is also attributed to the binding affinity of VL9 to HLA-E, which is much lower than the average binding affinity of other MHC-I binding peptides^{253,283-285}.

HLA-E targeting by CMV-based vaccines

Peptide-presentation of HLA-E is further exploited in the more recently developed cytomegalovirus (CMV)-based vaccines, studied in rhesus macaques which express the HLA-E homologue Mamu-E. rhCMV-vectored vaccines against genes of the simian immunodeficiency virus (SIV) elicited a strong HLA-E-restricted CD8⁺ T cell response to SIV peptides causing efficient eradication of a subsequent SIV infection, compared to a relatively slower T cell response from comparable adenovirus-vectored vaccines.

It is hypothesized that the rhCMV-derived VL9 peptide stabilizes the hydrophobic binding groove of Mamu-E, allowing a broader range of SIV-derived peptides to bind, improving presentation of SIV-derived antigens to non-classical CD8⁺ T cells. These findings, combined with the lack of polymorphism of HLA-E in the human population²⁸⁶, show a promising role of CMV-based vaccination against HIV and other viruses in humans.

HLA-E as target

HLA-E is overexpressed on various types of hematopoietic and solid tumors, and is associated with worse prognosis and disease outcome in lung cancer²⁸⁷, glioma^{288,289}, renal cell carcinoma²⁹⁰, colon cancer^{37,291–293}, breast cancer^{36,228}, and ovarian cancer^{275,294,295}. Tumor infiltrating lymphocytes in certain cancers show higher expression of NKG2A, which is also correlated with poor prognosis^{296–298}. Because overexpression of HLA-E on cancer cells is a mechanism of immune-evasion, blockade of the interaction between NKG2A and HLA-E may enhance the anti-tumor immune response and cancer therapies. In fact, the monoclonal NKG2A-targeting antibody Monalizumab has successfully been used in combination with PD-L1-targeting or EGFR-targeting therapies to treat colorectal cancer and squamous cell head-and-neck cancer respectively. Blocking of NKG2A alone had no effect on cancer growth^{296,299}.

The role of the cytoplasmic tail on HLA-E trafficking and peptide presentation deserves further study. As mentioned, the cytoplasmic tail is also the feature distinguishing HLA-E from other MHC-I molecules. Thus, antibodies against the HLA-E cytoplasmic tail could provide a useful tool for studying the cytoplasmic tail interactions, as well as for other purposes where targeting of HLA-E specifically is necessary, such as staining of tumor tissues for diagnostics.

Targeting of proteins can be done with monoclonal antibodies, an approach we used for the cytoplasmic tail of HLA-E, or camelid-derived heavy-chain only fragments, called nanobodies or VHHs, which we use for targeting MICA. The difference between conventional antibodies and VHHs is described in Chapter 2.

Chapter 2:

Nanobodies in cancer

Elisha R. Verhaar¹, Andrew W. Woodham^{1,2}, Hidde L. Ploegh^{1,2}

¹ Program in Cellular and Molecular Medicine, Boston Children's Hospital,
Boston, MA

² Department of Pediatrics, Harvard Medical School, Boston, MA

Seminars in Immunology

2021 Feb;52(363):101425

DOI: 10.1016/j.smim.2020.101425

Abstract

For treatment and diagnosis of cancer, antibodies have proven their value and now serve as a first line of therapy for certain cancers. A unique class of antibody fragments called nanobodies, derived from camelid heavy chain-only antibodies, are gaining increasing acceptance as diagnostic tools and are considered also as building blocks for chimeric antigen receptors as well as for targeted drug delivery. The small size of nanobodies (~15 kDa), their stability, ease of manufacture and modification for diverse formats, short circulatory half-life, and high tissue penetration, coupled with excellent specificity and affinity, account for their attractiveness. Here we review applications of nanobodies in the sphere of tumor biology.

Introduction

In this review we capture developments in the application of antibody fragments, called nanobodies, to tumor biology, covering both diagnostics and therapeutics. Spontaneous or engineered, immune responses against cancers are seen as a powerful adjunct to other forms of treatment. The ensemble of antigen presenting cells (APCs), CD4⁺ T cells, CD8⁺ T cells and B cells regulate adaptive immunity. CD4⁺ T cells (helper T cells) respond when they recognize antigen presented on class II major histocompatibility complex (MHC-II) molecules on the surface of APCs. Activated helper T cells and their products enhance the adaptive immune response through activation of B cells, NK cells and macrophages. B cells present antigen via MHC-II, which is recognized by helper T cells. Helper T cells then secrete signals to differentiate B cells into immunoglobulin (Ig)-secreting plasma cells. Secreted Ig serves various purposes, from neutralization of infectious agents to enhancement of phagocytosis or complement-assisted destruction of pathogens. These effector functions are attributable mostly to crosslinking of fragment crystallizable (Fc) receptors.

In most mammals, Igs are composed of a heavy chain and a light chain, each containing a variable and a constant region. A unique type of Igs, devoid of light chains, was discovered in sharks³⁰⁰ and in camelid species in 1989³⁰¹. Engineering of the heavy chains of the camelid heavy-chain only antibodies (hcAbs) yields single-domain antibody (sdAb) fragments, also known as nanobodies (Nb) or VHHs (figure 1A). In select cases, it has been possible to generate sdAbs from the heavy chain variable segments of human and mouse (conventional) Igs³⁰²⁻³⁰⁶. While such human or mouse V_H segments can be

expressed in the absence of a light chain and retain proper solubility and antigen binding properties^{307,308}, this is not always the case. Therein lies the importance of the discovery and development of the camelid hcAbs.

Of late, sdAbs are having a major impact on how Igs and their derivatives are used in research and in practical applications. Despite being only ~1/10th the size of their full-sized counterparts, nanobodies retain the characteristics of antigen specificity and binding affinity. Other favorable attributes of nanobodies are their solubility³⁰⁹ and stability³¹⁰, as well as ease of production in bacteria, thus enabling large-scale production³¹¹. Their small size (~15 kDa) endows nanobodies with excellent tissue penetration³¹² and rapid clearance from the circulation ($t_{1/2} < 30$ min)³¹³. Because of their unique characteristics and relative ease of production, nanobodies are increasingly used in a variety of applications, such as delivery of drugs or radioisotopes, as well as imaging of tumors and other tissue types. The half-life of nanobodies can be extended at will, for instance by chemical modification with polyethylene glycol (PEG)³¹⁴, through fusion of the nanobody to serum albumin nanoparticles³¹⁵ or to a serum albumin-binding nanobody³¹³.

The field of nanobodies continues to advance rapidly. Several excellent reviews on the generation, properties and application of nanobodies across broad areas of biomedical interest have appeared^{195,311,316–326}. The purpose of this review is to focus on recent applications of nanobodies in tumor immunology, primarily in the context of diagnostics, imaging, and therapeutics. We provide an overview of available nanobodies and the (tumor) targets they recognize, as well as their applications. While in many cases nanobodies are used in lieu of conventional antibodies, possibly to avoid intellectual property conflicts, it is helpful to think of nanobodies as immunological tools with unique properties.

Tumor-targeting nanobodies

Nanobodies have similar antigen-binding properties as conventional antibodies. However, because nanobodies employ a single Ig variable domain for antigen recognition, they can access epitopes that are beyond the reach of conventional antibodies or antibody derivatives such as single chain Fv fragments (scFvs). For example, nanobodies can penetrate into a cleft on a protein's surface or at a domain-domain interface. Currently available nanobodies for tumor-relevant targets are listed in Table 1. Figure 1B shows an overview of nanobody targets in relation to the tumor (microenvironment).

In some cases, the nanobodies cross-react with homologous targets from other species. This may facilitate the transition from pre-clinical to clinical applications. Examples include cross-reactivity with human and murine antigen for the anti-EGFR nanobody 8B6³²⁷, the anti-HER2 nanobody 2Rs15d³²⁸ and the nanobody directed against the EIIIB splice variant of fibronectin³²⁹.

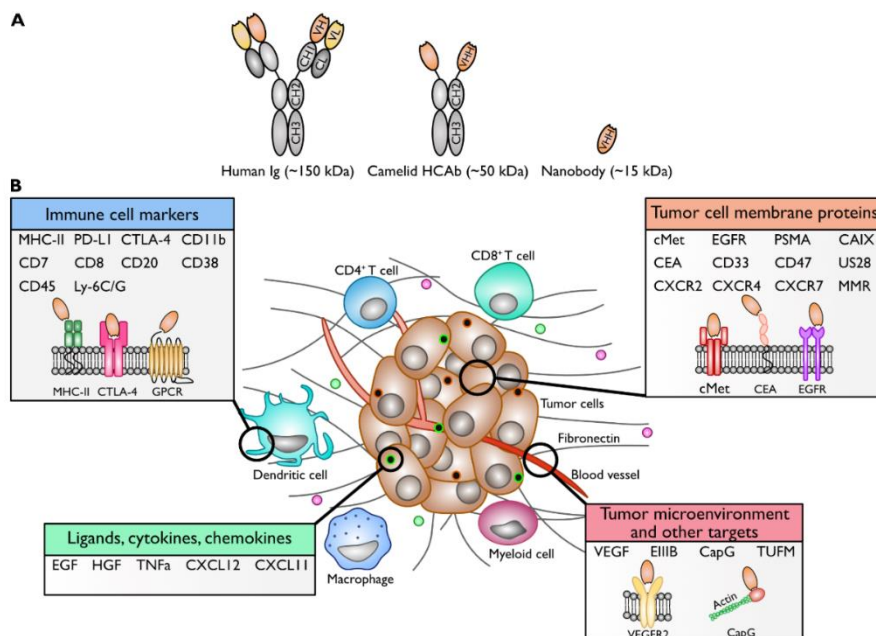


Figure 1. Nanobodies and their targets in relation to the tumor (micro-environment). (A) Schematic representation of a conventional human Ig, camelid HCab, and a nanobody. (B) Schematic overview of the tumor-associated targets for which nanobodies have currently been established. Important targets are immune cell markers, tumor cell (membrane) proteins, receptor ligands, and proteins associated with the tumor microenvironment.

EGFR family

Members of the epidermal growth factor receptor (EGFR) family are often over-expressed on the surface of tumor cells of epithelial origin and play a role in their proliferation, survival, and in angiogenesis³³⁰. Antibodies that target the EGF receptor have been proven successful in cancer treatment. An example is cetuximab, a full-size chimeric mouse/human monoclonal antibody specific for the EGFR³³¹. Therefore, EGFR family members have been

among the first tumor markers targeted by nanobodies. EGFR₁-targeting nanobodies were identified by phage display, using competitive elution with the ligand EGF to identify specific binders³³². Using the same EGFR phage nanobody repertoire and selecting for the EGFR extracellular domain, the nanobodies 7C12 and 7D12³³³ and 9G8³³² were identified.

The former competes with cetuximab, the latter does not. Multivalent nanobody molecules can be built by fusion of individual nanobody gene segments or through chemical conjugation methods. EGFR-specific nanobodies were formatted into bivalent molecules in different combinations, all of which inhibited tumor cell proliferation in an *in vitro* epidermoid cancer model. Specifically, the combination of 7D12-9G8 anti-EGFR nanobodies performed best in inhibiting EGFR signaling and reduced the growth of human epidermoid carcinoma A431 cells. When linked to Alb1, a serum albumin-binding nanobody, the construct was called CONAN-1, which strongly inhibited EGF-induced signaling, leading to tumor regression in A431 xenograft-bearing mice³³⁴.

Using similar methods, the anti-EGFR nanobodies 8B6 and OA-cb6 were obtained^{327,335}. Nanobodies that recognize HER2, another member of the EGFR family, specifically target HER2⁺ SKOV3 ovarian cancer cell-derived tumors *in vivo*³²⁸. HER2-targeting nanobodies 11A4³³⁶ and 5F7GGC³³⁷ have been used for a variety of (clinical) applications, described elsewhere in this review.

VEGFR2 and VEGF

Vascular epithelial growth factor receptor 2 (VEGFR₂) is part of the human VEGFR family of receptors and is present on vascular endothelial cells. Its ligand, VEGF, is secreted by cell types such as macrophages and tumor cells, thereby inducing downstream signaling pathways involved in cell proliferation, angiogenesis and metastasis^{338,339}. This makes VEGF and VEGFR₂ appealing targets for nanobody-based therapies, for example to prevent the formation of new blood vessels on which tumors rely for nutrient and oxygen supply. The anti-VEGFR₂ nanobody 3VGR19 was obtained by phage display on recombinant extracellular domains of the VEGFR₂ receptor. It inhibits VEGFR₂ signaling, thereby inhibiting the formation of capillary-like structures, as shown in an *in vitro* study on human umbilical vein endothelial cells (HUVEC)³⁴⁰. Ma et al. isolated an anti-angiogenic VEGFR₂-D3 specific nanobody NTV1 from HuSdlTM, a human single domain antibody

library of 'camelized' human antibodies³⁴¹. In similar fashion, nanobodies specific for VEGF were obtained. These inhibit endothelial cell proliferation in an *in vitro* angiogenesis assay using HUVECs³⁴². A humanized version of one of these nanobodies, Nb42, has also been generated³⁴³. Lastly, the nanobody VA12, which specifically targets the binding domain of VEGF-A, showed anti-angiogenic potential in a chorioallantoic membrane assay³⁴⁴.

c-Met and HGF

Hepatocyte growth factor (HGF) binds to the c-Met receptor³⁴⁵, which activates pathways responsible for cancer progression, angiogenesis and metastasis³⁴⁶. For several different epithelial and nonepithelial cancers, overexpression of HGF and the c-Met receptor are associated with a poor prognostic outcome^{347,348}. Nanobodies against c-Met and HGF have been produced. The anti-cMet nanobody G2 competes with HGF for binding to the c-Met receptor³⁴⁹. Schmidt Slørdahl et al. used a bispecific nanobody, with one nanobody to target c-Met and the other nanobody to enable binding to human serum albumin for half-life extension. This bispecific anti-c-Met nanobody inhibited the interaction of c-Met with HGF and led to a reduction in cell migration and adhesion in multiple myeloma cells. This bispecific nanobody was even more efficient at inhibiting tumor growth than a conventional bivalent monoclonal anti-c-Met antibody³⁵⁰.

The bispecific albumin- and HGF-specific 1E2-Alb8 and 6E10-Alb8 nanobodies showed a dose-dependent inhibition of HGF-induced proliferation of Bx-PC3 human pancreatic cancer cells. Nude mice bearing human glioma U-87 MG xenografts were treated with an anti-HGF nanobody, resulting in significant inhibition in tumor growth compared to the control group. Both 1E2-Alb8 and 6E10-Alb8 nanobodies show potential as a treatment option for multiple myeloma and other HGF-c-Met driven cancer types³⁵¹.

Other targets

In addition to the molecules described above, many other tumor-associated antigens have served as targets for nanobody development. Chemokine receptors, which are G-protein coupled receptors (GPCR), are overexpressed in a wide variety of malignancies³⁵². Chemokines and their receptors drive migration and activation of a variety of cell types relevant for both innate and adaptive immune responses. If the goal is to interfere with cell migration, these molecules would appear to be ideal targets in view of the superior tissue

penetration of nanobodies. Such nanobodies might neutralize the inhibition of chemorepellent signals, which would otherwise prohibit access of therapeutically efficacious immune cells to the tumor microenvironment. Conversely, immunosuppressive cells require chemoattractants to arrive at the site of the tumor. Nanobodies that target GPCRs and its ligands include reagents specific for human CXCR2³⁵³, CXCR4³⁵⁴⁻³⁵⁶, CXCR7³⁵⁷, CXCL11 and CXCL12³⁵⁸, and the viral GPCR US28³⁵⁹⁻³⁶¹.

Furthermore, nanobodies have been identified that target human tumor-associated (trans)membrane proteins such as carcinoembryonic antigen (CEA)³⁶²⁻³⁶⁴, prostate-specific membrane antigen (PSMA)³⁶⁵⁻³⁶⁹, and human and murine macrophage mannose receptor (MMR)^{370,371}.

Other important targets are immune cell markers such as human CD7^{372,373}, human and murine CTLA-4^{374,375}, human and murine PDL-1³⁷⁶⁻³⁸⁰, murine CD8³⁸¹, murine CD11b^{325,382,383}, human CD2³⁸⁴, human CD38³⁸⁵, mouse CD45³⁸², mouse Ly-6C/Ly-6G³⁸⁶, human and murine MHC-II^{387,388}. Other targets include fibronectin³²⁹, TUFM³⁸⁹, CapG³⁹⁰, CAIX^{391,392}, CD33³⁹³, human and murine CD47^{394,395}, murine ARTC2³⁹⁶, and TNF α ³⁹⁷ (table 1).

Nanobodies for diagnosis through imaging

Molecular imaging has become an important tool in cancer research, both for understanding the underlying biology of a disease, as well as for diagnosis and therapy³⁹⁸. Molecular imaging requires a targeting moiety labeled with a diagnostic radioisotope³⁹⁹ or a suitable fluorophore. Radiolabeled monoclonal antibodies have been used extensively as targeting moieties, but their effectiveness is limited by the large size of full-sized Igs and their comparatively long circulatory half-life⁴⁰⁰. Notwithstanding their large size, conventional fully human monoclonal antibodies used for therapy have been converted into imaging agents. This strategy has the obvious advantage that agents approved for clinical use can be used with only slight modification for imaging purposes, and with minimal risk of immunogenicity and unexpected adverse outcomes, especially given the modest amounts of imaging agent administered. Only recently have nanobodies been used in first human trials³²³. Aside from the kidneys, uptake of radiolabeled nanobodies in non-targeted organs is usually low, resulting in a high target-to-background ratio shortly after administration.

This allows same-day imaging and the use of shorter-lived radioisotopes, in contrast to the low target-to-background ratio found shortly after administration of ^{89}Zr -labeled full-sized monoclonal antibodies used for the same purpose^{400,401}. These characteristics explain why nanobodies have been used in molecular imaging techniques such as positron emission tomography (PET)⁴⁰², single photon emission computed tomography (SPECT)³²⁷, near-infrared fluorescence imaging (NIR)⁴⁰³, and ultrasound-based molecular imaging⁴⁰⁴ (figure 2A).

PET imaging

PET imaging uses positron-emitting radiotracers. Positrons collide with electrons in the tissue. This produces energy in the form of photons, which can be detected with a PET scanner⁴⁰⁵. Isotopically labeled Igs and Ig fragments used as PET imaging agents show exquisite specificity for select targets *in vivo*^{406,407}. The EGFR-targeting 7D12 nanobody, radiolabeled with $^{68/67}\text{Ga}$ or ^{89}Zr , was among the first nanobodies to be used for PET imaging. The PET images of A341 tumor-bearing mice show clearly visible tumors with good tumor-background contrast⁴⁰².

Some anti-HER2 nanobodies have also been used for imaging purposes, and the lead compound 2Rs15d has been studied in some detail. Coupled to ^{68}Ga -NOTA, the nanobody yielded high-contrast images of tumors in SKOV3 tumor-bearing rats⁴⁰⁸. The use of this nanobody has also successfully been translated to the clinic, with the first in-human phase I study of ^{68}Ga -NOTA-2Rs15d used in PET/CT scans of HER2-overexpressing cancer patients. The nanobody-based imaging agent showed favorable biodistribution and high accumulation in the primary lesions and/or metastases of the patients without side effects, indicating its safety and clinical potential⁴⁰⁹. Two phase II studies with this tracer have since been initiated, evaluating its potential to detect local and distant metastases in breast cancer patients (clinicaltrials.gov, NCT03331601 and NCT03924466). A similar approach with the anti-MMR nanobody 3.49 in 3LL-R tumor-bearing mice gave equally encouraging results, with promise for use in a phase I and II clinical trial (clinicaltrials.gov, NCT04168528)⁴¹⁰.

Labeling of biomolecules with ^{68}Ga requires a specific $^{68}\text{Ge}/^{68}\text{Ga}$ generator. The relatively short half-life of ^{68}Ga ($T_{1/2} < 68 \text{ min}$)⁴¹¹ can result in low resolution PET images. These challenges can perhaps be overcome using ^{18}F for radiolabeling of nanobodies. ^{18}F has a half-life of $\sim 109.8 \text{ min}$ ⁴¹² and

radiolabeling with ^{18}F provides better biodistribution and tumor targeting, as has been shown *in vivo* in PET/CT images of HER2⁺ SKOV3-tumor bearing mice when compared to labeling with ^{68}Ga ⁴¹³. ^{18}F labeling has also been performed on the anti-MMR 3.49 nanobody and resulted in specific visualization of the tumors of 3LL-R tumor-bearing mice³⁷¹.

Imaging of the myeloid compartment within the tumor microenvironment (TME) via PET is considered a desirable goal, as tumors are often infiltrated with myeloid-derived suppressor cells (MDSCs)³¹⁴. Treatment with checkpoint blocking antibodies such as anti-PD-1 and anti-CTLA4 has changed the landscape of tumor therapy^{414,415}, and can likewise affect the distribution of myeloid cells within the tumor^{416–418}. Thus, imaging the myeloid compartment within tumors can aid in understanding responses to cancer immunotherapies³¹⁴. Nanobodies modified for use as PET imaging agents have now been applied to a variety of targets in pre-clinical models, directed against class II MHC (VHH7, VHH4), PD-L1, CTLA-4, fibronectin EIIIB (NJB2), CD8 (X118), CD11b (DC13), CD36 (DC20), and CD45^{314,329,380,387,388,419,420} labeled with ^{18}F , ^{64}Cu , or ^{89}Zr . Several tumor models have thus been examined, including the mouse B16 melanoma, PANC02 pancreatic adenocarcinoma, MC38 colorectal adenocarcinoma, and C3.43 human papillomavirus-induced cancer models. All of these agents visualize tumors by virtue of the fact that myeloid cells and lymphocytes are present in the TME³²⁵.

SPECT with Micro-CT imaging

Single photon emission computed tomography (SPECT) imaging uses gamma-emitting radioisotopes. EGFR-targeting nanobodies 7D12 and 7C12, labeled with $^{99\text{m}}\text{Tc}$, have been used in SPECT and micro-CT applications. Both nanobodies showed clear localization to the tumors of A431 xenograft-bearing mice³³³. SPECT imaging with the $^{99\text{m}}\text{Tc}$ -labeled anti-EGFR nanobody 8B6 also showed good tumor localization in mice bearing DU145 and A431 tumor xenografts³²⁷. When $^{99\text{m}}\text{Tc}$ -2Rs15d was evaluated for tumor accumulation by SPECT and Micro-CT, it showed clear accumulation at the tumor site of HER2⁺ SKOV3 or LS174T xenograft-bearing mice, whereas no tumor localization of $^{99\text{m}}\text{Tc}$ -2Rs15d was observed in tumors of HER2⁻ xenografted mice³²⁸. $^{99\text{m}}\text{Tc}$ -labeled NbCEA5, evaluated by total pinhole SPECT and Micro-CT, showed rapid clearance from the blood and efficient tumor targeting in LS174T xenografted mice⁴²¹. The same held true for the $^{99\text{m}}\text{Tc}$ -labeled anti-MMR nanobody cl1 evaluated for tumor-targeting potential in TS/A and 3LL-R

tumor-bearing mice, imaged using pinhole SPECT and Micro-CT³⁷⁰. For diagnostic purposes, visualization of PD-L1 expression levels in patients can be valuable. SPECT imaging with ^{99m}Tc-labeled anti-PD-L1 nanobodies showed intense and specific uptake in PD-L1-overexpressing tumor models of melanoma and breast cancer in mice³⁷⁷. Moreover, these results were translated for human application in a phase I clinical trial on sixteen patients with non-small cell lung cancer (NSCLC), where an ^{99m}Tc labeled anti-PD-L1 nanobody showed clear visualization of the primary NSCLC tumors and metastases, while presenting favorable biodistribution and limited side-effects³⁷⁹.

NIR fluorescence

The use of isotopically labeled imaging agents has as an obvious drawback the risk of radiation exposure for both patient and physician. Shorter lived isotopes with a high positron yield such as ¹⁸F in principle allow imaging shortly after administration of the ¹⁸F-labeled agent, but this requires that tissue penetration and clearance from the circulation are compatible with visualization of the target of interest. Methods that do not rely on the use of radioisotopes therefore remain attractive alternatives, although these, too, have their limitations. Fluorescence-based methods suffer from absorption of light of the excitation and emission wavelengths by tissue and bodily fluids. Nonetheless, suitably labeled nanobodies have been used in these optical applications.

The HER2-targeting nanobody 11A4 conjugated to a near-infrared fluorophore IRDye 800CW, localized specifically to the tumor site of HER2⁺ SKBR3 xenograft-bearing mice, while maintaining good biodistribution. Near-infrared fluorescence imaging (NIR) has been exploited to enable image-guided surgery for the precise resection of HER2⁺ tumors. In a clinical setting, this NIR-conjugated anti-HER2 nanobody should allow specific non-invasive classification of HER2-positive tumors and more precise surgical tumor resection³³⁶. A similar approach was used to label the EGFR-targeting nanobody 7D12. NIR fluorescence identified OSC-19 tongue tumors. *Ex vivo* fluorescence imaging of histology sections showed localization of the nanobody to cervical lymph node metastases⁴²².

The anti-carbonic anhydrase IX (CAIX) nanobody B9 has been exploited for the same purpose and yielded acceptable images in an orthotopic xenograft mouse model³⁹². Because the tumor microenvironment is often hypoxic and

CAIX is a marker enzyme of hypoxia, this approach should allow its non-invasive visualization. Kijanka et al. conjugated the 11A4 and B9 nanobodies to either IRDye 800CW or IRDye 680RD and injected both simultaneously into MCF10DCIS breast cancer xenograft-bearing mice. The results indicate the possibility of imaging and surgical resection of heterogeneous tumors at improved tumor-to-background ratios³³⁶. Using the 2Rs15d nanobody labeled with IRDye 800CW, NIR fluorescence image-guided surgery aided the precise debulking of ovarian tumors in SKOV3 xenograft-bearing mice⁴²³.

The anti-ARTC2 nanobody S+16a has been conjugated to the fluorescent dye AlexaFluor-680 and was used for *in vivo* NIR imaging and *ex vivo* dissection of ARTC2-positive tumors in mice⁴²⁴. Combined, these examples show that fluorescence-based methods that exploit nanobodies as the targeting moieties have considerable potential, not only in the characterization of the tumor microenvironment, but also as an adjunct to surgery aimed at physical elimination of a tumor. Nevertheless, a study comparing the biodistribution of random and site-specific labeled 2Rs15d nanobodies shows the effect of different conjugation strategies on nanobodies' properties, which should be considered when developing nanobody-based fluorescent imaging agents⁴²⁵.

Ultrasound-based molecular imaging

A wide branch of molecular imaging is ultrasound-based. Microbubbles or nanobubbles can be used as ultrasound contrast agents⁴²⁶. Nanobubbles can have various types of shells (polymers or phospholipids) and cores (gas, liquid, or solid)^{427,428}. They can carry antibodies specific for tumor-associated antigens, aiding in the early diagnosis of different malignancies. The large molecular weight of full-sized antibody-particle complexes results in a limited number of nanobubbles that actually reach the intended target site. Therefore, the use of nanobodies may improve nanobubble performance⁴⁰⁴ as tested with nanobubbles filled with C₃F₈ ultrasound imaging gas and carrying an anti-PSMA nanobody. The modified nanobubble specifically adhered to prostate cancer cells and displayed high specificity in prostate cancer xenograft imaging *in vivo*³⁶⁸.

Several issues must be addressed before nanobodies can be fully implemented for imaging in a clinical setting. Importantly, nanobodies show high renal retention due to reabsorption in the proximal tubules, caused by megalin receptors⁴²⁹. Kidney retention can lead to renal damage, especially when the nanobody is labeled with a radioisotope or equipped with a cytotoxic drug.

Kidney retention also produces a strong signal in several imaging applications, possibly overshadowing the signal of the desired molecular targets when physically close to the kidneys. Several strategies have been pursued to address these issues, such as coadministration of gelofusin or positively charged amino acids, which interact with megalin receptors and thereby reduce kidney retention⁴²⁹. Modification of nanobody imaging agents with PEG can also mitigate this problem, as observed with the anti-CD8 nanobody X118, used to image T cell infiltration into mouse B16 and Panc02 tumors *in vivo* via PET³⁸¹. Lastly, incorporation of a brush border enzyme-cleavable linker, a glycine-lysine dipeptide, between the ¹⁸F-containing moiety and the 2Rs15d nanobody reduced renal activity levels as seen in micro-PET/CT images of SKOV-3 xenograft bearing mice⁴³⁰.

Nanobodies for therapy

Nanobodies as checkpoint blockade therapies

Conventional checkpoint blockade therapies use monoclonal antibodies to bind to immune checkpoints such as PD-1 or CTLA-4 to improve the anti-tumor immune response^{414,415,431,432}. The anti-PD-L1 nanobody KNo35 fused to Fc (KNo35-Fc) induced strong T cell responses and inhibited tumor growth of A375-PD-L1 cells in NOD-SCID mice *in vivo* [78]. The anti-CTLA-4 nanobody H11 alone failed to control B16 tumor growth in mice treated with the GVAX immunotherapy, but when linked to a murine Fc region, H11 resulted in better overall survival than an anti-mouse CTLA-4 monoclonal antibody³⁷⁵. CD47 is an antiphagocytic ligand (the “don’t eat me” signal) exploited by tumors. It does so by blunting antibody-mediated phagocytosis through binding to signal regulatory protein alpha (SIRP α) on phagocytes. The anti-CD47 nanobody A4 alone or in combination with a tumor-specific antibody fails to generate antitumor immunity against syngeneic B16 tumors, but CD47 antagonism substantially improved response rates against B16 tumors when used in combination with PD-L1 blockade³⁹⁵. Interestingly, administration of the A4 nanobody synergized with PD-L1, but not CTLA4 blockade⁴³³.

Nanobody-drug conjugates

Specific tumor-targeted therapies include the use of antibody-drug conjugates (ADCs). ADCs exploit the targeting efficiency of antibodies combined with the action of the cytotoxic payload conjugated to it^{434,435}. This ought to result in specific targeting of the cancer cells, thus alleviating off-target side-effects. The appeal of this approach is reflected by the large

number of clinical trials that use ADCs (registered on clinicaltrials.gov), with almost 40 being completed and over 80 in progress. Popular targets for ADCs are HER2, c-MET, CD30, and PSMA.

Despite evidence for the effectiveness of ADCs, there are drawbacks to the use of monoclonal antibodies in cancer therapy. These include a limited capacity of antibodies to penetrate the tumor due to their relatively large size. Smaller antigen-binding fragments such as Fabs, scFVs, minibodies, and diabodies have therefore attracted attention as a platform for ADCs. Nonetheless, the efficiency of these smaller formats is often limited because of decreased stability, lower affinity, or difficulties in production³¹¹. Nanobodies can overcome most of these challenges, due to their shorter circulatory half-life, increased tissue penetration, stability and ease of production⁴³⁴. Figure 2B shows an overview of the described uses for nanobodies in cancer therapy.

Nanobody-drug conjugates under investigation include a nanobody-albumin nanoparticle (NANAP), which has an albumin core modified on its surface with EGFR-targeting nanobodies conjugated to PEG (EGa1-PEG). The NANAP is loaded with the multikinase inhibitor 1786. When internalized and digested in lysosomes, it causes the intracellular release of the kinase inhibitor and inhibition of proliferation of EGFR-positive 14C squamous head and neck cancer cells³⁴⁵. Furthermore, conjugation of the drug Mertansine (DM1) to an MHC-II targeting nanobody, VHH7, resulted in a reduction in liver metastases in mice engrafted with the Azo lymphoma⁴³⁶. The central role of MDSCs in driving cancer progression has raised interest in their depletion via ADCs for therapeutic benefit. In mice, CD11b is expressed on several myeloid cell types including monocytes, macrophages, and granulocytes, whereas Ly-6C is highly expressed on monocytes with lower levels on granulocytes, while Ly-6G is expressed on granulocytes^{437,438}. Thus, the anti-CD11b nanobody DC13 and Ly-6C/Ly-6G-specific nanobodies (VHH16 and VHH21, respectively) were conjugated to *Pseudomonas* exotoxin A to deplete myeloid cells *in vitro* and *in vivo*³⁸⁶. All conjugates showed cytotoxicity *in vitro*. However, granulocytes were more sensitive than monocytes to Ly-6C/Ly-6G-specific immunotoxins *in vivo* despite similar binding of the nanobody-immunotoxins to each cell type, indicating the need to thoroughly characterize myeloid-specific ADC candidates.

Targeted radionuclide therapy (TRNT)

TRNT is an increasingly prevalent anti-cancer therapy, designed to deliver cytotoxic radiation to cancer cells, with delivery vehicles such as monoclonal antibodies, antibody fragments, or other small molecules equipped with a suitable radioisotope. Targeted delivery should limit exposure of healthy tissue to radiation. TRNT using antibodies has been approved by the FDA for Ibritumomab tiuxetan, a ^{90}Y -labeled CD20-targeting monoclonal antibody for radioimmunotherapy of non-Hodgkin's lymphoma⁴³⁹⁻⁴⁴¹, and the similar ^{131}I -tositumomab⁴⁴². Furthermore, promising results in early clinical trials have been obtained for antibodies specific for CD33^{443,444}, or preclinical results for a combination of CD20 and CD22 targeting antibodies^{445,446}. Nevertheless, the targeting of (large) solid tumors remains a challenge, as shown in trials with antibodies specific for MUC1⁴⁴⁷, CEA⁴⁴⁸⁻⁴⁵⁰, and CEA⁴⁵¹. Because the poor penetration of labeled antibodies into solid tumor tissue is to a large extent due to their size, smaller labeled molecules such as peptides and nanobodies, have been explored as alternatives for TRNT, especially for the treatment of solid tumors.

D'Huyvetter et al. were the first to use a nanobody for TRNT, in a study with mice bearing HER2⁺ SKOV3 xenografts treated with the ^{177}Lu -DTPA-2Rs15d nanobody. The treated mice showed an almost complete arrest in tumor growth and significantly longer disease-free survival compared to the control group, while no evidence of renal inflammation or necrosis was observed⁴⁵². The same nanobody, labeled with ^{131}I , has been used in a phase I clinical trial with breast cancer patients (NCT02683083)⁴⁵³. The 5F7GGC nanobody, labeled with the residualizing agent *N*-succinimidyl 4-guanidinomethyl 3-^{125/131}I-iodobenzoate (*I-SGMIB), designed to trap radioiodine inside a tumor cell⁴⁵⁴, showed promising results in targeting HER2⁺ cancers with different radioisotopes useful for TRNT⁴⁵⁵.

The promising results with Ibritumomab tiuxetan prompted researchers to repeat this strategy with CD20-specific nanobodies, which should limit the toxicity seen with mAbs in non-targeted tissues. The nanobody 9o79, radiolabeled with ^{177}Lu , showed better disease-free survival when used for treating mice with B16 melanoma compared to controls. More importantly, minimal renal toxicity was seen when mice were treated with ^{177}Lu -DTPA-sdAb 9o79³⁸⁴.

The results of these preclinical studies underscore how the unique characteristics of nanobodies could be leveraged perhaps also in a clinical setting. Further optimization to decrease renal retention is necessary to further reduce any possible adverse effects.

Nanobody-based carrier delivery systems

To increase tumor efficacy and decrease toxicity in non-targeted tissues, it is important to target the delivery of a drug or compound to the tumor. Nanoparticles used as carriers for targeted drug delivery include liposomes, polymeric nanoparticles, micelles, and albumin nanoparticles⁴⁵⁶. Despite their differences in structure and mechanism of action, they all depend on a targeting ligand at the surface of the nanocarrier to achieve adequate specificity.

Conjugation of the anti-EGFR nanobody EGa1 to PEGylated liposomes induced internalization and downregulation of EGFR in 14C cells, both *in vitro* and *in vivo*⁴⁵⁷. When formulated as a polymeric PEGylated micelle, similar receptor binding and internalization were observed, making micelles promising systems for active drug targeting⁴⁵⁸. To this end, EGa1-decorated micelles were loaded with temoporfin (mTHPC), a photosensitizer compound used in the clinic for photodynamic therapy (PDT) of head and neck squamous cell carcinoma (HNSCC). These micelles show prolonged circulation *in vivo* compared to free mTHPC, indicating a potential of these micelles to improve the selectivity and efficacy of PDT in EGFR⁺ tumors⁴⁵⁹. Extracellular vesicles (EV) are also being explored as nanoparticles for therapeutic purposes⁴⁶⁰. To be tumor specific, such EVs must be equipped with a targeting moiety. By anchoring EVs through a glycosyl-phosphatidylinositol (GPI) anchor to the EGa1 nanobody, the engineered EVs showed localization to and internalization in EGFR-expressing cells, but the conditions will require further improvement for pre-clinical use⁴⁶¹.

Tumor vaccination, lentiviral vector-based cancer therapy, and CAR-T cells

Vaccination against cancer would be a valuable prophylactic or therapeutic strategy and would benefit from specifically delivering tumor antigens to APCs. To this end, lentiviral vectors (LVs) have been used to deliver cancer autoimmune antigens to APCs⁴⁶². Antibodies⁴⁶³, and more importantly nanobodies, can be used to specifically deliver these LVs to APCs. LVs displaying the dendritic cell-targeting nanobody DC2.1 exclusively transduce

only DCs and macrophages *in vitro* and *in vivo*⁴⁶⁴. Tropism of human adenovirus serotype 5 (Ad5), which can efficiently transduce human cells, can be altered by capsid modifications that incorporate a nanobody against human CEA (hCEA). These CEA nanobody-expressing Ad5 vectors successfully transduced murine MC38 cells that express hCEA³⁶⁴. In a similar manner, nanobodies can be used to improve the targeting and transduction of adeno-associated viral vectors, as shown by the successful transduction of myeloma cells with AAV1P5 displaying an anti-CD38 nanobody⁴⁶⁵.

Another vaccination strategy focuses on activating cytotoxic CD8⁺ T cells through targeted delivery of cancer antigens to APCs by anti-CD11b nanobodies⁴⁶⁶. This has been explored for HPV⁺ tumors driven by the E6 and E7 genes of the oncogenic HPV type 16 strain. Vaccination based on anti-cd11b nanobodies conjugated to E7-peptide antigens elicited a strong CD8⁺ T cell response *in vivo* and showed slower tumor growth and longer overall survival in an *in vivo* C3.43 cancer model³²⁵. These results highlight a new role for nanobodies in tumor vaccination strategies. In a similar approach, a strong Th1 immune response against the tumor-specific antigen MUC1 was generated by attaching a site-specifically glycosylated MUC1 peptide to the class II MHC-targeting nanobody VHH7⁴²⁰. The enhanced production of antibodies in response to immunization with the nanobody-peptide adduct implied the induction of an adequate CD4 T helper response *in vivo*.

Adoptive cell transfer (ACT) employs a patient's own immune cells to target cancer cells. The T cells are engineered to express a cloned T cell receptor (TCR) or chimeric antigen receptor (CAR) that targets a tumor antigen of interest, the latter allowing for recognition of non-MHC restricted antigens. An ACT strategy using T cells engineered with a CAR comprised of an scFv against mouse VEGFR2 was effective in eliminating several different vascularized syngeneic tumors in mice⁴⁶⁷. Multiple CAR-T cells derived from antibodies or ScFvs are currently under investigation in a clinical setting. Some clinical trials show an immune response directed against the CAR-T cells⁴⁶⁸⁻⁴⁷⁰, presumably due to immunogenicity to the non-human scFv component in the CAR constructs⁴⁷¹. This problem might be solved by using humanized nanobody-based CARs. Albert et al. used their UniCAR system, a unique type of CAR T cell that can be redirected via simultaneously infused target modules (TM), allowing the UniCAR to be switched off in the absence of target modules. The UniCAR decorated with anti-EGFR nanobodies effectively target A431 cells *in vivo*⁴⁷², and showed an even better anti-tumor

responses when formulated as a bivalent α -EGFR-EGFR nanobody-based UniCAR⁴⁷³. A VEGFR2-nanobody specific CAR showed promising results *in vitro*, with high concentrations of secreted IL-2 and IFN- γ by the CAR T-cells, as well as a cytotoxic activity measured by an LDH release assay in response to the VEGFR2 antigen on target cells⁴⁷⁴. Bispecific CAR-T cells that target two antigens simultaneously might be effective to counteract potential antigen-escape in tumor cells. *In vitro* experiments show the great potential of a bispecific anti-CD20 and anti-HER2 nanobody-based CAR, which targets and kills Jurkat cells expressing either one or both antigens⁴⁷⁵. Targeting the TME rather than the tumor directly can be beneficial for targeting multiple tumor types. Anti-PD-L1-nanobody based CAR-T cells slow tumor growth rates *in vivo* in B16 and MC38 models. CAR-T cells based on a nanobody against the fibronectin splice variant EIIIB, which is exclusively expressed on tumor stroma and in the neovasculature, as found around tumors, significantly slowed B16 melanoma growth *in vivo*⁴⁷⁶. The anti-tumor efficacy of the EIIIB-nanobody CAR-T cells was improved in cells that simultaneously secreted nanobodies against PD-L1 or CTLA4, and their systemic cytotoxicity was reduced by secretion of a CD47 nanobody by the CAR T cells⁴⁷⁷. Because the sequence of the EIIIB splice variant is identical for mouse and man, there may be a future for the clinical use of human CAR T cells equipped with this nanobody as a recognition module.

These examples primarily focus on engineering the patient's autologous T cells. However, selecting non-malignant T cells is difficult for patients with T cell-specific cancer such as T-ALL. To overcome this problem, CAR-NK cells can be used. An anti-CD7 nanobody-based CAR on NK cells showed an inhibitory effect on tumor cells in a PDX mouse model²¹⁰. Bispecific anti-CD38 nanobody-based CAR-NK cells effectively deplete CD38⁺ cells from patient-derived multiple myeloma bone marrow cells *in vitro*⁴⁷⁸. Nanobody-based CAR-T cell therapy is now being pursued in clinical trials for CD19/CD20 bispecific targeting in patients with B Cell lymphoma (NCT03881761) and BCMA targeting in multiple myeloma (NCT03664661).

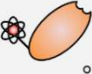
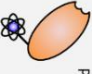

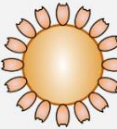
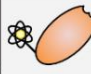
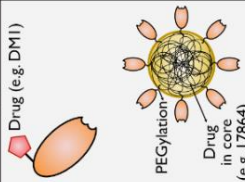
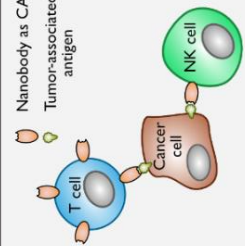
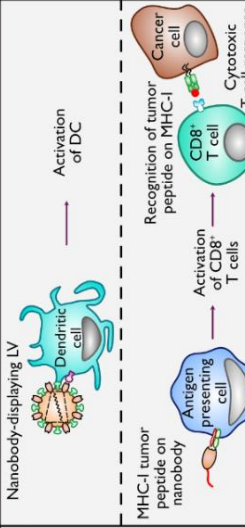
Diagnosis				
A	Positron emission tomography	Single photon emission computed tomography	Near-infrared fluorescence imaging	Ultrasound-based molecular imaging
	 <p>Nanobody labeled with ^{68}Ga, ^{89}Zr, ^{64}Cu, or ^{18}F</p> <p>Advantages:</p> <ul style="list-style-type: none"> - High tumor-background ratio - Imaging of tumors and tumor microenvironment - Limited side effects - Favorable biodistribution <p>Drawbacks:</p> <ul style="list-style-type: none"> - Short isotope half-life - Renal retention - Requires radioactive material 	 <p>Nanobody labeled with $^{99\text{m}}\text{Tc}$</p> <p>Advantages:</p> <ul style="list-style-type: none"> - Rapid clearance from blood - Imaging of tumors and tumor microenvironment - Limited side effects - Favorable biodistribution <p>Drawbacks:</p> <ul style="list-style-type: none"> - Short isotope half-life - Renal retention - Requires radioactive material 	 <p>Nanobody conjugated to IRDye 800CW or IRDye 680CW</p> <p>Advantages:</p> <ul style="list-style-type: none"> - No radioactivity - Imaging for precise surgical resection <p>Drawbacks:</p> <ul style="list-style-type: none"> - Different strategies for Nb labeling have effect on biodistribution 	 <p>Shell: polymers or phospholipids, targeting nanobodies Core: ultrasound imaging gas</p> <p>Advantages:</p> <ul style="list-style-type: none"> - No labeling with radioisotope or fluorescent marker <p>Drawbacks:</p> <ul style="list-style-type: none"> - Large in size, may limit biodistribution
Therapy				
B	Radionuclide therapy	Nanobody-drug conjugates	CAR-(T/NK) cell therapy	Anti-tumor vaccination
	 <p>Nanobody labeled with ^{177}Lu or ^{131}I</p> <p>Advantages:</p> <ul style="list-style-type: none"> - Specific targeting of tumors; less side-effects - Treatment of solid tumors <p>Drawbacks:</p> <ul style="list-style-type: none"> - Renal toxicity from radioactive material 	 <p>Drug (e.g. DM1)</p> <p>PEGylation/Drug in core (e.g. 17864)</p>	 <p>Nanobody as CAR Tumor-associated antigen</p>	 <p>Nanobody-displaying LV</p> <p>Activation of DC</p> <p>MHC-I tumor peptide on nanobody</p> <p>Recognition of tumor peptide on MHC-I</p> <p>Activation of CD8⁺ T cell</p> <p>Cytotoxic T cell response</p>

Figure 2. Overview of the applications of nanobodies in cancer diagnosis and therapy. (A) Nanobodies have been successful in diagnosis through molecular imaging techniques such as PET, SPECT, NIR, and ultrasound-based molecular imaging. (B) Nanobodies can be used in a variety of tumor therapies, such as targeted radionuclide therapy, nanobody-drug conjugates, adoptive cell transfer, and vaccination.

Conclusions

Research has illuminated a valuable role for nanobodies in cancer diagnostics and therapy. Their biophysical properties are fundamentally distinct from those of their conventional two-chain counterparts. The small size, antigen specificity, binding affinity, and stability of nanobodies allows successful targeting of antigens in the tumor, the tumor microenvironment and of the immune cells that are recruited there. Nanobodies are increasingly being used as a diagnostic tool in molecular imaging techniques such as PET, SPECT and NIR fluorescence imaging, as evidenced also by successful early clinical trials. As therapeutic agents, nanobodies can aid delivery of drugs or radioisotopes and can be used for tumor vaccination strategies and CAR-T cell therapy. The full range of possible applications of nanobodies has yet to be explored, but as a complement or an alternative to conventional immunoglobulins: nanobodies are here to stay.

Target	Disease examples	Origin	Model system tested	Nanobody name	Refs
ARTC2		<u>Murine</u> (ART2.2 in <i>Llama matahari</i>)	CD38 KO mice	S+16a	479
CAIX	Breast Cancer (ductal carcinoma)	rCAIX in <i>Camelus dromedarius</i>	PC3 and HeLa cell lines	K24	480
		<u>Human</u> (HeLa cells in <i>Llama glama</i>)	DCIS and CAIX xenograft-bearing SCID/beige mice	B9	481
CapG	Breast Cancer TNBC, melanoma, PDAC	<u>Human</u> (Recombinant CapG in <i>Llama glama</i>)	MDA-MB-231 cells, MDA-MB-231 cells in nude mice	CAPNb2	482
CD11b	Innate immune cell marker	Murine (BMDC in <i>Llama glama</i>)	BMDC and macrophage cell lines	V36, 76, 51, 81, Bio and 42	483
			HPV E7 xenograft bearing mice	VHH _{CD11b} (also known as VHH _{DC13})	484
CD20	B16 melanoma Melanoma, lung cancer, breast cancer	<u>Human</u> (hCD20-encoding plasmid and hCD20pos cells in <i>Llama glama</i>)	hCD20 _{pos} B16 xenograft-bearing mice	9077, 9079	485
CD33	AML	rCD33 in <i>Llama glama</i>	THP-1 tumor xenograft-bearing mice	Nb_7, Nb_21, Nb_22	486
CD38	Multiple myeloma	<u>Human</u> (rCD38 ectodomain, C-terminal domain, or cDNA expression vector for full-length CD38 in <i>Llama glama</i>)	LP-1, OPM2 and RPMI8226 myeloma cell lines, Primary malignant plasma cells	MU375, MU1053, MU551	487
			Human CD38-expressing DC27.10 cells in nude mice	WF211, MU1067, JK36, JK2, MU523, WF14 and MU738	488
CD45		<u>Mouse</u> (Mouse BDMC cells in <i>Llama glama</i>)	<i>In vitro</i> assays	G7 and 32b	483
CD47	AML, NHL, gastric, ovarian,	<u>Mouse</u> (Ig-like V-type	Tubo-EGFR mouse breast	A4	489

	colon and hepatocellular cancer	domain (ECD) of mouse CD47 in alpaca)	cancer cell line, BALB/c BMDMs, B16F10 cells		
			BMDMs and B16F10 xenograft-bearing C57BL/6 mice	A4 fusion to IgG2a Fc (A4Fc)	490
		<u>Human</u> (hCD47(ECD)-Fc in <i>Camelus bactrianus</i>)	Raji cell lymphoma NOG mice, cynomolgus monkeys	HuNb1-IgG4	491
CD7	Leukemia	<u>Human</u> (CD7+ Jurkat cells in <i>Llama glama</i>)	Leukemia cell lines, CEM xenograft-bearing nude mice	VHH6	492
			T-ALL PDX model for humanized VHH6	Humanized VHH6	493
CD8	B16 melanoma, pancreatic cancer	<u>Human and mouse</u> (recombinant mouse CD8αβ heterodimer in alpacas)	C57BL/6 mice with B16 and B16 GVAX, MMTV-PyMT transgenic mouse model, human biopsy tumor sections	VHH-X118	494
CEA	Epithelial cancers (lung, thyroid, pancreas, uterus, breast, ovary, colorectal)	<u>Human and murine</u> (CEA in <i>Camelus dromedarius</i>)	LS174T cells and LS174T xenograft-bearing mice	cAb-CEA5	495
		<u>Human</u> (CEA in <i>Vicugna pacos</i>)	LS174T cells and MC38(CEA) mouse colon cancer cells	JJB-B2	496
			H460 xenograft-bearing nude mice	^{99m} Tc-nanobody	497
c-Met	Brain, liver, pancreatic and gastric cancer, multiple myeloma	<u>Human</u> (c-MET-Fc in <i>Llama glama</i>)	hMSCs	Anti-c-Met nanobody, bispecific	498 Nb patent by Beste et
		<u>Human</u> (A431 cells in <i>Llama glama</i>)	A549 cells, MKN-45 cells	G2	499
CTLA-4	B16 melanoma	<u>Human</u> (CTLA-4 protein in	B16/B6 melanoma cell injected	Nb16	500

		<i>Camelus dromedarius</i>)	C57BL/6 mice		
		<u>Murine</u> (CTLA-4 ECD fused to Fc domain in <i>alpaca</i>)		H11	501
CXCL11	Pre-B lymphoma	<u>Human</u> (Chemokine mixture in <i>Llama glama</i>)	HEK293T cells	11B1, 11B7	502
CXCL12				12A4	
CXCR2	Acute and chronic inflammatory diseases, cancer metastases	<u>Human</u> (CXCR2-expressing cells or pVAX1-hCXCR2 DNA in <i>Llama glama</i>)	CHO-CXCR2 cells	127D1, 163E3	503
CXCR4	HIV-1, tumor growth and metastasis, WHIM syndrome	<u>Human</u> (CXCR4-expressing HEK293T cells in <i>Llama glama</i>) 90% sequence identity with murine ortholog	Cynomolgus monkeys	238D2 and 238D4 (mono- and biparatopic)	504
			HEK293T and CXCR4-R334X overexpressing K652 cell lines	10A10	505
		<u>Human</u> (CXCR4-expressing lipoparticles in <i>Llama glama</i>)	SUP-T1 and Jurkat cells	VUN400, VUN401, VUN402	506
CXCR7	Head and neck cancer	<u>Human</u> (CXCR7-expressing HEK293 cells or pVAX1-CXCR7DNA in <i>Llama glama</i>)	22A xenograft-bearing nude mice	NB1, NB2, NB3, NB4, NB5 (mono- and biparatopic)	507
EGFR	Epithelial cancers	<u>Human</u> (EGFRvIII peptide in <i>Camelus bactrianus</i>)	Ascites fluid of NSCLC	OR1-83, OR2-83	508
		<u>Human</u> (A431 cells in <i>Llama glama</i>)	Murine xenograft models	Ia1, IIIa3, L2-3.40, 9G8	509
				EGa1	510
				8B6	511

				aEGFR- aEGFR-aAlb	512
				7C12, 7D12	513
				CONAN-1 (7D12-9G8- Alb1)	514
				OA-cb6	515
				OR1-83, OR2- 83	508
Fibro- nectin (EIIIB)	Mammary carcinoma	Mixture of ECM proteins, domains and peptides in <i>alpaca</i>	LM2 xenografts in NSG mice	NJB2	516
HER2	Breast cancer	<u>Human</u> (HER2- Fc recombinant fusion protein in <i>Camelus dromedarius</i>)	HER2+ SKOV3 tumor bearing mice	2Rs15d, 1R136d	517,518
		<u>Human</u> (MCF7 or BT474 cells in <i>Llama glama</i>)	SKBR3 xenograft- bearing mice	11A4	519
		<u>Human</u> (SKBR3 cells in <i>Llama glama</i>)	BT474M1 xenograft-bearing mice	5F7GGC	520
HGF	Glioma	<u>Human</u> (HGF in <i>Llama glama</i>)	U87 MG xenograft-bearing mice	1E2-Alb8, 6E10-Alb8	521
Ly-6C/ Ly-6G	Myeloid cells in immune diseases and cancer	<u>Mouse</u> (mouse splenocytes in <i>alpaca</i>)	NUP98/HOXB4 cells and C57BL/6j mice	VHH16, VHH21	522
MHC-II	Pancreatic cancer	<u>Murine</u> (murine splenocytes in <i>alpaca</i>)	panco2-tumors in C57/BL6 mice	VHH7, VHHDC8, and VHHDC15	523
	Graft versus Host Disease	<u>Human</u> (Purified HLA antigen in <i>Vicugna pacos</i>)	Xenograft model of GvHD	VHH4	524
MMR	TAMs infiltrating tumors	<u>Human</u> (MMR EC in <i>Vicugna pacos</i>)	TS/A and 3LL-R tumor-bearing mice	Nb cl1	525
		<u>Human</u> and <u>murine</u> (recomb. Monomeric		3-49	526

		fusion proteins in <i>Vicugna pacos</i>)			
PD-L1	NSCLC, colon, thyroid, uterus, pancreas, and ovary cancer	<u>Human</u> (PD-L1 Fc fusion protein in <i>Camelus bactrianus</i>)	PD-L1 ⁺ A375 cells + hPBMCs xenograft-bearing nude mice	KN035	527
		<u>Murine</u> (RAW264.7 cells in <i>Camelus dromedarius</i>)	TC-1 (WT and PD-L1 KO) in WT or PD-L1 KO mice	C3, E2	528
		<u>Human</u> (PD-L1-Fc protein in <i>alpaca</i>)	PD-L1 ⁺ MCF7 and 624-MEL xenograft-bearing nude mice	K2	529
		<u>Human</u> clinical trial	Human NSCLC patients	NM-01	530
PSMA	Prostate cancer	<u>Human</u> (Purified PSMA antigen in <i>Camelus dromedarius</i>)	<i>In vitro</i> binding predictions	C9, C24, N14, N50	531
		<u>Human</u> (rPSMA in <i>Camelus bactrianus</i>)	LNcaP and PC3 cells	C3	532
		<u>Human</u> (LNCaP cells, PSMA peptide, rPSMA EC in <i>Camelus dromedarius</i>)	PC-3 and LNCaP xenograft-bearing nude mice	PSMA30	533
		<u>Human</u> (4 different PCa cell lines in <i>Llama glama</i>)	PC-310 and PC-3 xenograft-bearing NMRI mice	JVZ-007	534
			LNcaP, C4-2 or MKN45 xenograft bearing BALB/c-nu nude mice		535
TNFα	Sarcomas, melanomas, carcinomas	DNA sequences encoding the camelidae antihuman TNF α single-domain)	MCF-7, T-47D and MDA-MB-231 cell lines, 4T-1 breast cancer mouse model	anti-TNF-VHH	536

TUFM	Glioblastoma	<u>Human</u> (GBM stem-like cells in <i>Alpaca</i>)	Several GBM cell lines and tissues	Nb206	537
VEGF/VEGFR	Angiogenesis in solid tumors	<u>Human</u> (293KDR cells in <i>Camelus dromedarius</i>)	HUVEC cells	3VGR19	538
		<u>Human</u> (VEGF ₁₂₁ in <i>Camelus dromedarius</i>)		Nb22, Nb23, Nb35, Nb42; Humanized Nb42	539,540
		<u>Human</u> sdAb from HuSdI™		NTV1	541
			Chorioallantoic membrane	VA12	542
Viral GPCR US28	Glioblastoma	pVAX1-US28 DNA boosted with HEK293T-US28 expressing cells in <i>Llama glama</i>	U251 cells, intracranial GBM mouse model	(bivalent) US28 nanobody	543
		pcDEF3 vector encoding for VHL/E US28 in <i>Llama glama</i>	U251 cells	VUN100	544
			<i>In silico</i>	Nb7	545

Table 1. Currently available nanobodies for tumor-relevant targets.

Outline of this thesis

In this thesis, we describe the targeting of tumor-specific proteins for cancer diagnosis and therapy. The thesis is divided into two parts.

Part 1, chapter 3 goes into detail on the establishment and characterization of nanobodies targeting MICA. These nanobodies, VHH-A1 and VHH-H3, show specific recognition of the most common alleles of MICA on cancer cells (MICA*008 and MICA*009). Therapeutically, we produced a nanobody-drug conjugate (NDC) by fusion of VHH-A1 to the Mertansine derivative molecule DM1. We treated the T-cell lymphoma cell line “EL-4” - stably transfected to express MICA - with the NDC in an *in vitro* model. We see excellent cytotoxicity of MICA⁺ cells compared to WT cells, with a clear reduction in IC₅₀ and specific targeting of MICA⁺ cells. In **chapter 4**, we describe unpublished data on the nanobody-drug conjugate used for the *in vivo* treatment of EL-4 MICA⁺ tumors. Although the *in vitro* results of the DM1-based nanobody-drug conjugate showed promising results, we did not observe significant reduction in tumor growth in EL-4 MICA⁺ tumor-bearing mice treated with intraperitoneal VHH-A1 nanobody-drug conjugate. In **chapter 5**, we describe the construction of a chimeric antigen receptor (CAR), using VHH-A1 and VHH-H3 nanobodies as the targeting domains. We expressed the construct in human NK-92 cells. We confirmed the localization of the VHH-A1-based CAR NK cells to MICA⁺ tumors in a lung metastases model with PET imaging, using a ⁸⁹Zr-labeled nanobody targeting the transferrin receptor on the surface of the NK cells. Therapeutically, we confirm the ability of these CAR NK-92 cells to kill MICA⁺ cancer cells *in vitro* on MICA⁺ EL-4 and B16F10 melanoma cells, and *in vivo* on MICA⁺ B16F10 tumors. In **chapter 6**, we describe unpublished data on the production of nanobody-based CAR T cells, and their use in *in vitro* cytotoxicity experiments. We confirmed specific cytotoxicity of MICA⁺ B16F10 and EL-4 cells when co-cultured with VHH-based CAR T cells.

Part 2, chapter 7 goes into detail on the establishment and characterization of a monoclonal antibody which recognizes a unique 13-amino acid epitope in the cytoplasmic tail of HLA-E. The epitope is not found on other human proteins. The antibody should thus show no cross-reactivity to other MHC-I molecules, and can be used as antibody-epitope pair with the corresponding epitope. We modified the antibody to contain an LPETG motif (for sortase-

mediated modification) and a (His)₆-tag (to facilitate purification on a NiNTA matrix) on the C-termini of both heavy and light chains. We show that the antibody can be modified by a site-specific and efficient sortase-catalyzed transpeptidation reaction to install fluorophores or biotin. The antibody, either modified or unmodified, can be used for labeling HLA-E intracellularly in flow cytometry, immunofluorescence, immunohistochemistry, and immunoblot. The antibody is thus a great tool for diagnostic purposes, and the antibody-epitope pair can also be used for tagging non-HLA-E specific targets.

In **Chapter 8**, the results of the abovementioned projects are summarized and discussed, and future perspectives are described.



Chapter 3:

MICA-specific nanobodies for diagnosis and immunotherapy of MICA⁺ tumors

Elisha R. Verhaar^{1,2}, Anouk Knoflook¹, Novalia Pishesha¹, Willemijn J.C. van Keizerswaard¹, Xin Liu¹, Kai Wucherpfennig³, Hidde L. Ploegh^{1,2*}

¹Program in Cellular and Molecular Medicine, Boston Children's Hospital, Harvard Medical School, Boston, MA 02115, USA

²Department of Cell and Chemical Biology, Leiden University Medical Centre, Leiden, The Netherlands

³Harvard Medical School, Boston, MA 02215, USA; Department of Cancer Immunology and Virology, Dana-Farber Cancer Institute, 450 Brookline Avenue, Boston, MA 02215, USA

Frontiers in Immunology

2024 March:15

DOI: 10.3389/fimmu.2024.1368586

Abstract

MICA and MICB are Class I MHC-related glycoproteins that are upregulated on the surface of cells in response to stress, for instance due to infection or malignant transformation. MICA/B are ligands for NKG2D, an activating receptor on NK cells, CD8⁺ T cells, and $\gamma\delta$ T cells. Upon engagement of MICA/B with NKG2D, these cytotoxic cells eradicate MICA/B-positive targets. MICA is frequently overexpressed on the surface of cancer cells of epithelial and hematopoietic origin. Here, we created nanobodies that recognize MICA. Nanobodies, or VHHs, are the recombinantly expressed variable regions of camelid heavy chain-only immunoglobulins. They retain the capacity of antigen recognition but are characterized by their stability and ease of production. The nanobodies described here detect surface-disposed MICA on cancer cells *in vitro* by flow cytometry and can be used therapeutically as nanobody-drug conjugates when fused to the Maytansine derivative DM1. The nanobody-DM1 conjugate selectively kills MICA positive tumor cells *in vitro*.

Introduction

The Class I MHC-like molecules MICA and MICB are stress-induced surface glycoproteins, absent from healthy cells but upregulated on virus-infected or malignantly transformed human cells²²⁴. MICA/B are ligands for NKG2D, an activating receptor on NK cells, CD8⁺ T cells, and $\gamma\delta$ T cells²¹⁸. Upon engagement of NKG2D, these cytotoxic cells can eradicate MICA-positive targets, assisted by secretion of cytokines^{219–221}. Elevated levels of MICA/B occur in hematopoietic malignancies, as well as in epithelial solid tumors such as colorectal cancer²²⁵, ovarian cancer²²⁶, cervical cancer²²⁷, breast cancer²²⁸, pancreatic cancer²²⁹, melanoma²³⁰ and cholangiocarcinoma²³¹. MICA/B are thus considered possible targets for immunotherapy.

Nanobodies, a registered trademark, are also referred to as VHHs. They are the smallest immunoglobulin fragments that retain the capacity of antigen binding. They are the recombinantly expressed variable regions of camelid heavy chain-only immunoglobulins³⁰¹. Nanobodies have a short circulatory half-life, are poorly immunogenic, and show excellent tissue penetration compared to conventional full-sized immunoglobulins^{312,313}. Many nanobodies do not require disulfide bonds for their stability, nor do they depend on glycosylation for expression. They are therefore easily and affordably produced in prokaryotic cells^{309–311}.

Nanobodies have proven valuable as the point of departure for the construction of PET imaging agents^{314,329,380,387,388,419,420}, nanobody-drug conjugates^{315,386,436}, and chimeric antigen receptors in cell-based therapies^{210,474–478,546–551}.

Because MICA is expressed on stressed and cancerous cells, the ability to detect such aberrations *in vivo* would be an important diagnostic tool to detect premalignant and malignant lesions. Here, we report the generation of nanobodies that recognize MICA, and apply these nanobodies to detect surface-bound MICA *in vitro* by flow cytometry. Fused to the microtubule inhibitor Maytansine (DM1), these nanobodies can be used therapeutically as nanobody-drug conjugates.

Materials and methods

Alpaca immunization and phage library construction

We immunized an alpaca with 250 µg of the purified extracellular portion of MICA*009 (obtained by baculovirus expression in the lab of K.W. Wucherpfennig²⁴²) comprising the α_1 , α_2 , and α_3 domains in alum adjuvant, followed by 3 booster injections at 2-week intervals. Immunizations were carried out by Camelid Immunogenics. The immune response of the animal was checked by immunoblot (Supplementary figure 1). Briefly, 1 µg of antigen was resolved by SDS PAGE and transferred to a PVDF membrane. The membrane was incubated with at 1:5000 dilution of alpaca serum collected 2 weeks after the last boost. HRP-linked goat-anti-llama (0.05 µg/mL; Bethyl, NC9656984) was used as the secondary antibody. Membranes were developed with ECL Western Lightning Plus. Mononuclear cells from peripheral blood of the immunized alpaca were isolated by Ficoll gradient separation. The VHH library was generated according to an established protocol (Maas et al., 2007). Briefly, RNA was extracted (RNeasy RNA purification kit, Qiagen) and cDNA was prepared (Superscript III first-strand synthesis system, Invitrogen). The DNA sequences from conventional and heavy-chain only Ig genes are not distinguishable based on the use of specific primers, but two distinct hinge regions are generated between the VHH domain and the CH₂ region. We amplified the VHH repertoire from the alpaca using VHH-specific primers that target these hinge sequences (Supplementary table 1). We pooled the VHH PCR products and ligated them into a phagemid vector in-frame with the pIII gene of the M13 phagemid to construct a phagemid library display. We performed two rounds of panning against MICA*009 immobilized on an ELISA plate, following previously described protocols⁵⁵².

Production of recombinant VHHs and sortase reactions

DNA from positive clones was sequenced and 9 clones were selected for further characterization. The relevant VHH sequences were subcloned into a pHEN6 expression vector with C-terminal modifications, so that each nanobody sequence included an LPETG motif recognized by sortase A, followed by a (His)₆-tag to facilitate recovery and purification. Briefly, VHH sequences were amplified from the phagemid vector by PCR (primers in supplementary table 1) and the pHEN6 vector was linearized using the NcoI and BstEII restriction enzymes. Gibson assembly was performed following manufacturer's directions (Gibson Assembly[®] Master Mix, NEB). Positive VHH clones were expressed in WK6 *E. coli* in terrific broth and periplasmic protein expression was activated by induction with isopropyl β-D-thiogalactopyranoside (1 mM) at an OD₆₀₀ of 0.6. VHHs were harvested from the periplasm by osmotic shock. The C-terminal (His)₆-tag allows purification of the recombinant proteins using Ni-NTA agarose beads (Qiagen), followed by FPLC purification on an S75 column by FPLC (ÄKTA, Cytiva Life Sciences). Sortase reactions were performed by incubating each nanobody with a 10-fold molar excess of GGG-nucleophile in the presence of 25 μM Sortase 7M⁵⁵³ overnight at 4°C. Because the LPETG sequence is cleaved during transpeptidation, the (His)₆-tag immediately C-terminal of the LPETG motif is lost. This allows enrichment of the desired modified product by depletion of His-tagged sortase and unreacted nanobody on a NiNTA matrix, while the unbound fraction contains the modified nanobody.

Competitive ELISA and estimation of binding affinity

An ELISA was performed to determine the concentration at which each biotinylated nanobody showed ~80% binding to recombinant MICA*009 (5 mg/mL) immobilized on an ELISA plate. Biotinylated nanobody at a concentration that yielded 80% of the maximum attainable binding value was then mixed with a 500-fold excess of unlabeled competitor nanobody and allowed to compete for binding to 5 μg/mL MICA*009 coated on an ELISA plate. Plates were incubated with streptavidin-HRP (0.00025 μg/mL) for 45-60 minutes at room temperature. After addition of TMB substrate, absorbance was read out at 450 nm on a Spectramax iD5 plate reader (Molecular Devices). If the unlabeled nanobody binds to an epitope distinct from that recognized by the biotinylated nanobody, no diminution of the signal at 450 nm is expected. Nanobodies that recognize the same epitope as that seen by the biotinylated nanobody will show a reduction in the signal at 450nm.

We estimated the binding affinity of VHH-A1 and VHH-H3 by performing an affinity ELISA as previously described⁵⁵⁴. Briefly, we incubated plates coated with 100µL PBS containing 2.5 µg/mL recombinant MICA*009 or GFP as negative control with biotinylated VHH-A1 and VHH-H3 in various concentrations (10-fold serial dilutions; 0.000001 nM – 1000 nM). Streptavidin-HRP at 0.00025 µg/mL was used as detection agent. After addition of TMB substrate, absorbance was read at 450 nm on a Spectramax iD5 plate reader (Molecular Devices). Binding affinity was estimated by calculating the IC₅₀ obtained from three experimental replicates with each sample added in duplicates. Recombinant MICA*009 was produced by transfection of EXPI-293 cells with pcDNA3.1(+) vector encoding for extracellular MICA*009 containing a C-terminal LPETG sortase motif followed by a His₍₆₎-tag to facilitate recovery and purification on a NiNTA matrix (Supplementary figure 2). EXPI-293 cells were transfected using the ExpiFectamine™ 293 Transfection Kit, according to manufacturer's directions (Gibco).

Cell culture

B16F10 and EL-4 cells and their MICA⁺ transfectants were a gift from the lab of Kai Wucherpfennig. B16F10 cells were cultured in complete DMEM (DMEM with 4.5 g/L glucose, substituted with 10% Fetal Bovine Serum (FBS) and 100 U/mL penicillin/streptomycin). EL-4 cells were cultured in complete RPMI 1640 (RPMI 1640, substituted with 10% FBS and 100 U/mL penicillin/streptomycin). Cells were maintained at optimal densities in a humidified 5% CO₂ incubator at 37°C.

Flow cytometry

EL-4 WT and MICA⁺ cells, or B16F10 WT and MICA⁺ cells, were stained with biotinylated VHH-A1 and VHH-H3 for 30 minutes on ice, washed, and incubated with a cocktail of Streptavidin-conjugated PE at 0.0025 µg/mL (Invitrogen) and 2 µg/mL propidium iodide (Life technologies) for EL-4 or LIVE/DEAD™ Fixable Violet Dead Cell Stain Kit (Invitrogen) for B16F10, both according to manufacturer's directions for 30 minutes on ice. Cells were analyzed on an LSR Fortessa flow cytometer (BD Biosciences). Gating strategies were based on cell lines stained with the appropriate controls, where single cells and live cells were appropriately selected.

VHH-drug conjugate creation and in vitro cytotoxicity assays

VHH-DM1 was produced in a sortase-mediated transpeptidation reaction. Briefly, 500-1000 µg of VHH containing a C-terminal LPETG-motif was mixed with a 10-fold molar excess of GGG-DM1 and incubated with 25 µM Sortase

for 16 hours at 4°C. GGG-DM1 was produced in-house by modifying a GGG-peptide linker to contain a maleimide group and allowing it to react with the thiol group on DM1 (Broadpharm) (Supplementary figure 3A). Unreacted VHH and Sortase, both containing a (His)₆-tag, were depleted by incubation with NiNTA agarose (Qiagen or Promethues). Excess free GGG-DM1 was removed by desalting on a PD-10 desalting column (Cytiva). We plated 4000 cells/well in a 96-well plate and incubated cells with serial 3-fold dilutions of VHH-drug adduct or free DM4 (Broadpharm), a structural analog of DM1 (supplementary figure 3B) at 37°C in a humidified 5% CO₂ atmosphere. After 72 hours, we measured cell viability by CellTiter Glo™ assay according to the manufacturer's directions (Promega). For co-culture experiments, MICA expression was determined after a 72-hour incubation. Each treatment was performed in duplicates. For flow cytometry, the duplicate wells of each condition were combined, and the cell mixture was stained with 0.0006 µg/mL biotinylated anti-human MICA/B antibody (Clone 6D4, Biolegend) for 30 minutes on ice. Cells were washed and incubated with Streptavidin-conjugated PE at 0.0025 µg/mL (Invitrogen) and LIVE/DEAD™ Fixable Violet Dead Cell Stain Kit according to manufacturer's directions (Invitrogen) for 30 minutes on ice. Cells were washed and viability and MICA positivity were determined by flow cytometry on an LSR Fortessa flow cytometer (BD Biosciences).

Statistical analysis

All statistical analysis was performed with GraphPad Prism 8. Flow cytometry data was analyzed with FlowJo (v10.8.1 and v10.9.0).

Results

Alpaca immunization and phage display panning yields MICA-specific nanobodies

We immunized an alpaca with purified recombinant MICA*009 in alum adjuvant, followed by 3 booster injections at 2-week intervals. We checked the immune response of the animal by immunoblot using serum samples collected prior to each boost. Having recorded a positive response after the 3rd boost, construction of a phage display library, followed by screening for MICA-reactive hits, yielded positive clones. DNA from positive clones was sequenced and 9 clones were selected for further characterization. Because nanobodies interact with their antigen mainly via their CDR3 region, and to a lesser extent via the germline-encoded CDR1 and CDR2⁵⁵⁵, we chose clones that were unique in their CDR3. A detailed comparison of the nanobody

clones based on sequence similarity in the framework and CDR regions is described in the caption of Figure 1.

Relevant VHH sequences were subcloned into a pHEN6 expression vector to encode a VHH product with C-terminal modifications, so that each VHH sequence included an LPETG motif at its C-terminus, recognized by sortase A, and a (His)₆-tag to facilitate recovery and purification (Figure 1). This arrangement enables the installation of fluorophores, biotin, and other substituents by a site-specific and efficient sortase-catalyzed transpeptidation reaction⁵⁵³. Because the LPETG sequence is cleaved during transpeptidation, the (His)₆-tag immediately C-terminal of the LPETG motif is lost. This allows enrichment of the desired modified product by depletion of His-tagged sortase and unreacted nanobody on a NiNTA matrix, while the unbound fraction contains the modified nanobody.

	FR1	CDR1	FR2	CDR2	FR3			
D8	QLQLVESGGGLVQPGGSLRLSCAASGFTLDYIAIGWFRQAPGKERE	GVSCI	SSDGSSTYYADSVKGRFTISR	DNAK				
C12	QLQLVESGGGLVQPGGSLRLSCAASGFTLDYIAIGWFRQAPGKERE	GVSCI	SSDGSSTYYADSVKGRFTISR	DNAK				
2A9	QLQLVETGGGLVQPGGSLRLSCAASGFTLDYIAIGWFRQAPGKERE	GVSCI	SSDGSSTYYADSVKGRFTISR	DNAK				
A1	QVQLVESGGGLVQPGGSLRLSCAASGFTLDYIDIGWFRQAPGKERE	GVSCI	SSDGSSTYYADSVKGRFTISR	DNAK				
B11	QVQLVETGGGLVQPGGSLRLSCAASGFTLDYIAIGWFRQAPGKERE	GVSCI	SSDGSSTYYADSVKGRFTISR	DNAK				
2B5	QVQLVETGGGLVQPGGSLRLSCAASGFTLDYIAIGWFRQAPGKERE	GVSCI	SSDGSSTYYADSVKGRFTISR	DNAK				
E9	QVQLVETGGGLVQPGGSLRLSCAASGFTLDYIAIGWFRQAPGKERE	GVSCI	SSDGSSTYYADSVKGRFTISR	DNAK				
2D5	QLQLVETGGGLVQPGGSLRLSCAASGFTLDYIAIGWFRQAPGKERE	GVSCI	SSDGSSTYYADSVKGRFTISR	DNAK				
H3	QVQLVETGGGLVQAGGSLRLSCAASGRTFSSYAMGWFRQAPGKERE	FVAGIS	WSGGSTYYGDSVKGRFTISR	DNAK				
	1	10	20	30	40	50	60	70

	FR3	CDR3	FR4	C-terminal modification			
D8	NTVYLQMNSLKPEDTAVYYCA	---DCLSSWT---	S-----AYLGGGTQVTVSS	GGLPETGGHHHHH			
C12	NTVYLQMNSLKPEDTAVYYCA	---DCLSSWT---	S-----AYLGGGTQVTVSS	GGLPETGGHHHHH			
2A9	NTVYLQMNSLKPEDTAVYYCA	---NCLSSNWS---	S-----GYNGGTQVTVSS	GGLPETGGHHHHH			
A1	NTVYLQMNSLKPEDTAVYYCA	---DCTPKQK---	KT-----EANGGTQVTVSS	GGLPETGGHHHHH			
B11	NTVYLQMNSLKPEDTAVYYCA	---DCLSSWT---	N-----AYLGGGTQVTVSS	GGLPETGGHHHHH			
2B5	NTVYLQMNSLKSED	TA	VYYCA---DCTRQG--RK	-----DYNGGTQVTVSS	GGLPETGGHHHHH		
E9	NTVYLQMNSLKPEDTAVYYCA	---DCLSSNWT---	S-----AYLGGGTQVTVSS	GGLPETGGHHHHH			
2D5	NTVYLQMNSLKPEDTAVYYCA	---DCLSSWT---	G-----AYLGGGTQVTVSS	GGLPETGGHHHHH			
H3	NTVYLLMNSLKPEDTAVYYCA	ADLVR	SYSGSSPSLFQFRNPEDVQDGM	DYVKGTLTVTVSS	GGLPETGGHHHHH		
	80	90	100	110	120	130	140

Figure 1. Alpaca immunization and nanobody panning. After construction of a phage display library and screening for positive clones with plate-based panning, nanobody sequences were determined and 9 unique clones were selected. Neutral amino acid substitutions attributable to somatic hypermutations are underscored. Unique substitutions in framework regions are highlighted in blue and in CDR's are highlighted in red. Nanobodies harboring such mutations are more likely derived from different germline V regions rather than somatic hypermutation. The framework regions of nanobodies D8 and C12 are identical. The alpaca IGHHV-3-3*01 gene is the possible germline version of these nanobodies⁵⁵⁶. The single difference of VHH A1 with D8 and C12 in its framework regions is an L2V substitution. A1 may thus be derived from the same germline V gene as D8 and C12 by a single (somatic) point mutation. LEGEND CONTINUES ON THE NEXT PAGE.

*The framework regions of nanobodies 2A9 and 2D5 are mostly identical to each other, with a single S49A substitution between them. Nanobody E9 has both a D29E and a R45Q substitution, indicating that E9 may be derived from a different V gene. In comparison with the other MICA-specific nanobodies, H3 has the largest number of differences in its framework regions and is clearly derived from a different germline V gene, likely the alpaca IGHHV3-1*01⁵⁵⁶. The CDR1 and CDR2 regions are mostly conserved. The most obvious deviation is a deletion at position 53 in VHH C12, B11, 2A9, 2D5, and E9. The MICA-specific nanobodies have CDR3 regions of 13-16 amino acids, but H3 has a 31-residue CDR3. Except for VHH H3, A1 and 2B5, the remaining CDR3 regions are enriched for the sequence "AxDCLSSxWRx". The VHH sequences were subcloned into the pHen6 expression vector and modified at the C-terminus to contain an LPETG motif and (His)₆ tag.*

Nanobodies recognize recombinant MICA and surface-exposed MICA on cancer cells

To determine whether the isolated MICA-specific nanobodies recognized similar or distinct epitopes on MICA, we performed cross-competition experiments by ELISA. Competition of unlabeled nanobodies with a biotinylated nanobody for binding to MICA showed that this set of nanobodies recognizes two distinct epitopes, one defined by the H3 nanobody and the second by all the other nanobodies. None of the nanobodies compete for binding with the 7C6 monoclonal antibody, an agent that inhibits shedding of MICA²⁴³ (Figure 2A). Typically, not all nanobodies are suitable for use in immunoblotting experiments, but the biotinylated versions of A1 and H3 yielded a strong and specific signal in immunoblots on recombinant MICA (Figure 2b). The binding affinities of VHH-A1 and VHH-H3 are both in the nanomolar range, at ~0.2 and ~0.4 nM for A1 and H3 respectively (Figure 2C), as estimated by ELISA assay. By examining the binding of the A1 and H3 nanobodies to a subset of MICA/B allelic products, available in purified form, we conclude that the A1 and H3 nanobodies recognize the MICA*008 and MICA*009 alleles (Figure 2D) which, combined, cover 51.1% of the Caucasian population⁵⁵⁷. To verify that A1 and H3 also recognize surface-disposed MICA, we used B16F10 transfectants that express MICA*009, and EL-4 transfectants that express MICA*008, with B16F10 and EL-4 wild type cells serving as negative controls. Both A1 and H3 showed excellent staining of the MICA transfectants by flow cytometry and yielded no signal for the untransfected parental cell lines (Figure 2E) with a significant difference determined by mean fluorescence intensity (MFI) (Figure 2F). Gating strategies are shown in supplementary figure 4.

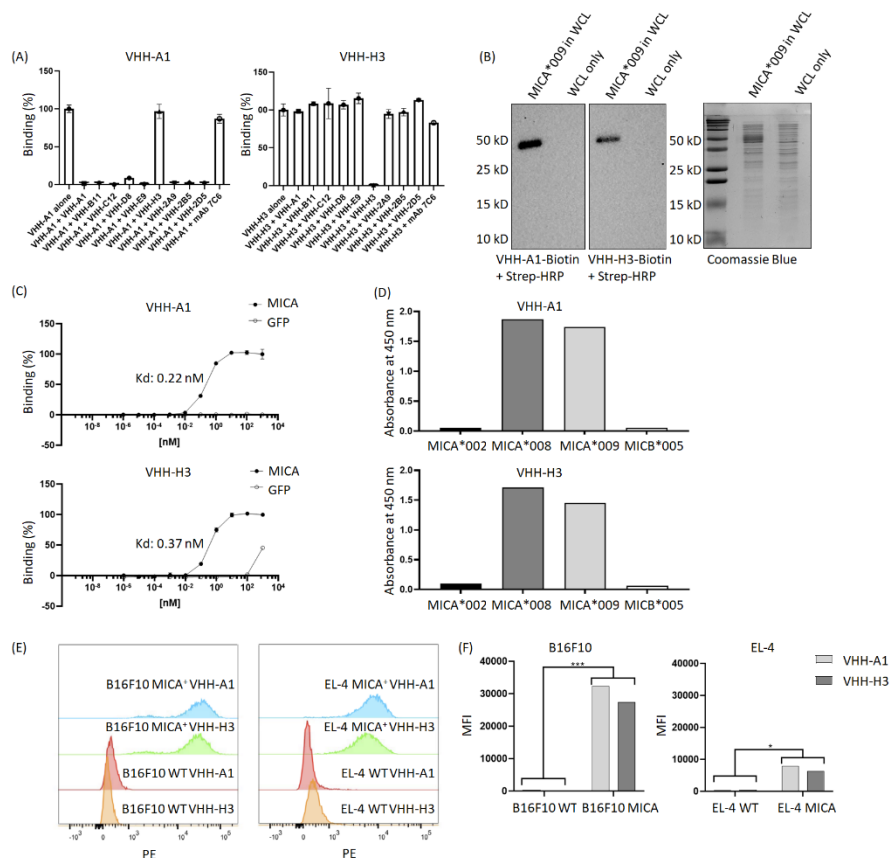


Figure 2. Characterization of MICA-specific VHVs. (A) Cross-competition ELISA shows that VHH-A1 and VHH-H3 recognize distinct epitopes on MICA. Neither VHH cross-competes for binding with the monoclonal antibody 7C6. (B) VHH-A1 and VHH-H3 recognize MICA in immunoblot. 500 ng recombinant MICA*009 in non-specific *E. coli* whole cell lysate (WCL) was separated by SDS-PAGE and transferred to a PVDF membrane. Blots were stained with 1 µg/mL biotinylated VHH-A1 or VHH-H3 respectively. Detection with strep-HRP (0.3 ng/mL) shows a clear signal for both VHVs. (C) Binding affinity as estimated by ELISA coated with 2.5 µg/mL recombinant MICA*009, or GFP as the negative control. Estimated K_d values are 0.22 nM and 0.37 nM for VHH-A1 and VHH-H3 respectively. (D) ELISA coated with different recombinant MICA alleles shows that VHH-A1 and VHH-H3 both recognize MICA*008 and MICA*009. (E) Flow cytometry with biotinylated VHH-A1 and VHH-H3, using streptavidin-conjugated PE as secondary agent, shows a clear signal in the PE channel for MICA⁺ EL-4 and B16F10 cells, but not for the WT cells, indicating recognition of membrane-disposed MICA on the surface of cells by both nanobodies. Gating strategies for flow cytometry are shown in supplementary figure 1. **LEGEND CONTINUES ON THE NEXT PAGE**

(F) We calculated the MFI after flow cytometry. The MFI of B16F10 WT cells was 394 for VHH-A1 and 299 for VHH-H3. The MFI of B16F10 MICA⁺ cells was 23430 for VHH-A1 and 27411 for VHH-H3. The MFI of EL-4 WT was 310 for VHH-A1 and 511 for VHH-H3. MFI of EL-4 MICA⁺ cells was 7955 for VHH-A1 and 6417 for VHH-H3. We averaged the MFI from the WT or MICA⁺ cells and determined a significant difference in nanobody staining of WT versus MICA⁺ cells ($p = 0.00713$ for B16F10; $p = 0.0128$ for EL-4, calculated by multiple T-test).

Anti-MICA nanobodies fused to Maytansine (DM1) for targeted cytotoxicity of MICA⁺ cancer cells

The reactivity of VHH-A1 and VHH-H3 make them appealing candidates for the construction of nanobody-drug conjugates. To test this, we ligated the Maytansine derivative DM1, a microtubule disrupting agent, to VHH-A1 or to a VHH that targets mouse MHC-II (VHH_{MHC-II})⁵⁵⁸ as a negative control via a sortase-mediated transpeptidation reaction (Figure 3A) and confirmed successful ligation with SDS-PAGE (Figure 3B). We performed an in vitro cytotoxicity assay by titration of VHH_{MHC-II}-DM1, VHH_{A1}-DM1, or free DM4 (a functional analog of DM1) on EL-4 WT and MICA⁺ cells. EL-4 MICA⁺ cells were sensitive to VHH_{A1}-DM1, with a stronger cytotoxic effect at lower doses of the VHH-drug conjugate compared to VHH_{MHC-II}-DM1, as estimated by IC₅₀. The IC₅₀ of VHH_{A1}-DM1 treated EL-4 MICA⁺ cells was comparable to that of cells treated with free DM4. Similarly treated WT cells showed no obvious reduction in viability with either nanobody-drug conjugate (Figure 3C).

To further validate selectivity of VHH_{A1}-DM1 for MICA⁺ cells, we co-cultured EL-4 WT and EL-4 MICA⁺ cells at a 1:1 ratio, and added VHH_{MHC-II}-DM1, VHH_{A1}-DM1, or free DM4 at different concentrations. We determined the ratio of viable EL-4 WT and EL-4 MICA⁺ cells after 72 hours by flow cytometry using a live/dead cell stain. We stained the MICA⁺ cells in the co-culture with a biotinylated α MICA mAb, using streptavidin-conjugated PE as secondary reagent. Gating on live cells and MICA⁺ cells showed specific elimination of MICA⁺ cells at adduct concentrations between 1.71 nM and 416 nM for VHH_{A1}-DM1. A difference in ratio between WT and MICA⁺ cells was not observed in cells treated with VHH_{MHC-II}-DM1 or free DM4. Because WT cells proliferate slightly faster than MICA⁺ cells in culture, the distribution shifted to ~65% WT and 35% MICA⁺ cells after 72 hours in culture. Thus, numbers were normalized according to the percentage of cells of either line in the untreated ("0 nM") group (Figure 3D). Gating strategies are shown in supplementary figure 5.

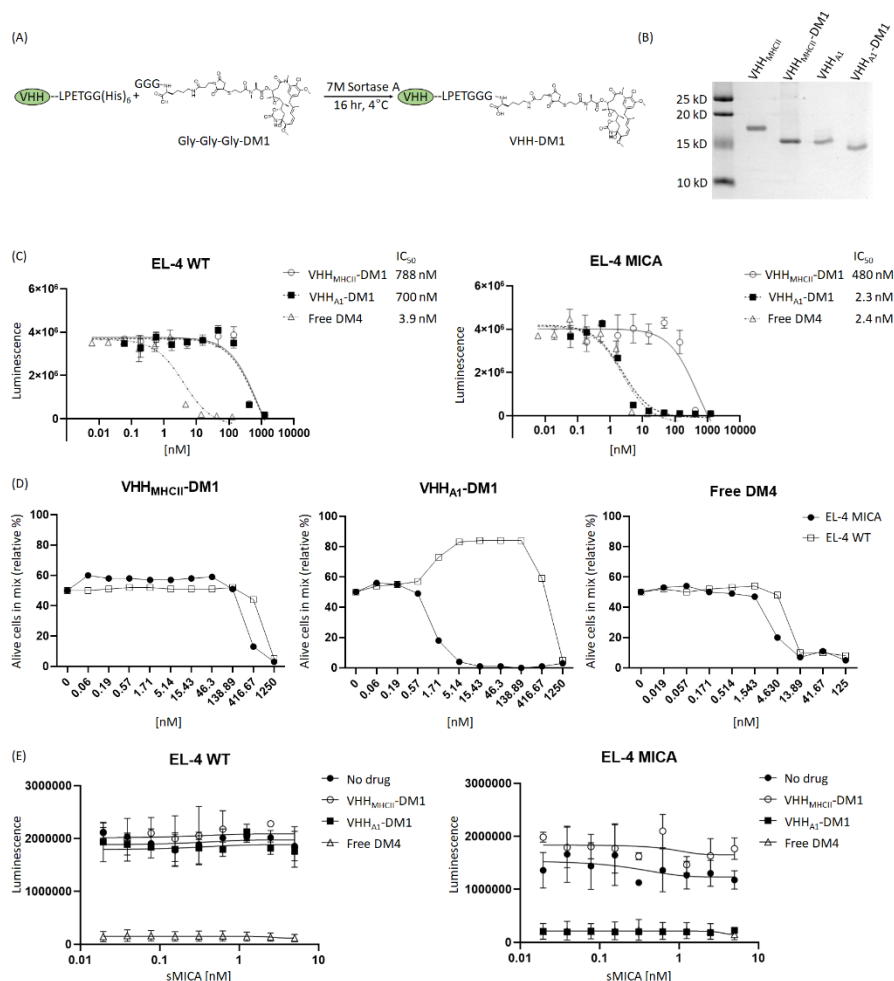


Figure 3. Anti-MICA VHHs as nanobody-drug conjugate with the Maytansine derivative DM1. (A) We ligated the microtubule inhibitor Maytansine GGG-DM1 to VHH-AI or VHH_{MHC-II} as non-targeting control through sortase-mediated transpeptidase reaction. (B) Because GGG-DM1 has a slight positive charge, the modified VHHs will migrate slightly lower on the SDS-PAGE gel compared to the unmodified VHHs. (C) The *in vitro* cytotoxicity assay was performed with limited dilutions of VHH_{MHC-II}-DM1, VHH_{AI}-DM1, or free DM4 on EL-4 WT cells and their MICA⁺ counterparts. After incubation for 72 hours, we measured cell viability by CellTiter Glo™ assay. MICA⁺ cells treated with VHH_{AI}-DM1 showed a significant reduction in IC₅₀, and thus a reduction in viability with smaller amounts of drug added, compared to similarly treated WT cells, or cells treated with the non-targeting VHH_{MHC-II}-DM1. **LEGEND CONTINUES ON THE NEXT PAGE**

(D) We co-cultured EL-4 WT and EL-4 MICA⁺ cells at a 1:1 ratio and added VHH_{MHCII}-DM1, VHH_{A1}-DM1, or free DM4 at different concentrations. Viability of EL-4 WT and MICA⁺ cells was determined using a live/dead cell stain. MICA⁺ cells were stained with a biotinylated anti-MICA mAb, using streptavidin-PE as secondary agent. Gating on live cells and PE showed elimination of MICA⁺ cells at VHH-drug adduct concentrations between 1.71 nM and 416 nM for VHH_{A1}-DM1. A difference in [WT:MICA] was not observed in cells treated with VHH_{MHCII}-DM1 or free DM4. (E) We incubated EL-4 WT and MICA⁺ cells with 2.5 nM of VHH_{MHCII}-DM1, VHH_{A1}-DM1, or free DM4 in the presence of sMICA (two-fold dilutions; 0-5 nM/0-170 ng/mL) for 72 hours. We measured viability by CellTiter Glo™ assay. We did not observe a decreased effect on cytotoxicity of VHH_{A1}-DM1 on MICA⁺ cells with addition of sMICA in the medium.

Tumor cells can downregulate surface expression of MICA through shedding, mediated by proteolytic cleavage at the $\alpha 3$ domain. Increased levels of soluble MICA (sMICA) in the serum of patients are associated with poor prognosis and worse disease progression^{229,233-235}. To address the possible competition of sMICA for binding with the anti-MICA nanobody, we performed an in vitro cytotoxicity assay. EL-4 WT and MICA⁺ cells were incubated with VHH_{MHCII}-DM1, VHH_{A1}-DM1, or free DM4 at a fixed concentration of 2.5 nM, in the presence of sMICA at various concentrations (serial 2-fold dilutions; 0-5 nM/0-170 ng/mL). We observed no reduction in cytotoxicity of VHH_{A1}-DM1 on MICA⁺ cells upon addition of sMICA to the medium (Figure 3E). Publications report concentrations of sMICA in the serum of MICA⁺ patients in the range of 0.1-15 ng/mL⁵⁵⁹⁻⁵⁶¹ which is at least 10-fold lower than the sMICA concentration in our competition assay. We thus expect little to no impact of sMICA in patients' serum on the ability of these nanobodies to target membrane-bound MICA *in vivo*.

Discussion

MICA and MICB are Class I MHC-related proteins expressed on stressed and cancerous cells. Their presence can serve not only as a diagnostic marker but may also be exploited as a target for therapy. While the typical immunoglobulins exert their functional properties through Fc effector functions, their size compromises efficient tissue penetration. Nanobodies offer an appealing alternative to immuno-globulins for the purpose of launching an immune attack on MICA-positive tumors. Nanobodies are characterized by their small size, showing superior tissue penetration compared to intact immunoglobulins, and ease of production and modification^{309,310,312,313}. Lastly, nanobodies are poorly immunogenic, presumably because of their considerable sequence homology with human V_H regions⁵⁵⁶.

Because nanobodies lack an Fc portion, for them to exert cytotoxic activity they require functionalization, for example with a cytotoxic drug creating a nanobody-drug conjugate, as done here for the VHH-DM1 adducts. Compared to antibody-drug conjugates using conventional immunoglobulins, the small size of the nanobody allows superior penetration into tumor tissue. Furthermore, owing to the relatively short circulatory half-life, the nanobody-drug conjugate that is not bound to its target will be eliminated more quickly from the circulation, resulting in less systemic cytotoxicity by slow release of the drug attached to the antibody-drug conjugate.

We produced and characterized in further detail two nanobodies, A1 and H3, that recognize the MICA alleles *008 and *009 with nM affinities. An analysis of the MICA-specific nanobodies shows that they are unique sequences, thus the isolated nanobodies were likely derived from a few different germline V genes (see Figure 1 and legend). The germline sequences of the V genes of the (outbred) alpaca used for immunization are not known. We can only compare the sequences of the MICA-specific nanobodies with each other, and with reference germline sequences from unrelated alpacas.

The alpaca IGHHV-3-3*01 gene is the possible germline version of the D8 and C12 nanobodies⁵⁵⁶. The single difference of VHH A1 with D8 and C12 in its framework regions is an L2V substitution, thus A1 may be derived from the same germline V gene as D8 and C12 by somatic mutation. Nanobody E9 has a D29E and an R45Q substitution, indicating that E9 may be derived from a different V gene. In comparison with the other MICA-specific nanobodies, H3 has the largest number of differences in its framework regions and is clearly derived from a different germline V gene, likely the alpaca IGHHV3-1*01⁵⁵⁶.

Highly similar CDR regions, specifically CDR3, imply recognition of related antigens⁵⁶²⁻⁵⁶⁵. For the MICA-specific nanobodies, the CDR1 and CDR2 regions are mostly conserved. The most obvious deviation in the CDR2 region is a deletion at position 53 in VHH C12, B11, 2A9, 2D5, and E9. Somatic hypermutation can produce deletions and insertions in V genes⁵⁶⁶⁻⁵⁶⁸ but given the overall similarity in framework regions, the use of a distinct V gene that lacks residue 53 is the more plausible explanation. Except for H3, A1 and 2B5, the remaining CDR3 regions are enriched for the sequence "AxDCLSSxWRx".

We show that these nanobodies bind to surface-disposed MICA on cells and can thus be used for diagnostic and therapeutic purposes. The specific targeting of MICA⁺ cells make them suitable candidates as diagnostic markers, as building blocks for nanobody-drug conjugate, or for the

construction of chimeric antigen receptors^{472,475,476,550}. MICA and MICB are highly polymorphic in the human population, with hundreds of alleles for MICA and MICB identified so far^{557,569}. The isolated nanobodies were tested for recognition of the MICA alleles *002, *008 and *009, and MICB allele *005. Of the tested alleles, the nanobodies recognize MICA*008 and MICA*009, which together cover over 50% of the investigated German population⁵⁵⁷. Expanding the nanobody pool to cover a larger portion of the alleles of MICA and MICB should be considered. We recognize the limitations of using a MICA⁺ cell line obtained by transfection. The availability of a suitable patient-derived cell line that expresses the correct alleles of MICA is a limiting factor. We think this is worth exploring in future research.

We created a nanobody-drug conjugate by conjugating the microtubule inhibitor DM1 to VHH-A1. We show increased cytotoxicity of MICA⁺ tumor cells compared to WT tumor cells *in vitro*, with efficacy comparable to that of free drug but with much higher specificity for MICA⁺ cells. The production of these nanobody adducts should be scaled up for testing on *in vivo* tumor models. The creation of different VHH-drug combinations, for example by inclusion of DNA damaging agents or other cytotoxic drugs^{570–572}, or even radiopharmaceuticals for targeted radiotherapy^{573,574}, deserves consideration as well.

Cleavage of the $\alpha 3$ domain involving the disulphide isomerase ERp5 and ADAM-type proteases such as ADAM10 and ADAM17^{232–236}, and thus shedding of the MICA/B from the cancer cell surface, may lead to immune evasion and failure to be recognized by NKG2D-positive cytotoxic cells. The monoclonal antibody 7C6 inhibits the shedding of MICA/B, and thus increases the density of MICA/B proteins on the surface of tumor cells²⁴³. Although we saw no reduction in efficacy of VHH_{A1}-DM1 on MICA⁺ cells upon addition of sMICA to the medium, the combination of anti-MICA nanobody adducts with the 7C6 antibody might therefore be therapeutically more attractive than either treatment alone.

Conflict of Interest

K.W.W. serves on the scientific advisory boards of DEM BioPharma, Solu Therapeutics, D2M Biotherapeutics and Nextechinvest. He is a co-founder of Immunitas Therapeutics and receives sponsored research funding from Novartis and Fate Therapeutics.

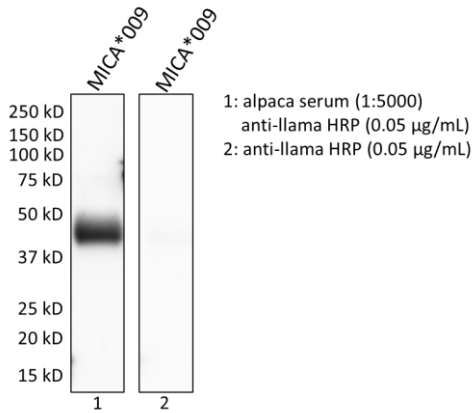
Author Contributions

The authors confirm their contribution to the paper as follows: E.R.V and H.L.P designed the study, supervised data collection. E.R.V., A.K, and W.v.K collected data. N.P. performed alpaca immunizations and produced the nanobody phage library. X.L. produced the GGG-DMi and provided invaluable feedback on nanobody-drug conjugate studies. K.W. provided recombinant MICA proteins and MICA⁺ cell lines. E.R.V. and H.L.P. wrote the paper. All authors reviewed the results and approved the final version of the manuscript.

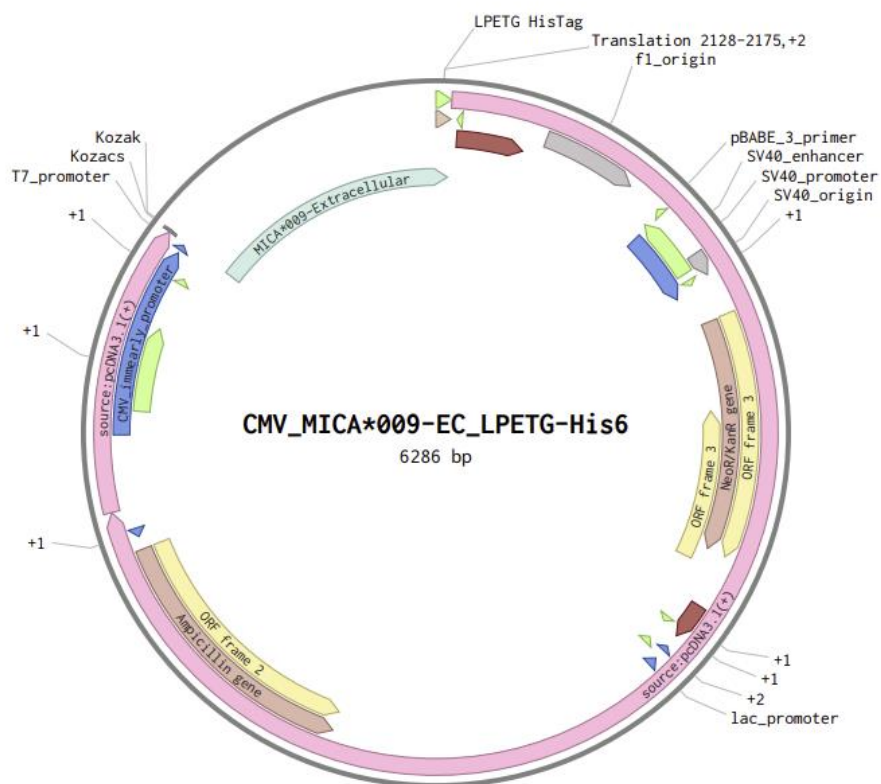
Acknowledgments

This research was supported by the NIH Pioneer Grant (DP1AI150593-05) to H.L.P and an Ro1 from NCI (CA238039) to K.W.W. We gratefully acknowledge Dr. Thomas Balligand for helpful discussions.

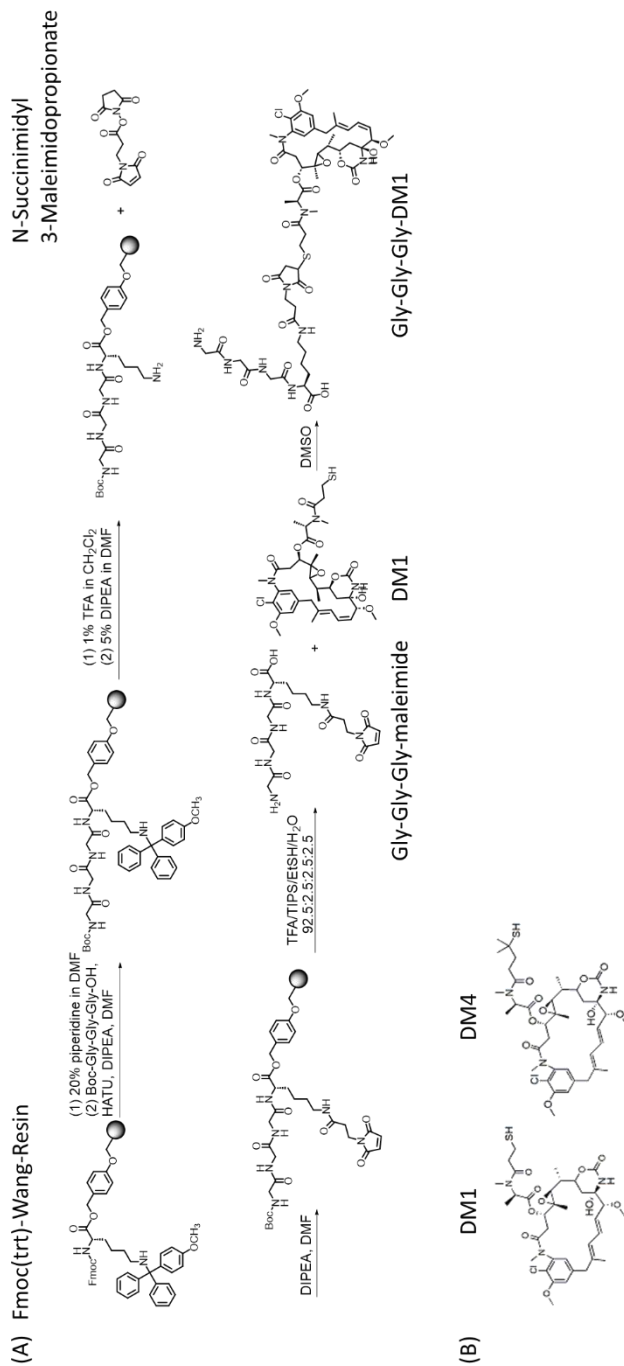
Supplementary figures



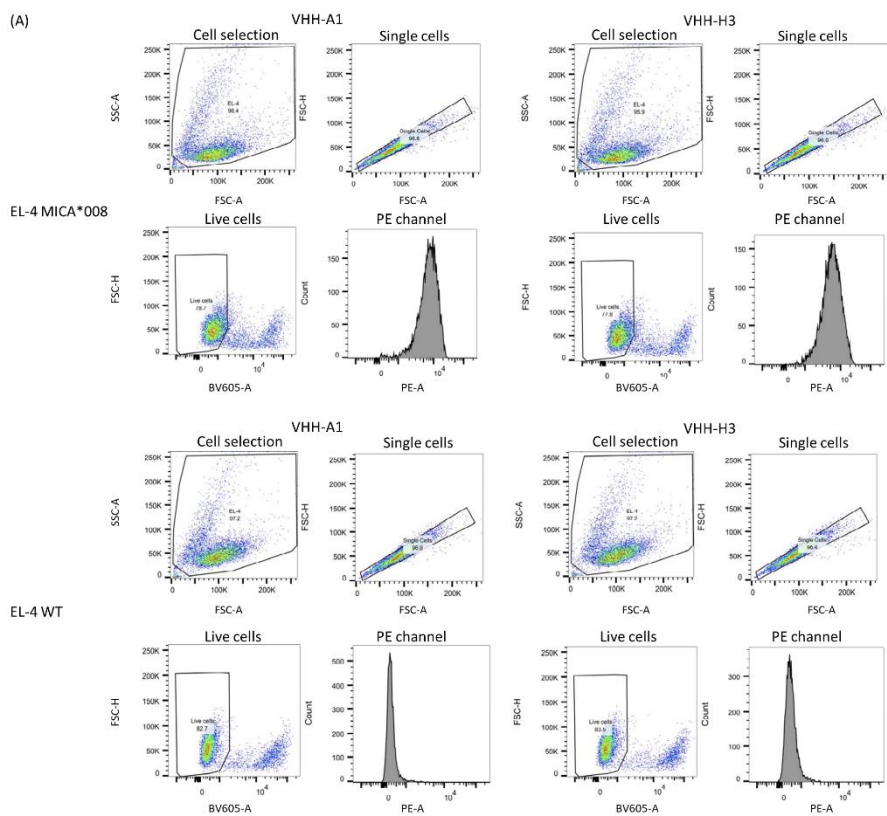
Supplementary figure 1. Immunoblot to determine the immune response of the alpaca after 4 immunizations with recombinant MICA*009. 1 µg of antigen was resolved by SDS PAGE and transferred to a PVDF membrane. The membrane was incubated with at 1:5000 dilution of alpaca serum collected 2 weeks after the last boost. HRP-linked goat-anti-llama (0.05 µg/mL; Bethyl, NC9656984) was used as the secondary antibody. Membranes were developed with ECL Western Lightning Plus. To rule out a non-specific signal from the secondary antibody, a membrane with MICA*009 was incubated with the secondary antibody only and developed under the same conditions.

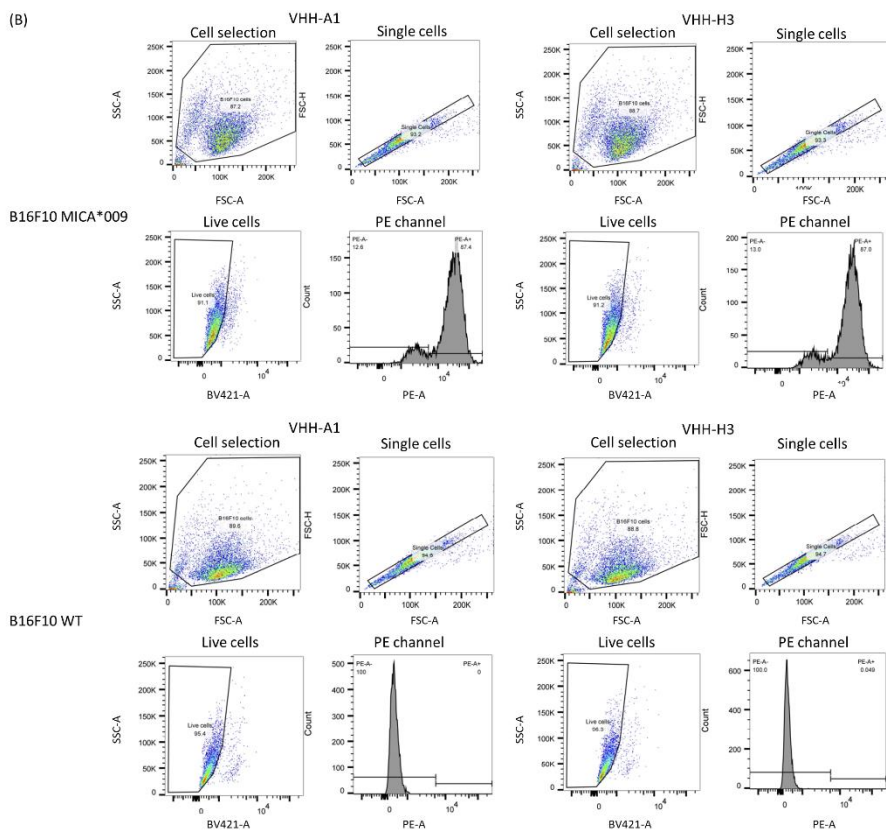


*Supplementary figure 2. pcDNA3.1(+) vector containing the sequence for extracellular, secreted MICA*009-LPETG-His₍₆₎.*

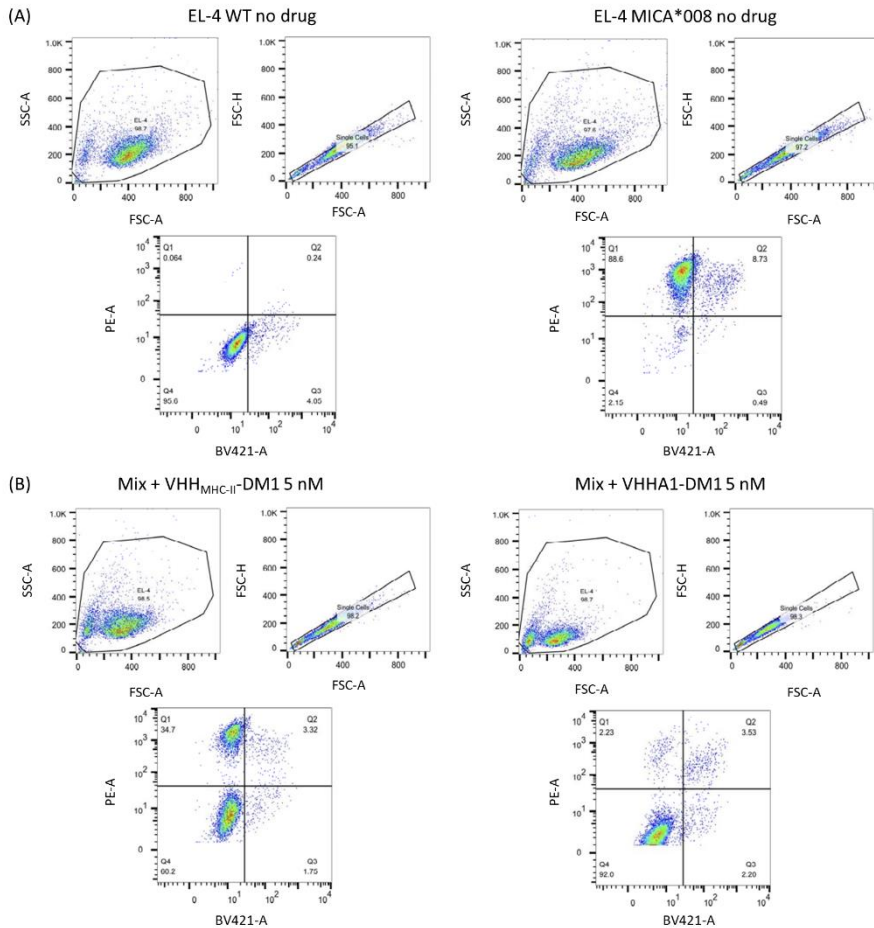


Supplementary figure 3. Chemical synthesis of GGG-DM1. (A) We modified a GGG-peptide linker to contain a maleimide group and allowed it to react with the thiol group of commercially obtained DM1. (B) Chemical structures of unmodified DM1 and DM4.





Supplementary figure 4. Gating strategy to determine VHH-A1 and VHH-H3 binding to surface-disposed MICA on EL-4 (A) and B16F10 (B) cells. Cells were stained with biotinylated VHH-A1 and VHH-H3 (1 $\mu\text{g/mL}$) for 30 minutes on ice, washed, and stained with a cocktail of streptavidin-PE (2.5 $\mu\text{g/mL}$) and propidium iodide (for EL-4) or LIVE/DEAD™ Fixable Violet Dead Cell Stain (for B16F10) for 30 minutes on ice. Cells were washed and analyzed on an LSR Fortessa flow cytometer (BD Biosciences). Gating strategies are shown for cells stained with biotinylated VHH, Streptavidin-PE, and viability dye, but the appropriate negative staining controls were added to determine gates. First all cells were selected based on FSC and SSC. Then, we selected singlets based on FSC-A and FSC-H. We determined viability in the BV605 channel for EL-4 and BV421 channel for B16F10 cells. MICA-staining was determined by signal in the PE channel.



Supplementary figure 5. Gating strategy to determine viability in a mixed population of EL-4 WT and MICA⁺ cells undergoing treatment with nanobody-drug conjugate. Cells were stained with 0.0006 $\mu\text{g/mL}$ biotinylated anti-human MICA/B antibody (Clone 6D4, Biolegend) for 30 minutes on ice. Cells were washed and incubated with Streptavidin-conjugated PE at 0.0025 $\mu\text{g/mL}$ (Invitrogen) and LIVE/DEAD[™] Fixable Violet Dead Cell Stain Kit according to manufacturer's directions (Invitrogen) for 30 minutes on ice. Viability and MICA positivity were determined by flow cytometry. (A) Gating was performed on unmixed EL-4 WT or MICA⁺ cells which were kept in the same culture conditions, without the addition of drug. Cells were deemed viable if they stained negatively in the BV-421 channel. Cells were deemed MICA⁺ if they stained positive in the PE channel (upper left quadrant) or WT if they stained negative in the PE channel (lower left quadrant). (B) Representative gating pattern for mixed EL-4 WT and MICA⁺ cells, here shown for those treated with 5 nM VHH_{MHC-II}-DM1 (left panels) or 5 nM VHH_{A1}-DM1 (right panels). The ratio of WT and MICA⁺ cells were normalized to the relative ratio of untreated WT:MICA⁺ cells.

Target	Usage	Sequence [5' -> 3']
VHH hinge	Library construction (forward primer)	CTTGGGCGCTCAGKTGCAGCTGTGGAGWNGNGG
VHH short hinge	Library construction (reverse primer)	GATCGGGCGCCGAGGGTCTTCGCTGTGTGCG
VHH long hinge	Library construction (reverse primer)	GATCGGGCGCCGGTTGTGCTTTTGGTGTCTTGGG
VHH in phagemid vector	Forward primer for PCR of VHH sequence from phagemid vector	CGCGCCCCAGCCGGCCATGGCCCCAGGTGCAGCTCCAGG
VHH in phagemid vector	Reverse primer for PCR of VHH sequence from phagemid vector	AGTCCTCCTGAGGAGACGGTGACCTGGGTCCCCTGG
LacZ	Sequence validation of VHH insertion into pHEN6 vector	CAGGAAACAGCTATGAC

Supplementary table 1. Primer sequences for creating the VHH phage library, validation of VHH sequences, and Gibson assembly into the pHEN6 vector.

Chapter 4:

MICA-specific nanobody-drug conjugate for in vivo treatment of MICA⁺ EL-4 tumors

Elisha R. Verhaar^{1,2}, Xin Liu¹, Hidde L. Ploegh^{1,2*}

¹Program in Cellular and Molecular Medicine, Boston Children's Hospital,
Harvard Medical School, Boston, MA 02115, USA

²Department of Cell and Chemical Biology, Leiden University Medical Centre,
Leiden, The Netherlands

Unpublished data

Abstract

MICA and MICB are MHC-I related glycoproteins, upregulated on the surface of cells in response to stress, for instance when a cell is infected or malignantly transformed. MICA/B act as ligands for NKG2D, the activating receptor on NK cells, CD8⁺ T cells, and $\gamma\delta$ T cells. Upon engagement of MICA/B with NKG2D, these cytotoxic cells get activated and can eradicate MICA/B-positive targets. We have created nanobodies that specifically target MICA on the surface of cancer cells. We have shown that these nanobodies, when fused to the Maytansine derivative DM1, selectively kill MICA positive EL-4 T cell lymphoma cells *in vitro*. Here, we describe the results of an *in vitro* study in which we treated MICA⁺ B16F10 melanoma cells with nanobody-DM1 adducts. We next performed *in vivo* experiments, attempting treatment of MICA⁺ EL-4 tumor-bearing mice with the MICA nanobody-DM1 conjugate.

Introduction

The MHC Class I-associated glycoproteins MICA and MICB (MICA/B) are upregulated on the surface of human cells under stress, for instance due to viral infection or malignant transformation²²⁴. MICA/B act as ligands for the NKG2D activating receptor found on NK cells, CD8⁺ T cells, and $\gamma\delta$ T cells²¹⁸, engagement of which activates these cytotoxic cells to eradicate MICA/B-positive targets by secretion of granzymes, perforins, and cytokines^{219–221}. High levels of MICA/B are found in hematopoietic malignancies, as well as in many solid tumors of epithelial origin²³⁵. MICA/B are thus considered possible targets for immunotherapy.

Nanobodies, also referred to as VHHs, are the recombinantly expressed variable regions of camelid heavy chain-only immunoglobulins³⁰¹. Nanobodies retain excellent antigen-binding capabilities and are characterized by their small size, short circulatory half-life, and excellent tissue penetration compared to conventional full-sized immunoglobulins^{312,313}. Nanobodies have proven valuable for the construction of nanobody-drug conjugates^{315,386,436}. We have developed nanobodies, VHH A1 and VHH H3, that recognize surface-bound MICA with high affinity. When fused to the microtubule inhibitor Maytansine (DM1), we showed that VHH A1 can be used therapeutically as a nanobody-drug conjugate in an *in vitro* study in which we targeted MICA⁺ EL-4 T cell lymphoma cells⁵⁷⁵. Here, we use the nanobody-drug conjugate to test its *in vitro* cytotoxicity of B16F10 MICA⁺ melanoma cells. Furthermore, we describe the results of an *in vivo* experiment to treat mice bearing MICA⁺ EL-4 primary tumors with the VHH A1-based nanobody drug conjugate.

Materials and methods

Production of recombinant nanobodies and sortase reactions

Nanobody sequences were subcloned into a pHen6 expression vector, including C-terminal modifications of an LPETG motif recognized by Sortase A, and a (His)₆-tag for recovery and purification on a NiNTA matrix⁵⁷⁵. Nanobodies were expressed in WK6 *E.Coli* in terrific broth by periplasmic protein expression, activated with isopropyl β -thiogalactopyroniside (1mM) once an OD₆₀₀ of 0.6 was reached. Nanobodies were harvested from the periplasm by osmotic shock. The (His)₆-tag allows purification of nanobodies with NiNTA Agarose beads (Qiagen). Nanobodies were purified on an S75 column by FPLC (ÄKTA, Cytiva Life Sciences). GGG-DM₁ and GGG-DM₄ were produced in-house by modifying a GGG-peptide linker to contain a maleimide group and allowing it to react with the thiol group on DM₁ or DM₄ (Broadpharm) as described (Chapter 3, supplementary figure 2). For sortase reactions, nanobodies were incubated with a 10-fold molar excess of GGG-DM₁ or GGG-DM₄ and incubated with 25 μ M Sortase for 16 hours at 4°C. Unreacted VHH and Sortase, both containing a (His)₆-tag, were depleted by incubation with NiNTA agarose (Qiagen or Prometheus). Excess free GGG-DM_{1/4} was removed by desalting on a PD-10 desalting column (Cytiva). Fractions were eluted in 500 μ L PBS. To prevent inclusion of free GGG-DM_{1/4}, only the fractions eluting early were selected and combined for downstream further applications.

Cell culture

MICA-expressing mouse-derived EL-4 T cell lymphoma cells or B16F10 melanoma cells, and their wild type (WT) counterparts, were a gift from K. Wucherpfennig (Dana Farber Cancer Institute). EL-4 cells were cultured in complete RPMI 1640 (RPMI 1640 supplemented with 10% fetal bovine serum (FBS) + 100 U/mL penicillin/streptomycin (pen/strep)). B16F10 cells were cultured in complete DMEM (DMEM with 4.5 g/L glucose, supplemented with 10% FBS + 100 U/mL pen/strep)

Nanobody-drug conjugate treatment *in vitro*

We plated 4000 B16F10 or EL-4 WT or MICA⁺ cells per well in a 96-well plate. We incubated the cells with serial 3-fold dilutions of VHH-drug adduct at 37°C in a humidified 5% CO₂ atmosphere. After 72 hours, we measured cell viability by CellTiter Glo™ assay according to the manufacturer's directions (Promega).

Nanobody-drug conjugate treatment *in vivo*

C57/B6 mice were injected subcutaneously in the right flank with 0.5×10^6 EL-4 MICA⁺ cells in PBS. On day 2 after injection, intraperitoneal injections of 100 μ g (~5 mg/kg) per mouse were given every 2 or 3 days until day 21. Tumor size was measured by calipers and tumor volume was calculated using the following formula: $V = 0.5 \times L \times W^2$. Mice were sacrificed when the tumor volume exceeded 2000mm³ or when ulcerations were observed.

Mice

C57BL/6J mice were purchased from the Jackson Laboratory or bred in-house. Mice were used at 8-12 weeks of age. Experiments were performed in accordance with the guidelines of the Institutional Animal Care and Use Committee (IACUC) of Boston Children's Hospital.

Results

Nanobody-drug conjugate fails to induce cytotoxicity of B16F10 MICA⁺ tumor cells *in vitro*

Because of the promising results in *in vitro* cytotoxicity of VHH_{A1}-DM1 on EL-4 MICA⁺ cells, we tested the efficacy of this nanobody drug conjugate on a different MICA⁺ cancer cell line. We used the aggressive mouse-derived B16F10 melanoma line, transfected to stably express MICA on the cell surface. We used a VHH that targets mouse MHC-II (VHH_{MHC-II})⁵⁵⁸ as a negative control. We ligated the microtubule inhibitor Maytansine (DM1) to the nanobodies by a sortase-mediated transpeptidation reaction (Figure 1A). After the sortase reaction, unreacted VHH and Sortase, both containing a (His)₆-tag, were depleted by incubation with NiNTA agarose. We performed an *in vitro* cytotoxicity assay by titration of VHH_{MHC-II}-DM1 or VHH_{A1}-DM1 on B16F10 WT and MICA⁺ cells. We did not observe an increased sensitivity, measured by IC₅₀, to VHH_{A1}-DM1 by the MICA⁺ cells compared to VHH_{MHC-II}-DM1. We also did not observe a significant difference in IC₅₀ between WT and MICA⁺ B16F10 cells treated with either nanobody (Figure 1B). These results indicate that the VHH A1-based nanobody-drug conjugate is ineffective in treating the aggressive B16F10 MICA⁺ melanoma line *in vitro*.

Using the same strategy, we evaluated the efficacy of VHH A1 conjugated to DM4, the functional analog of DM1 with as the only difference the presence of a cleavable linker (Chapter 3, Supplementary figure 2B) in killing EL-4 WT or MICA⁺ cells. We did not observe an increased sensitivity, measured by IC₅₀, to VHH_{A1}-DM4 by the MICA⁺ cells compared to VHH_{MHC-II}-DM4 (Figure 1C).

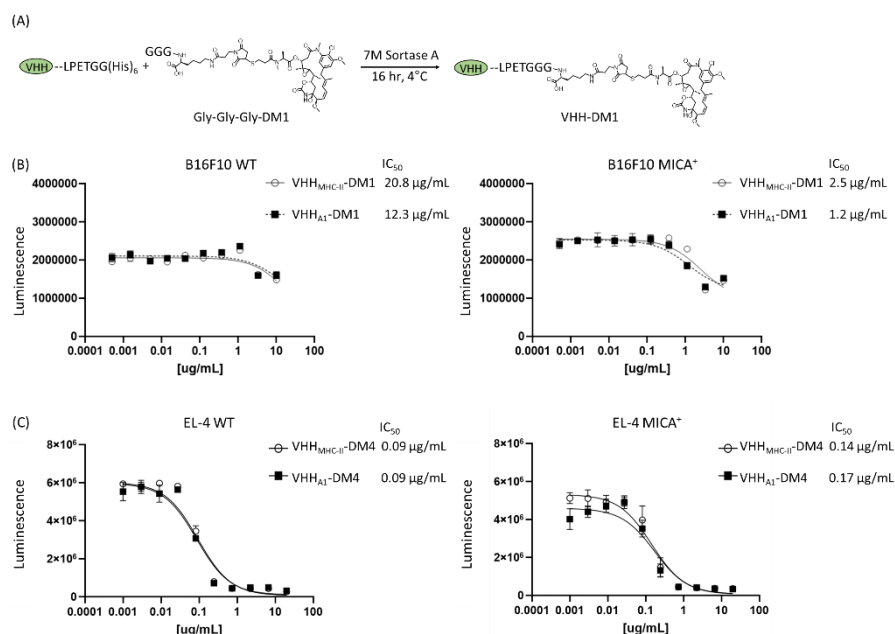


Figure 1. Anti-MICA VHs as nanobody-drug conjugate with the Maytansine derivative DM1. (A) We ligated the microtubule-inhibitor GGG-DM1 to VHH A1 or VHH_{MHC-II} as a non-targeting control through sortase-mediated transpeptidation reaction. (B) We performed an *in vitro* cytotoxicity assay by incubating 4000 B16F10 WT or MICA⁺ cells with VHH_{MHC-II}-DM1 or VHH_{A1}-DM1 at 3-fold serial dilutions. After 72 hours, we measured proliferation by CellTiter Glo™ assay. We observed a similar IC₅₀ in cells incubated with either non-targeting or MICA-targeting nanobody-drug conjugate, thus there is no effect on proliferation of MICA⁺ cells treated with VHH_{A1}-DM1.

Half-life extension of nanobody-drug conjugate for *in vivo* cytotoxicity of EL-4 MICA⁺ tumor cells

Despite the resistance of B16F10 cells to treatment with the nanobody-drug conjugate, we previously had striking results in treating EL-4 MICA⁺ cells with the VHH A1-based nanobody drug conjugate). The efficacy of treatment of EL-4 MICA⁺ cells with VHH_{A1}-DM1 was comparable to that of cells treated with free DM4, a functional analog of DM1. Because of their small size, unbound nanobody is rapidly cleared from the circulation, with an *in vivo* half-life of less than 2 hours⁵⁷⁶. Thus, to use the VHH A1-based nanobody-drug conjugate for treatment of MICA⁺ tumors *in vivo*, we reasoned that half-life extension of the nanobody might be useful.

To this end, we created a genetic C-C fusion of VHH-A₁ to a mouse immunoglobulin kappa-light chain targeting nanobody (VHH_{mKappa}). This nanobody recognizes the κ light chains of mouse immunoglobulins⁵⁷⁷. As a negative control, we used a genetic C-C fusion of VHH_{mKappa} to a nanobody that targets influenza virus hemagglutinin (VHH_{SD36}). We created VHH_{A1}-VHH_{mKappa}-DM1 or VHH_{SD36}-VHH_{mKappa}-DM1 using sortase-mediated transpeptidation (Figure 2A). We combined fractions 1-6 for VHH_{A1}-VHH_{mKappa}-DM1 and fractions 3-6 for VHH_{SD36}-VHH_{mKappa}-DM1. We confirmed successful ligation by SDS-PAGE (Figure 2B).

To test the efficacy of VHH_{A1}-VHH_{mKappa}-DM1, we performed an *in vitro* cytotoxicity assay by titration of VHH_{A1}-VHH_{mKappa}-DM1, VHH_{SD36}-VHH_{mKappa}-DM1, or free DM4 on EL-4 WT and MICA⁺ cells. 72 hours after co-culture, we measured proliferation by CellTiter Glo assay. EL-4 MICA⁺ cells were sensitive to VHH_{A1}-VHH_{mKappa}-DM1 with a stronger cytotoxic effect at lower doses of the VHH-drug conjugate compared to VHH_{SD36}-VHH_{mKappa}-DM1, as estimated by IC₅₀. Despite the reduction in IC₅₀, the sensitivity of EL-4 MICA⁺ cells was lower for treatment with VHH_{A1}-VHH_{mKappa}-DM1 compared to free DM4. Similarly treated WT cells showed no obvious reduction in proliferation with either nanobody-drug conjugate (Figure 2C).

Nanobody-drug conjugates fail to reduce growth of MICA⁺ tumors *in vivo*

Mice bearing subcutaneously grafted EL-4 MICA⁺ tumors were treated every 2 or 3 days until day 21 with an intraperitoneal injection of 5 mg/kg of VHH_{A1}-VHH_{mKappa}-DM1 or VHH_{SD36}-VHH_{mKappa}-DM1 (Figure 3A). Although tumor growth in the treated mice was delayed relative to mice treated with a non-targeting nanobody-drug conjugate, once treatment was stopped this delay no longer applied. In fact, treated mice showed accelerated tumor growth upon cessation of treatment (Figure 3B). We also did not observe a significant difference in survival probability between the mice treated with VHH_{A1}-VHH_{mKappa}-DM1 and VHH_{SD36}-VHH_{mKappa}-DM1 (Figure 3C).

Discussion

MICA/B are MHC-I related proteins expressed on stressed and malignant cells. Their presence can serve as a target for therapy. We produced the MICA-targeting nanobody (VHH A₁) and conjugated it to the Maytansinoid DM1, a microtubule inhibitor. We observed increased, specific cytotoxicity *in vitro* of VHH_{A1}-DM1 on MICA⁺ EL-4 T cell lymphoma tumor cells, compared to WT EL-4 cells.

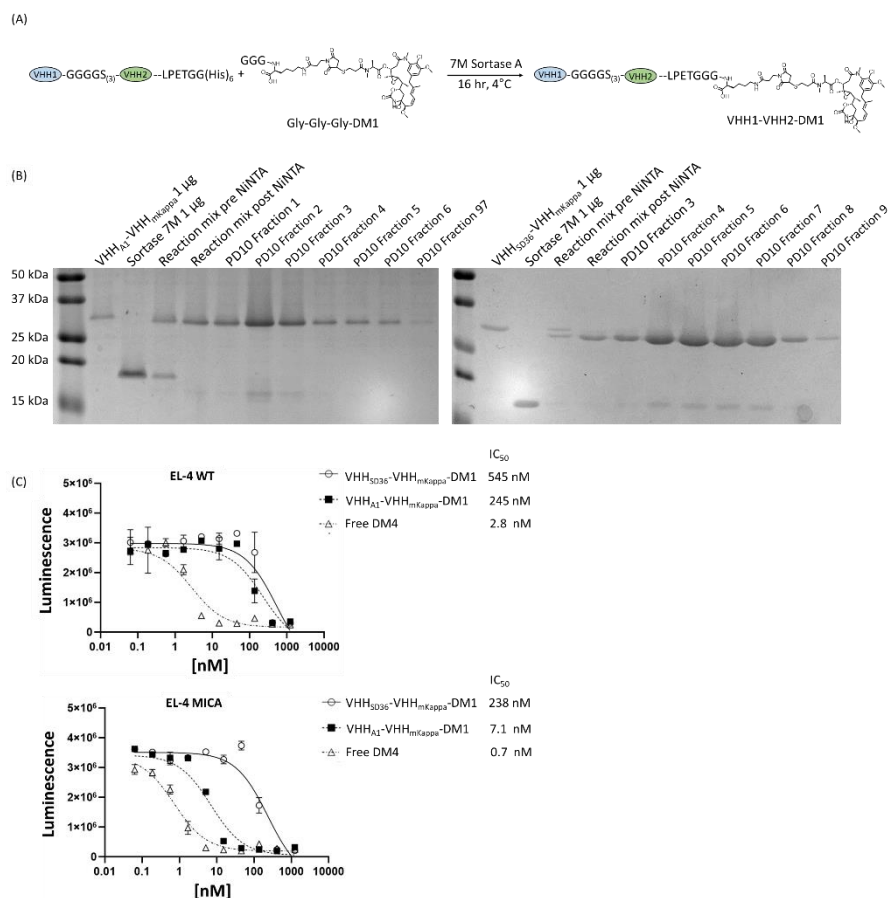


Figure 2. Production of nanobody-drug conjugate with the Maytansine DM1 and calculation of IC₅₀. (A) We ligated DM1 to this fusion by sortase-mediated transpeptidation reaction to create VHH_{A1}-VHH_{mKappa}-DM1 or VHH_{SD36}-VHH_{mKappa}-DM1. (B) After the sortase reaction, unreacted VHH and Sortase, both containing a (His)₆-tag, were depleted by incubation with NiNTA agarose. Excess free GGG-DM1 was removed by desalting on a PD-10 desalting column, eluting in fractions of 500 μ L PBS. We selected and combined fractions 1 – 6 for VHH_{A1}-VHH_{mKappa}-DM1 and fractions 3-6 for VHH_{SD36}-VHH_{mKappa}-DM1. We confirmed successful ligation by SDS-PAGE. (C) We performed an *in vitro* cytotoxicity assay by titration of VHH_{A1}-VHH_{mKappa}-DM1, VHH_{SD36}-VHH_{mKappa}-DM1, or free DM4 on EL-4 WT and MICA⁺ cells. After incubation for 72 hours, we measured cell viability by CellTiter Glo™ assay. EL-4 MICA⁺ cells treated with VHH_{A1}-VHH_{mKappa}-DM1 showed a significant reduction in IC₅₀, and thus a decrease in viability with a lower concentration of drug added, compared to similarly treated EL-4 WT cells, or EL-4 cells treated with the non-targeting VHH_{SD36}-VHH_{mKappa}-DM1.

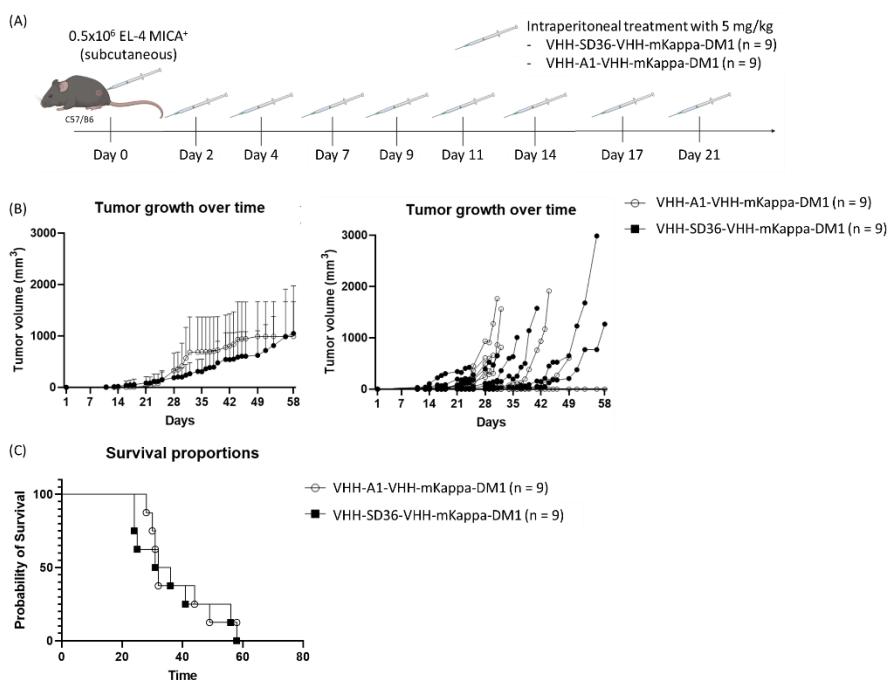


Figure 3. In vivo cytotoxicity of nanobody-drug conjugate in MICA⁺ tumor-bearing mice. (A) We subcutaneously grafted 0.5x10⁶ EL-4 MICA⁺ cells in C57/B6 mice. Treatment with 5 mg/kg of VHH_{A1}-VHH_{mKappa}-DM1 (n = 9) or VHH_{SD36}-VHH_{mKappa}-DM1 (n = 9) started on day 2. Treatments were administered intraperitoneal every 2-3 days until day 21. (B) Tumors were measured daily by calipers. The average tumor volumes with standard deviations are plotted in the left graph. The measurements of each mouse individually are depicted in the right graph. We did not see a significant reduction in tumor growth in the mice treated with VHH_{A1}-VHH_{mKappa}-DM1 compared to the mice treated with VHH_{SD36}-VHH_{mKappa}-DM1. (C) We did not observe a significant difference in survival probability between the mice treated with VHH_{A1}-VHH_{mKappa}-DM1 or VHH_{SD36}-VHH_{mKappa}-DM1.

Here, we tested the efficacy of VHH A1-based nanobody-drug conjugate on MICA⁺ B16F10 cells, a highly aggressive mouse-derived melanoma cell line. The VHH A1-based nanobody-drug conjugate was ineffective in treating B16F10 MICA⁺ cells *in vitro*. Published literature suggests a certain resistance of B16F10 cells to DM1 treatment⁵⁷⁸. Because of the promising results obtained when using the EL-4 cell line, we suggest inclusion of more cell lines that represent different tumor types to determine the extent of resistance to VHH_{A1}-DM1 across a broader spectrum of malignancies.

For our *in vivo* model, we extended the half-life of the nanobody drug conjugate by creating a genetic C-C fusion of VHH A1 to an anti-mouse kappa light chain nanobody (VHH_{mKappa}). Using a sortase reaction, we ligated DM1 to this fusion and created VHH_{A1}-VHH_{mKappa}-DM1. We used VHH_{SD36}, a nanobody that targets the influenza virus hemagglutinin, fused to VHH_{mKappa} and DM1, as a negative control. We treated mice bearing subcutaneous EL-4 MICA⁺ cells 3x weekly with an intraperitoneal injection of 5 mg/kg of the fusions and showed that the VHH_{A1}-VHH_{mKappa}-DM1 was ineffective in treating the EL-4 MICA⁺ tumors. Possibly, intravenous administration of the drug might improve delivery to the tumor, but this was not tested by experiment.

The creation of different VHH-drug combinations, for example with other tubulin inhibitors like Auristatins, immunomodulators like STING agonists, or DNA damaging agents like Exatecans, deserves further research.

Chapter 5:

Nanobody-based CAR NK-92 cells for possible immunotherapy of MICA⁺ tumors

Elisha R. Verhaar^{1,2}, Willemijn J.C. van Keizerswaard¹, Anouk Knoflook¹,
Thomas Balligand¹, Hidde L. Ploegh^{1,2}

¹Program in Cellular and Molecular Medicine, Boston Children's Hospital, Harvard Medical
School, Boston, MA 02115, USA

²Department of Cell and Chemical Biology, Leiden University Medical Centre, Leiden, The
Netherlands

PNAS Nexus

2024 May;3(5)

DOI: 10.1093/pnasnexus/pgae184

Abstract

The glycoproteins MICA and MICB are upregulated on the surface of cells undergoing stress, for instance due to (viral) infection or malignant transformation. MICA/B are the ligands for the activating receptor NKG2D, found on cytotoxic immune cells like NK cells, CD8⁺ T cells, and $\gamma\delta$ T cells. Upon engagement of NKG2D, these cells are activated to eradicate the MICA/B-positive targets, assisted by the secretion of cytokines. Nanobodies, or VHHs, are derived from the variable regions of camelid heavy-chain only immunoglobulins. Nanobodies are characterized by their small size, ease of production, stability, and specificity of recognition. We generated nanobodies that recognize membrane-bound MICA with high affinity. Here, we use these nanobodies as building blocks for a chimeric antigen receptor (CAR) to establish VHH-based CAR NK cells. These anti-MICA nanobody-based CAR NK cells recognize and selectively kill MICA-positive tumor cells *in vitro* and *in vivo*. We track localization of the VHH-based CAR NK cells to MICA-positive lung metastases by immuno-positron emission tomography (PET) imaging.

Significance statement

MICA is a Class I MHC-related surface glycoprotein, upregulated by virus-infected or malignantly transformed cells. MICA is overexpressed on cancers of hematopoietic and epithelial origin but is absent from healthy cells. We generated nanobodies, the recombinantly expressed variable regions of camelid heavy-chain only immunoglobulins, that recognize MICA with high affinity. We use the nanobodies as building blocks for chimeric antigen receptors (CAR) on NK-92 cells, which recognize and selectively kill MICA⁺ tumor cells *in vitro* and *in vivo*. We track the localization of the nanobody-based CAR NK cells to lung metastases of mice by immuno-PET imaging. The presence of MICA on many tumor types, and absence from healthy tissue, makes it a promising target for cancer immunotherapy.

Introduction

The MHC class I chain-related proteins A and B (MICA and MICB) are surface glycoproteins that are absent from healthy cells but upregulated on malignantly transformed or otherwise stressed human cells²²⁴. High levels of MICA/B have been reported in cancers of both hematopoietic and epithelial origin^{219,224–228}. MICA/B are ligands for the activating receptor NKG2D, found on NK cells, CD8⁺ T cells, and $\gamma\delta$ T cells²¹⁸. Upon engagement of MICA/B with NKG2D, these cytotoxic immune cells are activated to eradicate MICA-positive target^{219–221}.

The tumor microenvironment (TME) affects surface expression of the ligands of NKG2D transcriptionally and post-translationally. Surface expression of MICA and MICB on tumor cells can be downregulated through shedding, mediated by proteolytic cleavage involving ADAM-type metalloproteases at the MICA $\alpha 3$ domain²³⁶. Loss of surface-bound MICA renders tumor cells less sensitive to NKG2D-positive NK cells^{233,235}.

Nanobodies, also known as VHHs, are the variable heavy-chain fragments of camelid-derived heavy-chain only immunoglobulins³⁰¹. Nanobodies are characterized by their small size compared to conventional immunoglobulins (15 kD versus 150 kD), which allows for excellent tissue penetration, stability, solubility, and ease of production^{309–311}. Nanobodies are poorly immunogenic and have a short circulatory half-life, making them valuable tools for the construction of PET imaging agents^{314,329,380,387,388,419,420}, nanobody-drug conjugates^{315,386,436}, and chimeric antigen receptors in cell-based therapies^{210,474–478,546–551}.

The latter is based on a cornerstone of immunotherapy known as adoptive cell transfer (ACT), in which immune cells (often the patient's own lymphocytes) are given to a patient as cancer therapy. When using tumor infiltrating lymphocytes expanded ex vivo, this form of treatment is referred to as TIL therapy. In another form of ACT, the patient's T or NK cells are engineered to express a chimeric antigen receptor (CAR) that targets the tumor and exerts cytotoxic activity upon binding to the target recognized by the CAR. In such cells, the CAR dictates the antigen specificity of the cell towards a target of choice. The CAR also contains intracellular signaling domains derived from several proteins such as 4-1BB, CD28, and CD3 ζ . These signaling domains activate the CAR cell in response to antigen recognition^{579,580} and trigger cytotoxic activity as well as cytokine release. Typically, the antigen recognition domain of the CAR is based on a single-chain variable fragment (scFv), derived from a full-sized immunoglobulin by connecting the variable regions of the immunoglobulin heavy and light chains by means of a short linker into a single construct. The affinity and specificity of scFvs must be carefully compared to that of the source immunoglobulin to maintain its functional properties. When expressed in mammalian cells, domain swaps can lead to self-aggregation of scFv-based CARs^{581–584}. The possible immunogenicity of the scFv is a factor to be considered as well. Nanobodies are poorly immunogenic in humans, presumably because of the pronounced homology between camelid and human variable heavy (V_H) chain sequences^{196,197}.

The FDA has approved several CAR T cell therapies for hematopoietic cancers, such as relapsed or refractory B-cell lymphoma or acute lymphatic leukemia, based on CD19 targeting with an scFv, and relapsed or refractory multiple myeloma, based on CARs that target B-cell maturation antigen (BCMA) via either an scFv or a VHH⁵⁸⁵⁻⁵⁸⁷, the latter with remarkable clinical efficacy. A major reported side effect of CAR T therapy is cytokine release syndrome, which is systemic inflammation caused by excessive cytokine secretion by the CAR T cells. The cytokines released by NK cells do not induce such inflammation, and thus do not cause cytokine release syndrome²¹⁷. For these reasons, CAR NK cell therapy is potentially a safer alternative to CAR T cell therapy.

CAR NK cells can be produced from a variety of sources: from the patient's or a donor's peripheral blood, from a placenta or from umbilical cord blood, existing immortalized NK cell lines (NK-92) or manufactured from induced pluripotent stem cells (iPSC)²⁰⁵⁻²¹⁰. Unlike T cells, NK cells do not pose the risk of GVHD in an allogeneic setting. In fact, NK cells are believed to protect against GVHD in other T cell-based cancer treatments²¹¹⁻²¹⁵. Furthermore, NK cells also allow the inclusion of a wider range of co-stimulatory domains, using not only traditional intracellular domains derived from CAR T therapies based on CD28, 4-1BB, and CD3ζ, but also NK-specific domains such as CD244, CD137, and NK-Ars^{209,216,217}. If a tumor were to downregulate the CAR's target in an attempt at immune escape, the NK cells might still be effective against the tumor cells because of their intrinsic cytotoxic activity. NK cell-based therapies have entered clinical trials for targeting NY-ESO-1 in synovial carcinoma, myxoid liposarcoma, multiple myeloma, or certain solid tumors. These NK cells are harvested from cord blood and modified with an NY-ESO-1 TCR and IL-15 receptors. Several other pre-clinical studies with CAR NK cells include CARs that target CD19 and CD20 in B cell lymphoma and leukemia⁵⁸⁸⁻⁵⁹⁵, GD2 in neuroblastoma and breast cancer⁵⁹⁶⁻⁵⁹⁸, and HER2 in breast cancer and other epithelial cancers^{599,600}.

Ideally, the target of CAR immune cells is present only on tumor cells and absent from normal tissue, to reduce unwanted off-target effects. Because MICA is expressed primarily on stressed and cancerous cells, MICA is an appealing target for adoptive cell transfer. We have described the production of MICA-targeting nanobodies, VHH-A1 and VHH-H3. These nanobodies recognize the MICA*008 and *009 alleles with nanomolar affinity and recognize surface-disposed MICA on cancer cells⁵⁷⁵.

Here, we use these anti-MICA nanobodies to establish VHH-based CAR NK cells. We show that these CAR NK cells recognize and selectively kill MICA-positive tumor cells *in vitro* and *in vivo*.

Materials and methods

Cell culture

The NK-92 cells were obtained from S.K. Dougan (Dana Farber Cancer Institute). NK-92 cells were cultured in complete α MEM (α MEM; no nucleosides, supplemented with 12.5% horse serum, 12.5% fetal bovine serum (FBS), 2mM L-glutamine, 0.1 M 2-mercaptoethanol, 0.02 mM folic acid, 100 U/mL recombinant IL-2 and 100 U/mL penicillin/streptomycin). B16F10 murine melanoma cells and EL-4 lymphoma cells, and their MICA⁺ transfectants, were obtained from K. Wucherpfennig (Dana Farber Cancer Institute). HEK293T and B16F10 cells were cultured in complete DMEM (DMEM with 4.5 g/L glucose supplemented with 10% FBS and 100 U/mL penicillin/streptomycin). To avoid proteolytic cleavage of membrane-bound MICA, we dissociated adherently grown B16F10 cells from the plate using a 0.5 mM EDTA solution (Gibco). EL-4 cells were cultured in complete RPMI 1640 (RPMI 1640 supplemented with 10% FBS and 100 U/mL penicillin/streptomycin). All cells were cultured to maintain optimal densities and kept in a humidified 5% CO₂ incubator at 37°C. Recognition of surface-disposed MICA by the nanobodies was verified by flow cytometry⁵⁷⁵.

Expression of the CAR construct was verified by flow cytometry. Briefly, cells were stained with Cy5-conjugated recombinant extracellular MICA*009 (1 μ g/mL) for 30 minutes on ice. Cells were washed and viability was determined with LIVE/DEAD™ Fixable Violet Dead Cell Stain Kit (Invitrogen) according to manufacturer's directions. Cells were analyzed on an LSR2 Flow Cytometer (BD Biosciences). Recombinant MICA*009 was produced in-house by transfection of EXPI-293 cells⁵⁷⁵.

Mice

C57BL/6J mice and Rag1-deficient mice were purchased from the Jackson Laboratory or bred in-house. Mice were used at 7-12 weeks of age. Experiments were performed in accordance with the guidelines of the Institutional Animal Care and Use Committee (IACUC) of Boston Children's Hospital. Mice were housed under specific pathogen-free conditions in a controlled environment with a 12-hour light-dark cycle and ad libitum access to standard laboratory chow and water. Health status and welfare of the mice were monitored regularly throughout the study.

Design of the VHH CAR construct and virus production

The gene fragments for the CAR were inserted by 'sticky-end' cloning using the BamHI and ClaI restriction enzymes (both from New England Biolabs) into a lentiviral backbone with a mammalian EF-1 α promoter (lenti-EF1 α -IRES-GFP, a gift from David Williams (Boston Children's Hospital) (Supplementary figure 1). For lentiviral production, we transfected HEK-293T cells with 3 μ g of CAR plasmid, 2 μ g of psPAX2 packaging vector, a gift from Didier Trono (Addgene plasmid #12260; <http://n2t.net/addgene:12260>; RRID:Addgene_12260) and 1 μ g of pMD2.G envelope vector, a gift from Didier Trono (Addgene plasmid #12259; <http://n2t.net/addgene:12259>; RRID:Addgene_12259) in 500 μ l of serum-free DMEM (Gibco). This DNA mixture was added to 100 μ l of serum-free DMEM at a 6:1 ratio of FuGENE6 transfection reagent (Promega) and incubated for 15-30 minutes at room temperature. The mixture was then added to ~70% confluent HEK293T cells grown in 10mL of complete DMEM. The medium was replaced ~16 hours after transfection. Lentivirus was harvested 24 and 48 hours after the medium change, the media combined, and concentrated by centrifugation at 45,000xg for 2 hours at 4°C.

Lentiviral transduction and selection of transduced NK-92 cells

NK cells were transduced by centrifugal inoculation. Briefly, 1×10^5 NK cells were added to a well of a 6-well plate, at a 1:3 ratio of concentrated viral supernatant and complete α MEM. Polybrene infection agent (Sigma-Aldrich) (8 μ g/mL) was added to improve transduction. BX795 (1.5 μ M), IL-2 (500 IU/mL) and IL-12 (20 ng/mL, all from PeproTech) were added for optimal cell viability. Cells were centrifuged at 2000xg at 30°C, for 90 minutes, resuspended, and incubated in the viral culture medium at 37°C in a humidified 5% CO₂ atmosphere for 4 hours. Centrifugation was repeated at 2000xg at 30°C, for 60 minutes. The medium was then replaced with complete α MEM.

Activation of CAR NK cells by co-culture with MICA-expressing B16F10 cells

WT or MICA-expressing B16F10 or EL-4 cells were incubated at 25,000 cells per well of a 96-well plate together with CAR NK cells at various effector to target ratios in a total volume of 100 μ l (1:1 ratio of complete DMEM and complete α MEM) at 37°C in a humidified 5% CO₂ atmosphere. After 24 hours, the IFN- γ concentration in the medium was determined by ELISA, using the human IFN- γ matched antibody pair (ThermoFisher scientific) according to the manufacturer's instructions. Cell death was determined with a lactate

dehydrogenase (LDH) Cytotoxicity Assay (Abcam, Ab65393) performed according to the manufacturer's instructions.

CAR NK-92 treatment *in vivo*

Rag1^{-/-} mice were subcutaneously injected in the right flank with 4x10⁵ B16F10 MICA⁺ cells in PBS. Retro-orbital injections of CAR NK were started on day 3 and treatment injections were given twice weekly at 5-10x10⁶ cells per injection. Tumor size was measured by calipers and tumor volume was calculated using the formula ($V = 0.5 \times L \times W^2$). Mice were sacrificed once the tumor volume reached 2000mm³ or when ulcerations were observed.

PET-CT imaging

To create the imaging agents for PET-CT imaging, we ligated GGG-DFO-Azide to VHH₁₈₈ by sortase-mediated transpeptidation. For sortase reactions, the nanobody was incubated with a 10-fold molar excess of GGG-DFO-Azide and 25 μM Sortase 7M⁵³³ overnight at 4°C. Reaction mixtures were depleted of unreacted VHH and Sortase, both containing a C-terminal (His)₆-tag on a NiNTA matrix and elimination of free nucleophile by desalting on a PD-10 column (Cytiva), eluting in fractions of 500 μL PBS. We selected and combined fractions 6, 7, and 8 (Supplementary figure 2A). To extend the half-life of the nanobody *in vivo*, the nanobodies were PEGylated by incubation with a 10-fold molar excess of DBCO-PEG20 overnight at 4°C. The reaction was cleaned with a PD-10 column (Cytiva), eluting in fractions of 500 μL PBS. We selected and combined fractions 6, 7, and 8 (Supplementary figure 2B). ⁸⁹Zr was ordered from the UW-Madison Cyclotron Lab (University of Wisconsin-Madison, USA) and neutralized to a pH of 7.4 by addition of 2M Na₂CO₃ and 1M HEPES. Nanobodies were labeled with ⁸⁹Zr by DFO-mediated chelation in chelexed PBS and excess, unbound ⁸⁹Zr was removed by desalting on a PD-10 column and eluted in fractions of 600 μL chelexed PBS (Supplementary figure 3). Radioactivity of the individual fractions was determined and ~60 μCi VHH₁₈₈-PEG20-⁸⁹Zr was injected per mouse via retro-orbital injection. Mice were anaesthetized using 2% isoflurane in O₂ at a flow rate of 1 liter per minute. PET/CT scans were obtained 1-, 24-, 48-, and 72-hours post injections on a G8 PET-CT small-animal scanner (PerkinElmer). Each scan had a PET acquisition time of 10 minutes, followed by a CT-scan for 1.5 minutes. PET images were processed and analyzed using VivoQuant software.

Statistical analysis

All statistical analysis was performed with GraphPad Prism 8. Flow cytometry data was analyzed with FlowJo (v10.8.1 and v10.9.0).

Results

Transduction with lentiviral anti-MICA VHH-based CAR constructs yielded stable CAR NK-g2 cells

The design of CAR NK cells was based on previously described VHH-based CAR T cells⁴⁷⁶ (Figure 1A). We designed a GBlock™ Gene fragment that encodes GFP, followed by a P2A proteolytic processing site to separate the GFP portion from the CAR itself. The CAR antigen recognition domain is encoded by the MICA-specific VHHs A1 or H3, followed by the CD8 hinge and CD8 transmembrane segment and the cytoplasmic signaling and costimulatory domains of CD28 and CD3ζ. The characterization of the anti-MICA VHHs has been described⁵⁷⁵. Cells bearing these VHH-based CARs will be referred to as A1 and H3 CAR NK cells.

As a control, we transduced NK cells with a lentiviral vector containing only a GFP cassette, referred to as empty vector ("EV"). For the NK cells, we observed a low transduction efficiency between 0.3 and 5% (Figure 1B). We therefore sorted the GFP⁺ cells to establish a stably transduced cell line. We included a PE channel to eliminate dead auto-fluorescent cells that show up in the PE channel. Flow cytometry performed on the H3 CAR NK cells shows the presence of two distinct populations of GFP⁺ cells, attributed to the combination of two cell lines transduced on separate days, done to obtain adequate numbers of cells (Figure 1C). To verify CAR surface expression, we stained the CAR NK cells with Cy5-conjugated MICA protein, which binds to the extracellularly exposed nanobodies that are part of the CAR. Flow cytometry produced a clear signal in the Cy5 channel for the A1 CAR NK cells, showing surface expression of the VHH-A1 based CAR. We saw a weak signal in the Cy5 channel for the H3 CAR NK cells, indicating weaker expression of the VHH-H3 based CAR (Figure 1D).

For the H3 CAR NK cells, both the GFP^{hi} and the GFP^{lo} population show the same signal in the Cy5 channel (supplementary figure 4). Immunoblots prepared with anti-CD3ζ antibodies (signal at 40 kD in A1 and H3 CAR NK cells) showed expression of the CAR. The GFP polypeptide produced by the Lenti-EF1α A1 and H3 NK cell lysates migrates slightly higher on SDS -PAGE than the GFP produced by the Lenti-EF1α empty vector, attributable to the continued presence of the P2A peptide sequence downstream of the GFP in the CAR construct (Figure 1E). Gating for flow cell sorting and flow cytometry is shown in supplementary figures 5-7.

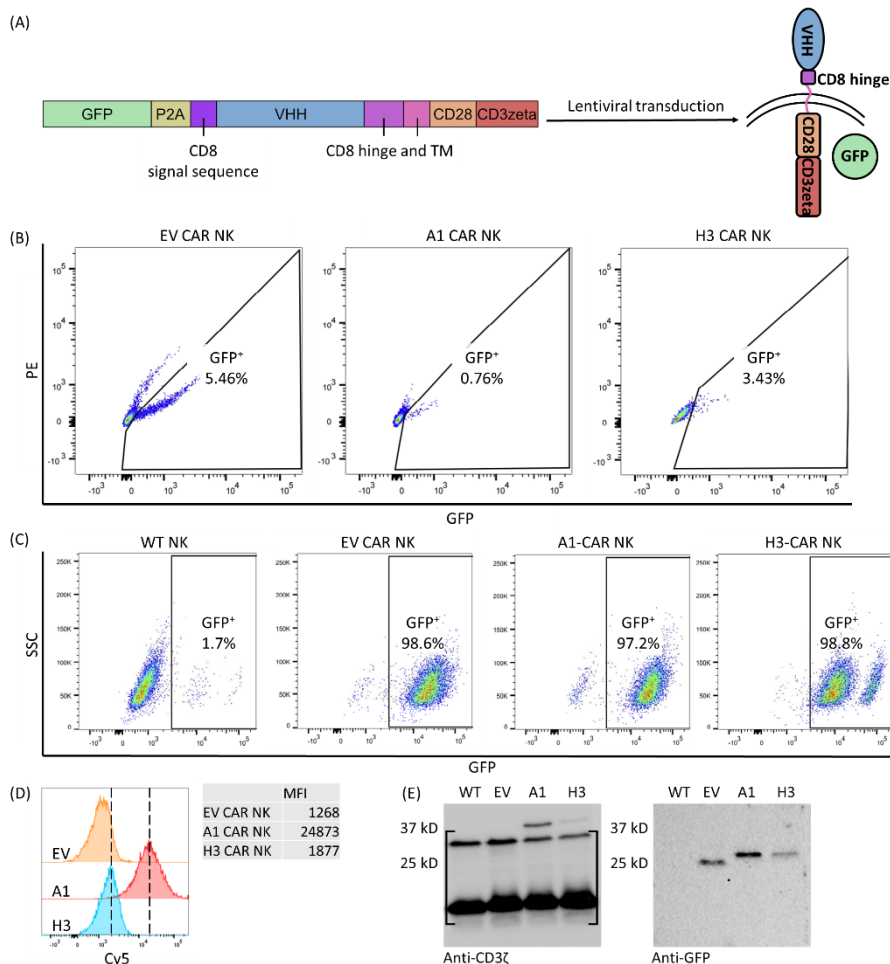


Figure 1. The production and establishment of stable CAR NK cells. (A) Schematic overview of the CAR construct as transduced into NK cells. We used a lentiviral backbone with a mammalian EF1 α promoter and incorporated the sequences of either VHH A1 or VHH H3, the costimulatory and activation signals of CD28 and CD3 ζ , and GFP separated from the rest of the construct by a P2A peptide cleavage signal. Construct maps for A1 CAR NK, H3 CAR NK and EV CAR NK are shown in supplementary figure 1. (B) After transduction, GFP positive cells were deemed to be transduced successfully, and therefore sorted by FACS. We included a PE channel to eliminate dead, auto-fluorescent cells. Gating shown in supplementary figure 5. (C) We continually monitored GFP expression in the CAR NK cells and found a stable expression after at least 4 months in culture, with a GFP positive population of 98.6% for the EV NK cells, 97.2% for the A1 CAR NK cells, and 98.8% for H3 CAR NK cells. Gating shown in supplementary figure 6. **LEGEND CONTINUES ON THE NEXT PAGE.**

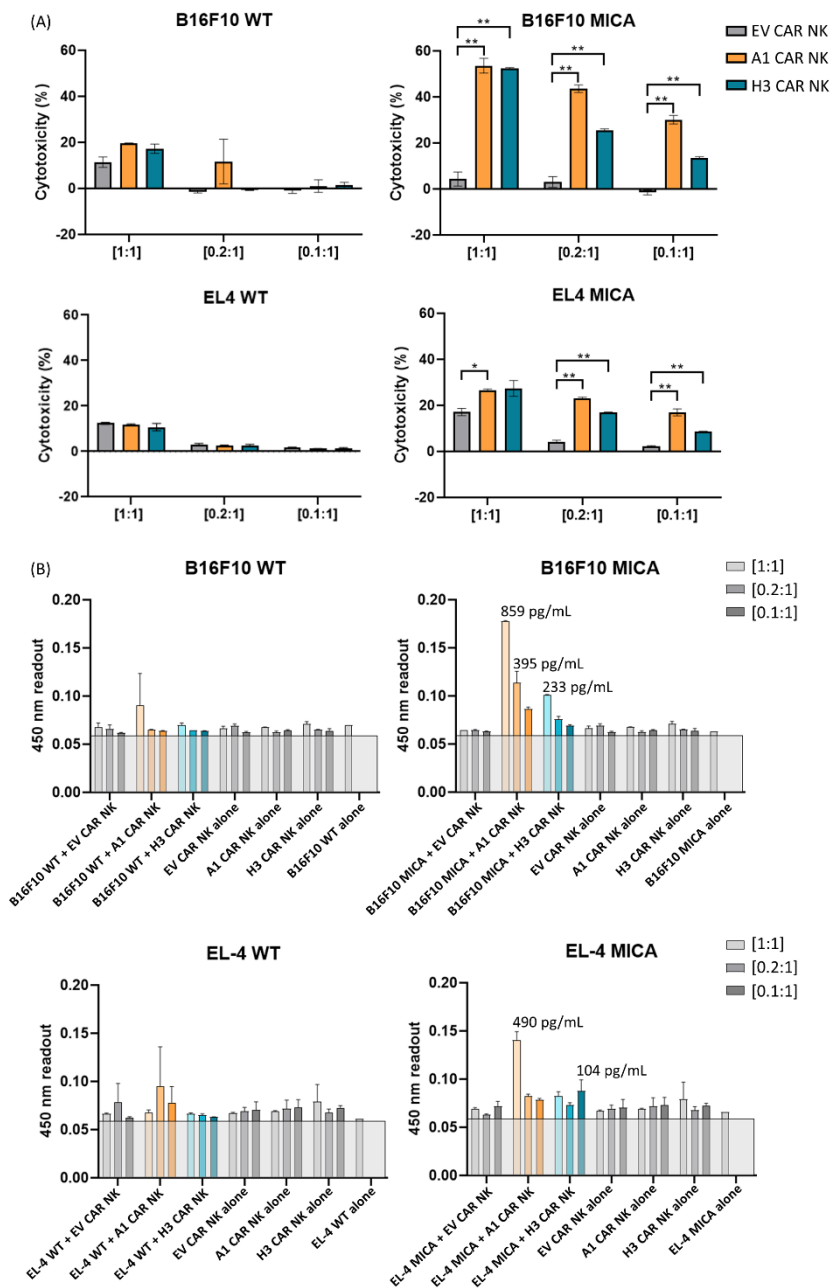
(D) To verify CAR surface expression by flow cytometry, we stained the CAR NK cells with Cy5-conjugated recombinant MICA protein. We observed a clear signal in the Cy5 channel for the A1 CAR NK cells, thus establishing surface expression of VHH-A1 as part of the CAR. We saw a weak signal in the Cy5 channel for the H3 CAR NK cells, indicating weaker expression of the VHH-H3-bearing CAR. Gating is shown in supplementary figure 7. (E) Immunoblots prepared with anti-CD3ζ antibodies showed expression of the actual CAR portion of the viral vector with a signal at 40 kD in A1 and H3 CAR NK cells and an absence of signal in WT and EV CAR NK cells. The GFP polypeptide produced by the Lenti-EF1α A1 and H3 NK cell lysates runs slightly higher than that of GFP produced by the Lenti-EF1α empty vector cell lysate, which we attribute to the presence of the P2A peptide sequence downstream of the GFP in the CAR construct. The weaker signal observed for the H3 CAR NK cells matches that observed by flow cytometry. The signal in brackets is non-specific.

MICA-expressing tumor cells activate A1 and H3 CAR NK-92 cells and elicit cytotoxicity

Because mice lack a protein homologous to human MICA, we used MICA transfectants of the mouse-derived B16F10 melanoma (MICA*009) and EL-4 T cell lymphoma (MICA*008) lines. We incubated A1 and H3 CAR NK cells with WT or MICA⁺ B16F10 cells or with WT or MICA⁺ EL-4 cells. We co-cultured effector cells and target cells at different ratios ([1:1], [0.2:1] and [0.1:1]), keeping the number of target cells constant and varying the number of effector cells. For the A1 and H3 CAR NK cells, at all [E:T] ratios, we observed a significant increase in cell death of MICA⁺ cells as measured by LDH release. Co-culture of MICA⁺ cells with EV CAR NK cells showed no such increase in cytotoxicity. No cytotoxicity was observed when co-culturing WT B16F10 cells with the A1 or H3 CAR NK cells. We observed a significant increase in cytotoxicity of EL-4 MICA⁺ cells co-cultured with A1 CAR NK cells or H3 CAR NK cells when compared to cytotoxicity exerted by EV CAR NK cells. No significant increase in cytotoxicity was observed in WT EL-4 cells co-cultured with EV, A1, or H3 CAR NK cells (Figure 2A).

To relate this cytotoxicity to activation of CAR NK cells, we measured IFNγ secretion by ELISA. Upon co-culture with B16F10 MICA⁺ we observed an increase in IFNγ secretion for the A1 and H3 CAR NK cells, but not for the EV CAR NK cells. CAR NK cells co-cultured with B16F10 WT cells showed no such increase. We observed an increase in IFNγ expression when A1 CAR NK cells were co-cultured with EL-4 MICA⁺ cells at [1:1], but not for any of the other conditions, despite the observed significant difference in cytotoxicity (Figure 2B). We attribute this to the fact that we observed lower MICA expression levels on the surface of the EL-4 MICA⁺ cells compared to the B16F10 MICA⁺ cells⁵⁷⁵. Furthermore, EL-4 cells are suspension cells, while

B16F10 cells are adherent, potentially facilitating an interaction with NK cells. These results indicate the possibility of CAR NK cells to treat MICA positive tumors *in vivo*.



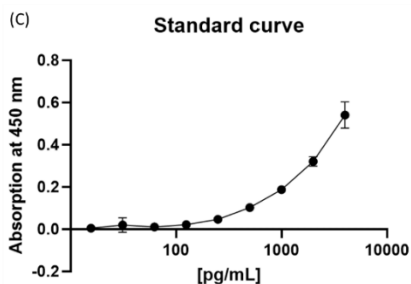


Figure 2. In vitro cytotoxicity of CAR NK cells co-cultured with MICA⁺ targets. We incubated EV, A1, and H3 CAR NK cells with WT B16F10 or EL-4 cells, or B16F10 or EL-4 cells that stably express MICA. We incubated at effector to target ratios [E:T] of [1:1], [0.2:1], or [0.1:1], keeping the number of target cells consistent and varying the number of effector cells. (A) 24 hours after co-culture, cytotoxicity was determined by measuring LDH release in the medium. Cytotoxicity percentages were normalized to target cells without CAR NK co-culture as a background control (0% cell death), or lysed target cells as a high control (100% cell death). We observed a significant increase in cytotoxicity of B16F10 MICA⁺ cells co-cultured with A1 CAR NK cells and H3 CAR NK cells compared to EV CAR NK cells at all [E:T] ([1:1] $p = 0.004$ for A1; $p = 0.002$ for H3, [0.2:1] $p = 0.0024$ for A1; $p = 0.0055$ for H3 and [0.1:1] $p = 0.0022$ for A1; $p = 0.0027$ for H3). EL-4 MICA⁺ cells showed a lower overall cytotoxicity of 15-30% when co-cultured with A1 and H3 CAR NK cells. We observed a significant increase in cytotoxicity of EL-4 MICA⁺ cells co-cultured with A1 CAR NK cells or H3 CAR NK cells compared to EV CAR NK cells at most [E:T] ([1:1] $p = 0.015$ for A1; $p = 0.061$ for H3, [0.2:1] $p = 0.0011$ for A1; $p = 0.0016$ for H3, [0.1:1] $p = 0.0055$ for A1; $p = 0.0014$ for H3). No significant increase in cytotoxicity was observed when WT cells were co-cultured with EV, A1, or H3 CAR NK cells. (B) After 24 hours of co-culture, the concentration of IFN γ in the medium was determined by sandwich ELISA with a matched human IFN γ antibody pair. We observed a significant increase in IFN γ secretion in the A1 and H3 CAR NK cells, but not in EV CAR NK cells, when co-cultured with B16F10 MICA⁺. We show the raw values of the ELISA plate read-out at 450 nm and the estimated IFN γ production in pg/mL by extrapolation from the standard curve (C).

MICA⁺ tumor-bearing mice treated with A1 CAR NK-92 cells show reduced tumor growth and increased survival probability

We inoculated RAG1^{-/-} mice with 4×10^5 B16F10 MICA⁺ cells via subcutaneous injection. Twice weekly, we treated the mice with EV CAR NK cells ($n = 3$) or A1 CAR NK cells ($n = 7$) by retro-orbital injection for a total of 5 injections and followed tumor growth by caliper measurements (Figure 3A). Mice treated with A1 CAR NK cells show a significant delay in tumor growth compared to mice treated with EV CAR NK cells ($p = 0.0075$) (Figure 3B). Furthermore, mice treated with A1 CAR NK cells showed a significant increase in survival probability ($p = 0.0011$) (Figure 3C). Of the mice treated with EV CAR NK

cells, one mouse was euthanized on day 17 because of severe ulcerations. Two mice were euthanized on day 17 and 18 when the tumor volume exceeded 2000mm³. Of the mice treated with A1 CAR NK cells, one mouse was euthanized on day 20 and one on day 21, both because of severe ulcerations. All other mice were euthanized when the tumor volume exceeded 2000 mm³. These results support the possibility of nanobody-based CAR NK cells to treat MICA⁺ tumors.

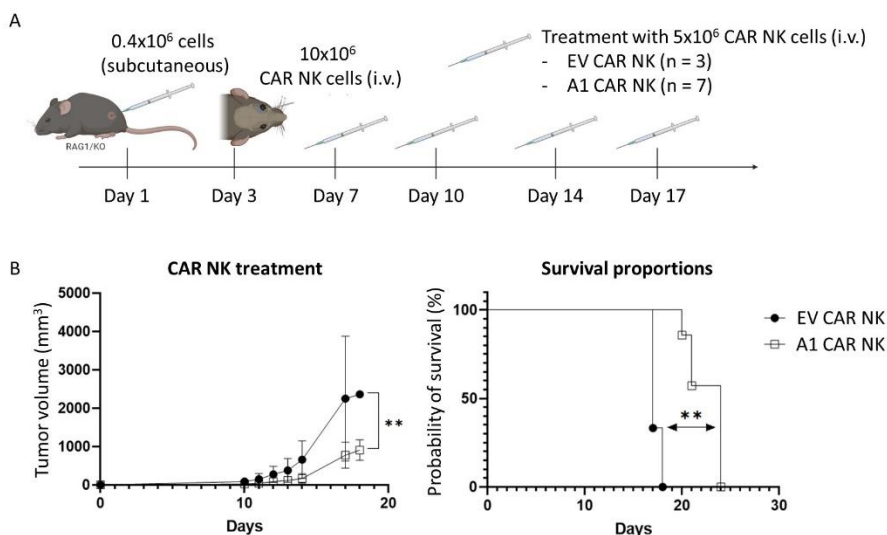


Figure 3. In vivo cytotoxicity of CAR NK cells in MICA⁺ tumor-bearing mice. (A) We challenged RAG1/KO mice with B16F10 MICA cells by subcutaneous injection. On day 3 post tumor graft, we treated the mice with a retro-orbital dose of 10x10⁶ CAR NK cells and reduced the dose to 5x10⁶ cells per mouse for the treatments twice weekly thereafter. (B) Mice treated with A1 CAR NK cells show a significant delay in tumor growth compared to mice treated with EV CAR NK cells ($p = 0.0075$) (Calculated with two-way ANOVA). (C) Mice treated with A1 CAR NK cells showed a significant increase in survival probability ($p = 0.001$) (Calculated with the Mantel-Cox test).

Immuno-PET traces CAR NK-92 cells to MICA⁺ tumors

To track the localization of CAR NK cells to MICA⁺ tumors, we inoculated C57/B6 mice with B16F10 MICA⁺ tumors by tail vein injection and allowed lung metastases to form for 15 days. We used PEGylated ⁸⁹Zr-labeled VHH₁₈₈ (Supplementary figure 2), a nanobody that targets the human transferrin receptor on the NK cells, which are of human origin (Supplementary figure 8) for immuno-PET imaging. VHH₁₈₈ does not recognize the mouse transferrin receptor⁶⁰¹. On day 1 of imaging, mice were injected with either EV CAR NK cells or A1 CAR NK cells (both 5x10⁶ cells/mouse) into one retro-orbital cavity,

and ^{89}Zr -labeled PEGylated VHH₁₈₈ (60 $\mu\text{Ci}/\text{mouse}$) into the other retro-orbital cavity.

We were able to localize the CAR NK cells to the lungs of the mice that received B16F10 MICA⁺ tumors up to 72 hours after NK cell injection (Figure 4B). We observed slightly more positive nodules in the lungs of the mice that received A1 CAR NK cells compared to EV CAR NK cells at 72 hours post-injection, although it is difficult to draw a meaningful conclusion based on these small differences, seen only at the 72-hour timepoint. Possibly the EV CAR NK are cleared from the circulation more rapidly, due to their inability to bind to a MICA target. Upon dissection of the lungs, we saw clear metastatic lesions on the surface of the lungs (Figure 4C). The resolution of the PET images used is ~ 1.4 mm, which makes it difficult to visualize positive signal in greater detail.

Discussion

MICA and MICB are Class I MHC-related proteins expressed on stressed and cancerous cells. Their presence can serve not only as a diagnostic marker of malignancies, but also as a possible target for therapy. While typical immunoglobulins exert their functional properties through Fc effector functions, their size compromises efficient tissue penetration. Nanobodies offer an appealing alternative to immunoglobulins for the purpose of launching an immune attack on MICA-positive tumors. We previously produced high affinity nanobodies, A1 and H3, that recognize the extracellular portion of MICA, alleles *008 and *009, on the surface of MICA⁺ B16F10 melanoma cells and MICA⁺ EL-4 T-cell lymphoma cells.

Adoptive cell transfer is widely explored as a possible cancer therapy. The success of VHH-based CAR T cells in tumor treatment has been recorded⁴⁷⁶, with the first VHH-based CAR T cell therapy (Carvykti) approved for treatment of relapsed or refractory multiple myeloma⁶⁰². Despite the success of CAR T cells, significant drawbacks and side-effects deserve consideration. T cells are often sourced from the patient's own peripheral blood and require expansion *ex vivo* after modification. CAR NK cells can be obtained from a wider range of sources, such as the patient's or a donor's peripheral blood, from placenta or umbilical cord blood, existing immortalized NK cell lines (NK-92) or manufactured from induced pluripotent stem cells (iPSC)²⁰⁵⁻²¹⁰.

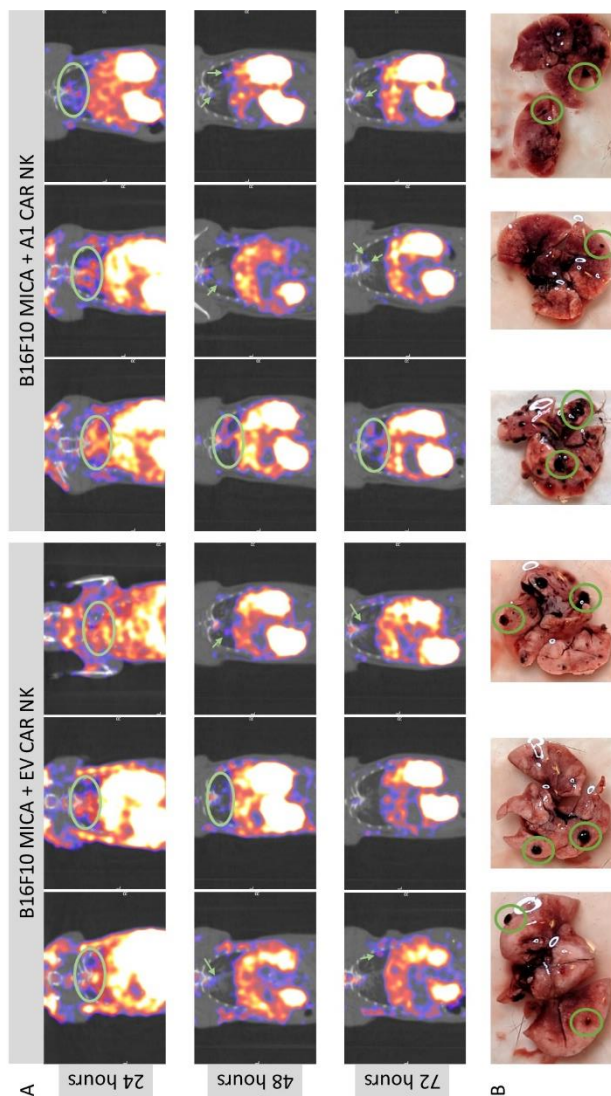


Figure 4. PET imaging to track localization of CAR NK cells to MICA⁺ lung metastases. (A) We injected C57/BL6 mice with B16F10 MICA⁺ cells by tail vein injection and allowed metastases to form for 15 days. On day 1 of imaging, EV and A1 CAR NK cells and ⁸⁹Zr-VHH₁₈₈ were injected retro-orbitally. We were able to localize the A1 CAR NK cells to the lungs of the mice that received B16F10 MICA⁺ tumors up to 72 hours after NK cell injection (circles and arrows). Little if any signal remained at the 72-hour timepoint for mice that received EV CAR NK cells. Regardless of the type of CAR NK cells transferred, strong PET signals were seen in the liver. In grayscale: CT density in HU (Hounsfield units), in color: PET intensity in Bq/mL. Coronal sections through the lungs are shown. For full images and intensity scales, see supplementary figure 9. For 3D videos, see 10.6084/m9.figshare.25471795. (B) We dissected the lungs of each mouse and observed metastases on the lung surface (several highlighted by circles).

A major reported side effect of CAR T therapy is cytokine release syndrome (CRS), a systemic inflammation caused by excessive secretion of cytokines such as IL-2 and IL-6 released by the CAR T cells. Other immune cells may respond to cytokines produced by the CAR T cells and also contribute to pathology. Most of the cytokines released by NK cells (IL-3, and TNF- α) do not induce such inflammation, and thus are less likely to cause CRS²¹⁷, although CRS due to overexpression of IFN- γ has been reported in a patient receiving CAR NK cells, thus careful monitoring is still required⁶⁰³. For these reasons, CAR NK cell therapy is potentially a more effective and safer alternative to CAR T cell therapy.

Here, we developed VHH_{MICA}-based CAR NK cells that target and selectively kill MICA⁺ B16F10 and MICA⁺ EL-4 cells *in vitro*. Immuno-PET shows that the A1 CAR NK cells localize to the lungs of mice bearing MICA⁺ B16F10 lung metastases. We see such localization until 72 hours post injection. The CAR NK cells are also cytotoxic towards MICA⁺ B16F10 cells *in vivo*. MICA⁺ B16F10 tumor-bearing mice treated with A1 CAR NK cells show a significant reduction in the rate of tumor growth and increase in overall survival compared to mice treated with EV CAR NK cells.

We recognize the limitation of using mouse-derived cancer cells that have been rendered MICA-positive by transfection. A major constraint is the availability of patient-derived cancer cell lines that not only express the correct alleles of MICA but that are also suitable for transplantation. Using such lines for engraftment of immunocompetent mice poses a risk of a possible xenogeneic response independent of MICA expression, and thus requires the use of immunodeficient recipients.

Although MICA is generally absent from healthy tissue, expression of MICA is seen in gut epithelium, although primarily intracellularly^{604,605}. Since gut epithelia are capable of rapid repair, this risk may be manageable, should MICA-specific CAR NK cells indeed attack gut epithelia. Nevertheless, since mice do not possess a MICA homolog, the use of MICA-transgenic mice⁶⁰⁶ might allow an assessment of any “off-tumor, on-target” effects when using MICA-targeting CAR NK cells.

The genetic instability of NK-92 cells requires their irradiation prior to infusion in a patient, which impairs their proliferation and limits their persistence *in vivo*⁶⁰⁷. Patient-specific induced pluripotent stem cell-derived NK cells (iPSC-NKs) may be better for CAR T and CAR NK cell therapy.

iPSC-NK cells express the CD16 Fc receptor and are thus capable of antibody-dependent cellular cytotoxicity (ADCC)^{207,608–610}.

Despite excellent results in the treatment of certain hematological cancers, the efficiency of CAR treatment in solid tumors remains poor. The CARs used in this study are based on what is referred to as a “second-generation” CAR, which includes a CD3 ζ signaling domain and CD28 co-stimulatory domain. Possible improvements to this CAR design include the addition of a cytokine auto-stimulation domain, such as IL-15^{611,612}. Third- and fourth-generation CARs employ additional co-stimulatory domains such as CD27 or STAT3/5 binding motifs. Other modifications, such as enhanced CD28 signaling domains or the inclusion of ITAMs 2 and 3 in CD3 ζ may increase the stability of CAR cells and thus show better tumor control *in vivo*⁶¹³.

The tumor microenvironment often shows deposition of extracellular matrix (ECM) components and may cause encapsulation of a solid tumor that limits access to the tumor for CAR T or CAR NK cells. Instead of CAR T or CAR NK cells, MICA-specific CAR macrophages might help degrade the ECM by secretion of proteases and improve the outcome of immunotherapy^{614–619}. Because VHH A1 and VHH H3 recognize different epitopes on MICA⁵⁷⁵, we could use H3-based CAR macrophages to help degrade the ECM and attract A1-based CAR NK cells to aid in tumor-specific cytotoxicity, without the different cell types competing for binding to MICA.

Conflict of Interest

The authors declare that the research was conducted in the absence of any commercial or financial relationships that could be construed as a potential conflict of interest.

Author Contributions

The authors confirm their contribution to the paper as follows: E.R.V and H.L.P designed the study and supervised data collection. E.R.V and W.v.K designed and produced the CAR NK cells. E.R.V and A.K. performed research with the CAR NK cells. T.B provided guidance on PET imaging and the work with the anti-transferrin receptor nanobody. E.R.V. and H.L.P. wrote the paper. All authors reviewed the results and approved the final version of the manuscript.

Acknowledgments

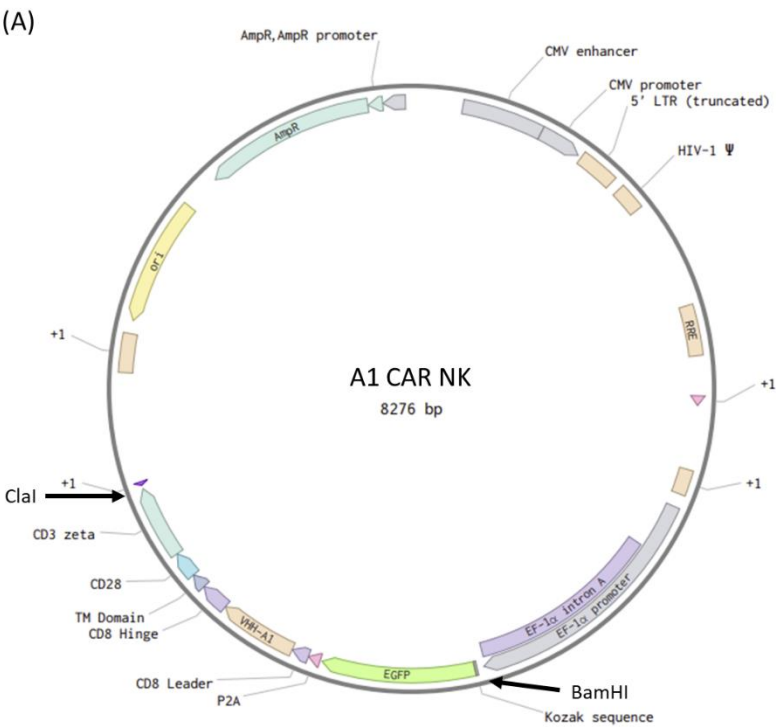
This research was supported by the NIH Pioneer Grant (DP1AI150593-05). T.B. was supported by fellowships from the Belgian American Educational Foundation and from Wallonie-Bruxelles International (WBI.World). We

gratefully acknowledge Dr. Maarten Dewilde (KU Leuven) and Dr. Bart De Strooper (KU Leuven) for providing VHH188. We gratefully acknowledge Dr. Ryan Alexander for helpful discussions regarding the CAR NK production, Dr. Xin Liu for helpful discussions and performing tail vein injections in mice, and Claire Carpenet, MSc, for guidance with PET imaging and PET imaging data analysis.

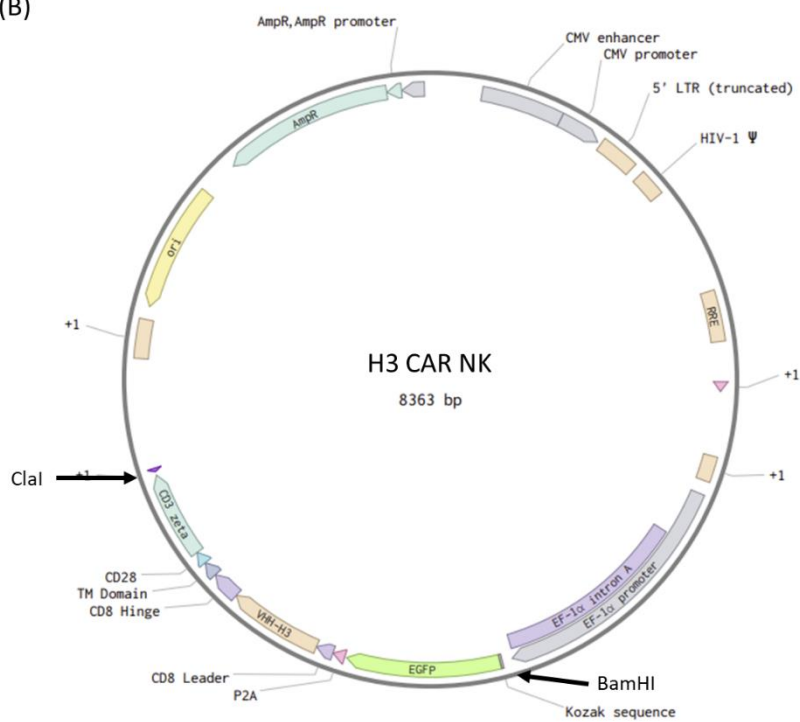
Data availability

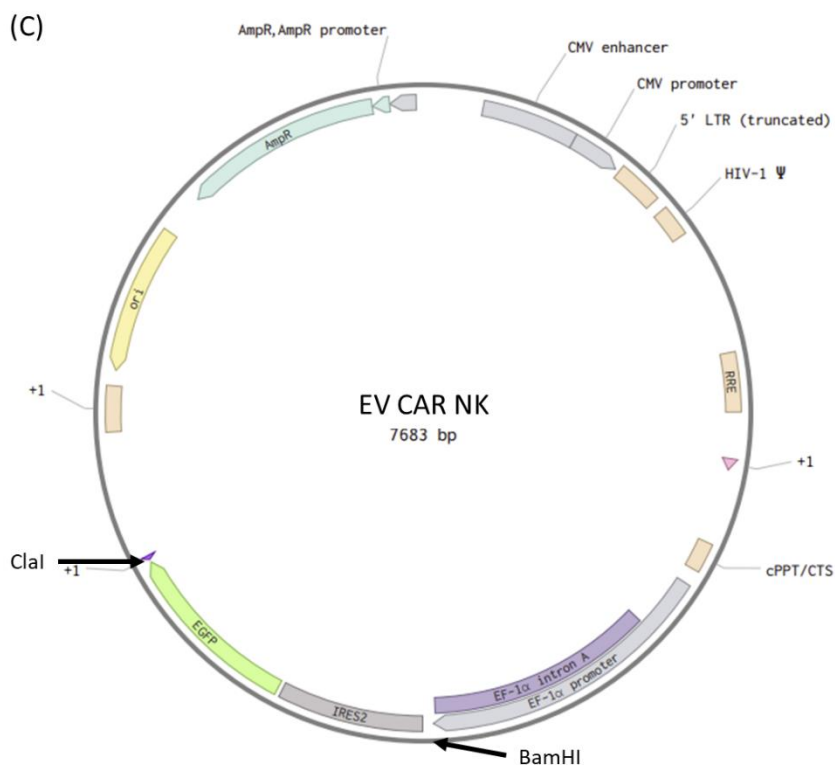
All data is included in the manuscript and supporting information. 3D videos of PET/CT imaging available at [10.6084/m9.figshare.25471795](https://doi.org/10.6084/m9.figshare.25471795). All data underlying this publication, including but not limited to raw data, designs, diagrams, data files, statistical records, unique materials, graphs, and other research data will be available upon request.

Supplementary figures

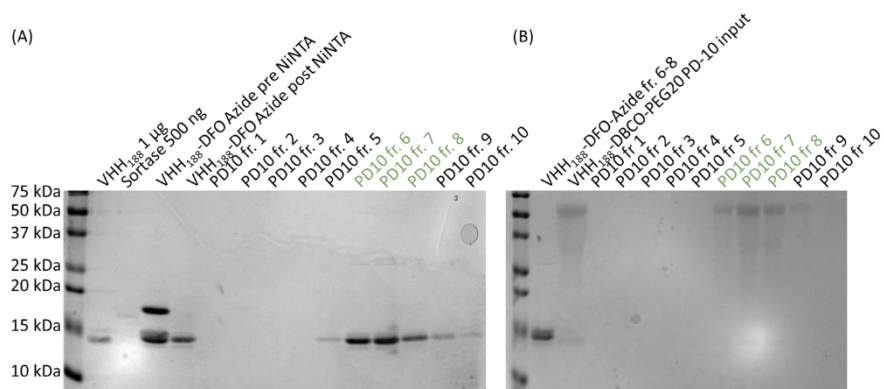


(B)

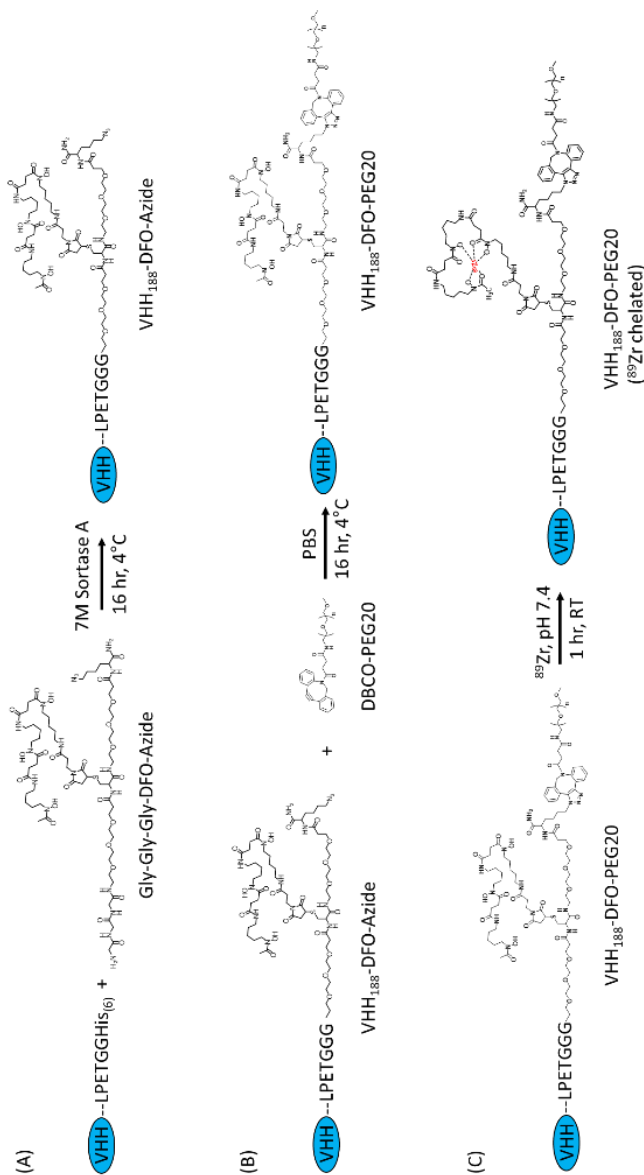




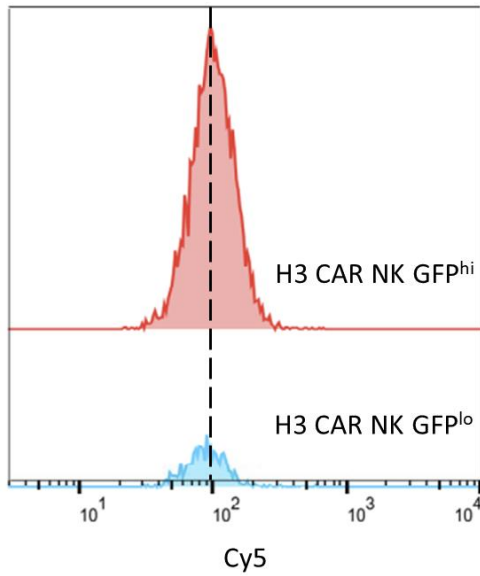
Supplementary figure 1. Lentiviral vector maps used for the transduction of NK-92 cells. We designed a GBlockTM gene fragment that encodes for EGFP, followed by a P2A proteolytic processing site separating the EGFP from the CAR. The CAR antigen recognition domain is encoded by the amino acid sequence of VHH A1 (A) or VHH H3 (B), separated by a CD8 hinge from the transmembrane segment and the cytoplasmic signaling and costimulatory domains of CD28 and CD3ζ. The gene fragments were inserted into a Lentiviral backbone with the mammalian EF-1α promoter by 'sticky-end' cloning using the BamHI and ClaI restriction enzymes (both from New England Biolabs). For the empty vector (EV) CAR NK-92 cells, we transduced NK-92 cells with the unmodified lentiviral vector containing only the EGFP cassette (C).



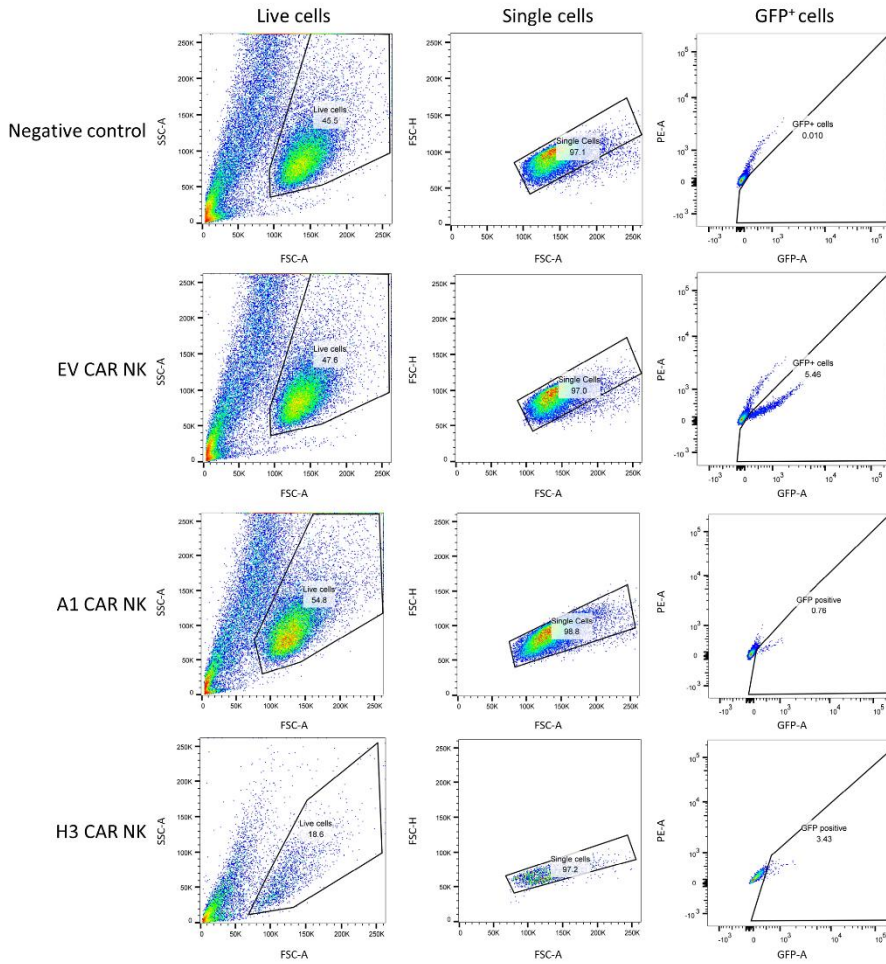
Supplementary figure 2. Preparation of VHH₁₈₈-DFO-PEG₂₀ for labeling with ⁸⁹Zr to be used in PET imaging. (A) We installed DFO-Azide on VHH₁₈₈, a nanobody targeting the human transferrin receptor found on the NK cells, with a sortase reaction. The reaction was depleted of unreacted nanobody and sortase, both containing a (His)₆-tag, on a NiNTA matrix. The reaction was depleted of unreacted DFO-Azide using a PD-10 desalting column. (B) Fractions 6, 7, and 8 were used to install DBCO-PEG₂₀ on the nanobody by means of a click-reaction between the DBCO and Azide. The reaction was depleted of unreacted DBCO-PEG₂₀ with a PD-10 desalting column. Fractions 6, 7, and 8 were combined for labeling with ⁸⁹Zr.



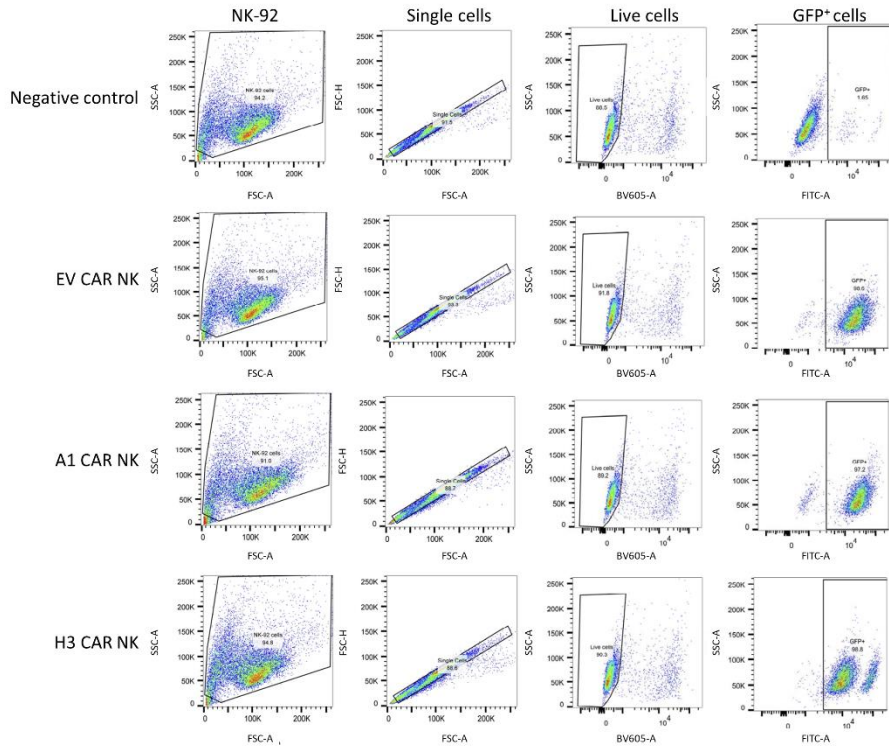
Supplementary figure 3. Schematic overview of the production of VHH₁₈₈-PEG20-⁸⁹Zr. (A) We ligated GGG-DFO-Azide to VHH₁₈₈ by sortase-mediated transpeptidation. We incubated the nanobody, containing a C-terminal LPETGG sortase motif and (His)₆-tag, with a 10-fold molar excess of GGG-DFO-Azide and 35 μM “7M Sortase A, overnight at 4°C. The reaction mixture was depleted of unreacted VHH and Sortase, both containing a C-terminal (His)₆-tag, on a NiNTA matrix. Free nucleophile was eliminated by desalting on a PD-10 column. (B) To extend the half-life of the nanobody in vivo, the nanobodies were PEGylated by incubation with a 10-fold molar excess of DBCO-PEG20 overnight at 4°C. (C) ⁸⁹Zr was neutralized to a pH of 7.4 by addition of 2M Na₂CO₃ and 1M HEPES. Nanobodies were labeled with ⁸⁹Zr by DFO-mediated chelation in chelexed PBS.



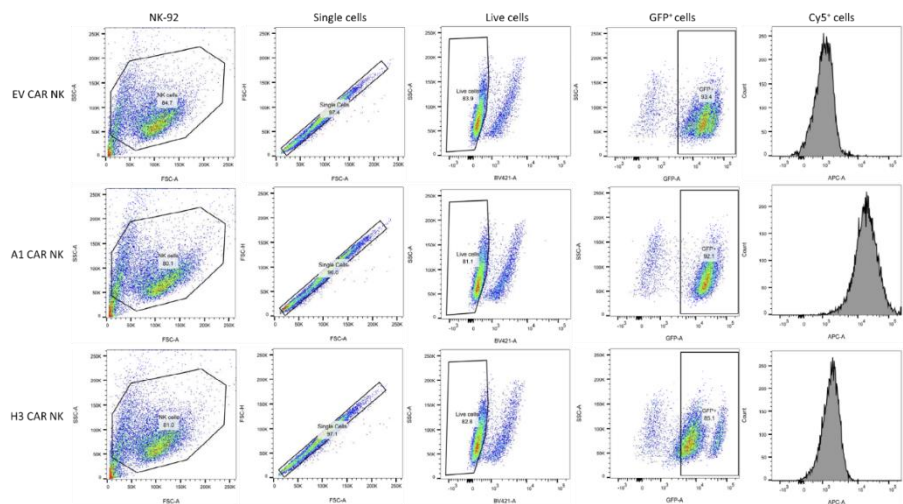
Supplementary figure 4. H3 CAR NK Cy5 expression based on dividing the CAR NK cells in a GFP^{hi} and GFP^{lo} population. We stained cells with Cy5-conjugated recombinant MICA (1 μ g/mL) for 30 minutes on ice. We determined viability with LIVE/DEAD Cell stain (1:200). Both populations show similar signal in the Cy5 channel.



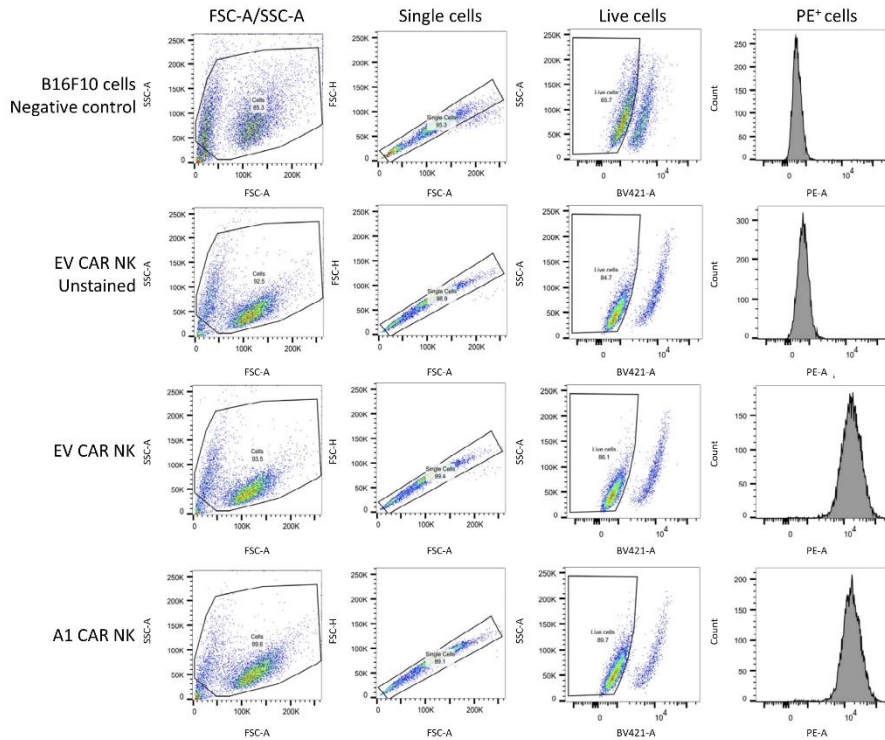
Supplementary figure 5. Gating strategy for the sorting of CAR NK-92 cells. Due to transduction on different days all cell lines (EV, A1, and H3 CAR NK-92) were sorted on different days, but we used comparable gating for all samples. A negative (untransduced) control was added for each sample, here the negative control used for sorting of EV CAR NK-92 cells is shown. First, we gated on live cells determined by FSC and SSC. Next, we gated on singlets, determined by FSC-H and FSC-A. We sorted the GFP-positive cells based on a gate set for the negative (untransduced) control cells.



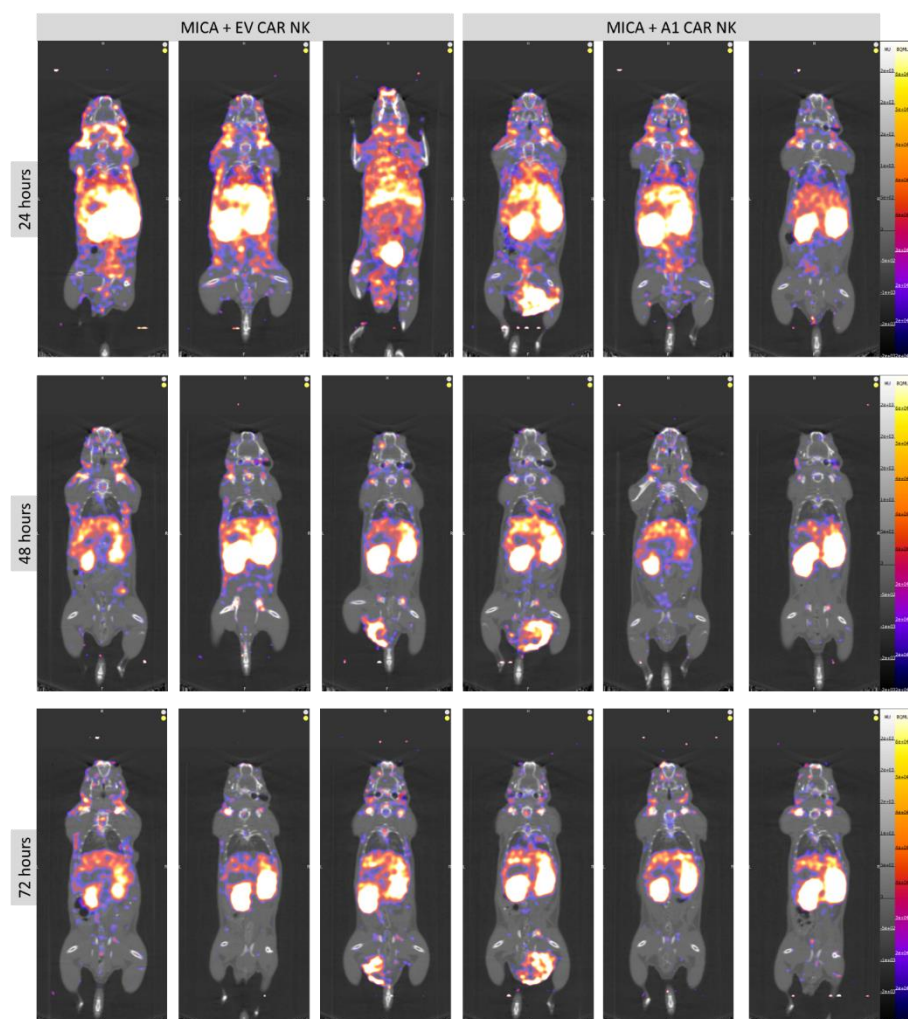
Supplementary figure 6. Gating strategy for determining stability of sorted CAR NK-92 cells. A negative (untransduced) control was used to determine the GFP-negative population. Cells were stained with propidium iodide to determine viability. First, we selected the cells based on FSC and SSC. Next, we gated on singlets, determined by FSC-H and FSC-A. We measured GFP expression in the FITC channel on live cells, which stain negative in the BV605 channel.



Supplementary figure 7. Gating strategy for determining extracellular expression of nanobody-based CAR construct. We stained cells with Cy5-conjugated recombinant MICA (1 $\mu\text{g}/\text{mL}$) for 30 minutes on ice. We determined viability with LIVE/DEAD Cell stain (1:200).



Supplementary figure 8. Gating strategy for determining human transferrin receptor staining with VHH₁₈₈ on CAR NK-92 cells. We stained cells with biotinylated anti-transferrin receptor nanobody VHH₁₈₈ (1 µg/mL) and streptavidin-conjugated PE (2.5 µg/mL) and determined viability with LIVE/DEAD Cell stain (1:200). To ensure a positive signal is from binding of VHH₁₈₈, a control stained with only Strep-PE and viability dye was added for both cell lines (shown here for EV CAR NK-92). A murine B16F10 cell line, which should stain negative with VHH₁₈₈, was added as negative control. First, we selected the cells based on FSC and SSC and gated these cells on singlets, determined by FSC-H and FSC-A. We selected live cells that stained negative in the BV421 channel. We measured human Transferrin-receptor staining in the PE channel.



Supplementary figure 9. Full-body immuno-PET images with ^{89}Zr -labeled VHH_{188} of mice injected with EV CAR NK or A1 CAR NK at $t = 24$ hours, 48 hours, and 72 hours after injection. Coronal sections through the lungs are shown here. In grayscale: CT density in HU (Hounsfield units), in color: PET intensity in Bq/mL.

Chapter 6:

Nanobody-based CAR T cells for selective cytotoxicity towards MICA⁺ cancer cells in vitro

Elisha R. Verhaar^{1,2}, Anouk Knoflook¹, Ryan Alexander¹, Hidde L. Ploegh^{1,2}

¹Program in Cellular and Molecular Medicine, Boston Children's Hospital,
Harvard Medical School, Boston, MA 02115, USA

²Department of Cell and Chemical Biology, Leiden University Medical Centre,
Leiden, The Netherlands

Unpublished data

Abstract

The stress-induced surface glycoproteins MICA and MICB are MHC-I related proteins that are upregulated on the surface of virus-infected cells or malignant cells. MICA and MICB act as ligands for NKG2D, one of the activating receptors on NK cells, CD8⁺ T cells, and $\gamma\delta$ T cells. When MICA binds to NKG2D, these cytotoxic immune cells become activated and can eradicate the MICA/B-positive targets through cytotoxicity and secretion of cytokines. Nanobodies, also referred to as VHHs, are the variable regions of camelid heavy chain-only immunoglobulins. We previously created nanobodies that recognize MICA and used these nanobodies as building blocks for the construction of chimeric antigen receptors (CAR) for expression in human CAR NK-92 cells. Here, we use these nanobodies to establish VHH-based CAR T cells and show that these cells recognize and selectively kill MICA positive tumor cells *in vitro*.

Introduction

The MHC class I chain-related proteins A and B (MICA and MICB) are upregulated on the surface of human cells undergoing stress, for instance due to virus infection or malignant transformation²²⁴. MICA/B are ligands for NKG2D, an activating receptor on NK cells, CD8⁺ T cells, and $\gamma\delta$ T cells, which can eradicate MICA-positive targets through cytotoxicity and secretion of cytokines²¹⁸. Elevated levels of MICA/B on the surface of hematopoietic and epithelial solid tumors are associated with better prognosis^{225–231}.

Nanobodies, or VHHs, are the recombinantly expressed variable regions of camelid heavy chain-only immunoglobulins³⁰¹ which are characterized by their solubility, stability, and ease of production^{309–311}. Due to their small size of 15 kD (versus 150 kD for conventional full-sized antibodies), nanobodies have a short circulatory half-life and show excellent tissue penetration. Nanobodies are attractive building blocks for the construction of chimeric antigen receptors for cell-based therapies^{210,474–478,546–551}.

We have developed nanobodies, VHH A1 and VHH H3, that target MICA on the surface of tumor cells. We used these nanobodies to establish anti-MICA VHH-based CAR NK-92 cells and showed that these cells recognize and selectively kill MICA positive targets *in vitro* and *in vivo*⁶²⁰.

Although CAR NK cells may have an advantage in terms of safety and versatility, research on CAR NK cell-based therapy is still in the early stages of development. CAR T cell therapy has been more widely studied, with several CAR T cell therapies approved for treatment of hematopoietic cancers, such

as relapsed or refractory B-cell lymphoma or acute lymphatic leukemia based on CD19 targeting (Axicabtagene ciloleucel, brexucabtagene autoleucel, lisocabtagene maraleucel, and tisagenlecleucel), and relapsed or refractory multiple myeloma, based on B-cell maturation antigen (BCMA) targeting (idecabtagene vicleucel and ciltacabtagene autoleucel)²⁰². Here, we report the generation of nanobody-based CAR T cells that recognize and selectively kill MICA⁺ cells *in vitro*.

Materials and methods

Cell culture

MICA-expressing B16F10 murine melanoma cells and EL-4 T cell lymphoma cells, and their wild type (WT) counterparts, were a gift from K. Wucherpfennig (Dana Farber Cancer Institute). B16F10 cells and HEK293T cells were both cultured in complete DMEM (high glucose DMEM supplemented with 10% fetal bovine serum (FBS) and 100 U/mL penicillin/streptomycin). To avoid proteolytic cleavage of membrane-bound MICA, we dissociated the adherently grown B16F10 cells from the plates using an EDTA-based versene solution (Gibco). EL-4 cells were cultured in complete RPMI 1640 (RPMI 1640 supplemented with 10% FBS + 100 U/mL penicillin/streptomycin). Mouse primary T cells were cultured in BMDC medium (RPMI 1640 supplemented with 10% FBS, 1mM sodium pyruvate, 10 mM MEM-NEAA, 50 mM β -mercaptoethanol, and 100 U/mL penicillin/streptomycin). To ensure active cell proliferation, 100 IU/mL murine IL-2 (Peprotech) was added. All cells were cultured to maintain optimal densities, unless otherwise specified, and incubated at 37°C in a humidified 5% CO₂ atmosphere.

Mice

C57BL/6J mice were purchased from the Jackson Laboratory or bred in-house. Mice were used at 8-12 weeks of age. Experiments were performed in accordance with the guidelines of the Institutional Animal Care and Use Committee (IACUC) of Boston Children's Hospital. Mice were housed under specific pathogen-free conditions in a controlled environment with a 12-hour light-dark cycle and ad libitum access to standard laboratory chow and water. Health status and welfare of the mice were monitored regularly throughout the study.

VHH CAR construct design and virus production

We designed a GBlockTM Gene fragment that encodes GFP, followed by a P2A proteolytic processing site to separate the GFP portion from the CAR itself. The CAR antigen recognition domain is encoded by the amino acid sequence of VHH A1 or VHH H3, separated by a hinge from the transmembrane segment of CD8 and the cytoplasmic signaling and costimulatory domains of CD28 and CD3 ζ . The gene fragments for the CAR were inserted by 'sticky-end' cloning into a retroviral backbone with a mammalian MSCV promoter, modified in-house to include the desired sticky-end restriction sites (MSCV-IRES-GFP was a gift from Tannishtha Reya (Addgene plasmid #20672; <http://n2t.net/addgene:20672>; RRID: Addgene_20672). For retroviral production, we transfected HEK-293T cells with 7.5 μ g of CAR plasmid and 7.5 μ g of pCL-Eco (pCL-Eco was a gift from Inder Verma (Addgene plasmid #12371; <http://n2t.net/addgene:12371>; RRID: Addgene_12371⁶²¹) in 1000 μ l of OptiMEM. This DNA mixture was added to 500 μ l of OptiMEM with 45 μ l of TransIT[®]-LT1 (Mirus Bio LLC) and incubated for 30 minutes at room temperature. The mixture was added to ~70% confluent HEK293T cells in 10mL of DMEM + 10% FBS and retrovirus was harvested 48 hours after transfection.

Isolation of mouse T cells

Freshly isolated and transduced T cells were used for each CAR T cell experiment. T cells were isolated from the spleens of 8- to 12-week-old C57/B6 mice. Spleens were collected aseptically, homogenized, and filtered through a 40 μ m cell strainer. Red blood cells were lysed with 0.8% ammonium chloride for 10 minutes on ice. T cells were isolated using the Dynabeads Untouched T cell isolation kit (Invitrogen) according to manufacturer's protocol. T cells were resuspended at 1×10^8 cells/mL in isolation buffer (PBS with 2% FBS and 2mM EDTA). Heat-inactivated FBS (200 mL) and 200 mL antibody mix was added and incubated on ice for 20 minutes. Cells were washed with and resuspended in isolation buffer and added to the Mouse Depletion DynabeadsTM. The cell-bead mixture was incubated for 15 minutes at room temperature on a rotating platform and diluted with isolation buffer prior to placement in a neodymium magnet for 2 minutes to retrieve the magnetic beads. The supernatant containing the untouched T cells was transferred to a fresh tube. T cells were activated with DynabeadsTM Mouse T-Activator CD3/CD28 (Invitrogen) at 1 ml of beads per 40,000 cells. Cells were cultured at 1.5×10^6 cells per mL in BMDC medium with murine IL-2 (100 IU/mL) until further applications.

Retroviral transduction and selection of transduced murine T cells

For T cell transduction, a non-tissue culture treated, plastic bottom 6-well plate was coated with RetroNectin® according to the manufacturer's directions. Retroviral particles were adsorbed to the plate by centrifugation for 2 hours at 2000xg at 30°C. Viral supernatant was removed and T cells were added to the well and transduced by centrifugation for 1-1.5 hours at 2000xg at 30°C. After 24 hours the expression of GFP was measured by flow cytometry. If a transduction efficiency of at least 25% was achieved, CAR T cells were then used for further experiments.

***In vitro* cytotoxicity and cytokine production assays**

For co-culture experiments, 3×10^5 WT or MICA⁺ B16F10 or WT or MICA⁺ EL-4 cells were plated per well on a tissue culture-treated 96-well flat-bottom plate in complete RPMI supplemented with IL-2 (50 IU/ml). A1 CAR T cells or untransduced T cells were added to each well at different effector-to-target [E:T] ratios, keeping the number of target cells constant and varying the number of effector cells. After 24 hours, the IFN- γ concentration in the medium was determined using a mouse IFN- γ ELISA kit (ThermoFisher scientific, #88-7314-22) according to the manufacturer's instructions. Relative cell death was determined with a lactate dehydrogenase (LDH) Cytotoxicity Assay (Abcam, Ab65393) performed according to the manufacturer's instructions.

Results

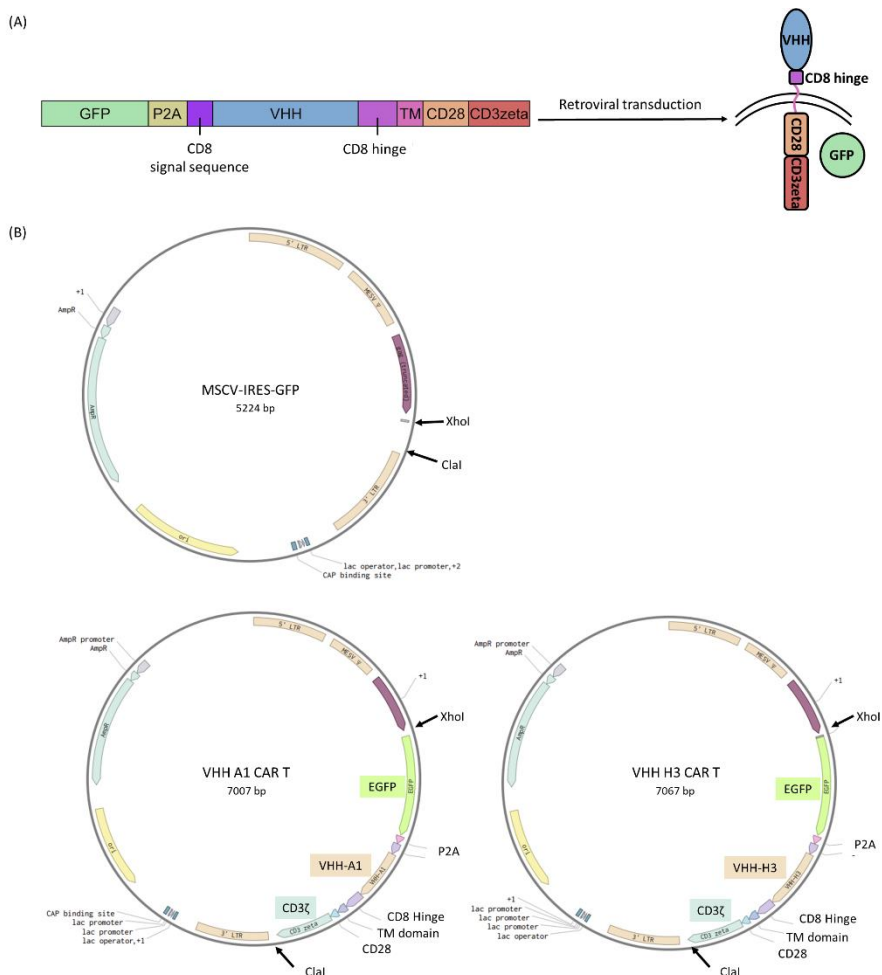
Transduction with retroviral VHH-based CAR constructs yielded MICA-specific CAR T cells

Design of CAR T cells was based on previously established VHH-based CAR T cells⁴⁷⁶. We designed a GBlock™ Gene fragment that encodes GFP followed by a P2A domain separating the actual CAR construct. The extracellular CAR antigen recognition domain is encoded by the amino acid sequence of VHH A1 or VHH H3, separated by a hinge from the transmembrane segment and the cytoplasmic signaling and costimulatory domains of CD28 and CD3 ζ (Figure 1A). The gene fragments for the CAR were inserted by 'sticky-end' cloning into a retroviral backbone carrying a mammalian MSCV promoter (Figure 1B) and used for retroviral production in HEK-293T cells. We transduced freshly isolated T cells from mouse splenocytes by spinoculation using RetroNectin® reagent. Cells bearing these VHH-based CARs will be referred to as A1 and H3 CAR T cells. As a negative control for CAR T cells, we used untransduced T cells that underwent the same transduction protocol but in the absence of retrovirus. Because primary T cells have a finite lifespan

in culture, we produced a fresh batch of transduced T cells for each experiment. On average, we observed a transduction efficiency between 25% and 50% for A1 CAR T cells and between 20% and 30% for H3 CAR T cells. Flow cytometry data for one representative transduction are shown in Figure 1C.

A1 CAR T cells are activated by and selectively kill MICA⁺ tumor cells

We incubated A1 and H3 CAR T cells, or untransduced T cells as negative control, with WT B16F10 or EL4 cells, or B16F10 or EL4 cells that stably express MICA at different effector to target ratios ([E:T]), keeping the amount of target cells constant and varying the number of effector cells.



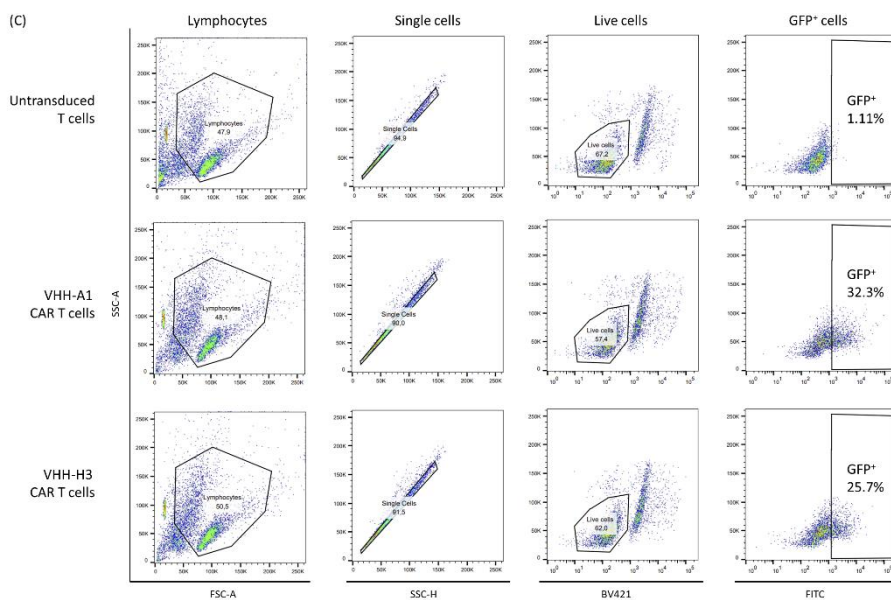


Figure 1. Design of the CAR construct and production of CAR T cells. (A) Schematic overview of the CAR construct as transduced into the mouse primary T cells. We ordered GBlock™ gene fragments encoding for EGFP, followed by a P2A proteolytic cleavage domain separating the EGFP from the CAR construct. The CAR construct contains the amino acid sequence of VHH A1 or VHH H3 as extracellular targeting domain, and the costimulatory and activation domains of CD28 and CD3ζ. (B) We used a retroviral backbone with a mammalian MSCV promoter, modified in-house to contain XhoI and ClaI restriction sites. We cloned the GBlock™ gene fragments with ‘sticky-end’ cloning. These plasmids were used to create retrovirus for the transduction of isolated primary mouse T cells. (C) 24 hours after transduction, we determined the transduction efficiency by flow cytometry. Viability was determined using the LIVE/DEAD Fixable Dye (Invitrogen). We used T cells that underwent the same retroviral transduction protocol, but in the absence of retrovirus, as negative control. GFP positive cells were deemed transduced successfully. If a transduction efficiency of >25% was reached, cells were used for downstream applications.

We measured cell death by determining the release of lactate dehydrogenase (LDH) in the culture medium. We normalized the level of cytotoxicity by subtracting the LDH released by the T cells due to reduced viability, determined by using wells containing only T cells at the appropriate cell densities. At a [E:T] ratio of [15:1], we observe significant cell death of the MICA⁺ B16F10 cells when co-cultured with A1 CAR T cells. We do not observe significant cell death when co-culturing the B16F10 WT cells with A1 CAR T cells. We do not observe significant cell death in MICA⁺ cells when co-cultured with untransduced T cells, or when co-cultured with H3 CAR T cells. For the MICA⁺ EL-4 cells, we observed significant cell death when co-cultured

with A1 CAR T cells at an [E:T] of [5:1] and [15:1]. We do not observe significant cell death in EL-4 WT cells co-cultured with A1 or H3 CAR T cells, or EL-4 MICA⁺ cells co-cultured with untransduced T cells (Figure 2A).

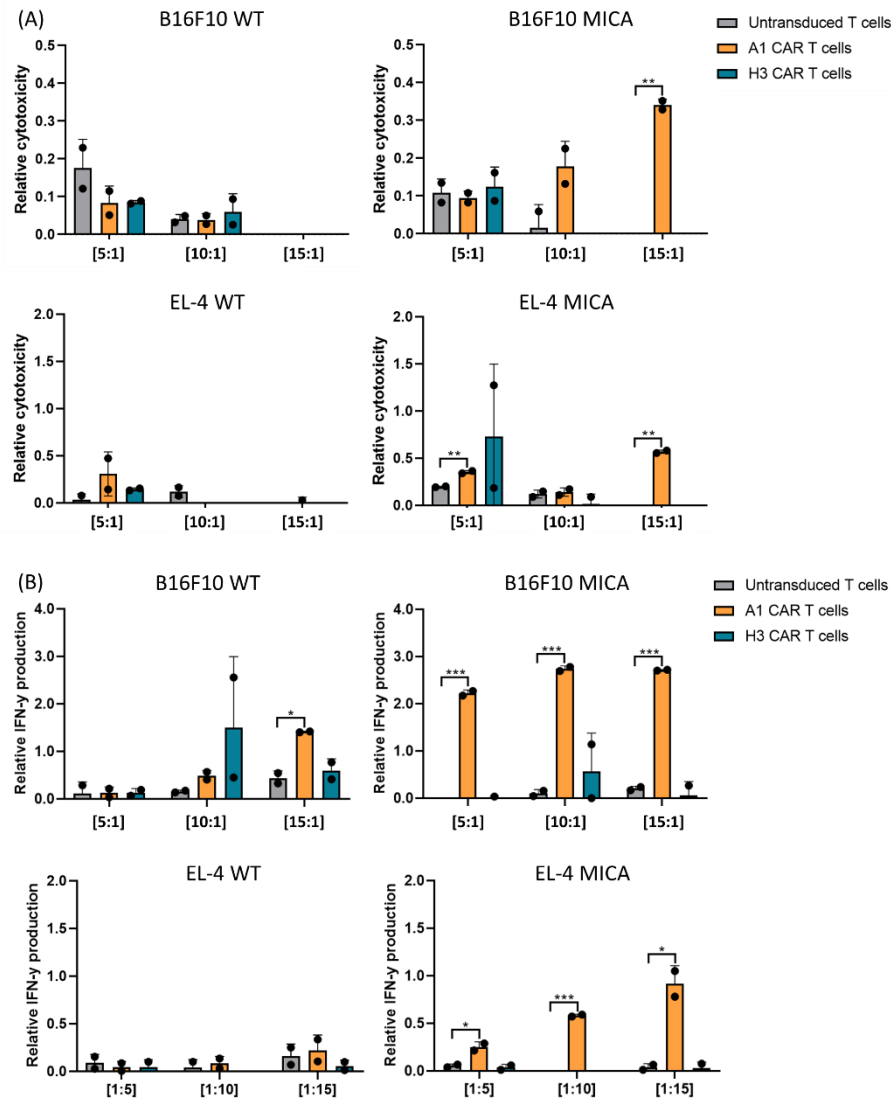


Figure 2. In vitro cytotoxicity of CAR T cells co-cultured with MICA⁺ targets.
LEGEND CONTINUES ON THE NEXT PAGE.

We incubated untransduced T cells, and A1 and H3 CAR T cells with WT B16F10 or EL-4 cells, or B16F10 or EL-4 cells that stably express MICA. We incubated for 24 hours at effector-to-target ratios [E:T] of [5:1], [10:1], or [15:1], keeping the number of target cells consistent and varying the number of effector cells. (A) Cytotoxicity was determined by measuring the LDH released in the medium. LDH concentration was normalized for the concentration of LDH released by the T cells alone due to reduced viability. At an [E:T] ratio of [15:1], we observe significant cell death of the MICA⁺ cells when co-cultured with A1 CAR T cells ($p = 0.01$). We observe significant cell death of EL-4 MICA⁺ cells when co-cultured with A1 CAR T cells at an [E:T] of [5:1] ($p = 0.007$) and [15:1] ($p = 0.001$). We observe no significant cell death in MICA⁺ cells when co-cultured with untransduced T cells. No significant increase in cell death was observed when WT B16F10 or EL-4 cells were co-cultured with untransduced T cells, or A1 or H3 CAR T cells. (B) The relative levels of IFN γ were determined by sandwich ELISA with a matched murine IFN γ antibody pair. We observed significant increase in IFN γ secretion in the A1 CAR T cells when co-cultured with B16F10 and EL-4 MICA⁺ cells at all [E:T] ratios (B16F10 MICA⁺: [5:1] $p = 0.0005$; [10:1] $p = 0.0007$; [15:1] $p = 0.0002$, EL-4 MICA⁺: [5:1] $p = 0.04$; [10:1] $p = 0.0003$; [15:1] $p = 0.02$). No significant release of IFN γ was observed in untransduced T cells or H3 CAR T cells co-cultured with any type of target cell, or A1 CAR T cells co-cultured with WT B16F10 or EL-4 cells. All significance was determined with multiple T-test.

To attribute the cytotoxicity to effector cell activation, we measured the secretion of IFN γ in the culture medium. We normalized IFN γ secretion by subtracting the spontaneous IFN γ secretion by the T cells, determined by using wells containing only T cells at the appropriate cell densities. We observed a significant increase in IFN γ secretion by A1 CAR T cells when co-cultured with B16F10 MICA⁺ cells and EL-4 MICA⁺ cells at all [E:T] ratios, but not when co-cultured with WT cells (Figure 2B). We did not see activation of H3 CAR T cells in the presence of either WT or MICA⁺ target cells. Our previous data shows less cytotoxicity for the H3 CAR NK-92 cells as well, likely due to the lower expression of the H3-based CAR⁶²⁰. Although we have not determined and compared the CAR expression levels for the A1 and H3 CAR T cells, the data for H3-based CAR T cells is consistent with the previous findings for H3-based CAR NK cells.

Discussion

The Class I MHC-related proteins MICA and MICB, expressed on the surface of cells undergoing stress, can serve as both a diagnostic marker for certain cancers, and as a target for cancer therapy. We have produced high-affinity nanobodies A1 and H3, both of which target MICA on the surface of cells⁵⁷⁵. Nanobodies have been used as the targeting portion of CAR T cells, with the first nanobody-based CAR T cell (Carvykti) approved for treatment of relapsed or refractory multiple myeloma⁴⁷⁶.

We have shown that the MICA-targeting nanobodies VHH-A1 and VHH-H3 can serve as antigen-recognition domains in CAR NK cells⁶²⁰. While advantages of using CAR NK cells over CAR T cells for therapy have been claimed^{217,622}, the success of CAR T cell therapy makes the production of nanobody-based CAR T cells an interesting possibility. Here, we developed VHH-based CAR T cells by retroviral transduction of T cells isolated from the spleens of mice. When co-culturing these CAR T cells with WT or MICA⁺ cells of the murine-derived B16F10 melanoma line or EL-4 T-cell lymphoma line, we observed an increase in cytotoxicity of the MICA⁺ cells compared to the WT cells, when co-cultured with high doses of A1 CAR T cells. Furthermore, we see a dose-dependent increase in IFN- γ release in the A1 CAR T cells co-cultured with MICA⁺ B16F10 or EL-4 cells, compared to WT B16F10 or EL-4 cells. We see no such effect when co-culturing these cells with untransduced T cells. These results indicate that the A1 CAR T cells selectively target and kill MICA⁺ B16F10 and MICA⁺ EL-4 cells *in vitro*.

Although the *in vitro* data are promising, the efficacy of these VHH-based CAR T cells *in vivo* remains to be tested. A major limitation is the relatively low transduction efficiency of the T cells. Despite extensive troubleshooting steps, we have been unable to reach a transduction efficiency of, on average, more than 35%. Our method of isolation of T cells from splenocytes does not discriminate between CD4⁺ and CD8⁺ T cells, only the latter of which are responsible for cytotoxicity. Because the T cell fraction of mouse splenocytes consists for ~20% of CD8⁺ T cells⁶²³, we hypothesize that the total population of VHH-based CAR T cells capable of cytotoxicity may be no more than ~7%. This number limits the effectiveness of CAR T cell-based cytotoxicity *in vitro*, since high [E:T] are necessary to obtain an effective dose.

For *in vivo* experiments, it may be necessary to increase the number of cytotoxic CAR T cells transferred. Considering that 5×10^6 successfully transduced CAR NK-92 cells were effective at eliminating MICA⁺ tumors *in vivo*⁶²⁰, it would be desirable to attain a similar number of successfully transduced CD8⁺ CAR T cells. Based on transduction efficiency, we need to inject $\sim 72 \times 10^6$ cells per mouse per injection. Each spleen yields approximately 40×10^6 T cells, thus requiring several spleens as the starting material. At 3 injections per week, treatment of one mouse for one week requires the use of 6 spleens.

The troubleshooting steps we have undertaken have increased the average transduction efficiency from 12% to 35%, while simultaneously increasing cell viability. This improvement was mainly caused by switching from a

polybrene-based retroviral transduction to RetroNectin®, since polybrene is known to inhibit T cell viability⁶²⁴. We have also experimented with the addition of different stimulating cytokines, like varying concentrations of IL-2 and IL-15, the latter of which decreased the average cell viability and transduction efficiency.

An alternative option is to switch from retroviral to lentiviral transduction of T cells. Lentiviruses can infect non- or slowly dividing cells and establish long-term gene expression⁶²⁵. Lentiviral-based transduction has several other advantages, including a higher viral titer and virion stability, which could improve transduction efficiency.



Chapter 7:

A monoclonal antibody that recognizes a unique 13-residue epitope in the cytoplasmic tail of HLA-E

Elisha R. Verhaar^{1,2}, Jin Gan¹, Susan Buhl³, Ziao Li⁴, Amir Horowitz⁴, and
Hidde L. Ploegh^{1,2*}

¹Program in Cellular and Molecular Medicine, Boston Children's Hospital,
Harvard Medical School, Boston, MA 02115, USA

²Department of Cell and Chemical Biology, Leiden University Medical Centre,
Leiden, The Netherlands

⁴Department of Cell Biology, Albert Einstein College of Medicine, 1300 Morris
Park Avenue, NY 10461, USA

⁴Department of Oncological Sciences, Precision Immunology Institute, Tisch
Cancer Institute, Icahn School of Medicine at Mount Sinai,
New York, NY, USA.

Molecular Immunology

2024 June, in press

Article Reference: MIMM6935

Abstract

The Class I MHC molecule (MHC-I) HLA-E presents peptides that are derived from the signal sequences, either those of other MHC-I products, or of viral type I membrane glycoproteins. Monoclonal antibodies with proven specificity for HLA-E, and with no cross-reactions with other MHC-I products, have yet to be described. To obtain anti-HLA-E-specific antibodies suitable for a range of applications, we generated monoclonal antibodies against a unique feature of HLA-E: its cytoplasmic tail. We created an immunogen by performing an enzymatically catalyzed transpeptidation reaction to obtain a fusion of the cytoplasmic tail of HLA-E with a nanobody that recognizes murine Class II MHC (MHC-II) products. We obtained a mouse monoclonal antibody that recognizes a 13-residue stretch in the HLA-E cytoplasmic tail. We cloned the genes that encode this antibody in expression vectors to place an LPETG sortase recognition motif at the C-terminus of the heavy and light chains. This arrangement allows the site-specific installation of fluorophores or biotin at these C-termini. The resulting immunoglobulin preparations, labeled with 4 equivalents of a fluorescent or biotinylated payload of choice, can then be used for direct immunofluorescence or detection of the tag by fluorescence or by streptavidin-based methods. We also show that the 13-residue sequence can serve as an epitope tag, independent of the site of its placement within a protein's sequence. The antibody can be used diagnostically to stain HLA-E on patient tumor samples, as an antibody-epitope tag for extracellular proteins, and to research the unique role of the cytoplasmic tail of HLA-E.

Introduction

Class I MHC proteins are composed of a membrane-embedded glycoprotein heavy chain in tight, non-covalent association with the soluble light chain beta2-microglobulin. Class I MHC molecules (MHC-I) are found on the surface of all nucleated cells in vertebrates and present fragments of intracellular antigens in the form of peptides to CD8⁺ cytotoxic T lymphocytes (CTL) to enable elimination of intracellular pathogens. Virus-infected and malignantly transformed cells can escape immune cell recognition by down-regulation of MHC-I products, which can be achieved transcriptionally and post-transcriptionally⁶²⁶. MHC-I molecule HLA-E presents a unique case, as it is specialized in the presentation of peptides that are derived from the signal sequences of other MHC-I products, or of viral type I membrane glycoproteins²⁵²⁻²⁵⁹. HLA-E is frequently overexpressed on tumors and on virus-infected cells, where it serves as a ligand for CD94/NKG2A, -B, and -C on NK and T cells, thereby regulating their

cytotoxic activity^{258,269-277}. Thus, even if a virus were to succeed in down-regulation of the classical Class I HLA-A, -B and -C products to escape detection by CTLs, their signal peptides would continue to be produced and could serve as peptide cargo for HLA-E, rendering the infected cell more resistant to lysis by NK and T cells.

HLA-E-specific monoclonal antibodies have been used to detect expression in tumors and normal tissues, but the available reagents that are in wide use to detect HLA-E (3-D12 and MEM-E/o2) have been reported to cross-react with certain allelic products of the HLA-B and HLA-C⁶²⁷. Here, we set out to generate monoclonal antibodies that are specific for HLA-E, with no anticipated cross-reactions with conventional MHC-I products. The ectodomains of the MHC-I products, including those of HLA-E, are highly homologous. There are few locus-specific features present in the ectodomains that would allow an unambiguous assignment of a sequence to the HLA-A, -B or -C locus, and locus-specific tools for use in immunochemistry are comparatively rare⁶²⁸⁻⁶³². In contrast, the cytoplasmic tails of the classical MHC-I products do show locus-specific features, shared among virtually all alleles at that locus (Figure 1). The cytoplasmic tail of HLA-E is highly conserved and shows no allelic variation. The two known HLA-E alleles, HLA-E*01:01 and HLA-E*01:03, vary only by a single replacement substitution of an arginine to a glycine at position 107 in exon 3 (underscored in Figure 1)^{633,634}.

The cytoplasmic tail of MHC-I is involved in trafficking peptide-bound MHC-I from the endoplasmic reticulum to the cell membrane. In addition, the cytoplasmic tail is believed to play a role in the relocation of HLA-E to late and recycling endosomes^{281,282}. Antibodies against the HLA-E cytoplasmic tail would thus provide a useful tool for studying the cytoplasmic tail interactions, as well as for other purposes where detection of HLA-E is called for, such as staining of tumor tissues by conventional immunohistochemistry.

We used an immunization strategy that exploits a nanobody that targets mouse Class II MHC⁺ antigen presenting cells^{420,466,558} (VHH_{MHCII}) fused to the HLA-E C-terminal sequence (GGCSKA^{EW}SDSAQGS^{ES}HS^L, hereafter referred to as “HLA-E_{tail}”) by means of a sortase reaction^{553,635}. We obtained 23 monoclonal antibodies and selected three with unique sequences for further analysis. All of them recognize a 13-residue stretch in the HLA-E cytoplasmic tail.

To enhance the applicability of the HLA-E specific monoclonal antibody, we site-specifically modified the IgG molecules with 4 moles of fluorophore or biotin by installing sortase recognition motifs (LPETG) at the C-termini of its

IgG heavy and light chains, thus avoiding the need for secondary antibodies as staining agents. The monoclonal antibody detects HLA-E in immunoblots and immunoprecipitation on HLA-E positive cell lysates, formalin-fixed, paraffin-embedded tissue sections, and can be used for immunofluorescence and flow cytometry of permeabilized cells. The 13-residue sequence and the monoclonal antibody that recognizes it also serves as an effective epitope tag/detection pair, regardless of its location in the protein of interest, in an otherwise HLA-E negative environment. We show that antigen-specific elution with the synthetic cytoplasmic tail peptide is an effective means of retrieval of the tagged protein.

Figure 1. Alignment of the consensus amino sequences of HLA-E, -A, -B, -C, -F, and -G. In blue are highlighted the amino acids that differ from the consensus sequence. The ectodomains show very few locus-specific features to which antibodies could be directed. In contrast, the cytoplasmic tails of the classical Class I MHC products, highlighted in the black box, do show locus-specific features, and could therefore be used to generate HLA-E specific antibodies. The cytoplasmic tail of HLA-E is highly conserved and shows no allelic variation. The two known HLA-E alleles, HLA-E*01:01 and HLA-E*01:03, vary only by a single replacement substitution of an arginine to a glycine (underscored in figure)

Materials and methods

Sortase reactions to create VHH_{MHCII}-HLA-E_{tail}, GFP-HLA-E_{tail}, or 10-mer HLA-E_{tail} derivatives

Recombinant VHH_{MHCII} equipped with LPETG (an amino acid sequence recognized by sortase) and a (His)₆-tag was expressed by periplasmic expression in *Escherichia coli* WK6 (ATCC). Recombinant GFP-LPETG was expressed by cytoplasmic expression in *E. coli* BL21 (Thermo Scientific). The C-terminal (His)₆-tag allows purification of the recombinant proteins using Ni-NTA agarose beads (Qiagen), followed by FPLC purification on an S75 column by FPLC (ÄKTA, Cytiva Life Sciences). HLA-E cytoplasmic tail peptide was obtained from Genscript at ~85% purity. 10-mer peptides were produced by solid phase peptide synthesis and provided by the lab of Jacques Neefjes, Leiden University Medical Center. Each peptide carries an N-terminal Gly-Gly sequence to allow fusion to the VHH or GFP by means of a sortase reaction. Sortase reactions were performed in PBS at 4°C overnight with final reagent concentrations of 1 mg/ml protein, 500 mM GG-peptide, and 25 mM 7M-Sortase A⁵⁵³. Unmodified VHH_{MHCII} or GFP that retained the sortase motif, as well as 7M-Sortase A, all containing the (His)₆-tag, were removed by depletion on NiNTA beads for 20-60 minutes at 12°C. Completion of the sortase reactions was confirmed by LC-MS and SDS-PAGE.

Mice

C57BL/6J mice were purchased from the Jackson Laboratory. Mice were used at 8-12 weeks of age and were housed under specific pathogen-free conditions. Experiments were performed in accordance with the guidelines of the Institutional Animal Care and Use Committee of Boston Children's Hospital, protocol number 00001880.

Mouse immunization and hybridoma production

Mice were immunized intraperitoneally at ~10-day intervals with 40-50 µg VHH_{MHCII}-HLA-E_{tail} in Freund's adjuvant. Immune responses were monitored using ELISA on GFP-HLA-E_{tail} to measure the peptide-specific response. As the donor of the spleen used for hybridoma production, we chose one mouse whose immune response as measured by ELISA was detectable at a serum dilution of >1:40,000. Mice were given an intraperitoneal injection of ~100 µg VHH_{MHCII}-HLA-E_{tail} in PBS five days and four days prior to harvesting splenocytes to absorb free circulating antibody and boost the splenocytes, respectively. Hybridomas were produced by fusing splenocytes with the Ag8.653 myeloma cell line according to previously described protocols⁶³⁶. Hybridoma were allowed to expand in hybridoma medium (DMEM with 4.5

g/L glucose (Gibco), substituted with 20% fetal bovine serum (FBS), 10% NCTC-109 (Gibco), 1% non-essential amino acids (Gibco), 100 U/mL penicillin/streptomycin, 2% hypoxanthine-aminopterin-thymidine (HAT) (Sigma-Aldrich), substituted for 2% HT (Gibco) after ~12 days in culture). Hybridoma supernatant was tested by ELISA on GFP-HLA-E_{tail}, because the immunized mice have not been exposed to GFP at any point, this screening strategy ensures selection for antibodies that recognize the attached HLA-E tail and not GFP. Positive clones were expanded, and single-cell clones were obtained through semi-solid cloning in ~0.4% SeaPlaque™ Agarose (Lonza) prepared in complete hybridoma medium substituted with 5% HyMax™ (Antibody Research Corporation). Clones that showed a positive response to GFP-HLA-E_{tail} on ELISA were expanded and positive hybridoma clones were selected.

Cloning and expression of LPETG-modified monoclonal immunoglobulins

mRNA was extracted from ~1x10⁷ cells of each positive hybridoma clone, following manufacturer's protocol (Qiagen). cDNA was transcribed with RT transcriptase and a random hexamer primer (5'-NNNNNN-3'), following manufacturer's protocol (Takara SMARTScribe™ Reverse Transcriptase kit). Immunoglobulin HC and LC were amplified by PCR, using a combination of low and highly degenerate primers flanking the sequence between FR₁ and FR₄ (supplementary table 1). HC and LC sequences, modified to contain LPETGG-(His)₆ on the HC and LC, were ordered as GBlock™ gene fragments and cloned into a pcDNA4 vector by InFusion cloning, following the manufacturer's protocol (Takara In-Fusion® Snap Assembly Master Mix) into a murine IgG (for the HC) or IgKappa (for the LC) backbone. Proteins were expressed in EXPI-293 cells following the manufacturer's instructions. EXPI-293 cells were diluted to 3x10⁶ cells/mL in Expi293™ Expression Medium (Gibco) and transfected with ExpiFectamine™ according to the manufacturer's instructions (ExpiFectamine™ 293 transfection kit, Gibco). Briefly, HC and LC DNA were mixed at a [1:3] ratio and incubated with ExpiFectamine™ 293 reagent for 20 minutes at room temperature. The mixture was added drop-wise to the cells followed by incubation in a shaking incubator at 37°C in a humidified 5%CO₂ atmosphere. 16-24 hours after transfection, ExpiFectamine™ 293 Transfection Enhancers were added according to the manufacturer's instructions. Cells were harvested 4 days after transfection and centrifuged for 45 minutes at 2000xg.

Immunoglobulins were purified from the culture medium on a Ni-NTA agarose column (Qiagen) and further purified by size exclusion on a HiLoad Superdex 200 column (Cytiva Life Sciences) using FPLC (ÄKTA, Cytiva Life Sciences).

DNA constructs

The Halo-Tev-Flag-Ube2v2 (#110070, Addgene) construct has been described previously⁶³⁷. This plasmid was used as a substrate for the introduction of epitope tags recognized by monoclonal antibody 19-H12 (Supplementary figure 1). For site-directed mutagenesis, a PCR mixture containing GFP-OTUB2 WT template, mutation primers, Phusion High-Fidelity PCR Master Mix, and MilliQ water in a 30 μ L reaction volume was subjected to PCR amplification using the following program: 98 °C for 30s (98 °C for 10 s; 55 °C for 1 min; 72 °C for 1 min/Kb) \times 30 cycles; 72 °C for 5 min. PCR products were digested with 1 μ L DpnI (ThermoFisher Scientific) overnight at 37 °C to remove methylated DNA template, then transformed into competent DH5 α (Thermo Scientific). All mutated constructs were verified by sequencing. All primers were purchased from IDT. For primer sequences, see supplementary table 2.

Cell culture and reagents

HEK293T (ATCC) were cultured in Dulbecco's modified Eagle's medium (DMEM) supplemented with 10% FCS and 1% penicillin/streptomycin at 37 °C and 5% CO₂. K-562 HLA-E KO and K-562 HLA-E⁺ cells were a gift from Alan Korman (VIR Biotechnology). Cells were maintained in Iscove's modification of DMEM with 10% FCS and 1% penicillin/streptomycin at 37 °C and 5% CO₂. Hybridomas were cultured in DMEM with 4.5 g/L glucose (Gibco), 20% FBS, 10% NCTC-109 (Gibco), 1% non-essential amino acids (Gibco), 1% pen/strep, and 1X HAT (Sigma-Aldrich). HAT was replaced with 1X HT (Sigma-Aldrich) after 2 weeks, and cells remained in HT⁺ medium. For transfection experiments, HEK293T cells were seeded to achieve 50–60% confluence the following day and transfected using polyethylenimine (PEI), Polysciences Inc., Cat# 23966) as follows: 200 μ L DMEM medium without supplements was mixed with DNA and PEI (1 mg/mL) at a ratio of 1:3 (e.g.: 1 μ g DNA : 3 μ g PEI), incubated at RT for 20 min, and added drop-wise to the cells. Cells were cultured for 24 hours prior to further analysis. The reaction mixtures were scaled to maintain a fixed component ratio, as follows: 6-well plate: 3 μ g DNA, 6 cm dish: 8 μ g DNA, 10 cm dish: 24 μ g DNA.

SDS-PAGE, in-gel fluorescence scan, and immunoblotting

Samples were resolved on 12% SDS-PAGE gels. For immunoblotting, proteins were transferred to a nitrocellulose membrane (#162-0112, 0.2 μ m, Biorad) at 300 mA for 3 hours at 4°C in transfer buffer (25 mM Tris, 192 mM glycine in PBS). The membranes were blocked in 5% (w/v) skim milk (non-fat dry milk powder, #Mo842, Lab Scientific) in 1 \times PBS, incubated with a primary antibody diluted in 5% (w/v) milk in PBS + 0.1% Tween-20 (PBS-T) overnight in a cold room, washed three times for 5 min in PBS-T. with rabbit anti-Flag (20543-1-AP, Proteintech, 0.3 μ g/mL) secondary antibody diluted in 5% (w/v) milk in PBS-T for 1 hour, and washed three times again in PBS-T. The signal was visualized using a BioRad ChemiDoc MP imaging system. For silver staining of SDS-PAGE gels, Pierce™ Silver Stain Kit (#24612) was used.

Immunoprecipitation

HEK293T cells were lysed for 20 min in a lysis buffer containing 50mM Tris-HCl (pH 8.0), 150mM NaCl, 4mM EDTA, 1% Triton X-100, protease inhibitor (Roche, complete EDTA-free, Cat# 05056489001). The crude lysate was centrifuged (20 min, 4 °C, ~16,000xg) and the supernatant was incubated with the respective antibodies by rotation at 4 °C for 1 hour. Pierce™ Protein G Agarose (#20398) beads were then added and incubated with agitation at 4 °C for 4 h. Beads were washed four times in lysis buffer. After removal of the washing buffer, reducing Laemmli SDS sample buffer (Alfa Aesar, #J61337-AD) was added at 1 \times to the beads, followed by 7 min incubation at 95 °C. Immunoprecipitated proteins were separated by SDS-PAGE for immunoblotting.

Immunoblot on K-562 cells

One million K562 HLA-E KO or K-562 HLA-E⁺ cells per lane of an immunoblot were lysed in 1 \times RIPA lysis buffer with DNase I for 30 minutes on ice. Proteins were denatured with SDS Laemmli sample buffer (Alfa Aesar, #J61337-AD) with fresh 9% (v/v) beta-mercaptoethanol at 80-90°C for 10 minutes and resolved on a 12% SDS-PAGE gel. Proteins were transferred onto a PVDF membrane with a Trans-Blot Turbo System (BioRad). Membranes were blocked for 2 hours at room temperature in blocking buffer (5% (w/v) skim milk in PBS + 0.02% Tween) and incubated overnight with 1 μ g/mL purified 19-H12. The next day, membranes were incubated with 0.3 ng/mL HRP-conjugated goat-anti-mouse IgG (H+L) secondary antibody (Invitrogen) for 45 minutes at room temperature and developed with Western Lighting ECL Plus (Perkin-Elmer). Images were recorded on the ChemiDoc Imaging System (BioRad).

Flow cytometry

K-562 KO or HLA-E⁺ cells were fixed at 4×10^5 cells per 100 μ l with cold 4% PFA for 15 minutes at room temperature. Cells were washed with PBS and either kept in PBS or permeabilized at 2×10^5 cells per 100 μ l of 0.1% Saponin and 2% FBS in PBS for 15 minutes at room temperature. Cells were stained with 19-H12-Cy5 at 2.5 μ g/mL and 3-D12-PE (BioLegend Cat# 342604, Lot #B353119) at 1.25 μ g/mL in either PBS (for non-permeabilized samples), or in permeabilization buffer (permeabilized samples) for 30 minutes on ice. Cells were washed twice with FACS buffer (2mM EDTA, 2% FBS in PBS) and analyzed on an LSR Fortessa (BD Biosciences). To control for non-specific intracellular retention of antibodies, we incubated permeabilized or non-permeabilized, fixed K-562 HLA-E KO or HLA-E⁺ cells with irrelevant antibodies (PE-conjugated murine IgG-kappa isotype control (Biolegend, 1 μ g/mL) and Cy5-conjugated anti-HA.11 epitope tag (Biolegend, 1 μ g/mL) using the above staining protocol. Gating strategies for flow cytometry described in supplementary figure 4.

Immunofluorescence microscopy

For immunofluorescent staining of K-562 cells, we used an adaptation of a previously described protocol⁶³⁸. Briefly, cells were pelleted for 5 minutes at 500xg and resuspended in PBS. Cells were transferred to a 12-well plastic-bottom tissue culture plate (Corning) at 1×10^6 cells per well and left to adhere for 30 minutes at room temperature. Non-adherent cells were removed by aspiration. Adherent cells were fixed with 500 μ l/well of 10% (v/v) formalin for 10 minutes at room temperature. Fixed cells were washed with PBS, followed by permeabilization for 10 minutes with 0.5% (w/v) Saponin in PBS, or left in PBS for the non-permeabilized control wells. Cells were washed with PBS and blocked with 1% (w/v) BSA in PBS for 30 minutes at room temperature and stained with staining solution containing either 1.25 μ g/mL 19-H12-Cy5, 2.7 μ g/mL 3-D12-PE (BioLegend), or both, in 1% (w/v) BSA in PBS for 1 hour at RT, in the dark. Cells were washed three times with PBS and nuclei were stained with Hoechst 33342 at 1 μ g/mL (Life Technologies) for 10 minutes at room temperature, in the dark. Cells were washed twice with PBS to remove excess dye. Cells were submerged in PBS (500 μ L/well) and imaged with a Keyence IX8 fluorescent microscope.

Immunohistochemistry staining

Formalin-fixed, paraffin embedded sections (3 μ M) of healthy human tonsils or NMIBC bladder tumors from patients were prepared for immunohistochemistry by deparaffinization with xylene and rehydration in a series of graded alcohols. Heat-induced antigen retrieval was done at 95°C

with Dako Target Retrieval Solution, pH 6 following manufacturer's directions (Agilent Solutions, S2369). Slides were blocked with peroxidase suppressor (Thermo Scientific, 35000) for 10 minutes, followed by incubation with Serum-free Protein Block (Dako, X090930-2) for 5 minutes. Primary antibodies MEM-E/02 (Abcam, ab2216) or 19-H12 were incubated at the indicated concentrations for 60 minutes at room temperature. EnVision+ Single Reagent, HRP mouse (Dako, K4001) was used as secondary reagent. Sections were developed with DAB⁺ (Dako, K3468), counterstained with Mayer's hematoxylin (Sigma-Aldrich, MHS32), dehydrated in a series of graded alcohols, and mounted with a coverslip. Whole tissue sections on the slide were converted into high-resolution digital data using a NanoZoomer S60 Digital slide scanner (Hamamatsu).

Results

Immunization and hybridoma production yields HLA-E specific monoclonal antibodies

The intact cytoplasmic tail of HLA-E, fused by means of a sortase reaction to the mouse MHC-II specific nanobody VHH_{MHCII} was used as immunogen^{436,558}. The identity of the ligation products was confirmed by mass spectrometry (Figure 2A). Mice were immunized in complete Freund's adjuvant and boosted with antigen until a serum antibody titer >1:40,000, as measured by ELISA, was reached (Figure 2B). To render the ELISA specific for the HLA-E cytoplasmic tail, plates were coated with recombinant GFP, modified at its C-terminus with the intact HLA-E_{tail}, again using a sortase reaction to install the HLA-E_{tail} peptide. The spleen from an appropriately responding mouse was used for the generation of hybridomas with assistance from Dr. Matthew D. Scharff and Ms. Susan Buhl from the Hybridoma Facility at the Albert Einstein College of Medicine⁶³⁶. Positive clones were identified by ELISA, again using GFP-HLA-E_{tail} as the target antigen. Single cell clones were expanded and the supernatants from growing clones were used as the primary antibody in immunoblotting experiments, using the GFP-HLA-E_{tail} fusion as the target. All clones tested by immunoblotting recognized this fusion protein (Figure 2C), clones 19-H12, 2-D12, and 10-C1 are highlighted in Figure 2.

The DNA sequences of the clones that were positive in ELISA and immunoblotting were determined by RT-PCR. We identified a single dominant V_H sequence, derived from the germline V_H IGHV1-72*01 sequence, in combination with the J IGHJ2*01 segment. A D element could not be unambiguously identified (Figure 3A). The VDJ sequence contains 4

mutations attributable to somatic hypermutation, as determined by reference to a consensus murine germline VH sequence. All mutations were present in the framework regions and caused amino-acid substitutions at positions 16, 51, and 62. One mutation, underscored in Figure 3A, was a silent replacement.

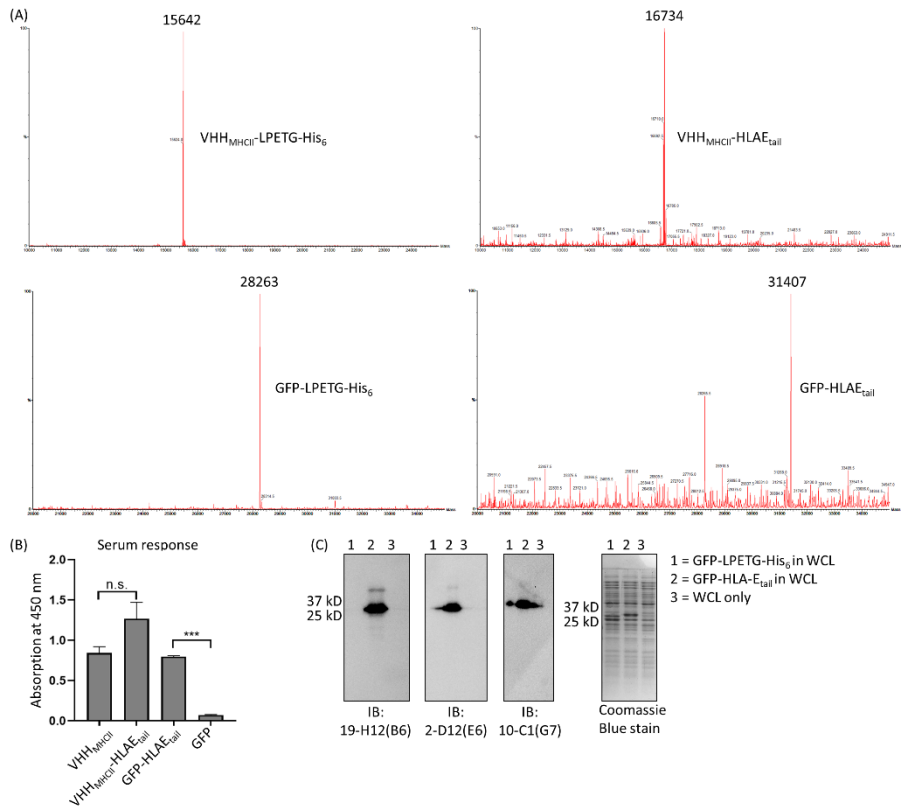


Figure 2. Immunogen production, quantification of serum titer, and immunoblot analysis of hybridoma clones. (A) The peptide comprising the cytoplasmic tail of HLA-E was fused by means of a sortase reaction to VHH7 (anti-mouse MHC-II) or GFP. The identity of the ligation products was confirmed by mass spectrometry. Intact VHH7-LPETG-(His)₆ has a calculated molecular weight of 15635 g/mol, VHH7-HLA-E_{tail} has a calculated molecular weight of 16691. GFP-LPETG-(His)₆ has a calculated molecular weight of 28250. GFP-HLAE_{tail} has a calculated molecular weight of 29306. The observed molecular weight of 31407 is attributed to the disulfide bond formed between the cysteine residues of two peptides, creating an expected molecular mass of 31329. The discrepancy between the calculated molecular weight and the observed molecular weight found with the LC-MS is within the normal range of error. **LEGEND CONTINUES ON THE NEXT PAGE.**

*(B) Mice were immunized in complete Freund's adjuvant and boosted with antigen until a serum antibody titer >1:40,000, as measured by ELISA, was reached. Because VHH7 is slightly immunogenic, the titer was determined on the response to GFP-HLAE_{tail}. A significant difference was reached in serum response to GFP-HLAE_{tail} compared to GFP ($p = 0.00019$, calculated by multiple T-test). (C) Per lane, 500 ng of protein (lane 1: GFP-LPETG-(His)₆, lane 2: GFP-HLA-E_{tail}) was loaded. To prevent non-specific signal, proteins were mixed with unrelated *E. coli* whole cell lysate (WCL). Supernatant of hybridoma clones was used as primary staining agent and HRP-linked anti-mouse secondary was used as secondary agent. To verify loading, a coomassie blue gel stain was made. All the clones recognized the fusion protein. The non-specific signal in lane 1 and 3 from the 2-D12 and 10-C1 blot are spillover of the proteins into the neighboring lanes.*

For the V κ sequences we identified 3 unique occurrences, based on the usage of the germline V κ gene IGKV1-135*01 and J-segment IGK1*01 for 19-H12, IGKV4-90*01 and IGKJ1*01 for 2-D12, and IGKV4-50*01 and IGKJ4*01 for 10-C1. 19-H12 has a V2I, N39S, and F67V mutations and 3 silent replacements. 2-D12 has mutations in the first six amino acids of the FR1, which we attribute to the primers used for amplification of the LC domain. 2-D12 has a P95Y substitution in the CDR3 region. 10-C1 has the same six amino-acid replacement in the FR1, and an S95F substitution in CDR3 (Figure 3B). We conclude that all hybridomas identified are derived from a single V_H rearrangement. Because antigen recognition is predominantly established by the identity of the V_H segment, more specifically its CDR3 region, these monoclonal antibodies are likely to all recognize the same epitope.

The DNA sequences of the clones that were positive in ELISA and immunoblotting were determined by RT-PCR. We identified a single dominant V_H sequence, derived from the germline V_HIGHV1-72*01 sequence, in combination with the JIGHJ2*01 segment. A D element could not be unambiguously identified (Figure 3A). The VDJ sequence contains 4 mutations attributable to somatic hypermutation, as determined by reference to a consensus murine germline V_H sequence. All mutations were present in the framework regions and caused amino-acid substitutions at positions 16, 51, and 62. One mutation, underscored in Figure 3A, was a silent replacement.

For the V κ sequences we identified 3 unique occurrences, based on the usage of the germline V κ gene IGKV1-135*01 for 19-H12, IGKV4-90*01 for 2-D12, and IGKV4-50*01 for 10-C1. 19-H12 has a V2I, N39S, and F67V mutations and 3 silent replacements. 2-D12 has mutations in the first six amino acids of the FR1, which we attribute to the primers used for amplification of the

LC domain. 2-D12 has a P95Y substitution in the CDR₃ region. 10-C1 has the same six amino-acid replacement in the FR₁, and an S95F substitution in CDR₃ (Figure 3B). We conclude that all hybridomas identified are derived from a single V_H rearrangement. Because antigen recognition is predominantly established by the identity of the V_H segment, more specifically its CDR₃ region, these monoclonal antibodies are likely to all recognize the same epitope.

(A)

IGHV1-72*01	CAG GTC CAA CTG CAG CAG CCT GGG GCT GAG CTT GTG AAG CCT GGG GCT TCA GTG AAG CTG TCC TGC AAG GCT TCT
mAb HC	Q V Q L Q Q P G A E L V K P G A S V K L S C K A S
	CAG GTC CAA CTG CAG CAG CCT GGG GCT GAG CTT GTG AAG CCT GGG ACT TCA GTG AAG CTG TCC TGC AAG GC TCT
	Q V Q L Q Q P G A E L V K P G T S V K L S C K A S
	CDR1FR2
IGHV1-72*01	GGC TAC ACC TTC ACC AGC TAC TGG ATG CAC TGG GTG AAG CAG AGG CCT GGA CGA GGC CTT GAG TGG ATT GGA AGG
mAb HC	G Y T F T S Y W M H W V K Q R P G R G L E W I G R
	GGC TAC ACC TTC ACC AGC TAC TGG ATG CAC TGG GTG AAG CAG AGG CCT GGA CGA GGC CTT GAG TGG ATT GGA AGG
	G Y T F T S Y W M H W V K Q R P G R G L E W I G R
	CDR2FR3
IGHV1-72*01	ATT GAT CCT AAT AGT GGT GGT ACT AAG TAC AAT GAG AAG TTC AAG AGC AAG GCC ACA CTG ACT GTA GAC AAA CCC
mAb HC	I D P N S G G T K Y N E K F K S K A T L T V D R P
	CTT GAT CCT AAT AGT GGT GGT ACT AAG TAC ACT GAG AAG TTC AAG AGC AAG GCC ACA CTG ACT GTA GAC AAA CCC
	L D P N S G G T K Y T E K F K S K A T L T V D K P
	FR3CDR3
IGHV1-72*01	TCC AGC ACA GCC TAC ATG CAG CTC AGC AGC CTG ACA TCT GAG GAC TCT GCG GTC TAT TAT TGT GCA AGA --- ---
mAb HC	S S T A Y M Q L S S L T S E D S A V Y Y C A R - -
	TCC AGC ACA GCC TAC ATG CAG CTC AGC AGC CTG ACA TCT GAG GAC TCT GCG GTC TAT TAT TGT GCA AGA CAT GGC
	S S T A Y M Q L S S L T S E D S A V Y Y C A R H G
	CDR3FR4
IGHV1-72*01	---
mAb HC	CTT GAG TAC TGG GGC CAA GGC ACC ACT CTC ACA GTC TCC TCA
	L E Y W G Q G T T L T V S S

(B)

IGKV-135*01	GAT GTT GTG ATG ACC CAG ACT CCA CTC ACT TTG TCG GTT ACC ATT GGA CAA CCA GCC TCC ATC TCT TGC AAG TCA
19-H12 LC	D V V M T Q T P L T L S V T I G Q P A S I S C K S
	GAC ATT GTG ATG ACA CAG ACT CCA CTC ACT TTG TCG GTT ACC ATT GGA CAA CCA GCC TCC ATC TCT TGC AAG TCA
	D I V M T Q T P L T L S V T I G Q P A S I S C K S
	CDR1FR2
IGKV-135*01	AGT CAG AGC CTC TTA GAT AGT GAT GGA AAG ACA TAT TTG AAT TGG TTG TTA CAG AGG CCA GGC CAG TCT CCA AAG
19-H12 LC	S Q S L L D S D G K T Y L N W L L Q R P G Q S P K
	AGT CAG AGC CTC TTA GAT AGT GAT GGA AAG ACA TAT TTG AGT TGG CTG TTA CAG AGG CCA GGC CAG TCT CCA AAC
	S Q S L L D S D G K T Y L S W L L Q R P G Q S P K
	CDR2FR3
IGKV-135*01	CGC CTA ATC TAT CTG GTG TCT AAA CTG GAC TCT GGA GTC CCT GAC AGG TTC ACT GGC AGT GGA TCA GGG ACA GAT
19-H12 LC	R L I Y L V S K L D S G V P D R F T G S G S G T D
	CGC CTA ATC TAT CTG GTG TCT AAA CTG GAC TCT GGA GTC CCT GAC AGG GTC ACT GGC AGT GGA TCA GGG ACA GAT
	R L I Y L V S K L D S G V P D R V T G S G S G T D
	CDR3
IGKV-135*01	TTG ACA CTG AAA ATC AGC AGA GTG GAG GCT GAG GAT TTG GGA GTT TAT TAT TGC TGG CAA GGT ACA CAT TTT CCT
19-H12 LC	F T L K I S R V E A E D L G V Y Y C W Q G T H F P
	TTG ACA CTG AAA ATC AGC AGA GTG GAG GCT GAG GAT TTG GGA GTC TAT TAT TGC TGG CAA GGT ACA CAT TTT CCT
	F T L K I S R V E A E D L G V Y Y C W Q G T H F P
	FR4
IGKV-135*01	---
19-H12 LC	CGG ACG TTC GGT GGA GGC ACC AAG CTG GAA ATC AAA
	R T F G G G T K L E I K

		FR1																									
IGKV-90*01		GAA	ATT	TTG	CTC	ACC	CAG	TCT	CCA	GCA	ATC	ATA	GCT	GCA	TCT	CCT	GGG	GAG	AAG	GTC	ACC	ATC	ACC	TGC	AGT	GCC	
2-D12 LC		E	I	L	L	T	Q	S	P	A	I	I	A	S	P	G	E	K	V	T	I	T	C	S	A	I	
		GAC	ATT	GTG	ATG	ACC	CAG	ACT	CCA	GCA	ATC	ATA	GCT	GCA	TCT	CCT	GGG	GAG	AAG	GTC	ACC	ATC	ACC	TGC	AGT	GCC	
		D	I	V	M	T	Q	T	P	A	I	I	A	S	P	G	E	K	V	T	I	T	C	S	A	I	
		CDR1						FR2														CDR2					
IGKV-90*01		AGC	TCA	AGT	GTA	AGT	TAC	ATG	AAC	TGG	TAC	CAG	CAG	AAA	CCA	GGA	TCC	TCC	CCC	AAA	ATA	TGG	ATT	TAT	GGT	ATA	
2-D12 LC		S	S	S	V	S	Y	M	N	N	W	Y	Q	Q	K	P	G	S	S	P	K	I	W	I	Y	G	I
		AGC	TCA	AGT	GTA	AGT	TAC	ATG	AAC	TGG	TAC	CAG	CAG	AAA	CCA	GGA	TCC	TCC	CCC	AAA	ATA	TGG	ATT	TAT	GGT	ATA	
		S	S	S	V	S	Y	M	N	N	W	Y	Q	Q	K	P	G	S	S	P	K	I	W	I	Y	G	I
		FR3														CDR3											
IGKV-90*01		TCC	AAC	CTG	GCT	TCT	GGA	GTT	CCT	GCT	CGC	TTC	AGT	GGC	AGT	GGG	TCT	GGG	ACA	TCT	TTC	TCT	ACA	ATC	AAC		
2-D12 LC		S	N	L	A	S	G	V	P	A	R	F	S	G	S	G	S	G	T	S	F	S	F	T	I	N	
		TCC	AAC	CTG	GCT	TCT	GGA	GTT	CCT	GCT	CGC	TTC	AGT	GGC	AGT	GGG	TCT	GGG	ACA	TCT	TTC	TCT	ACA	ATC	AAC		
		S	N	L	A	S	G	V	P	A	R	F	S	G	S	G	S	G	T	S	F	S	F	T	I	N	
		FR4																									
IGKV-90*01		AGC	ATG	GAG	GCT	GAA	GAT	GTT	GCC	ACT	TAT	TAC	TGT	CAG	CAA	AGG	AGT	AGT	TAC	CCA	CCC	---	---	---	---	---	
2-D12 LC		S	M	E	A	E	D	V	A	T	Y	Y	C	Q	Q	R	S	S	Y	P	P	-	-	-	-	-	
		AGC	ATG	GAG	GCT	GAA	GAT	GTT	GCC	ACT	TAT	TAC	TGT	CAG	CAA	AGG	AGT	AGT	TAC	CCG	TAC	CGC	TTC	GGA	GGG	GGG	
		S	M	E	A	E	D	V	A	T	Y	Y	C	Q	Q	R	S	S	Y	P	Y	P	Y	T	G	G	
IGKV-90*01		---	---	---	---	---	---	---	---	---	---	---	---	---	---	---	---	---	---	---	---	---	---	---	---	---	
2-D12 LC		ACC	AAG	CTG	GAA	ATA	AAA																				
		T	K	L	E	I	K																				
		FR1																									
IGKV-50*01		GAA	AAT	GTG	CTC	ACC	CAG	TCT	CCA	GCA	ATC	ATG	TCT	GCA	TCT	CTA	GGG	GAG	AAG	GTC	ACC	ATG	AGC	TGC	AGG	GCC	
10-C1 LC		E	N	V	L	T	Q	S	P	A	I	M	S	A	S	L	G	E	K	V	T	M	S	C	R	A	
		GAC	ATT	GTG	ATG	ACC	CAG	ACT	CCA	GCA	ATC	ATG	TCT	GCA	TCT	CTA	GGG	GAG	AAG	GTC	ACC	ATG	AGC	TGC	AGG	GCC	
		D	I	V	M	T	Q	T	P	A	I	M	S	A	S	L	G	E	K	V	T	M	S	C	R	A	
		CDR1						FR2														CDR2					
IGKV-50*01		AGC	TCA	AGT	GTA	AAT	TAC	ATG	TAC	TGG	TAC	CAG	CAG	AAG	TCA	GAT	GCC	TCC	CCC	AAA	CTA	TGG	ATT	TAT	TAC	ACA	
10-C1 LC		S	S	S	V	N	Y	M	Y	W	Y	Q	Q	K	S	D	A	S	P	K	L	W	I	Y	Y	T	
		AGC	TCA	AGT	GTA	AAT	TAC	ATG	TAC	TGG	TAC	CAG	CAG	AAG	TCA	GAT	GCC	TCC	CCC	AAA	CTA	TGG	ATT	TAT	TAC	ACA	
		S	S	S	V	N	Y	M	Y	W	Y	Q	Q	K	S	D	A	S	P	K	L	W	I	Y	Y	T	
		FR3														CDR3											
IGKV-50*01		TCC	AAC	CTG	GCT	CCT	GGA	GTC	CCA	GCT	CGC	TTC	AGT	GGC	AGT	GGG	TCT	GGG	AAC	TCT	TAT	TCT	CTC	ACA	ATC	AGC	
10-C1 LC		S	N	L	A	P	G	V	P	A	R	F	S	G	S	G	S	G	N	S	Y	S	L	T	I	S	
		TCC	AAC	CTG	GCT	CCT	GGA	GTC	CCA	GCT	CGC	TTC	AGT	GGC	AGT	GGG	TCT	GGG	AAC	TCT	TAT	TCT	CTC	ACA	ATC	AGC	
		S	N	L	A	P	G	V	P	A	R	F	S	G	S	G	S	G	N	S	Y	S	L	T	I	S	
		FR4																									
IGKV-50*01		AGC	ATG	GAG	GGT	GAA	GAT	GCT	GCC	ACT	TAT	TAC	TGC	CAG	CAG	TTT	ACT	AGT	TCC	CCA	TCC	---	---	---	---	---	
10-C1 LC		S	M	E	G	E	D	A	A	T	Y	Y	C	Q	Q	F	T	S	S	P	S	-	-	-	-	-	
		AGC	ATG	GAG	GGT	GAA	GAT	GCT	GCC	ACT	TAT	TAC	TGC	CAG	CAG	TTT	ACT	AGT	TCC	CCA	TTC	AGC	TTC	GGC	TCG	GGG	
		S	M	E	G	E	D	A	A	T	Y	Y	C	Q	Q	F	T	S	S	P	F	T	F	G	S	G	
IGKV-50*01		---	---	---	---	---	---	---	---	---	---	---	---	---	---	---	---	---	---	---	---	---	---	---	---	---	
10-C1 LC		ACA	AAG	TTG	GAA	ATA	AAA																				
		T	K	L	E	I	K																				

Figure 3. The DNA sequences of the clones that were positive in ELISA and immunoblotting were determined by RT-PCR. (A) We identified a single dominant V_H sequence, derived from the germline V_H IGHV1-72*01 sequence, in combination with the J IGHJ2*01 segment. A D element could not be unambiguously identified. The VDJ sequence contains 4 mutations attributable to somatic hypermutation, as determined by reference to the germline V_H sequence. All mutations, highlighted in red, were present in the framework regions and caused amino-acid substitutions (highlighted in blue). One mutation, underscored, was a silent (B) For the V_k sequences we identified 3 unique occurrences, based on the usage of the germline V_k gene IGKV1-135*01 and J-segment IGKJ1*01 for 19-H12, IGKV4-90*01 and IGKJ2*01 for 2-D12, and IGKV4-50*01 and IGKJ4*01 for 10-C1. 19-H12 has V2I, N39S, and F67V mutations and 3 silent replacements. 2-D12 has mutations in the first 6 amino acids which we attribute to the primers used for sequencing of the LC domain. The mutations P95Y in the CDR3 is attributable to somatic hypermutation. 10-C1 has this same 6 amino-acid replacement in the FR1, and an S95F mutation in the CDR3.

We cloned the sequences spanning the FR₁ to FR₄ of the heavy chain and light chain backbones on a murine IgG₁ (for the HC) or IgKappa (for the LC) backbone, both modified C-terminally with an LPETGG-(His)₆ motif. The 6x histidine tag allows easy purification of the recombinant IgG on a NiNTA matrix (Figure 4A). The LPETG motif allows sortase-mediated modification of both the heavy chain and light chain with a biotin or fluorophore. We produced the 19-H12 clone in EXPI-293T cells and modified it with biotin or Cy5 on the heavy chain and light chain for downstream applications such as cytofluorimetry or immunofluorescence (Figure 4B). Because the (His)₆-tag is lost upon modification of the IgG molecule with sortase, depletion of the sortase reaction mixture on a NiNTA column ensures that the final product, obtained in the NiNTA flow through, is homogeneously modified at all four C-termini. The homogeneously Cy5-modified 19-H12 was used where indicated for further experiments.

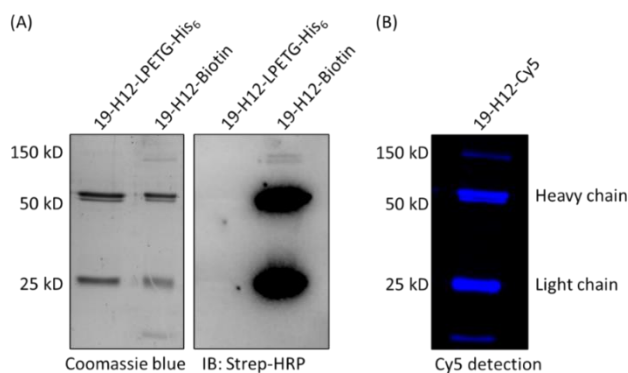


Figure 4. Production of antibody modified at the HC and LC C-terminus with an LPETG-His₆ motif. (A) We cloned the sequences spanning the FR₁ to FR₄ of the heavy chain and light chain in backbones on a murine IgG₁ (for the HC) or IgKappa (for the LC) backbone, both modified C-terminally with LPETG-(His)₆ motif and transfected the plasmids into EXPI-293 cells for protein production. The (His)₆-tag allows for easy purification of the recombinant IgG on a NiNTA matrix. The LPETG motif allows sortase-mediated modification of both the heavy chain and light chain with a biotin or fluorophore. (B) We modified the monoclonal antibody with Cy5 on the heavy chain and light chain. The final product has an equimolar amount of Cy5 on the C-termini of both heavy chains and light chains.

Monoclonal antibodies recognize a 13-residue HLA-E specific peptide

We mapped the epitope recognized by three monoclonal antibodies that make use of three distinct k light chains. A series of overlapping peptides with a 1-residue pitch was synthesized based on the sequence of the HLA-E_{tail}. Each peptide was extended at its N-terminus with a Gly-Gly-Ser sequence to ensure its suitability as a sortase nucleophile and to impart some degree of flexibility relative to the GFP to which the peptide is attached. Each peptide was individually ligated to a sortase-compatible, (His)₆-tagged GFP variant. Input (His)₆-tagged sortase and unreacted (His)₆-tagged GFP were removed from the reaction by depletion on a Ni-NTA matrix, so that the supernatant contained only the desired ligation product and free peptide, added in molar excess. Recognition of ligation products was done by immunoblot, using conditioned medium of the three monoclonal hybridomas as the primary detection agent. HRP-linked anti-mouse IgG was used as a secondary detection agent. The results unambiguously identified three overlapping peptides: (W)(S)(D)SAQGSES(H)(S)(L), thus identifying the sequence SAQGSES as the core of the epitope in the HLA-E cytoplasmic tail (Figure 5A).

To determine the smallest possible tag based on this epitope sequence, we inserted 8-mer, 10-mer, and 13-mer peptide sequences at the C-terminus of Halotag-Flag-UBE2V2 in a mammalian expression vector. The constructs were expressed in HEK-293T cells, and cell lysates were subjected to immunoblot using conditioned medium from hybridoma cultures. 19-H12 and 2-D12 clearly recognized the 13-mer at the C-terminus of the target protein. 10-C1 showed a weaker signal, which we attribute to the lower titer of the immunoglobulin in the hybridoma culture supernatant (Figure 5B). 19-H12 and 2-D12 both also recognize the 13-mer tag when positioned at the N-terminus or at the center of the protein, as validated with immunoblot on lysates of HEK-293T cells that express Halotag-Flag-UBE2V2 modified to express the 13-mer tag at the N-terminus (N₁₃ mer) or middle (M₁₃ mer) (Figure 5C). Immunoprecipitation further validated the interaction of purified 19-H12 mAb with the 13-mer tag (Figure 5D). Protein complexes immunoprecipitated with 19-H12 mAb can be eluted by addition of an excess of free synthetic peptide (Figure 5E, 5F).

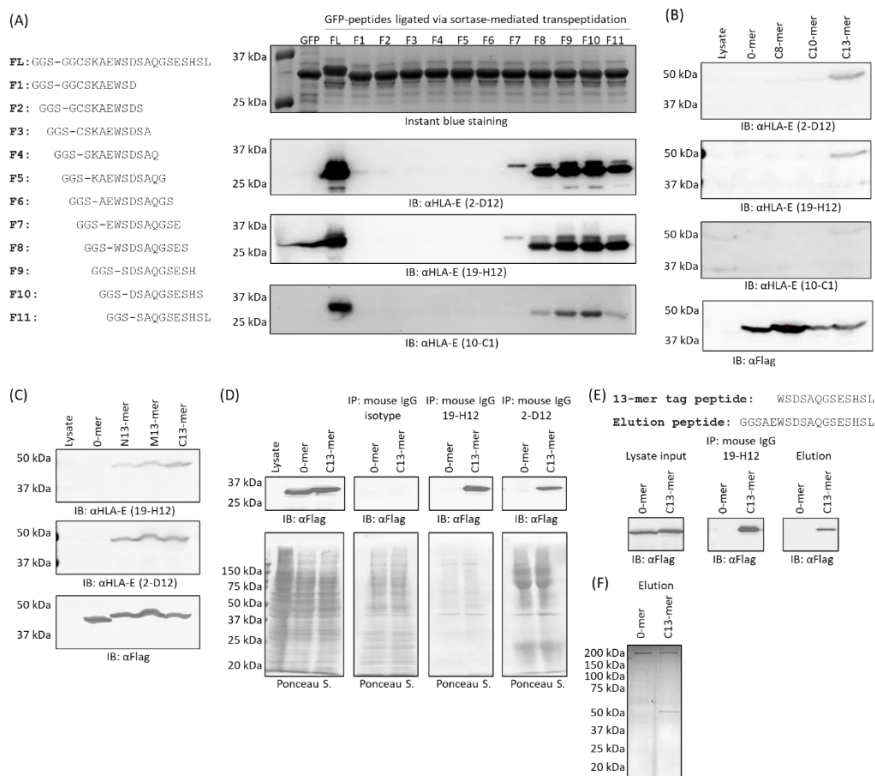


Figure 5. Monoclonal antibodies recognize a unique 13-residue HLA-E specific peptide (A) Epitope mapping with 10mers. 10-residue HLA-E specific peptides with a pitch of one residue were chemically synthesized and ligated to GFP C-terminus via sortase-mediated transpeptidation. The ligated products were subject to SDS-PAGE and immunoblots against selected monoclonal antibodies. (B) 8-mer, 10-mer or 13-mer peptide sequences were inserted at the C-terminus of the mammalian expression vector Halotag-Flag-UBE2V2 via PCR-based site-directed mutagenesis. The constructs were exogenously expressed in HEK293T cells, the cell lysates were subject to immunoblots against indicated antibodies. (C) The 13-mer tag was inserted into the mammalian cell expression vector at the N-terminus (N13-mer), Middle (M13-mer), or C-terminus (C13-mer) of Halotag-Flag-UBE2V2 via PCR-based site-directed mutagenesis. The indicated constructs were exogenously expressed in HEK293T cells, the cell lysates were subject to immunoblots against indicated antibodies. (D) The mammalian cell expression vector Halotag-Flag-UBE2V2 (o-mer) or Halotag-Flag-UBE2V2-13mer (C13-mer) constructs were exogenously expressed in HEK293T cells, the cell lysates were subject to immunoprecipitation with indicated antibodies. The immunoprecipitated protein complex was subject to immunoblots against Rabbit anti-Flag antibody. **LEGEND CONTINUES ON THE NEXT PAGE.**

(E) The mammalian cell expression vector Halotag-Flag-UBE2V2 (0-mer) or Halotag-Flag-UBE2V2-13mer (C13-mer) constructs were exogenously expressed in HEK293T cells, the cell lysates were subject to immunoprecipitation with purified 19-H12-B6 monoclonal antibody, the immunoprecipitated protein complex was competitively eluted with chemically synthesized elution peptide. (F) Silver staining of the eluted protein bands from immunoprecipitation.

Antibodies recognize HLA-E in immunoblot, flow cytometry, immunofluorescence, and immunohistochemistry

For recognition of HLA-E in cell lines, we used K-562 derivative cell lines where HLA-E was knocked out (K-562 KO), or where single chain HLA-E and beta-2-microglobulin, complexed with the HIV Gag69 peptide, were reintroduced (K-562 HLA-E⁺). For immunoblot, we transferred the lysate of 1×10^6 K-562 HLA-E KO and K-562 HLA-E⁺ cells to a PVDF membrane and blotted with purified mAb (19-H12) at 1 μ g/mL using HRP-conjugated anti-mouse IgG as secondary detection agent. We noted a clear signal around 55kD, corresponding to the molecular weight of the HLA-E Gag69 trimer. The signal around 37kD corresponds to the heavy chain of HLA-E. Potentially, the β 2-microglobulin got cleaved off (Figure 6A).

For flow cytometry, K-562 KO or K-562 HLA-E⁺ cells were fixed with 4% (v/v) PFA and permeabilized with 0.1% (w/v) saponin as described in methods. Cells were stained with 19-H12-Cy5 and with the commercially available anti-HLA-E antibody 3-D12-PE as described in methods. Non-specific staining was low, as characterized by the signal from permeabilized cells stained with irrelevant antibodies (Supplementary figure 2). Fixed, permeabilized K-562 HLA-E⁺ cells show a clear signal in the PE channel with the commercially available HLA-E antibody 3-D12, as well as in the Cy5 channel with the HLA-E specific antibody 19-H12. Permeabilized K-562 KO cells show no staining in either channel. Fixed, non-permeabilized cells were used as negative control for 19-H12, as the antibody binds an intracellular epitope. Non-permeabilized K-562 HLA-E⁺ cells show a clear signal in the PE channel with 3-D12, but not in the Cy5 channel with 19-H12. The 19-H12 antibody thus specifically recognizes the cytoplasmic tail of HLA-E and is suitable for flow cytometry on permeabilized cells (Figure 6B). To control for non-specific intracellular retention of antibodies, we incubated permeabilized or non-permeabilized fixed K-562 HLA-E KO or HLA-E⁺ cells with non-targeting antibodies (PE-conjugated murine IgG-kappa isotype control and Cy5-conjugated anti-HA.11 epitope tag). We see a negative signal in both the PE and Cy5 channel, confirming that any positive signal is not due to intracellular antibody retention (Supplementary figure 3)

To determine the suitability of 19-H12 in immunofluorescent imaging, we allowed K-562 KO or HLA-E⁺ cells to adhere to the bottom of a plastic 12-well tissue culture plate. Cells were fixed with 4% PFA and either permeabilized with saponin or left intact and stained with 19-H12-Cy5 and 3-D12-PE. We observed a clear signal of the cell membrane with either antibody in the formalin-fixed, permeabilized K-562 HLA-E⁺ cells, but not in similarly treated K-562 KO cells (Figure 6C). Cells that were fixed with formalin, but not permeabilized, showed clear staining of the cell membrane with 3-D12-PE but only little staining with 19-H12-Cy5, presumably due to some cellular damage inflicted by the small amount of methanol in the stock formaldehyde solution used for fixation. These results show that 19-H12 is suitable for immunofluorescence detection of HLA-E on the cell membrane.

For immunohistochemistry, we stained sections of healthy human tonsil and of a progressive non-muscle invasive bladder cancer (NMIBC) with 19-H12 or with the commercially available anti-HLA-E MEM-E/o2. The tonsil sections show clear staining of stromal cells. We observe specific staining at 40-fold lower concentrations of 19-H12 antibody (0.25 µg/mL), compared to the MEM-E/o2 (10 µg/mL) (Figure 7A). Progressive or recurrent human bladder cancer is generally high in HLA-E expression and low in expression of HLA-A, -B, and -C⁶³⁹. Tissue sections from progressive NMIBC shows clear staining of cancer cells at low concentrations of 19-H12 antibody (0.25 µg/mL) compared to MEM-E/o2 (10 µg/mL) (Figure 7B). In both the healthy tonsil and the NMIBC sections, we observe clear staining of the cytoplasm, which we attribute to staining of HLA-E in the endoplasmic reticulum or in recycling endosomes.

Discussion

HLA-E plays a unique role in antigen presentation and target recognition by cytotoxic T cells. In humans, HLA-E is specialized in the presentation of peptides derived from the signal sequences of other Class I MHC products. The signal sequences of viral glycoproteins likewise contribute to the pool of HLA-E ligands. Antibodies against the ectodomain of HLA-E have been reported to display varying degrees of cross-reactivity with alleles of HLA-B and HLA-C⁶²⁷. An inspection of the sequences of HLA-E and its comparison with the sequences of other Class I MHC molecules shows that the amino acid sequence of the cytoplasmic tail of HLA-E is unique. In fact, assignment of a given Class I MHC sequence to a particular locus is most readily achieved by inspection of the cytoplasmic tail sequence.

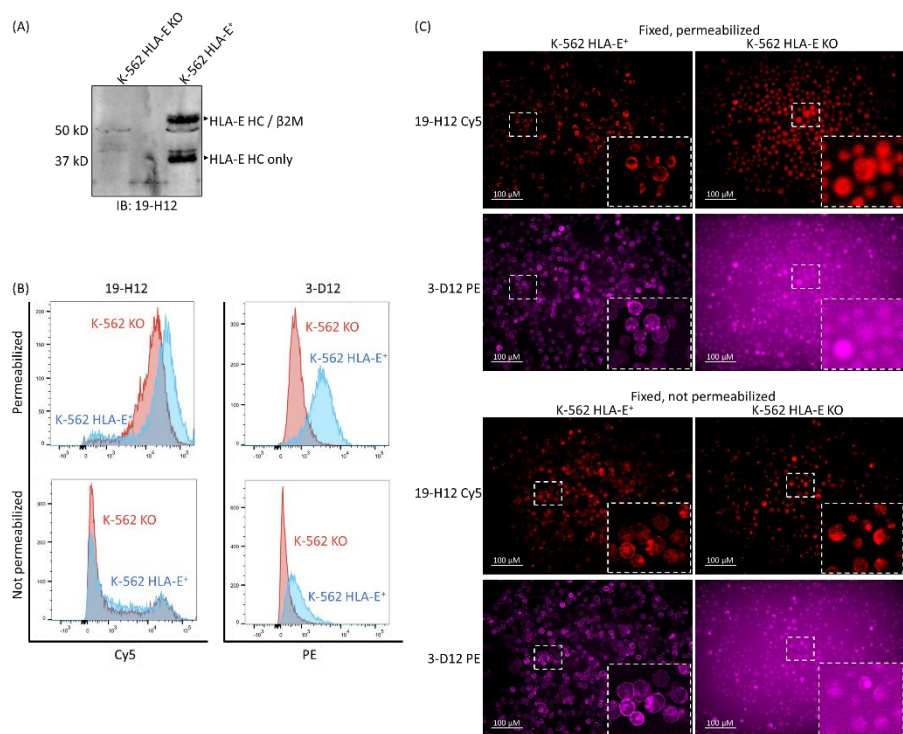


Figure 6. Cell-surface staining of HLA-E on K-562 HLA-E⁺ cells. (A) We transferred the lysate of 1×10^6 K-562 HLA-E KO or K-562 HLA-E⁺ cells to a PVDF membrane and blotted with purified 19-H12 mAb at 1 μg/mL. We used an HRP-conjugated anti-mouse IgG as secondary agent. We see a clear signal around 55kD, corresponding to the molecular weight of the single-chain trimer of the transfected HLA-E. The signal at ~37kD corresponds to the molecular weight of the heavy chain only. (B) K-562 KO or HLA-E⁺ cells were fixed and permeabilized and stained with PE-conjugated pan-HLA mAb 3-D12 or Cy5-conjugated HLA-E specific 19-H12. Fixed, non-permeabilized cells were used as negative control for 19-H12, as the antibody binds an intracellular epitope. Experiments were performed five times, representative data for one experiment shown here. (C) For immunofluorescence, K-562 KO or HLA-E⁺ suspension cells were adhered to a tissue culture 12-well plate by sedimentation through gravity in PBS. Cells were fixed with 4% PFA and either permeabilized with 0.1% saponin or left unpermeabilized. Cells were stained with a solution containing either 19-H12-Cy5 (1.25 μg/mL) or 3-D12-PE (2.7 μg/mL). Experiments were performed three times, representative data for one experiment shown here. Minor positive signal in the 19-H12 Cy5-stained HLA-E⁺ cells is explained by trace methanol in the formaldehyde stock solution, causing partial permeabilization of the cells.

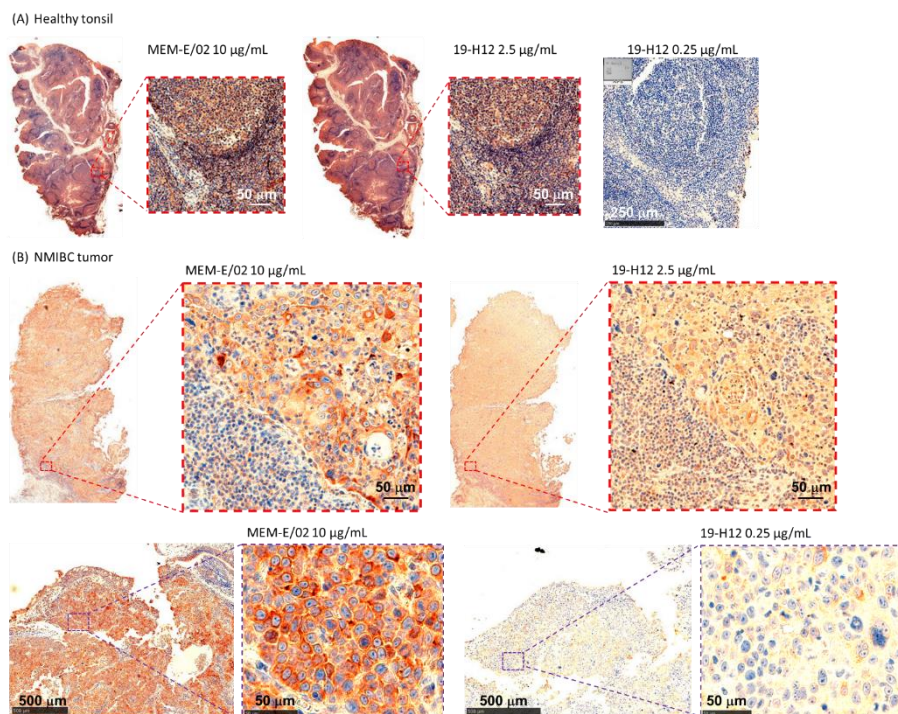


Figure 7. Immunohistochemistry on sections of human healthy tonsil and progressive non-muscle invasive bladder cancer (NMIBC). (A) We stained sections of a healthy human tonsil with the 19-H12 antibody or the commercially available anti-HLA-E MEM-E/o2. The tonsil sections show clear staining of stromal cells with 19-H12, even at lower concentration of antibody (0.25µg/mL), compared to MEM-E/o2 (10 µg/mL). (B) Tissue sections from progressive NMIBC shows very clear staining of cancer cells at low concentrations of 19-H12 antibody (0.25µg/mL) compared to the standard concentration for MEM-E/o2 (10 µg/mL).

The cytoplasmic tail of class I MHC molecules is involved in trafficking peptide-bound MHC class I from the endoplasmic reticulum to the cell membrane. The cytoplasmic tail of HLA-E in particular plays a role in the internalization and the reduced stability and surface expression of peptide-bound HLA-E²⁸¹.

To target the cytoplasmic tail peptide of HLA-E (HLA-E_{tail}) for production of monoclonal antibodies, we designed an immunogen based on our prior observations that targeted delivery of antigens to antigen presenting cells elicits strong B and T cell immunity^{420,466,558,640}. This is accomplished by fusing the antigen of interest to a nanobody that recognizes Class II MHC products. Fusions of this type can be obtained as genetic fusions or by a sortase-

catalyzed transpeptidation reaction, as was done here to create VHH_{MHC-II-HLAE_{tail}}. Screening of hybridomas was done by ELISA on a fusion of GFP-HLA-E_{tail}, also prepared by sortase-catalyzed transpeptidation. This ensured specificity for HLA-E_{tail} peptide in the ELISA assay, as the immunized mice were never exposed to GFP.

We obtained several hybridomas, all of which used the identical VDJ rearrangement for the Ig heavy chain locus, but with involvement of 3 distinct VJ kappa light chain rearrangements. Not surprisingly, this puts the weight of recognition of HLA-E_{tail} on the heavy chain CDRs. We mapped the epitope recognized within the HLA-E_{tail} to the core sequence SAQGSES. This core sequence was not sufficient to confer reactivity with any of the monoclonal antibodies with proteins carrying this minimal tag. Instead, we found that a 13-residue extended version of this core sequence was required for recognition in immunoblots. Given the strong reactivity of the antibody in immunoblots, this suggested its utility as an epitope tag. Indeed, by placing the WSDSAQGSESHSL sequence at the N- or C-terminus of a protein, or at an internal location, we confirmed retention of immunoreactivity with the antibody, independent of the placement of the tag. When running a search of the (W)(S)(D)SAQGSES(H)(S)(L) sequence against all available protein sequences, we found a hit only for HLA-E and its non-human primate homologs. Because in Class I MHC molecules this sequence is in the cytoplasm, use of the (W)(S)(D)SAQGSES(H)(S)(L) tag in extracellular proteins in cells of human or non-human primate origin would be possible. For all other species queried, no obvious cross-reactions of the (W)(S)(D)SAQGSES(H)(S)(L) tag with endogenous proteins is expected, thus expanding its utility.

Fluorescent labeling of antibodies is commonly done using NHS ester-fluorophores to target exposed lysine residues, or maleimide derivatives of fluorophores to target cysteine residues, either present endogenously or engineered into the antibody sequences at a particular site. These chemical modification strategies come with the attendant risk of placing fluorophores in the antibody's paratope, with possible loss of activity. Over-modification of antibodies with fluorophores can also result in an apparent loss of activity. The use of the sortase-catalyzed transpeptidation reaction ensures reproducibility, site-specificity, and produces the desired product in excellent yield, approximating >90% conversion. The sortase tags are located far away from the antigen binding site, thus minimizing the potential for loss of activity caused by the modification. While conventional methods for antibody detection, i.e., those involving the use of secondary antibodies, are

of course possible, direct modification with fluorophores or biotin eliminates the need for secondary antibodies. We modified the monoclonal antibody to carry the LPETG sortase motif on the C-termini of both heavy and light chains. The inclusion of a (His)₆-tag allows for easy purification after expression in EXPI-293T cells. Using 7M sortase, we successfully installed 4 moles of biotin or Cy5 on the mAb. We have shown the functionality of the modified HLA-E_{tail} specific mAb for cell staining in immunoblot, immunofluorescence, and flow cytometry.

We have also shown the use of this mAb in immunohistochemistry of paraffin embedded, formalin-fixed patient tumor samples, at much lower concentrations compared to the MEM-E/o2 antibody, suggesting the use of this mAb as a possible diagnostic tool in the clinic to detect HLA-E.

In conclusion, we have developed a monoclonal antibody that targets the cytoplasmic tail of HLA-E and thus we suspect no cross-reactivity to other Class I MHC molecules. This antibody can be used diagnostically for staining HLA-E on patient (tumor) samples, as an antibody-epitope tag for extracellular proteins, and to further the research to the role of the cytoplasmic tail on HLA-E trafficking from the ER and to endosomes.

Conflict of Interest

The authors declare that the research was conducted in the absence of any commercial or financial relationships that could be construed as a potential conflict of interest.

Author Contributions

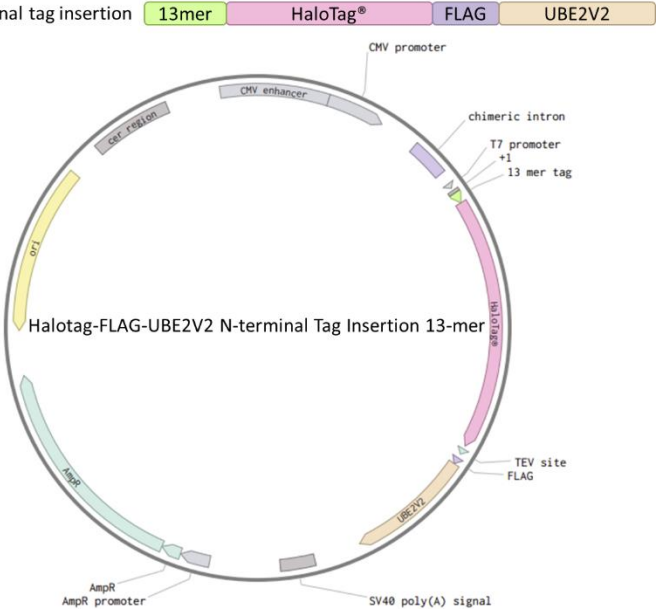
The authors confirm their contribution to the paper as follows: E.R.V and H.L.P designed the study and supervised data collection. E.R.V performed hybridoma analysis, single-cell cloning, and downstream applications with the monoclonal antibody. J.G. collected data on epitope mapping and immunoprecipitation with the 13-mer. S.B. and M.D.S. assisted in producing the hybridomas. Z.L. and A.H. performed immunohistochemistry staining. E.R.V. and H.L.P. wrote the paper. All authors reviewed the results and approved the final version of the manuscript.

Acknowledgements

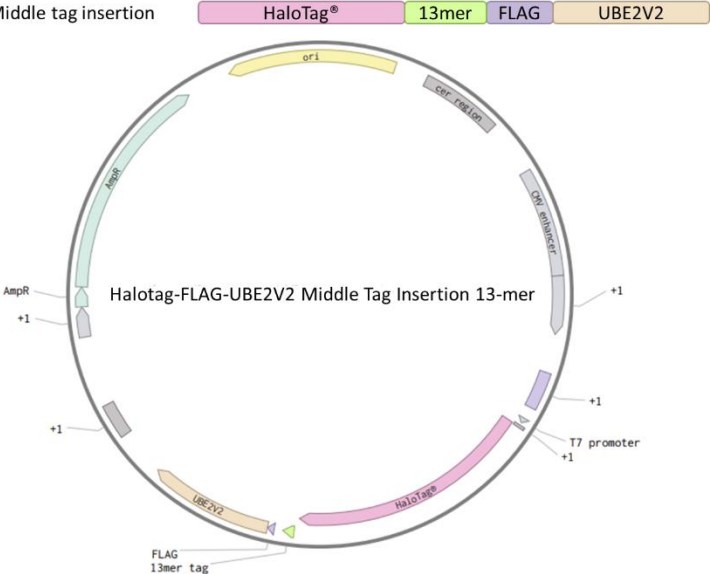
This research was supported by Vir Biotechnology (1800 Owens St. Suite 900. San Francisco, California 94158, US). We thank Dr. Alan Korman and Dr. Simon Belanger for their generous gift of the K-562 KO and HLA-E⁺ cell lines.

Supplementary figures

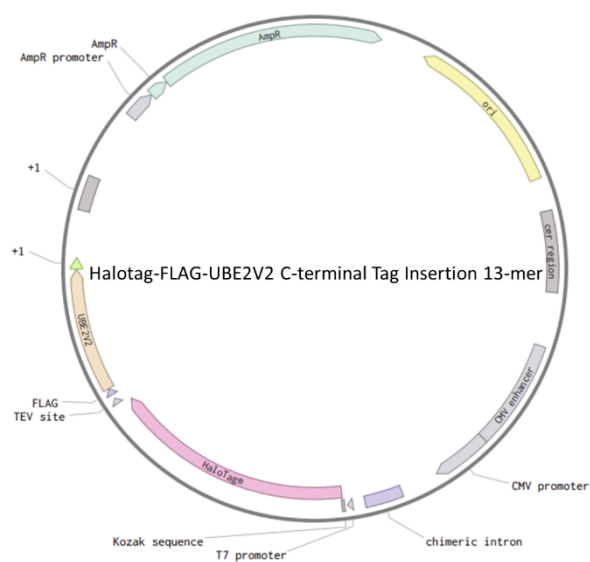
(A) N-terminal tag insertion



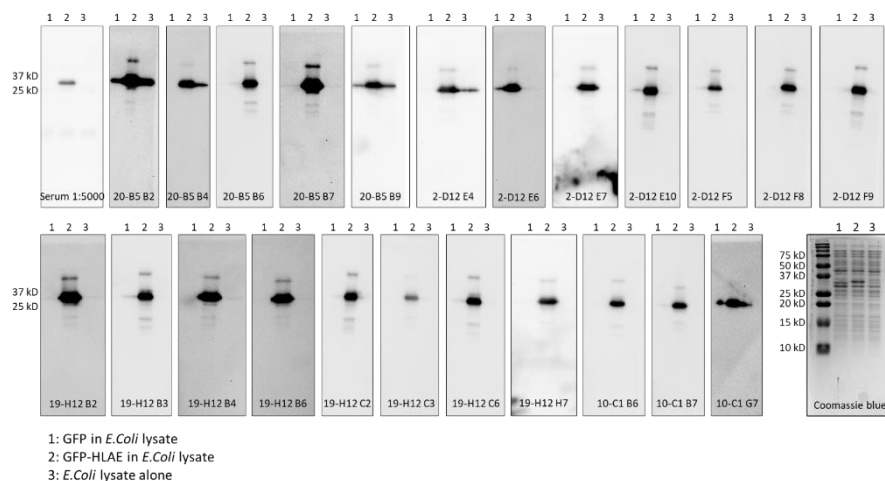
(B) Middle tag insertion



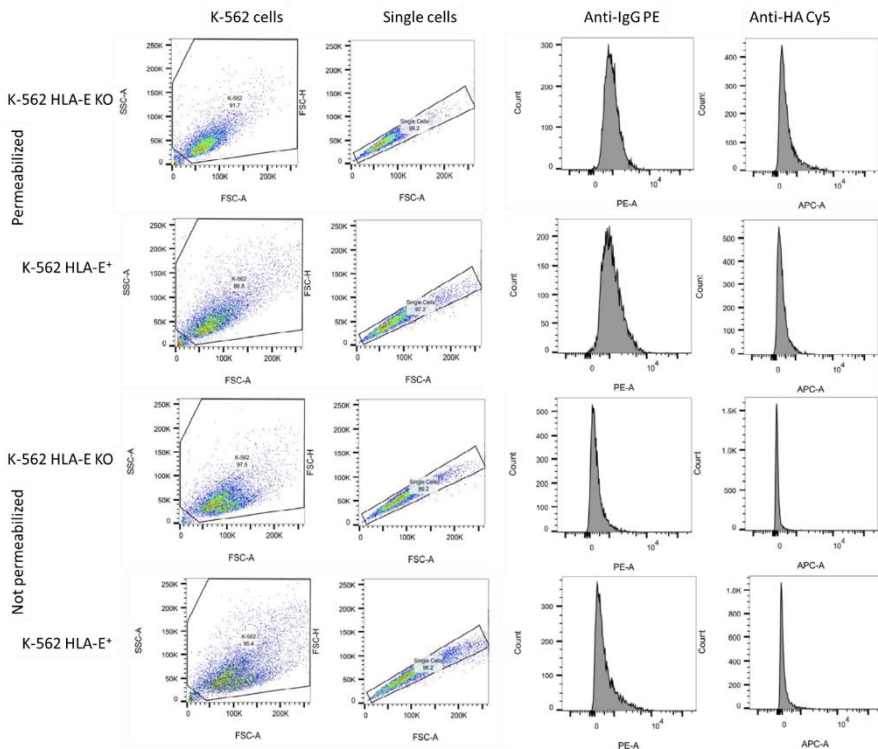
(C) C-terminal tag insertion HaloTag® FLAG UBE2V2 13mer



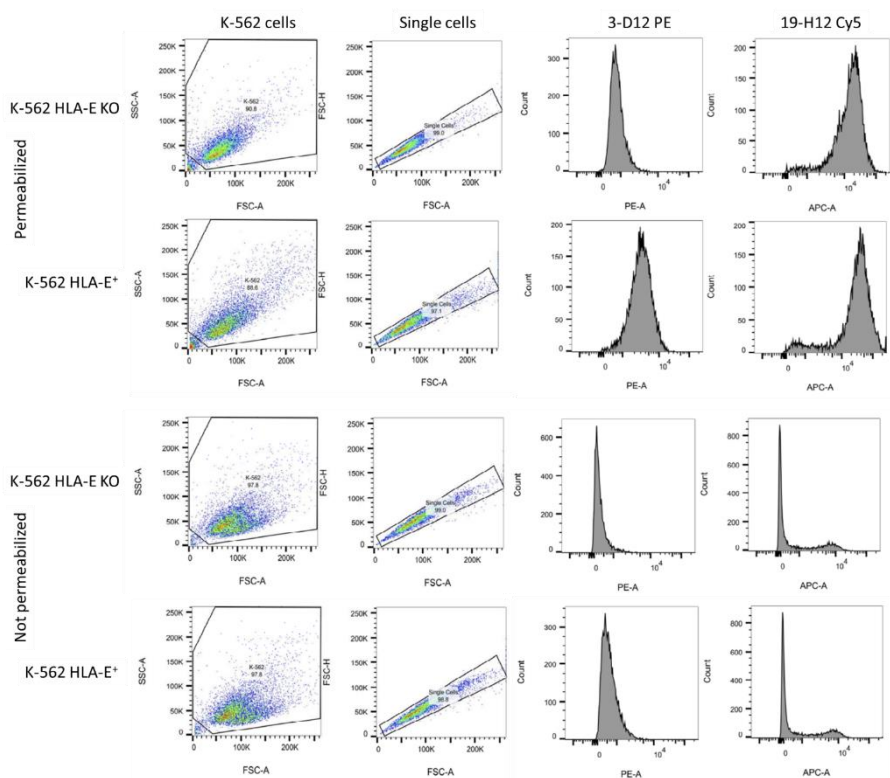
Supplementary figure 1. Schematic overview and plasmid map of the HaloTag-FLAG-UBE₂V₂ vector. We inserted the 13-mer epitope sequence (WSDSAQGSESHSL) in the N-terminus (A), middle (B) or C-terminus (C) of the protein complex.



Supplementary figure 2. Western blot on GFP and GFP-HLA_{Etail} for all hybridoma clones. Per lane, 500 ng of protein (lane 1: GFP-LPETG-His6, lane 2: GFP-HLA-E_{tail}) was loaded. To prevent non-specific signal, proteins were mixed with unrelated *E. Coli* whole cell lysate (WCL, lane 3). Supernatant of hybridoma clones was used as primary staining agent and HRP-linked anti-mouse IgG (H+L) antibody (0.3 µg/mL, Invitrogen) was used as secondary agent. To verify loading, a coomassie blue gel stain was made. To verify a positive signal, serum from the immunized mouse was used at 1:5000 dilution. All the clones recognized the fusion protein in lane 2. The non-specific signal in lane 1 and 3 of some blots are spillover of the proteins into the neighboring lanes.



Supplementary figure 3. K-562 cells stained with negative control antibodies. To control for non-specific intracellular retention of antibodies, we incubated permeabilized or non-permeabilized fixed K-562 HLA-E KO or HLA-E⁺ cells with non-targeting antibodies (PE-conjugated murine IgG-kappa isotype control (Biolegend, 1 μ g/mL) and Cy5-conjugated anti-HA.11 epitope tag (Biolegend, 1 μ g/mL). We see a negative signal in both the PE and Cy5 channel, confirming that any positive signal is not due to intracellular antibody retention.



Supplementary figure 4. Gating strategy for flow cytometry on K-562 HLA-E KO and HLA-E⁺ cells. We fixed cells with 4% (v/v) PFA in PBS and either permeabilized cells with 0.5% (w/v) saponin in PBS or left cells intact for the non-permeabilized control. Cells were stained with 2.7 $\mu\text{g/mL}$ 3-D12-PE (Biolegend) or 1.25 $\mu\text{g/mL}$ 19-H12-Cy5 in 1% (w/v) BSA in PBS. For flow cytometry, we selected cells based on FSC-A and SSC-A and selected singlets based on FSC-H and FSC-A. Positive signal coming from staining with the 3-D12-PE antibody was measured in the PE channel. Positive signal coming from staining with the 19-H12-Cy5 antibody was measured in the APC channel.

Target	Usage	Sequence (5' → 3')
IgG1	Reverse primer for IgG1 amplification	ATAGACAGATGGGGGTGTCGTTTGGC
IgG2A	Reverse primer for IgG2A amplification	CTTGACCAGGCATCTAGAGTCA
IgG2B	Reverse primer for IgG2B amplification	AGGGGCCAGTGGATAGACTGATGG
IgG3	Reverse primer for IgG3 amplification	AGGGACCAAGGGATAGACAGATGG
HC FR1 HD1	Forward primer for HC amplification (high degenerate)	SARGTNMAGCTGSAGSAGTC
HC FR1 HD2	Forward primer for HC amplification (high degenerate)	SARGTNMAGCTGSAGSAGTCWGG
HC FR1 LD1	Forward primer for HC amplification (low degenerate)	CAGGTTACTCTGAAAAGWGTSTG
HC FR1 LD2	Forward primer for HC amplification (low degenerate)	GAGGTCCARCTGCAACARTC
HC FR1 LD3	Forward primer for HC amplification (low degenerate)	CAGGTCCAACTVCAGCARCC
HC FR1 LD4	Forward primer for HC amplification (low degenerate)	GAGGTGAASSTGGTGAATC
HC FR1 LD5	Forward primer for HC amplification (low degenerate)	GATGTGAACTTGGAAGTGTC
LC Kappa	Reverse primer for Kappa LC amplification	GGATACAGTTGGTGCAGCATC
LC Kappa FR1	Forward primer for Kappa LC amplification (high degenerate)	GAYATTGTGMTSACMCARWCTMCA

Supplementary Table 1. Primer sequences for PCR amplification of hybridoma cDNA HC (IgG1, IgG2A, IgG2B, IgG3) and LC (Kappa). A mixture of low and high degenerate primers was used.

Target	Usage	Forward primer (5' -> 3')	Reverse (5' -> 3')
Halo-Tev-Flag-Ube2v2	C8mer	GCACAAGGATCTGAATCCCACTaaacgaattcg ggctcggtaccc	GGATTTCAGATCCTTGTGCGCTattgttgtatgttt gtccttctgggtggc
Halo-Tev-Flag-Ube2v2	C10mer	GCACAAGGATCTGAATCCCACTaaacgaa ttcgggctcggtaccc	GGATTTCAGATCCTTGTGCGCTGTCattgttgtat gtttgtccttctgtggc
Halo-Tev-Flag-Ube2v2	C13mer	GCACAAGGATCTGAATCCCACTaaac gaattcgggctcggtaccc	GGATTTCAGATCCTTGTGCGCTGTCGCTCCAat tgttgtatgtttgtccttctgtggc
Halo-Tev-Flag-Ube2v2	N13mer	GCACAAGGATCTGAATCCCACTagaaa tcggtaactggctttccattcg	GGATTTCAGATCCTTGTGCGCTGTCGCTCCAag ccatgggtggcttgcctagc
Halo-Tev-Flag-Ube2v2	M13mer	GCACAAGGATCTGAATCCCACTactgta ctttcagagcgataacgcg	GGATTTCAGATCCTTGTGCGCTGTCGCTCCAact cagtggttggctgcgcg

Supplementary table 2. Primer sequences for PCR amplification of Halo-Tev-Flag-Ube2v2 to insert the amino-acid sequences of the 8mer, 10mer, or 13mer (capitalized) into the C-terminus, N-terminus, or middle of the Ube2v2 protein (lowercase).

Chapter 8:

Summary

General discussion

Future perspectives

Tumor-specific antigens

This thesis is focused on two antigens expressed on the surface of tumor cells, MICA, and HLA-E. Both antigens are members of the MHC-I family of proteins, and both act as ligands for the NK receptors on NK cells and CD8⁺ T cells.

MICA

MHC-class I polypeptide-related sequence A (MICA), is often found overexpressed on the surface of cancer cells of hematopoietic and epithelial origin²²⁷. MICA is one of the ligands of NKG2D, an activating receptor found on NK cells and CD8⁺ T cells, and gd T cells²¹⁸. Engagement of NKG2D leads to their activation and triggers the cytotoxic activity of these immune cells. Because MICA is absent from the surface of healthy cells, we suspect that targeting this antigen to eliminate the cells that carry it should result in minimal harmful off-target effects.

While the typical immunoglobulins exert their effector functions through their Fc portion, their size compromises efficient tissue penetration. Intact immuno-globulins are less efficient at detecting their targets when using non-invasive imaging methods such as immuno-PET because of their comparatively poor tissue penetration and long circulatory half-life^{371,409,413}. Nanobodies, also referred to as VHHs, are engineered from the variable regions of camelid-derived heavy-chain only antibodies. Nanobodies are characterized by their small size, allowing superior tissue penetration compared to full-sized antibodies. Nanobodies retain their antigen binding properties and are easier to produce and modify than conventional immunoglobulins. Furthermore, because of significant homology between human V_H regions and the V regions in VHHs⁵⁵⁶ nanobodies are considered poorly immunogenic. Nanobodies thus offer an appealing alternative to immunoglobulins for the purpose of launching an immune attack on MICA-positive tumors.

Production and validation of MICA-targeting nanobodies

We produced nanobodies that recognize MICA by immunizing an alpaca with recombinant MICA*009, one of the most common alleles of MICA found in the Caucasian population. Plate-based panning of a phage library for binders yielded several nanobodies that recognize MICA*009 by ELISA. Based on sequence analysis, we chose clones that were unique in the CDR1, 2, and 3 regions (Chapter 3, Figure 1). Although sequence analysis and thorough

characterization of germline regions is impossible without access to the germline VH sequences of the source alpaca, with the help of literature reporting germline VH sequences of different alpacas, and by comparing the sequences of the obtained anti-MICA VHHs, we can hypothesize on the source of the anti-MICA nanobody sequences.

Based on sequence similarities found in the literature, we ascribe the alpaca IGHHV-3-3*01 germline gene to the D8, C12, and 2A9 nanobodies⁵⁵⁶. Somatic hypermutations occur mostly in the CDR regions, as the framework regions are generally less tolerant to such substitutions. VHH A1 and VHH B11 have a single L2V substitution in the framework region compared to the D8, C12, and 2A9 nanobodies. The A1 and B11 nanobodies could thus be derived from a different germline V gene, although neutral substitutions such as the L2V have been observed in framework regions as well⁶⁴¹. VHH A1 and B11 may thus also be derived from the same germline V gene as VHHs D8, C12, and 2A9.

Despite the homology in framework regions 1 and 2 of VHH 2B5, this nanobody has two non-neutral substitutions in framework region 3 compared to the consensus sequence of all the anti-MICA nanobodies. The R72S and N74I substitutions imply that VHH 2B5 is likely derived from a different germline V region. Nanobody E9 also has two substitutions, a neutral D29E in framework region 1 and a basic-to-polar R45Q in framework region 2. VHH E9 is thus likely derived from a different V gene. Nanobody 2D5 has a polar to non-polar S49A substitution in framework region 2 and is likely derived from a different germline V gene. Nanobody H3 shows the largest number of variations and based on alpaca germline sequences described in the literature, we hypothesize that this nanobody is derived from the alpaca IGHHV3-1*01 V gene⁵⁵⁶.

The CDR2 regions of VHH C12, 2A9, B11, E9, and 2D5 show a deletion at position 53. Although somatic hypermutation can produce deletions and insertions in V genes^{566–568}, given the overall dissimilarity in framework regions, the use of distinct V genes that lacks residue 53 is the more plausible explanation. Similar CDR regions, specifically CDR3, imply recognition of related antigens^{562–565}. Except for H3, A1 and 2B5, the remaining CDR3 regions are enriched for the sequence “AxDCLSSxWRx”.

To select which nanobodies to use for downstream applications, we performed an ELISA to estimate affinities, and a competition assay to determine whether the different VHHs recognize distinct epitopes on MICA. Based on those results, we chose VHH-A1 and VHH-H3 for downstream applications, because they bind to recombinant MICA*009 with high affinity

(~0.2 nM and ~0.4 nM respectively) (Chapter 3, figure 2C). The results of the competition ELISA suggest that these nanobodies can be used in synergy, since they seem to recognize different epitopes on the protein (Chapter 3, Figure 2A). Both VHH-A1 and VHH-H3 recognize the alleles MICA*008 and MICA*009 (Chapter 3, Figure 2D), which together cover >50% of the Caucasian population⁵⁵⁷. To our knowledge, these are the first examples of nanobodies specific to MICA.

These nanobodies can be modified at the C-terminus in a sortase-catalyzed reaction because of the presence of a C-terminal LPETG sortase recognition motif. This enables the addition of biotin, fluorophores, other molecules, and even intact proteins^{553,635}. By biotinylating the nanobodies and using a streptavidin-conjugated horse radish peroxidase (HRP) or fluorophore as detection agent, we show that VHH-A1 and VHH-H3 recognize immobilized or denatured recombinant MICA by immunoblot and ELISA (Chapter 3, Figure 2B and 2D). More importantly, we show that these nanobodies recognize surface-disposed MICA on MICA-transfected B16F10 and EL-4 cancer cells, assessed by flow cytometry (Chapter 3, Figure 2E). B16F10 and EL-4 cells are murine cells, derived from a melanoma and T-cell lymphoma respectively. Because mice do not express MICA/B or proteins that show cross-reactivity with anti-human MICA/B reagents, we could use the MICA transfectants of these cancer cell lines to apply the nanobodies *in vivo*.

MICA-targeting nanobodies can be used to generate nanobody-drug conjugates

Maytansines DM1 and DM4 are small molecules that disrupt microtubules. Adducts of antibodies with Maytansine have been approved for clinical use for the treatment of HER2⁺ breast cancer (ado-trastuzumab emtansine⁶⁴²) and folate receptor alpha positive, platinum-resistant epithelial ovarian, fallopian tube, or primary peritoneal cancer (Mirvetuximab soravtansine-gynx⁶⁴³).

We created a nanobody-drug conjugate (VHH-A1-DM1) by conjugating a Maytansine derivative DM1 to VHH-A1 in a sortase-mediated reaction (Chapter 3, Figure 3A and 3B). We observed decreased proliferation in EL-4 MICA⁺ tumor cells treated with VHH-A1-DM1 compared to EL-4 WT tumor cells *in vitro*. The calculated IC₅₀ is comparable to that of free Maytansine (DM4) (Chapter 3, Figure 3C and 3D). The difference between DM1 and DM4 is the inclusion of an additional dimethyl group next to the terminal cysteine in DM4, which increases the hydrophobicity and facilitates cell penetration of

DM4, thus increasing the cytotoxic effects⁶⁴⁴. In our experiments, an adduct of VHH-A1-DM4 proved ineffective in killing MICA⁺ cells (Chapter 4, Figure 1C). Perhaps the cleavable linker between VHH-A1 and DM4 releases the cytotoxic payload into the medium and decreases the intracellular cytotoxicity.

The VHH-A1-based nanobody-drug conjugate was ineffective in treating B16F10-derived MICA⁺ cells *in vitro* (Chapter 4, Figure 1B). Although B16F10 has been reported more resistant to treatment with DM1 alone, the precise reasons for this resistance remain to be identified⁵⁷⁸. Inclusion of cell lines that represent different tumor types will be required to determine the extent of resistance to VHH-A1-DM1.

For our *in vivo* model, we extended the half-life of the nanobody drug conjugate by creating a genetic C-C fusion of VHH-A1 to an anti-murine kappa light chain nanobody (VHH-mKappa). We ligated DM1 to this fusion by sortase reaction to create VHH-A1-VHH-mKappa-DM1 (Chapter 4, Figure 2A). Mice bearing subcutaneous EL-4 MICA⁺ cells were treated 3x weekly with an intraperitoneal injection of 5 mg/kg of this fusion (Chapter 4, Figure 3A). We showed that the VHH-A1-VHH-mKappa-DM1 was ineffective in treating EL-4 MICA⁺ tumors (Chapter 4, Figure 3B and 3C). Although tumor growth in the treated mice started slower compared to mice treated with a non-targeting nanobody-drug conjugate, once treatment was stopped this difference disappeared. In fact, the treated mice showed accelerated tumor growth upon cessation of treatment. Perhaps intravenous administration of VHH-A1-DM1 improves its delivery to the tumor. Further research is needed to validate the efficacy of VHH-A1-DM1 *in vivo*. Extending the half-life of the nanobody-drug conjugate is important for its persistence *in vivo* and might instead be achieved by conjugation of the nanobody-drug conjugate to polyethylene glycol (PEG20).

The creation of different VHH-drug combinations, for example using other tubulin inhibitors like Auristatins, DNA damaging agents like Exatecans, immuno-modulators like STING agonists, or radiopharmaceuticals for targeted radiotherapy, deserves consideration. We have not performed a direct comparison of the nanobody-drug conjugated to other MICA/MICB targeting agents, such as full-sized monoclonal antibodies. This could be done by engineering the coding sequence(s) for such reagents to contain a

sortase motif for site-specific conjugation, as was done in this thesis for the HLA-E cytoplasmic tail-specific monoclonal antibody.

MICA-targeting nanobodies can be used in VHH-based CAR NK cell therapy

A relatively new, now widely explored form of immunotherapy is adoptive cell transfer, and more specifically, the use of T and NK cells modified with a chimeric antigen receptor (CAR). scFv-based CAR T cell therapy is already considered as a possible cancer therapy, with several such therapies approved by the FDA for treatment of relapsed or refractory multiple myeloma and B-cell lymphoma, based on BCMA and CD19 targeting respectively. However, some limitations of scFv-based CARs merit discussion. First, scFvs used as targeting moieties may lack the affinity and specificity of the immunoglobulin from which they are derived. Furthermore, the immunogenicity of the scFv, as well as the potential of self-aggregation of scFv-based CARs, must be considered. This is relatively easy to diagnose and fix, for instance by grafting the CDR regions of the mouse-derived antibodies into human-derived framework region backbones⁶⁴⁵. In contrast, the single domain nature of VHHs precludes self-association, while VHHs retain excellent antigen recognition with binding constants typically in the nanomolar range. The clinical success of a nanobody-based CAR T cell, Carvykti, for the treatment of multiple myeloma is the first example of a clinically efficacious nanobody-based CAR T cell. This CAR contains a bi-paratopic ectodomain that recognizes the antigen BCMA, a protein highly expressed on fully mature plasma cells and on multiple myeloma⁶⁰². The success of Carvykti establishes the suitability of nanobodies as building blocks for the construction of CARs targeting other antigens.

Although CAR T cell therapy is widely studied in the clinic, there are several possible advantages of using CAR NK cells instead. First, NK cells are easier to source and expand *ex vivo* than T cells, with the ability of producing CAR NK cells not only from the patient's or a donor's peripheral blood, but also from umbilical cord blood, manufactured from iPSCs, or from existing immortalized NK cell lines (e.g. NK-92). Unlike T cells, NK cells do not pose the risk of graft-versus-host disease (GVHD) in an allogeneic setting and are not MHC-restricted. CARs to be installed on NK cells allow the inclusion of a wider range of co-stimulatory domains such as CD244, CD137, and NK activating receptors. Furthermore, NK cells have an inherent innate anti-tumor response. Even if a tumor were to downregulate the CAR target, CAR

NK cells might still exert a cytotoxic effect. Lastly, NK cells release the cytokines IL-3, TNF- α , and IFN- γ , only the latter of which is associated with cytokine release syndrome, a major side-effect of CAR T therapy caused by excessive secretion of IL-2, IL-6, and IFN- γ . For these reasons, we opted for the production of CAR NK cells instead of CAR T cells.

We developed VHH-based CAR NK cells by lentiviral transduction of NK-92 cells with a construct containing VHH-A1 or VHH-H3 as targeting moiety, followed by a transmembrane domain and the intracellular CD3 ζ co-stimulatory domain and the CD28 signaling domain (Chapter 5, Figure 1A). Successfully transduced cells were sorted based on GFP expression and expanded to create the stable A1 CAR NK, H3 CAR NK, or non-targeting empty vector (EV) CAR NK lines (Chapter 5, Figure 1B and 1C). We determined the efficacy of the CAR NK cells *in vitro* by co-culturing them with B16F10 melanoma cells or EL-4 T-cell lymphoma cells, and their MICA⁺ transfectants. By measure of LDH-release, we observed a significant increase in cytotoxicity of MICA⁺ B16F10 or MICA⁺ EL-4 cancer cells when co-cultured with VHH-A1-based CAR NK cells, compared to WT B16F10 or EL-4 cells co-cultured with A1 CAR NK cells, or either line co-cultured with the EV CAR NK cells (Chapter 5, Figure 2A). This cytotoxicity is caused by activation of the A1 and H3 CAR NK cells, confirmed by a significant increase in IFN γ released by the A1 and H3 CAR NK cells co-cultured with MICA⁺ B16F10 or MICA⁺ EL-4 cells, compared to these cells co-cultured with WT B16F10 and EL-4 cells (Chapter 5, Figure 2B).

In vivo, using an ⁸⁹Zr-labeled nanobody that targets the transferrin receptor on the NK-92 cells, we were able to track and localize the A1 CAR NK cells to MICA⁺ lung metastases in mice by immuno-PET imaging. We observed a PET signal, and thus localization, to the lungs of mice bearing MICA⁺ lung metastases until 72-hours after injection of A1 CAR NK cells. Less positive signal was observed in the lungs of mice bearing MICA⁺ lung metastases which received EV CAR NK cells (Chapter 5, Figure 4B). We conclude that the A1 CAR NK cells, by virtue of finding and binding to their MICA⁺ target cells, can persist longer *in vivo* than non-targeting CAR NK cells. This data provides us with insight into the parameters for administration of the VHH-based CAR NK cells for treatment of MICA⁺ tumors.

In an *in vivo* model of mice grafted with primary subcutaneous B16F10 MICA⁺ tumors, the A1 CAR NK cells are cytotoxic towards the MICA⁺ B16F10 tumors,

as shown by a significant reduction in the rate of tumor growth and an increase in overall survival for the treated mice compared to mice treated with EV CAR NK cells (Chapter 5, Figure 3B). These findings suggest a therapeutic potential for the VHH-based CAR NK cells. It is important to note the low group size of $n = 7$ for the A1 CAR NK treated group and $n = 3$ for the EV CAR NK treated group. During the first treatment injection, we injected 10×10^6 cells retro-orbitally, after which a third of the mice died. We suspect that the high number of cells injected at once created a blockage in the lung capillaries. Although the obtained results are significant, larger cohort sizes might increase our power. Given the PET imaging data with B16F10 metastasis model, it would be interesting to test the effect of treatment with the CAR NK cells on metastases formation.

MICA-targeting nanobodies to produce CAR T cells

Despite the potential benefits of CAR NK cell therapy over CAR T cell therapy, much work has already been conducted using CAR T cells and as mentioned, a nanobody-based CAR T cell therapy has been approved by the FDA. It would thus be interesting to pursue anti-MICA immunotherapy with CAR T cells. To this end, we produced VHH-based CAR T cells from murine primary T cells by retroviral transduction, using an MSCV-based vector. The CAR construct follows the same second-generation principal as the CAR NK cells, containing a GFP fluorophore followed by a P2A cleavage domain, VHH-A1 or VHH-H3 as targeting moiety, a transmembrane domain, and the intracellular CD3 ζ co-stimulatory domain and the CD28 signaling domain (Chapter 6, Figure 1A and 1B). We were able to reach transduction efficiencies of ~35%, based on GFP expression (Chapter 6, Figure 1C). When using these CAR T cells in co-culture experiments, we observed significant activation and cytotoxicity in co-culture of A1 CAR T cells with MICA⁺ B16F10 and MICA⁺ EL-4 cells (Chapter 6, Figure 2A and 2B). However, these effects were only measured at high effector-to-target ratios of [1:10] or more. Because of the relatively low transduction efficiency and considering that only ~20% of the isolated murine T cell population consists of CD8⁺ T cells (the population responsible for cytotoxicity), we more accurately have a VHH-based CD8⁺ CAR T cell pool of ~7%. When mixing the effector and target cells at a ratio of [1:10], we have an effective [E:T] of 1:0.3, which is likely insufficient to create significant anti-tumor responses. To increase the [E:T], we could increase the number of T cells in the well. We hypothesize that this will overcrowd the wells and reduce viability of the CAR T cells, because T cells have an optimal density of $1 - 2.5 \times 10^5$ cells/mL. To obtain more favorable [E:T] ratios without overcrowding the wells, we could decrease the amount of target cells.

Unfortunately, the assays we use currently for measuring cytotoxicity and IFN- γ release might not be appropriate for such low cell counts. We would thus have to find a more sensitive assay for measuring these parameters.

Due to the limitations in transduction efficiency of the CAR T cells, we did not pursue their *in vivo* properties. This remains an interesting avenue to pursue in future research since data from our lab and others has shown great potential of treating tumors with nanobody-based CAR T cells^{472,476,550}.

Future perspectives

For the present work, we created a second-generation CAR construct, utilizing co-stimulation and signaling by the CD28 and CD3 ζ domains. To improve stability, activation, and signaling of these CAR NK cells, improvements to the CAR construct might include addition of the 4-1BB signaling domain, known to enhance persistence of the CAR NK cells *in vivo*. Further enhancement could be reached by including a cytokine auto-stimulation ectodomain, such as IL-15 for the CAR NK cells⁶¹¹ or IL-2 for the CAR T cells⁶⁴⁶, inclusion of additional co-stimulatory domains such as CD27 or STAT3/5 binding motifs^{647,648}, enhancement of the CD28 signaling domains by incorporation of certain null mutations of the CD28 subdomains^{580,649} or the inclusion of immunoreceptor tyrosine-based activation motif (ITAMs) 2 and 3 in the CD3 ζ portion⁶⁵⁰.

The tumor microenvironment often shows increased deposition of extracellular matrix (ECM) components, which can cause encapsulation of a solid tumor and thus impose a physical barrier that limits access to the tumor for CAR T or CAR NK cells. CAR macrophages may help degrade the ECM by secretion of proteases, which improves the outcome of immunotherapy. Since we produced two nanobodies, H3 and A1, each recognizing a unique epitope on MICA, H3-based CAR macrophages might be able to help degrade the ECM and attract A1-based CAR T or CAR NK cells to aid in tumor-specific cytotoxicity.

For clinical translation of this research, several points are worth mentioning. Although MICA expression is typically absent from healthy cells, expression of MICA and MICB is seen in gut epithelium and could elicit a harmful ‘off-tumor on-target’ response⁶⁰⁴. Since gut epithelia are capable of rapid repair, this risk may prove to be manageable. Since mice do not possess a MICA/B homolog, this research should be extended to MICA⁺ animals such as non-human primates, which express MICA/B type molecules. The use of a MICA-

transgenic mouse harboring the correct allele of MICA could provide a useful alternative to the often highly regulated research in non-human primates⁶⁰⁶.

The genetic instability of NK-92 cells requires their irradiation prior to infusion in a patient to avoid the possibility of any malignant outgrowths of the NK population. However, irradiation impairs proliferation of the transferred NK-92 cells and thus limits their persistence *in vivo*. As an alternative, CAR NK cells could be created from patient-derived peripheral NK cells, although this method comes with its own limitations. NK cells only comprise 10% of circulating white blood cells, which requires *ex vivo* expansion on a cell line feeder layer, again incurring a risk⁶⁵¹. In addition, allogeneic NK cells sourced from healthy donors or umbilical cord blood also require expansion, and T cells need to be carefully removed to avoid GVHD. Other alternative NK cell sources are induced pluripotent stem cell-derived NK cells (iPSC-NKs), which can easily be produced from a standardized, homogeneous cell population and grown to clinical scale.

We recognize the limitations of using cell lines in which MICA is expressed through transfection. We thus can't conclude on the efficacy of the nanobodies on human cancer cell lines naturally expressing MICA. The limiting factor for us here was the availability of patient-derived cell lines expressing the correct alleles of MICA. We think these are excellent avenues to explore in future research.

In cancer patients, MICA is often shed from the cancer cell surface, rendering the cells invisible to MICA-targeted immune attack. Shedding occurs when the $\alpha 3$ domain of MICA undergoes ECM-induced proteolytic cleavage, facilitated by the disulphide isomerase ERp5 and ADAM-type proteases such as ADAM10 and ADAM17²³²⁻²³⁶. Wucherpfennig and coworkers have generated a monoclonal antibody, 7C6, that inhibits shedding of MICA/B and thus increases the density of MICA/B proteins on the surface of tumor cells²⁴³. Combination therapy of MICA-targeting nanobody-drug conjugates or nanobody-based CAR NK or T cells with the 7C6 antibody may therefore be worth exploring to enhance the efficacy of treatment.

HLA-E

Conventional MHC-I molecules (HLA-A, -B, and -C) present peptides derived mostly from intracellular antigens. In humans, HLA-E is specialized in the presentation of peptides derived from the signal sequences of other MHC-I products, as well as the signal sequences of certain viral glycoproteins. Tumors often downregulate the surface expression of the classical MHC-I molecules encoded by the HLA-A, -B, and -C loci, thereby evading cytotoxicity exerted by CD8⁺ T cells. In contrast, many cancer cells overexpress HLA-E. HLA-E acts, among other things, as a ligand of NKG2A, the inactivating or inhibitory receptor found on CD56^{hi} NK cells and on a subset of CD8⁺ T cells. Engagement of HLA-E by NKG2A inhibits the cytotoxicity of CD56^{hi} NK and CD8⁺ T cells, and thus can lead to immune evasion by the tumor⁶⁵².

Commercially available antibodies against the ectodomain of HLA-E, MEM-E/02 and 3-D12, display varying degrees of cross-reactivity with allelic products of the HLA-B and HLA-C loci⁶⁵³. A comparison of the sequences of HLA-E with those of other MHC-I molecules shows strong sequence conservation in the ectodomains. In contrast, the amino acid sequence of the cytoplasmic tail of HLA-E appears to be strongly conserved and distinct from the cytoplasmic tail sequences of the HLA-A, -B, and -C proteins (Chapter 7, Figure 1).

Peptide-bound HLA-E rapidly exits the endoplasmic reticulum (ER), traverses the secretory pathway, and is expressed at the cell surface. The cytoplasmic tail of MHC-I molecules plays a role in export from the ER and in endocytosis²⁸⁰. Most HLA-E, however, appears to be retained in an immature state in the ER, and it has been confirmed that the cytoplasmic tail of HLA-E plays a role in its ER retention and endocytosis²⁸¹.

Based on these observations, we developed a monoclonal antibody directed to the cytoplasmic tail of HLA-E. Because of the unique sequence of the cytoplasmic tail, we expect no cross-reactivity with other MHC-I molecules. This antibody can thus be used for diagnosis of HLA-E positive cancers. Furthermore, antibodies against the HLA-E cytoplasmic tail could be a useful tool for studying the cytoplasmic tail interactions.

A monoclonal antibody targeting the cytoplasmic tail of HLA-E

To target the cytoplasmic tail of HLA-E, we fused the peptide sequence of the cytoplasmic tail (GGCSKAEWSDSAQGSESHSL, referred to hereafter as

HLA-E_{tail}) to a murine MHC-II-targeting nanobody (VHH_{MHCII}) by a sortase-mediated reaction (Chapter 7, Figure 2A). Based on previous research, immunization of mice with this antigen-fused nanobody results in targeted delivery of antigen to antigen presenting cells and elicits strong B and T cell immunity^{420,463}. We immunized C57/Bl6 mice with VHH_{MHCII}-HLA-E_{tail} and selected a mouse that showed a high titer for hybridoma production (Chapter 7, Figure 2B). To obtain hybridomas that target the extracellular tail peptide, and not VHH_{MHCII}, we performed all screening ELISAs on a fusion of GFP with HLA-E_{tail}, obtained via sortase reaction. The mice were never exposed to GFP and should thus have no antibodies to this protein. So, any response on the ELISA plate would ensure specificity for the cytoplasmic tail peptide (Chapter 7, Figure 2C). We obtained several hybridomas, all of which used the identical heavy chain sequence derived from the VH IGHV1-72*01 and J IGHJ2*01 genes. The hybridomas used 3 VJ kappa light chain rearrangements, based on the usage of the germline Vκ IGKV1-135*01, IGKV4-90*01, and IGKV-50*01 genes (Chapter 7, Figure 3A and 3B)

By performing an immunoblot with the antibodies on GFP ligated to a series of overlapping peptides with a 1-residue pitch, we determined that the antibodies recognize a 7-residue epitope (“SAQGSES”) (Chapter 7, Figure 5A). This sequence alone was insufficient as an epitope tag in combination with the antibodies. To determine the smallest possible tag, we expanded the sequence and created an 8-mer, 10-mer, and 13-mer peptide which we incorporated at the C-terminus of an unrelated protein. We overexpressed this protein in HEK-293T cells by transfection and subjected cell lysates to immunoblot with conditioned medium from hybridoma cultures. The monoclonal antibodies “19-H12” and “2-D12” recognized the 13-mer (WSDSAQGSESHSL) at the C-terminus of the target protein, but not the 8-mer or 10-mer (Chapter 7, Figure 5B). We ran a search of the sequence against all available protein sequences and found a hit only for HLA-E in humans, and its non-human primate homologs. Because this sequence is located in the cytoplasm, the use of the WSDSAQGSESHSL-tag in extracellular proteins in cells of human or non-human primate origin would be possible.

To explore whether recognition of the 13-mer tag by the antibodies is sequence context-dependent, we placed the 13-mer peptide sequence at the N- or C-terminus, or at an internal location of UBE2V2 and confirmed

immunoreactivity with both the 19-H12 and 2-D12 antibodies, independent of the location of the tag, by immunoblot (Chapter 7, Figure 5C). Immunoprecipitation further validated the interaction of the 19-H12 mAb with the 13-mer tag. The immunoprecipitated protein complex can be eluted by addition of an excess of free synthetic peptide (Chapter 7, Figure 5D, 5E, and 5F). Given the strong reactivity of the antibody in immunoblots, and the lack of cross-reactivity with endogenous proteins, WSDSAQGSESHSL may thus have utility as an epitope tag.

Site-directed modification of the monoclonal antibody

We modified the C-termini of the 19-H12 heavy and light chains with an LPETG sortase recognition motif by cloning a GBlockTM into a mammalian expression vector and producing the hybridomas in EXPI 293 cells. The addition of the LPETG motif allows modification of the antibodies by sortase-mediated transpeptidation reaction (Chapter 7, Figure 4). This method, when compared to more conventional methods of labeling antibodies, ensures reproducibility, site-specificity, and produces the desired product in excellent yield. Site-directed modification with fluorophores or biotin eliminates the need for secondary antibodies for detection in assays like flow cytometry. We have shown the functionality of the HLA-E_{tail} specific mAb for cell staining in immunoblot, immunofluorescence, flow cytometry, and immunohistochemistry (Chapter 7, Figure 6 and Figure 7).

Future perspectives

In conclusion, we have developed the monoclonal antibody 19-H12 which, in combination with its 13-residue epitope, can be used as epitope tag for extracellular proteins, since the 13-residue peptide is not found in any other protein except HLA-E. The epitope tag could be further explored for detection or purification of, for instance, a poorly immunogenic protein, or other proteins in a setting where the set of available epitope tags in current use is exhausted. The epitope mapping revealed a core epitope of 7 amino acids long ("SAQGSES"). We had to extend this sequence to the 13-mer, which we did by inclusion of the flanking amino acids present in the cytoplasmic tail peptide. Perhaps the 7-mer is the smallest epitope recognized by the antibody, and the 5-residue extension facilitates binding by aiding the 3D confirmation. To investigate this, we could flank the SAQGSES core epitope with unrelated amino acids and determine binding of the antibody.

The monoclonal antibody 19-H12, either directly labeled with biotin or fluorophores, or by using a secondary antibody, targets the cytoplasmic tail of HLA-E intracellularly as assessed by flow cytometry, immunofluorescence, and immunohistochemistry. Because of its epitope, the antibody will likely not cross-react with other MHC-I molecules.

As shown with immunohistochemistry, we can detect aberrant HLA-E expression on samples of human progressive non-muscle invasive bladder cancer at high sensitivity compared to MEM-E/o2. These characteristics make 19-H12 a potential staple for diagnosis of HLA-E⁺ tumors in the clinic.

Furthermore, studies on the involvement of the cytoplasmic tail in HLA-E trafficking through the endoplasmic reticulum and turnover from the cell membrane might benefit from this newly developed reagent. Its use does not require genetic modification of the target recognized and could thus find application in samples or cell lines established from primary tumors. Monoclonal antibody 19-H12, when labeled, can be used for detection of HLA-E intracellularly. Although not pursued in the context of this thesis, the ability to retrieve otherwise unmodified HLA-E molecules in pulse chase experiments might add further refinement to the study of intracellular trafficking of HLA-E. Understanding the transport pathways of HLA-E is essential for further elucidating HLA-E-restricted CD8⁺ T cell responses, like those seen in the more recently developed cytomegalovirus (CMV)-based vaccines against SIV²⁸⁶.

Appendices

Nederlandse samenvatting

Algemene introductie

De meest voorkomende soorten kanker in de Verenigde Staten zijn prostaat-, long- en darmkanker bij mannen, en borst-, long-, en darmkanker bij vrouwen. Dankzij wetenschappelijk onderzoek in de afgelopen decennia is de overlevingskans van kanker aanzienlijk is gestegen, maar het is een aandoening die nog steeds verantwoordelijk is voor ongeveer 15% van alle sterfgevallen wereldwijd. Patienten worden vaak behandeld met chemotherapie, bestraling, of operatief om de tumor te verwijderen. Ondanks de effectiviteit van deze behandelingen zijn ze niet voor elke patient geschikt. Veel van deze vormen van therapie hebben ook ernstige bijwerkingen.

Een relatief nieuwe vorm van behandeling waar recent veel voortgang mee is geboekt is immunotherapie. Hierbij wordt het imuunsysteem van de patient zelf ingezet om kankercellen te herkennen en elimineren. Dit gebeurt onder andere door middel van antilichamen die bepaalde doeleiwitten, of antigenen, op de tumor herkennen. Deze antilichamen kunnen dan bijvoorbeeld medicijnen gericht naar de tumorcel brengen, de functie van de herkende eiwitten blokkeren, of immuuncellen activeren. Een andere vorm van immuuntherapie is gebaseerd op genetische manipulatie van de cellen van de patient zelf. Een voorbeeld van deze vorm van celtherapie maakt gebruik van chimere antigeen receptor (CAR) T cellen of CAR 'natural killer' (NK) cel therapie. CAR T of CAR NK cellen zijn lymfocyten die genetisch gemodificeerd zijn met als uiteindelijk doel om tumorcellen te herkennen en doden. Een voordeel van CAR NK cellen over CAR T cellen is dat NK cellen een minder kans geven op 'graft versus host disease' (GVDH)²¹¹⁻²¹⁵ met minder bijwerkingen veroorzaakt door overproductie van cytokines, zoals vaak wordt gezien na behandeling met CAR T cellen²¹⁷. NK cellen zijn daarnaast makkelijker te isoleren uit donorbloed, navelstrengbloed, pluripotente stamcellen, en cellijnen zoals NK-92²⁰⁵⁻²¹⁰.

Het CAR gedeelte van zo'n cel bestaat vaak uit een extracellulair 'single-chain variable fragment' (scFv), dat het tumor-antigeen herkent. Het intracellulaire gedeelte van een CAR bestaat uit domeinen betrokken bij signaal transductie om zo de T cel te activeren wanneer de CAR T of CAR NK cel het tumor-antigeen herkent. Het voor dat doel meest gebruikte domein is afkomstig van

het cytoplasmatisch segment van het CD3 ζ eiwit, in combinatie met CD28 of 4-1BB. Activatie van een CAR-dragende cel leidt tot een cytotoxisch effect en dus celdood van de tumorcel, dankzij de productie en uitscheiding van cytokines en cytotoxische eiwitten door de CAR T of NK cel.

Bij de meeste vormen van immuuntherapie is het dus belangrijk om een tumor-specifiek of tumor-geassocieerd doeleiwit ('target') te hebben dat door de immuuncellen of antilichamen kan worden herkend. In dit proefschrift beschrijf ik een aanpak gecentreerd op twee tumor-geassocieerde antigenen: MICA en HLA-E.

MICA

MICA, en het daaraan verwante MICB, komen voor op het oppervlak van cellen die door een virale infectie of transformatie tot tumorcel, gestressed zijn. Gezonde cellen brengen doorgaans geen MICA/B tot expressie. MICA/B is een ligand voor de activerende NKG2D receptor, aanwezig op NK cellen en cytotoxische T lymfocyten. Als MICA/B bindt aan NKG2D wordt de immuuncel geactiveerd en wordt de MICA/B-positieve cel gedood door uitscheiding van cytokinen en cytotoxische eiwitten zoals Granzyme B. MICA/B komt vaak voor op het celoppervlak van tumorcellen van hematopoietische oorsprong, maar ook op veel epitheliale tumoren, bijvoorbeeld darmkanker, eierstokkanker, baarmoederhalskanker, borstkanker, alvleesklierkanker, melanoom, en galblaaskanker.

In dit proefschrift beschrijven we de ontwikkeling van MICA-specifieke 'nanobodies'. Een 'nanobody', ook wel VHH genoemd, is het recombinant tot expressie gebrachte variabele segment van zware-keten antilichamen. 'Nanobodies' zijn klein: waar conventionele antilichamen een massa hebben van 150kDa, hebben 'nanobodies' een massa van 15kDa. Hierdoor penetreren ze makkelijker dieper in weefsels, zijn ze relatief eenvoudig te produceren, zijn ze stabiel bij hogere temperaturen en andere omstandigheden, en hebben ze uitstekende capaciteit om hun antigeen te binden.

MICA-specifieke nanobodies detecteren MICA op cellen en tumoren

We hebben nanobodies ontwikkeld door een alpaca te immuniseren met recombinant MICA eiwit. Na immunisatie werden de B cellen van de alpaca geïsoleerd en gebruikt om een bibliotheek van de variable segmenten van 'heavy chain-only' antilichamen te maken. Deze bibliotheek wordt in bacteriofagen tot expressie gebracht en geselecteerd op 'nanobodies' die aan

MICA binden. In totaal hebben we 8 verschillende nanobodies tegen MICA gevonden, waarvan we er twee geselecteerd hebben voor verdere toepassingen. Deze nanobodies, VHH-A1 en VHH-H3, binden beide aan MICA met hoge affiniteit (~ 0.2 en ~ 0.4 nM, respectievelijk), herkennen de allelen MICA*008 en MICA*009 (welke aanwezig zijn bij meer dan de helft van de menselijke populatie), en kunnen worden gebruikt in een immunoblot. Beide nanobodies herkennen verschillende epitopen op MICA en kunnen dus tegelijkertijd gebruikt worden voor verschillende doeleinden. De nanobodies herkennen MICA op het celoppervlak van MICA-positieve kankercellen B16F10 (melanoom) en EL-4 (T-cel lymfoom) (Hoofdstuk 3, Figuur 2). In deze cellijnen, afkomstig van de muis, wordt het MICA eiwit door middel van transfectie tot expressie gebracht.

MICA-specifieke nanobodies voor immunotherapie: nanobody-drug conjugate

Een vorm van immuuntherapie in opkomst is het gebruik van zogenaamde ‘antibody-drug conjugates’ (ADCs), waarbij celdodende medicijnen aan antilichamen worden gekoppeld. Wanneer het antilichaam aan het antigeen bindt wordt de celdodende stof specifiek aan de tumorcel afgeleverd. Dit staat in principe een enorme reductie toe in de hoeveelheid cytostaticum waaraan de patient wordt blootgesteld.

Wij gebruikten VHH-A1 gekoppeld aan de microtubulus-remmer Mertansine (DM1) als ‘nanobody-drug conjugate’ (NDC). We zagen dat MICA⁺ EL-4 cellen behandeld met VHH-A1-DM1 aanmerkelijk gevoeliger zijn voor de NDCs dan wildtype (WT) EL-4 cellen, of MICA⁺ EL-4 cellen behandeld met een niet-specifieke NDC (VHH_{MHCII}-DM1; EL-4 cellen brengen geen MHC-II tot expressie). We kunnen dus hetzelfde celdodende effect bereiken met een lagere dosis van het medicijn. We testten de specificiteit van VHH-A1-DM1 door MICA⁺ en WT EL-4 cellen te mengen en te behandelen met VHH-A1-DM1, VHH_{MHCII}-DM1, of vrij DM1. Celdood werd gemeten door middel van cytometrie. We zagen een significante afname in het aantal MICA⁺ cellen ten opzichte van WT cellen na toevoeging van VHH-A1-DM1. De cellen behandeld met VHH_{MHCII}-DM1 of vrij DM1 laten daarentegen een vergelijkbare afname zien in het aantal MICA⁺ cellen en WT cellen (Hoofdstuk 3, Figuur 3)

MICA-specifieke nanobodies voor immunotherapie: CAR NK cellen

Zoals eerder genoemd zijn CAR T cellen immuuncellen die zodanig genetisch gemodificeerd zijn om specifiek tumorcellen te herkennen en doden. In ons geval gebruiken we de nanobodies VHH-A1 en VHH-H3 als extracellulair antigeen herkennings domein, en als signaaldomeinen maken we gebruik van CD3 ζ en CD28. In plaats van CAR T cellen, hebben we CAR NK cellen geproduceerd, welke afgeleid zijn van de NK-92 cellijn.

De CAR NK cellen, A1 CAR NK en H3 CAR NK, samen met een “empty vector” (EV) CAR NK als negatieve controle, werden geproduceerd door transductie met lentivirus dat codeert voor het CAR construct. We bevestigden expressie van het CAR construct door de aanwezigheid van GFP te meten met immunoblot en cytometrie, en door CD3 ζ expressie aan te tonen in een immunoblot. We stelden WT en MICA⁺ B16F10 en EL-4 cellen bloot aan de CAR NK cellen en zagen een significante hoeveelheid celdood in MICA⁺ cellen in aanwezigheid van A1 en H3 CAR NK cellen, maar niet wanneer EV CAR NK cellen werden gebruikt. WT cellen blootgesteld aan A1, H3, of EV CAR NK cellen lieten minder celdood zien. We zagen activatie van CAR NK cellen aan de hand van een toename in expressie van IFN- γ in de A1 en H3 CAR NK cellen in combinatie met MICA⁺ tumorcellen, maar niet in combinatie met WT tumorcellen (Hoofdstuk 5, Figuur 2).

Een mogelijke behandeling van tumoren met de A1 CAR NK cellen werd onderzocht in muizen. We behandelden MICA⁺ B16F10 tumor-dragende muizen met A1 CAR NK cellen of EV CAR NK cellen. De muizen behandeld met A1 CAR NK lieten een significant tragere tumorgroei zien met een grotere overlevingskans dan muizen behandeld met EV CAR NK (Hoofdstuk 5, Figuur 3).

We toonden aan dat de CAR NK cellen specifiek naar de MICA⁺ tumoren gaan door middel van immuno-PET. Hiertoe gebruikten we een “nanobody” dat de transferrin receptor herkent. De nanobody herkent specifiek de humane versie van deze receptor, welke op de NK-92 cellen te vinden is, maar niet de receptor op de cellen van de muis. We injecteerden muizen met MICA⁺ B16F10 longmetastasen met EV CAR NK cellen of A1 CAR NK cellen, en de “nanobody” gelinkt aan ⁸⁹Zr. Tot 72 uur na injectie zien we een specifiek signaal in de longen van de muizen welke de A1 CAR NK cellen ontvingen, maar niet in de longen van de muizen geïnjecteerd met EV CAR NK cellen (Hoofdstuk 5, Figuur 4).

Conclusie

We hebben 'nanobodies' ontwikkeld tegen MICA, een MHC-I gerelateerd eiwit dat veel voorkomt op verschillende tumoren en op cellen die als gevolg van cellulaire 'stress' door het immuunsysteem moeten worden verwijderd. Deze 'nanobodies' kunnen worden ingezet voor diagnose en behandeling van MICA⁺ tumoren, bijvoorbeeld met behulp van cytometrie en immunoblot. Voor de behandeling van kanker kunnen we de nanobodies inzetten als nanobody-drug conjugate (NDC), gekoppeld aan de microtubulus inhibitor DM1. We verwachten dat andere celdodende medicijnen eveneens kunnen worden gebruikt in de vorm van een NDC. We hebben hoge verwachtingen dat we, na verdere optimalisering, de NDCs kunnen gebruiken voor behandeling van MICA⁺ tumoren in muizen.

Door de nanobodies te gebruiken als extracellulair, antigeen-bindend domein van een CAR construct hebben we MICA-specifieke CAR NK cellen gegenereerd. Deze cellen zijn in staat MICA⁺ tumorcellen specifiek te herkennen en doden in celweek. In muizen met MICA⁺ tumoren leidde de behandeling met A1 CAR NK cellen tot een tragere tumorgroei en verbeterde levensverwachting, in vergelijking met muizen behandeld met niet-specifieke CAR NK cellen.

Omdat MICA niet op gezonde cellen voorkomt, verwachten we weinig bijwerkingen bij eventuele klinische toepassing. Dit zou men kunnen onderzoeken door de MICA-specifieke nanobodies te testen in apen, welke een vergelijkbare versie van MICA hebben als mensen.

HLA-E

MHC-I eiwitten zijn aanwezig op het oppervlak van elke kernhoudende cel. MHC-I presenteert fragmenten in de vorm van peptiden van voornamelijk cytosolaire eiwitten aan cytotoxische T cellen. Een gezonde cel presenteert fragmenten van zijn eigen intracellulaire eiwit repertoire. Tijdens de ontwikkeling van het immuunsysteem worden T cellen op juist deze complexen gecalibreerd om mogelijke reactiviteit met lichaamseigen eiwitten te vermijden. Als een cel geïnfecteerd is met een bacterie of virus, of door mutaties getransformeerd is tot tumorcel, presenteert de cel fragmenten van deze lichaamsvreemde eiwitten aan het celoppervlak als een complex met MHC-I. De cytotoxische T cel herkent deze complexen en doodt de cel die ze draagt. Sommige geïnfecteerde cellen of tumorcellen voorkomen deze celdood door de expressie van MHC-I eiwitten uit te schakelen.

HLA-E is een uniek MHC-I eiwit dat peptiden presenteert die afkomstig zijn van de andere MHC-I eiwitten, of van virale membraaneiwitten. Met name de signaalsequenties, verantwoordelijk voor de insertie van uitgescheiden en membraan eiwitten in het endoplasmatisch reticulum, worden door HLA-E gepresenteerd. HLA-E is een ligand voor de NKG2A en NKG2C receptoren op NK cellen. NKG2A is een inhibitoire receptor, dus als HLA-E aan deze receptor bindt worden de NK cellen en cytotoxische T cellen geïnactiveerd. HLA-E wordt veel gezien op verschillende tumoren van hematopoietische en epitheliale oorsprong. Expressie van HLA-E is vaak geassocieerd met een slechtere prognose in long kanker, glioom, nierkanker, darmkanker, borstkanker, en eierstokkanker.

De extracellulaire domeinen vertonen een sterke mate van sequentie homologie voor de producten van de HLA-A,-B, -C en -E loci. Het ontwikkelen van een antilichaam dat specifiek HLA-E herkent, zonder kruisreactie met allelen van de HLA-A, -B en -C loci is niet eenvoudig gebleken. Echter, het intracellulaire deel van HLA-E, ook wel de cytoplasmatische ‘staart’ genoemd, is wat aminozuurvolgorde betreft uniek. De cytoplasmatische staart van MHC-I moleculen, en van HLA-E in het bijzonder, speelt een rol bij het transport van het endoplasmatisch reticulum (ER) naar het celoppervlak, alsook in de internalisatie en recycling, zowel vanaf het celoppervlak en vanuit endosomen^{281,282}. Omdat de ‘staart’ van HLA-E uniek is, en gezien de mogelijke rol bij stabilisatie en expressie van HLA-E op het celoppervlak, is dit een interessant doelwit om antilichamen tegen te ontwikkelen.

Ontwikkeling van een monoclonaal antilichaam tegen de cytoplasmatische staart van HLA-E

Het cytoplasmatische domein van HLA-E heeft als aminozuurvolgorde “SKAEWSDSAQGSESHL” (hierna HLA-E_{tail} genoemd). Door middel van een Sortase reactie⁵⁵³ hebben we HLA-E_{tail} gekoppeld aan VHH_{MHCII}, welk MHC-II in muizen herkent. Gebaseerd op eerder onderzoek in ons lab verbetert de koppeling van een peptide antigeen aan VHH_{MHCII} de immuunrespons tegen het peptide ⁵⁵⁸. Na immunisatie kozen we de muis met het hoogste titer voor productie van monoclonale antilichamen tegen HLA-E_{tail}. De antilichamen herkennen het epitoom “WSDSAQGSESHL”, een aminozuursequentie die uniek en alleen wordt aangetroffen in de cytoplasmatische ‘staart’ van HLA-E (Hoofdstuk 7, Figuur 2).

Deze sequentie, ingebouwd aan de C- of N-terminus, of ingevoegd in het midden van een onverwant eiwit, wordt herkend door de monoclonale antilichamen in immunoblot en in immunoprecipitatie experimenten (Hoofdstuk 7, Figuur 5). We hebben ook laten zien dat het 19-H12 antilichaam gebruikt kan worden in immunoblot, immunofluorescentie, cytometrie, en immunohistochemie. Vergeleken met het veelgebruikte MEM-E/02 antilichaam kunnen we het 19-H12 antilichaam gebruiken in immunohistochemische analyse van blaaskankerbiopten (Hoofdstuk 7, Figuur 6 en Figuur 7).

We hebben de C-terminus van de zware en lichte ketens van 19-H12 gemodificeerd met een LPETG sortase motief en een 6-Histidine 'tag'. De 6-Histidine 'tag' vergemakkelijkt de zuivering van de geproduceerde antilichamen met behulp van een NiNTA kolom. Het LPETG sortase motief maakt het mogelijk om specifiek de C-termini van de zware en lichte ketens te modificeren met een fluorofoor of biotine molecuul. Dit maakt het gebruik van een secundair antilichaam overbodig en staat detectie van 19-H12 toe met behulp van 'horse radish peroxidase' (HRP) (Hoofdstuk 7, Figuur 4). De C-termini van de zware en lichte ketens spelen geen rol bij de interactie van antilichaam met het antigeen. De sortase modificaties van het 19-H12 antilichaam hebben dus geen invloed op antigeenherkenning.

Conclusie

Het door ons ontwikkelde antilichaam, 19-H12, herkent een epitoom van ~13 aminozuren dat enkel aanwezig is als het intracellulaire deel van HLA-E. De combinatie van antilichaam en epitoom kan dus worden gebruikt als 'epitope-tag' voor de detectie en/of zuivering van eiwitten. Het 19-H12 antilichaam herkent dit epitoom in immunoblot, in cytometrie, immunofluorescentie, en immunohistochemie. We hebben een variant van het antilichaam gemaakt dat aan de C-termini van de zware en lichte ketens gemodificeerd is met een sortase motief, waardoor enzymatische modificatie met een fluorofoor, biotine, of ander molecuul mogelijk is. Doordat het cytoplasmatische deel van HLA-E betrokken is bij de stabiliteit van het molecuul op het celmembraan, is de beschikbaarheid van een antilichaam specifiek voor deze determinant nuttig voor verder onderzoek naar de eigenschappen van HLA-E.

List of abbreviations

ACT – Adoptive cell transfer	MHC – Major histocompatibility complex
APC – Antigen presenting cell	MICA/B – MHC class I chain-related protein A/B
BRCA1/2 – Breast cancer gene 1 / 2	MYC – Myelocytomatosis oncogene
CAR – Chimeric antigen receptor	NFAT – Nuclear factor of activated T-cells
CMV – Cytomegalovirus	NFκB – Nuclear factor kappa-light-chain enhancer of activated B cells
CTL – Cytotoxic T lymphocyte	NK cell – Natural killer cell
DAP-10 – DNAX-activating protein 10	NKG2A/D – Natural killer group 2 member A/D
DC – Dendritic cell	NKR – NK receptor
ECM – Extracellular matrix	PBMC – Peripheral blood mononuclear cells
EGF – Epidermal growth factor	PI3K – Phosphoinositide 3-kinase
EGFR – Epidermal growth factor receptor	PTEN – Phosphatase and tensin homolog
ELISA – Enzyme-linked immunosorbent assay	RAS – Rat sarcoma virus
EMT – Epithelial-to-mesenchymal transition	scFv – Single-chain variable fragment
FACS – Fluorescence-activated cell sorting	SIV – Simian immunodeficiency virus
GFB2 – Growth factor receptor bound protein 2	STAT3/5 – Signal transducer and activator of transcription 3/5
GFP – Green fluorescent protein	TAM – Tumor associated macrophage
GrzB – Granzyme B	Tcm – Central memory T cell
GVHD – Graft-versus-host disease	Tem – Effector memory T cell
HcAb – Heavy chain-only antibody	TGF-β – Transforming growth factor-β
HIV – Human immunodeficiency virus	TME – Tumor microenvironment
HLA – Human leukocyte antigen	Tfh cell – Follicular helper T cell
HPV – Human papillomavirus	Th cell – T helper cell
IFN-γ – Interferon γ	TNF-α/β – Tumor necrosis factor α/β
Ig – Immunoglobulin	Treg cell – Regulatory T cell
IL – Interleukin	Tscm – Stem cell memory T cell
ITAM – Immunoglobulin transactivation motif	ULBP – UL-16 binding protein
ITIM – Immunoreceptor tyrosine-based inhibitory motif	VEGF – Vascular endothelial growth factor
KIR – Killer cell immunoglobulin-like receptor	VHH – Variable domain of HcAb
LPS – Lipopolysaccharides	WCL – Whole cell lysate
mAb – Monoclonal antibody	WNT – Wingless-related integration site
MAPK – Mitogen activated protein kinase	

Publications

Inge Ubink, **Elisha R. Verhaar**, Onno Kranenburg, and Roel Goldschmeding. A potential role for CCN2/CTGF in aggressive colorectal cancer. *Journal of Cell Communication and Signaling*. 2016;10(3). DOI: 10.1007/s12079-016-0347-5

Elisha R. Verhaar, Andrew Woodham, and Hidde L. Ploegh. Nanobodies in Cancer. *Seminars in Immunology*. 2020;52(363):101425. DOI: 10.1016/j.smim.2020.101425

Novalia Pishesha, Thibault J. Harmand, Paul W. Rothlauf, Patrique Praest, Ryan K. Alexander, Renate van den Doel, Mariel J. Liebeskind, Maria A. Vakaki, Nicholas McCaul, Charlotte Wijne, **Elisha R. Verhaar**, William Pinney III, Hailey Heston, Louis-Marie Bloyet, Marjorie Cornejo Pontelli, Ma. Xenia G. Llagan, Robert Jan Lebbink, William J. Buchser, Emmanuel J. H. J. Wiertz, Sean P. J. Whelan, and Hidde L. Ploegh. A class II MHC-targeted vaccine elicits immunity against SARS-CoV-2 and its variants. *Proceedings of the National Academy of Sciences*. 2021;118(44):e2116147118. DOI: 10.1073/pnas.2116147118

Arthur W. Lambert, Christopher Fiore, Yogesh Chutake, **Elisha R. Verhaar**, Patrick C. Strasser, Mei Wei Chen, Daneyal Farouq, Sunny Das, Xin Li, Elinor Ng Eaton, Yun Zhang, Joana Liu Donaher, Ian Engstrom, Ferenc Reinhardt, Bingbing Yuan, Sumeet Gupta, Bruce Wollison, Matthew Eaton, Brian Bieri, John Carulli, Eric R. Olson, Matthew G. Guenther, Robert A. Weinberg. Δ Np63/p73 drive metastatic colonization by controlling a regenerative epithelial stem cell program in quasi-mesenchymal cancer stem cells. *Developmental Cell*. 2022;57(24):2414-2730.e8. DOI: 10.1016/j.devcel.2022.11.015

Elisha R. Verhaar, Anouk Knoflook, Novalia Pishesha, Xin Liu, Willemijn J.C. van Keizerswaard, Kai W. Wucherpfennig, Hidde L. Ploegh. MICA-specific nanobodies for diagnosis and immunotherapy of MICA⁺ tumors. *Frontiers in Immunology*. 2024;15. DOI: 10.3389/fimmu.2024.1368586

Elisha R. Verhaar, Willemijn J.C. van Keizerswaard, Anouk Knoflook, Thomas Balligand, Hidde L. Ploegh. Nanobody-based CAR NK cells for possible immunotherapy of MICA⁺ tumors. *PNAS Nexus*. 2024;5(3):pgae184 DOI: 10.1093/pnasnexus/pgae184

Elisha R. Verhaar, Jin Gan, Susan Buhl, Ziao Li, Amir Horowitz, Hidde L. Ploegh. A monoclonal antibody that recognizes a unique 13-residue epitope in the cytoplasmic tail of HLA-E. *Molecular Immunology*. 2024 article in press. Article reference: MIMM6935

Curriculum vitae

Elisha Verhaar is geboren op 17 januari, 1995 te Vlissingen. Zij behaalde haar VWO diploma aan het Dalton Lyceum in Barendrecht in 2013. In datzelfde jaar begon zij haar bachelorstudie “Biomedische Wetenschappen” aan de Universiteit Utrecht. Tijdens haar studie was ze actief bij meerdere studieverenigingen als hoofdredactrice van de redactie ter verenigingsblad “Tight Junction” der M.B.V. Mebiose, en theaterspecialist van de toneelcommissie “Produkcje”. Tijdens haar studie richtte ze zich op kanker- en stamcelonderzoek, onder meer met een onderzoeksstage in het UMC Utrecht naar de rol van connective tissue growth factor op de ontwikkeling van darmkanker, onder leiding van Onno Kranenburg en Roel Goldschmeding.

Na het behalen van haar bachelordiploma in 2016 startte ze aan de masterstudie “Cancer, Stem Cells, and Developmental Biology” aan de Universiteit Utrecht. Hier specialiseerde ze zich verder tot kankeronderzoek, onder meer met een stage aan het Hubrecht Instituut in het lab van Jacco van Rheenen, waar zij onderzoek deed naar celcompetitie in darmkanker organoids onder leiding van Saskia Suijkerbuijk. Hierna volgde ze een internationale stage in het lab van Robert Weinberg aan het MIT Whitehead Institute te Boston, Verenigde Staten. Onder leiding van Arthur Lambert deed zij onderzoek naar de rol van p63 en p73 op de epitheliale-naar-mesenchymale transitie van borstkankercellen.

Na het behalen van haar masterdiploma in 2018 werkte ze in de Weinberg groep aan hetzelfde project als onderzoeksassistent. In 2019 begon ze aan haar afstudeertraject in het lab van Hidde Ploegh, Boston Children’s Hospital, Verenigde Staten. In 2024 verdedigt ze haar proefschrift, en zal hierna waarschijnlijk werkzaam worden bij een biomedisch bedrijf in Boston, Verenigde Staten.

Acknowledgements

Beste Hidde, je gaf me alle vrijheid om zelf de teugels in handen te nemen maar stond altijd klaar om toch even een duwtje in de juiste richting te geven. Bedankt dat ik deze kans heb gekregen om mijzelf in jouw lab te ontwikkelen van “student” naar “wetenschapper”.

Beste Sjaak, bedankt voor het accepteren van deze gekke PhD situatie. Hoewel we elkaar welgeteld drie keer gezien hebben, kan ik met zekerheid zeggen dat het Neefjes lab een fantastische plek moet zijn. Bedankt voor de adviezen en feedback op mijn werk.

Dear Thomas, thank you for entertaining me every single day, not just literally (your French swearing was entertaining!) You also entertained my many, many, many questions. I could always turn to you for help and advice about lab work, cloning, PET imaging, data analysis, medical problems, personal issues... The list goes on and on. I am not sure what I would've done without you in the bay. Cool bay forever!

Dear Lotte and Claire, together we were the “three PhD’ers”. But we didn’t just bond over mutual suffering, we made an actual connection. You girls are the best lab mates anyone could ask for. Dealing with all the “llama llama holiday drama” was easy with you guys thanks to our friendship. Always up for a drink, a hangout, a dance party (cue TomM!), raclette, board games, but also a serious chat or a vent. Thank you for becoming my friends.

Lieve Willemijn and Anouk, you both came to work with me like a gift from the UVA Heaven! Your dedication to the projects was unmatched and I can’t even express how helpful the two of you have been. Your scientific mindset was a true inspiration to lift these projects to a higher level. You worked tirelessly on cloning vectors, creating virus, producing CAR NK and CAR T cells, designing and executing downstream applications, the list goes on... I am so lucky to have mentored you two incredible women and can’t wait to see what your future holds.

Dear David, my liefde. You met me the month before I started my PhD and have dealt with the ups-and-downs of #PhDLife throughout the many years that followed. David, I can’t emphasize enough how incredibly lucky I am to have you in my life and to be able to call you my husband. You have supported me in more ways than I could’ve ever hoped for. Not just by taking

over many of the household chores during my most busy times at work, but also by being there for me emotionally. You accepted when our plans had to change because I had to run experiments. You gave advice, even when I told you I wasn't looking for solutions. Liefje, you are always the solution. Coming home every day to yours and our cat's love, that's always been what's keeping me going.

Lieve papa. Wat zou ik graag willen dat je dit kon lezen... Ik weet hoe ontzettend trots je zou zijn geweest. Je vroeg zo vaak "en, ben je al bezig met het schrijven van je proefschrift?" en dan moest ik uitleggen dat ik nog steeds druk bezig was met experimenten, dus nee ik was nog niet aan het schrijven... Je stuurde me vaak linkjes naar interessante artikelen, en dan praatten we daar even over. Ik heb zo veel van jou geleerd en jij ook van mij. Hoewel jij nu niks meer van mij kunt leren, leer ik nog elke dag van jou. Papa, je meisje is nu echt klaar met haar proefschrift. Je had hem zo graag willen lezen. Ik draag hem op aan jou.

Lieve mama. Ik ben zo ontzettend blij dat ik dit moment met jou kan delen. Toen ik naar Boston verhuisde voor eens stage van 8 maanden zei je: "Meid, jij komt nooit meer terug naar Nederland". 'Onzin', dacht ik. Maar het is nu 6.5 jaar later en Boston is nog steeds mijn thuis. Ondanks de afstand hebben we elkaar zo vaak mogelijk gezien. Ik vind het zo bewonderingswaardig dat jij, zonder medische achtergrond, altijd zo geïnteresseerd was in mijn onderwerp. Je wist altijd de juiste vragen te stellen waardoor we heerlijk konden kletsen over biomedische wetenschappen en mijn onderzoek. Mama, dank je wel voor de afgelopen jaren, voor het aanhoren van mijn frustraties, voor de altijd goede raad. Ik hou zo veel van jou.

References

1. World Health Organization. Global cancer burden growing, amidst mounting need for services. (2024).
2. Fares, J., Fares, M. Y., Khachfe, H. H., Salhab, H. A. & Fares, Y. Molecular principles of metastasis: a hallmark of cancer revisited. *Signal Transduct Target Ther* **5**, (2020).
3. Neophytou, C. M., Panagi, M., Stylianopoulos, T. & Papageorgis, P. The Role of Tumor Microenvironment in Cancer Metastasis: Molecular Mechanisms and Therapeutic Opportunities. *Cancers (Basel)* **13**, 1–22 (2021).
4. McAllister, S. S. & Weinberg, R. A. The tumour-induced systemic environment as a critical regulator of cancer progression and metastasis. *Nat Cell Biol* **16**, 717–727 (2014).
5. Kurose, K. *et al.* Genetic model of multi-step breast carcinogenesis involving the epithelium and stroma: clues to tumour-microenvironment interactions. *Hum Mol Genet* **10**, 1907–1913 (2001).
6. Vogelstein, B., Lane, D. & Levine, A. J. Surfing the p53 network. *Nature* **408**, 307–310 (2000).
7. Wang, X. W. & Harris, C. C. p53 tumor-suppressor gene: clues to molecular carcinogenesis. *J Cell Physiol* **173**, 247–255 (1997).
8. Ford, D. *et al.* Genetic Heterogeneity and Penetrance Analysis of the BRCA1 and BRCA2 Genes in Breast Cancer Families. *Am J Hum Genet* **62**, 676–689 (1998).
9. Li, J. *et al.* PTEN, a Putative Protein Tyrosine Phosphatase Gene Mutated in Human Brain, Breast, and Prostate Cancer. *Science* (1979) **275**, 1943–1947 (1997).
10. Myers, M. P. *et al.* The lipid phosphatase activity of PTEN is critical for its tumor suppressor function. *Proceedings of the National Academy of Sciences* **95**, 13513–13518 (1998).
11. Tan, M. H. *et al.* Lifetime cancer risks in individuals with germline PTEN mutations. *Clinical Cancer Research* **18**, 400–407 (2012).
12. Wang, S.-C., Lin, S.-H., Su, L.-K. & Hung, M.-C. Changes in BRCA2 Expression during Progression of the Cell Cycle. *Biochem Biophys Res Commun* **234**, 247–251 (1997).
13. Fischer, M. Census and evaluation of p53 target genes. *Oncogene* **36**, 3943–3956 (2017).
14. Nusse, R., van Ooyen, A., Cox, D., Kai T. Fung, Y. & Varmus, H. Mode of proviral activation of a putative mammary oncogene (int-1) on mouse chromosome 15. *Nature* **307**, 131–136 (1984).
15. Giehl, K. Oncogenic Ras in tumour progression and metastasis. *Journal of Biological Chemistry* **386**, 193–205 (2005).
16. Barbacid, M. ras genes. *Annu Rev Biochem* **56**, 779–827 (1987).
17. Rajalingam, K., Schreck, R., Rapp, U. R. & Albert, S. Ras oncogenes and their downstream targets. *Biochim Biophys Acta Mol Cell Res* **1773**, 1177–1195 (2007).
18. Prior, I. A., Lewis, P. D. & Mattos, C. A comprehensive survey of ras mutations in cancer. *Cancer Res* **72**, 2457–2467 (2012).
19. Madden, S. K., de Araujo, A. D., Gerhardt, M., Fairlie, D. P. & Mason, J. M. Taking the Myc out of cancer: toward therapeutic strategies to directly inhibit c-Myc. *Mol Cancer* **20**, (2021).
20. Zhan, T., Rindtorff, N. & Boutros, M. Wnt signaling in cancer. *Oncogene* **36**, 1461–1473 (2017).
21. Duffy, M. J., O'Grady, S., Tang, M. & Crown, J. MYC as a target for cancer treatment. *Cancer Treatment Reviews* vol. 94 Preprint at <https://doi.org/10.1016/j.ctrv.2021.102154> (2021).

22. Rajalingam, K., Schreck, R., Rapp, U. R. & Albert, S. Ras oncogenes and their downstream targets. *Biochim Biophys Acta Mol Cell Res* **1773**, 1177–1195 (2007).
23. Sinn, E. *et al.* Coexpression of MMTV/v-Ha-ras and MMTV/c-myc genes in transgenic mice: Synergistic action of oncogenes in vivo. *Cell* **49**, 465–475 (1987).
24. Tsukamoto, A. S., Grosschedl, R., Guzman, R. C., Parslow, T. & Varmus, H. E. Expression of the int-1 gene in transgenic mice is associated with mammary gland hyperplasia and adenocarcinomas in male and female mice. *Cell* **55**, 619–625 (1988).
25. Maleno, I. *et al.* LOH at 6p21.3 region and HLA class I altered phenotypes in bladder carcinomas. *Immunogenetics* **58**, 503–510 (2006).
26. Maleno, I. *et al.* Distribution of HLA class I altered phenotypes in colorectal carcinomas: high frequency of HLA haplotype loss associated with loss of heterozygosity in chromosome region 6p21. *Immunogenetics* **56**, 244–253 (2004).
27. Hanigiri, T. *et al.* Prognostic implications of human leukocyte antigen class I expression in patients who underwent surgical resection for non-small-cell lung cancer. *Journal of Surgical Resection* **181**, 57–63 (2013).
28. Simpson, J. A. D. *et al.* Intratumoral T cell infiltration, MHC class I and STAT1 as biomarkers of good prognosis in colorectal cancer. *Gut* **59**, 926–933 (2010).
29. Watson, N. F. S. *et al.* Immunosurveillance is active in colorectal cancer as downregulation but not complete loss of MHC class I expression correlates with a poor prognosis. *Int J Cancer* **118**, 6–10 (2006).
30. Squire, R., Fowler, C. L., Brooks, S. P., Rich, G. A. & Cooney, D. R. The relationship of class I MHC antigen expression to stage IV-S disease and survival in neuroblastoma. *J Pediatr Surg* **25**, 381–386 (1990).
31. Feenstra, M. *et al.* HLA class I expression and chromosomal deletions at 6p and 15q in head and neck squamous cell carcinomas. *Tissue Antigens* **54**, 235–245 (1999).
32. Garrido, M. A. *et al.* HLA class I alterations in breast carcinoma are associated with a high frequency of the loss of heterozygosity at chromosomes 6 and 15. *Immunogenetics* **70**, 647–659 (2018).
33. Seliger, B. *et al.* Immune escape of melanoma: first evidence of structural alterations in two distinct components of the MHC class I antigen processing pathway. *Cancer Res* **61**, 8647–8650 (2001).
34. Martín-Villa, J. M. *et al.* HLA-G: Too Much or Too Little? Role in Cancer and Autoimmune Disease. *Front Immunol* **13**, (2022).
35. Morandi, F. & Pistoia, V. Interactions between HLA-G and HLA-E in physiological and pathological conditions. *Front Immunol* **5**, (2014).
36. de Kruijff, E. M. *et al.* HLA-E and HLA-G Expression in Classical HLA Class I-Negative Tumors Is of Prognostic Value for Clinical Outcome of Early Breast Cancer Patients. *The Journal of Immunology* **185**, 7452–7459 (2010).
37. Zeestraten, E. C. M. *et al.* Combined analysis of HLA class I, HLA-E and HLA-G predicts prognosis in colon cancer patients. *Br J Cancer* **110**, 459–468 (2014).
38. Henke, E., Nandigama, R. & Ergün, S. Extracellular Matrix in the Tumor Microenvironment and Its Impact on Cancer Therapy. *Front Mol Biosci* **6**, (2020).
39. Rice, A. J. *et al.* Matrix stiffness induces epithelial-mesenchymal transition and promotes chemoresistance in pancreatic cancer cells. *Oncogenesis* **6**, (2017).
40. Dongre, A. & Weinberg, R. A. New insights into the mechanisms of epithelial–mesenchymal transition and implications for cancer. *Nat Rev Mol Cell Biol* **20**, 69–84 (2019).
41. Wei, S. C. *et al.* Matrix stiffness drives epithelial-mesenchymal transition and tumour metastasis through a TWIST1-G3BP2 mechanotransduction pathway. *Nat Cell Biol* **17**, 678–688 (2015).

42. Greenburg, G. & Hay, E. D. Epithelia Suspended in Collagen Gels Can Lose Polarity and Express Characteristics of Migrating Mesenchymal Cells. *J Cell Biol* **95**, 333–339 (1982).
43. Ribatti, D., Tamma, R. & Annese, T. Epithelial-Mesenchymal Transition in Cancer: A Historical Overview. *Transl Oncol* **13**, (2020).
44. Hallmann, R. *et al.* The regulation of immune cell trafficking by the extracellular matrix. *Current Opinions in Cell Biology* **36**, 54–61 (2015).
45. Zhu, X. & Zhu, J. CD4 T helper cell subsets and related human immunological disorders. *Int J Mol Sci* **21**, 1–26 (2020).
46. Knutson, K. L. & Disis, M. L. Tumor antigen-specific T helper cells in cancer immunity and immunotherapy. *Cancer Immunology, Immunotherapy* **54**, 721–728 (2005).
47. Knutson, K. L. & Disis, M. L. Tumor antigen-specific T helper cells in cancer immunity and immunotherapy. *Cancer Immunology, Immunotherapy* **54**, 721–728 (2005).
48. Nonaka, K. *et al.* Th1 polarization in the tumor microenvironment upregulates the myeloid-derived suppressor-like function of macrophages. *Cell Immunol* **369**, (2021).
49. Laheurte, C. *et al.* Distinct prognostic value of circulating anti-telomerase CD4+ Th1 immunity and exhausted PD-1+/TIM-3+ T cells in lung cancer. *Br J Cancer* **121**, 405–416 (2019).
50. Aue, G. *et al.* Activation of Th1 Immunity within the Tumor Microenvironment Is Associated with Clinical Response to Lenalidomide in Chronic Lymphocytic Leukemia. *The Journal of Immunology* **201**, 1967–1974 (2018).
51. Haabeth, O. A. W. *et al.* Inflammation driven by tumour-specific Th1 cells protects against B-cell cancer. *Nat Commun* **2**, (2011).
52. Walker, J. A. & McKenzie, A. N. J. TH2 cell development and function. *Nat Rev Immunol* **18**, 121–133 (2018).
53. Steinke, J. W. & Borish, L. Th2 cytokines and asthma Interleukin-4: its role in the pathogenesis of asthma, and targeting it for asthma treatment with interleukin-4 receptor antagonists. *Respir Res* **2**, 66–70 (2001).
54. Wang, N., Liang, H. & Zen, K. Molecular mechanisms that influence the macrophage M1-M2 polarization balance. *Front Immunol* **5**, (2014).
55. Yao, Y., Xu, X. H. & Jin, L. Macrophage polarization in physiological and pathological pregnancy. *Front Immunol* **10**, (2019).
56. Murray, P. J. Macrophage Polarization. *Annu Rev Physiol* **79**, 541–566 (2017).
57. Chraa, D., Naim, A., Olive, D. & Badou, A. T lymphocyte subsets in cancer immunity: Friends or foes. *J Leukoc Biol* **105**, 243–255 (2019).
58. Jacenik, D., Karagiannidis, I. & Beswick, E. J. Th2 cells inhibit growth of colon and pancreas cancers by promoting anti-tumorigenic responses from macrophages and eosinophils. *Br J Cancer* **128**, 387–397 (2023).
59. Protti, M. P. & De Monte, L. Cross-talk within the tumor microenvironment mediates Th2-type inflammation in pancreatic cancer. *Oncoimmunology* **1**, 89–91 (2012).
60. Mattes, J. *et al.* Immunotherapy of cytotoxic T cell-resistant tumors by T helper 2 cells: An eotaxin and STAT6-dependent process. *Journal of Experimental Medicine* **197**, 387–393 (2003).
61. Boieri, M. *et al.* CD4+ T helper 2 cells suppress breast cancer by inducing terminal differentiation. *Journal of Experimental Medicine* **219**, (2022).
62. Nishimura, T. *et al.* Distinct Role of Antigen-specific T Helper Type 1 (Th1) and Th2 Cells in Tumor Eradication In Vivo. *Journal of Experimental Medicine* **190**, 617–627 (1999).
63. Jiang, Y. *et al.* TNF- α enhances Th9 cell differentiation and antitumor immunity via TNFR2-dependent pathways. *J Immunother Cancer* **7**, (2019).

64. Lu, Y. *et al.* Th9 cells promote antitumor immune responses in vivo. *Journal of Clinical Investigation* **122**, 4160–4171 (2012).
65. Kim, I. K. *et al.* GM-CSF promotes antitumor immunity by inducing Th9 cell responses. *Cancer Immunol Res* **7**, 498–509 (2019).
66. Végran, F. *et al.* The transcription factor IRF1 dictates the IL-21-dependent anticancer functions of TH9 cells. *Nat Immunol* **15**, 758–766 (2014).
67. Xue, G., Jin, G., Fang, J. & Lu, Y. IL-4 together with IL-1 β induces antitumor Th9 cell differentiation in the absence of TGF- β signaling. *Nat Commun* **10**, (2019).
68. Humblin, E. *et al.* IRF8-dependent molecular complexes control the Th9 transcriptional program. *Nat Commun* **8**, (2017).
69. Kim, I. K. *et al.* GM-CSF promotes antitumor immunity by inducing Th9 cell responses. *Cancer Immunol Res* **7**, 498–509 (2019).
70. You, F.-P. *et al.* Th9 cells promote antitumor immunity via IL-9 and IL-21 and demonstrate atypical cytokine expression in breast cancer. *Int Immunopharmacol* **52**, 163–167 (2017).
71. Wei, L., Laurence, A., Elias, K. M. & O'shea, J. J. IL-21 is produced by TH17 cells and drives IL-17 production in a STAT3-dependent manner. *Journal of Biological Chemistry* **282**, 34605–34610 (2007).
72. Yang, L. *et al.* IL-21 and TGF- β are required for differentiation of human TH17 cells. *Nature* **454**, 350–352 (2008).
73. Miossec, P., Korn, T. & Kuchroo, V. K. Mechanisms of Disease Interleukin-17 and Type 17 Helper T Cells. *New England Journal of Medicine* **361**, 888–98 (2009).
74. Noack, M. & Miossec, P. Th17 and regulatory T cell balance in autoimmune and inflammatory diseases. *Autoimmun Rev* **13**, 668–677 (2014).
75. Yang, L. *et al.* Expression of Th17 Cells in Breast Cancer Tissue and Its Association with Clinical Parameters. *Cell Biochem Biophys* 153–159 (2012) doi:10.1007/s12013-011-9276-3.
76. Baharlou, R. *et al.* Reduced levels of T-helper 17-associated cytokines in the serum of patients with breast cancer: Indicators for following the course of disease. *Central European Journal of Immunology* **41**, 78–85 (2016).
77. Chen, W.-C. *et al.* Interleukin-17-producing cell infiltration in the breast cancer tumour microenvironment is a poor prognostic factor. *Histopathology* **63**, 225–233 (2013).
78. Avalos-Navarro, G. *et al.* Circulating soluble levels of MIF in women with breast cancer in the molecular subtypes: relationship with Th17 cytokine profile. *Clin Exp Med* **19**, 385–391 (2019).
79. Eyerich, S. *et al.* Th22 cells represent a distinct human T cell subset involved in epidermal immunity and remodeling. *Journal of Clinical Investigation* **119**, 3573–3585 (2009).
80. Trifari, S., Kaplan, C. D., Tran, E. H., Crellin, N. K. & Spits, H. Identification of a human helper T cell population that has abundant production of interleukin 22 and is distinct from TH-17, TH1 and TH2 cells. *Nat Immunol* **10**, 864–871 (2009).
81. Duhon, T., Geiger, R., Jarrossay, D., Lanzavecchia, A. & Sallusto, F. Production of interleukin 22 but not interleukin 17 by a subset of human skin-homing memory T cells. *Nat Immunol* **10**, 857–863 (2009).
82. Jiang, R. *et al.* Interleukin-22 promotes human hepatocellular carcinoma by activation of STAT3. *Hepatology* **54**, 900–909 (2011).
83. Khosravi, N. *et al.* IL22 promotes kras-mutant lung cancer by induction of a protumor immune response and protection of stemness properties. *Cancer Immunol Res* **6**, 788–797 (2018).
84. Cui, G. TH9, TH17, and TH22 Cell Subsets and Their Main Cytokine Products in the Pathogenesis of Colorectal Cancer. *Front Oncol* **9**, (2019).

85. Crotty, S. T Follicular Helper Cell Differentiation, Function, and Roles in Disease. *Immunity* **41**, 529–542 (2014).
86. King, C. New insights into the differentiation and function of T follicular helper cells. *Nat Rev Immunol* **9**, 757–766 (2009).
87. Pandey, S. *et al.* IL-4/CXCL12 loop is a key regulator of lymphoid stroma function in follicular lymphoma. *Blood* **129**, 2507–2518 (2017).
88. Rawal, S. *et al.* Cross Talk between Follicular Th Cells and Tumor Cells in Human Follicular Lymphoma Promotes Immune Evasion in the Tumor Microenvironment. *The Journal of Immunology* **190**, 6681–6693 (2013).
89. Amé-Thomas, P. *et al.* CD10 delineates a subset of human IL-4 producing follicular helper T cells involved in the survival of follicular lymphoma B cells. *Blood* **125**, (2015).
90. Zhanshan Cha *et al.* Circulating CXCR5+CD4+ T cells assist in the survival and growth of primary diffuse large B cell lymphoma cells through interleukin 10 pathway. *Exp Cell Res* **350**, 154–160 (2017).
91. Goubet, A. G. *et al.* Escherichia coli-Specific CXCL13-Producing TFH Are Associated with Clinical Efficacy of Neoadjuvant PD-1 Blockade against Muscle- Invasive Bladder Cancer. *Cancer Discov* **12**, 2280–2307 (2022).
92. Gu-Trantien, C. *et al.* CD4+ follicular helper T cell infiltration predicts breast cancer survival. *Journal of Clinical Investigation* **123**, 2873–2892 (2013).
93. Noël, G. *et al.* Functional Th1-oriented T follicular helper cells that infiltrate human breast cancer promote effective adaptive immunity. *Journal of Clinical Investigation* **131**, (2021).
94. Niogret, J. *et al.* Follicular helper-T cells restore CD8+ -dependent antitumor immunity and anti-PD-L1/PD-1 efficacy. *J Immunother Cancer* **9**, (2021).
95. Phanthurane, C. *et al.* Intratumoral Niches of B Cells and Follicular Helper T Cells, and the Absence of Regulatory T Cells, Associate with Longer Survival in Early-Stage Oral Tongue Cancer Patients. *Cancers (Basel)* **14**, (2022).
96. Walunas, T. L., Akker, C. Y. B. & Bluestone, J. A. CTLA-4 Ligation Blocks CD28-dependent T Cell Activation. *Journal of Experimental Medicine* **183**, 2541–2550 (1996).
97. Walunas, T. L. *et al.* CTLA-4 can function as a negative regulator of T cell activation. *Immunity* **1**, 405–413 (1994).
98. Ruella, M. *et al.* Overcoming the immunosuppressive tumor microenvironment of Hodgkin lymphoma using chimeric antigen receptor T cells. *Cancer Discov* **7**, 1154–1167 (2017).
99. Crane, C. A. *et al.* TGF- β downregulates the activating receptor NKG2D on NK cells and CD8+ T cells in glioma patients. *Neuro Oncol* **12**, 7–13 (2010).
100. Huang, J. J. & Blobel, G. C. Dichotomous roles of TGF- β in human cancer. *Biochem Soc Trans* **44**, 1441–1454 (2016).
101. Bjorkman, P. J. *et al.* The foreign antigen binding site and T cell recognition regions of class I histocompatibility antigens. *Nature* **329**, 512–518 (1987).
102. Xing, Y. & Hogquist, K. A. T-Cell tolerance: Central and peripheral. *Cold Spring Harb Perspect Biol* **4**, 1–15 (2012).
103. Sigal, L. J. Activation of CD8 T Lymphocytes during Viral Infections. *Encyclopedia of Immunobiology* **4**, 286–290 (2016).
104. De Araujo-Souza, P. S., Hanschke, S. C. H. & Viola, J. P. B. Epigenetic control of interferon-gamma expression in CD8 T cells. *J Immunol Res* **2015**, (2015).
105. Araki, Y., Fann, M., Wersto, R. & Weng, N.-P. Histone Acetylation Facilitates Rapid and Robust Memory CD8 T Cell Response through Differential Expression of Effector Molecules (Eomesodermin and Its Targets: Perforin and Granzyme B). *The Journal of Immunology* **180**, 8102–8108 (2008).

106. Haring, J. S., Badovinac, V. P. & Harty, J. T. Inflaming the CD8+ T Cell Response. *Immunity* **25**, 19–29 (2006).
107. De Araujo-Souza, P. S., Hanschke, S. C. H. & Viola, J. P. B. Epigenetic control of interferon-gamma expression in CD8 T cells. *J Immunol Res* **2015**, (2015).
108. Araki, Y., Fann, M., Wersto, R. & Weng, N.-P. Histone Acetylation Facilitates Rapid and Robust Memory CD8 T Cell Response through Differential Expression of Effector Molecules (Eomesodermin and Its Targets: Perforin and Granzyme B) 1. *The Journal of Immunology* **180**, 8102–8108 (2008).
109. Djenidi, F. *et al.* CD8+CD103+ Tumor-Infiltrating Lymphocytes Are Tumor-Specific Tissue-Resident Memory T Cells and a Prognostic Factor for Survival in Lung Cancer Patients. *The Journal of Immunology* **194**, 3475–3486 (2015).
110. Noh, B. J., Kwak, J. Y. & Eom, D. W. Immune classification for the PD-L1 expression and tumour-infiltrating lymphocytes in colorectal adenocarcinoma. *BMC Cancer* **20**, (2020).
111. Kawai, O. *et al.* Predominant infiltration of macrophages and CD8+ T cells in cancer nests is a significant predictor of survival in stage IV nonsmall cell lung cancer. *Cancer* **113**, 1387–1395 (2008).
112. Zhul, Y. *et al.* Impact of Cytotoxic T Lymphocytes Immunotherapy on Prognosis of Colorectal Cancer Patients. *Clinics in Oncology* **7**, (2023).
113. Pal, A. & Kundu, R. Human Papillomavirus E6 and E7: The Cervical Cancer Hallmarks and Targets for Therapy. *Front Microbiol* **10**, (2020).
114. Peng, S. *et al.* Identification of human MHC-I HPV18 E6/E7-specific CD8 + T cell epitopes and generation of an HPV18 E6/E7-expressing adenosquamous carcinoma in HLA-A2 transgenic mice. *J Biomed Sci* **29**, (2022).
115. Hong, J. Y. *et al.* Claudin 18.2 expression in various tumor types and its role as a potential target in advanced gastric cancer. *Transl Cancer Res* **9**, 3367–3374 (2020).
116. Siehl, J. M. *et al.* Expression of Wilms' tumor gene 1 at different stages of acute myeloid leukemia and analysis of its major splice variants. *Ann Hematol* **83**, 745–750 (2004).
117. Kramarzova, K. *et al.* Real-time PCR quantification of major Wilms' tumor gene 1 (WT1) isoforms in acute myeloid leukemia, their characteristic expression patterns and possible functional consequences. *Leukemia* **26**, 2086–2095 (2012).
118. Busse, A. *et al.* Wilms' tumor gene 1 (WT1) expression in subtypes of acute lymphoblastic leukemia (ALL) of adults and impact on clinical outcome. *Ann Hematol* **88**, 1199–1205 (2009).
119. Strickland, K. C. *et al.* Association and prognostic significance of BRCA1/2-mutation status with neoantigen load, number of tumor-infiltrating lymphocytes and expression of PD-1/PD-L1 in high grade serous ovarian cancer. *Oncotarget* **7**, (2016).
120. Xu, K., Yang, S. & Zhao, Y. Prognostic significance of BRCA mutations in ovarian cancer: an updated systematic review with meta-analysis. *Oncotarget* **8**, 285–302 (2017).
121. Bailur, J. K., Gueckel, B., Derhovanessian, E. & Pawelec, G. Presence of circulating Her2-reactive CD8 + T-cells is associated with lower frequencies of myeloid-derived suppressor cells and regulatory T cells, and better survival in older breast cancer patients. *Breast Cancer Research* **17**, (2015).
122. Mitri, Z., Constantine, T. & O'Regan, R. The HER2 Receptor in Breast Cancer: Pathophysiology, Clinical Use, and New Advances in Therapy. *Chemother Res Pract* **2012**, 1–7 (2012).
123. Le, K. *et al.* Overexpression of mesothelin in pancreatic ductal adenocarcinoma (PDAC). *Int J Med Sci* **17**, 422–427 (2020).
124. Wang, K., Wei, G. & Liu, D. CD19: a biomarker for B cell development, lymphoma diagnosis and therapy. *Exp Hematol Oncol* **1**, (2012).

125. Tomiyama, H., Matsuda, T. & Takiguchi, M. Differentiation of Human CD8⁺ T Cells from a Memory to Memory/Effector Phenotype. *The Journal of Immunology* **168**, 5538–5550 (2002).
126. Cui, W. & Kaech, S. M. Generation of effector CD8⁺ T cells and their conversion to memory T cells. *Immunol Rev* **236**, 151–166 (2010).
127. Youngblood, B. *et al.* Effector CD8 T cells dedifferentiate into long-lived memory cells. *Nature* **552**, 404–409 (2017).
128. Akondy, R. S. *et al.* Origin and differentiation of human memory CD8 T cells after vaccination. *Nature* **552**, 362–367 (2017).
129. Turner, D. L. *et al.* Lung niches for the generation and maintenance of tissue-resident memory T cells. *Mucosal Immunol* **7**, 501–510 (2014).
130. Corgnac, S., Boutet, M., Kfoury, M., Naltet, C. & Mami-Chouaib, F. The emerging role of CD8⁺ tissue resident memory T (TRM) cells in antitumor immunity: A unique functional contribution of the CD103 integrin. *Front Immunol* **9**, (2018).
131. Farber, D. L., Yudanin, N. A. & Restifo, N. P. Human memory T cells: Generation, compartmentalization and homeostasis. *Nat Rev Immunol* **14**, 24–35 (2014).
132. Edwards, J. *et al.* CD103⁺ tumor-resident CD8⁺ T cells are associated with improved survival in immunotherapy-naïve melanoma patients and expand significantly during anti-PD-1 treatment. *Clinical Cancer Research* **24**, 3036–3045 (2018).
133. Park, S. L. *et al.* Tissue-resident memory CD8⁺ T cells promote melanoma–immune equilibrium in skin. *Nature* **565**, 366–371 (2019).
134. Malik, B. T. *et al.* Resident memory T cells in the skin mediate durable immunity to melanoma. *Sci Immunol* **2**, (2017).
135. Ganesan, A. P. *et al.* Tissue-resident memory features are linked to the magnitude of cytotoxic T cell responses in human lung cancer. *Nat Immunol* **18**, 940–950 (2017).
136. Koh, J. *et al.* Prognostic implications of intratumoral CD103⁺ tumor-infiltrating lymphocytes in pulmonary squamous cell carcinoma. *Oncotarget* **8**, 13762–13769 (2017).
137. Wang, Z. Q. *et al.* CD103 and intratumoral immune response in breast cancer. *Clinical Cancer Research* **22**, 6290–6297 (2016).
138. Peter Savas *et al.* Single-cell profiling of breast cancer T cells reveals a tissue-resident memory subset associated with improved prognosis. *Nat Med* **24**, 986–993 (2018).
139. Webb, J. R. *et al.* Profound elevation of CD8⁺ T cells expressing the intraepithelial lymphocyte marker CD103 (α E/ β 7 Integrin) in high-grade serous ovarian cancer. *Gynecologic Oncology* **118**, 228–236 (2010).
140. Duhen, T. *et al.* Co-expression of CD39 and CD103 identifies tumor-reactive CD8 T cells in human solid tumors. *Nat Commun* **9**, (2018).
141. Atri, C., Guerfali, F. Z. & Laouini, D. Role of human macrophage polarization in inflammation during infectious diseases. *Int J Mol Sci* **19**, (2018).
142. Shapouri-Moghaddam, A. *et al.* Macrophage plasticity, polarization, and function in health and disease. *J Cell Physiol* **233**, 2425–6440 (2018).
143. Mantovani, A. *et al.* The chemokine system in diverse forms of macrophage activation and polarization. *Trends Immunol* **25**, 677–686 (2004).
144. Italiani, P. *et al.* Transcriptomic profiling of the development of the inflammatory response in human monocytes in vitro e87680. *PLoS One* **9**, (2014).
145. Martinez, F. O., Gordon, S., Locati, M. & Mantovani, A. Transcriptional Profiling of the Human Monocyte-to-Macrophage Differentiation and Polarization: New Molecules and Patterns of Gene Expression. *The Journal of Immunology* **177**, 7303–7311 (2006).
146. Kadomoto, S., Izumi, K. & Mizokami, A. Macrophage Polarity and Disease Control. *Int J Mol Sci* **23**, (2022).

147. Zhang, F. *et al.* TGF- β induces M2-like macrophage polarization via SNAIL-mediated suppression of a pro-inflammatory phenotype. *Oncotarget* **7**, 52294–52306 (2016).
148. Mantovani, A., Sozzani, S., Locati, M., Allavena, P. & Sica, A. Macrophage polarization: tumor-associated macrophages as a paradigm for polarized M2 mononuclear phagocytes. *Trends Immunol* **23**, 534–555 (2002).
149. Murray, P. J. & Wynn, T. A. Protective and pathogenic functions of macrophage subsets. *Nat Rev Immunol* **11**, 723–737 (2011).
150. Sumitomo, R. *et al.* PD-L1 expression on tumor-infiltrating immune cells is highly associated with M2 TAM and aggressive malignant potential in patients with resected non-small cell lung cancer. *Lung Cancer* **136**, 136–144 (2019).
151. Cao, L. *et al.* M2 macrophage infiltration into tumor islets leads to poor prognosis in non-small-cell lung cancer. *Cancer Manag Res* **11**, 6125–6138 (2019).
152. Sumitomo, R. *et al.* M2 tumor-associated macrophages promote tumor progression in non-small-cell lung cancer. *Exp Ther Med* (2019) doi:10.3892/etm.2019.8068.
153. Hughes, R. *et al.* Perivascular M2 macrophages stimulate tumor relapse after chemotherapy. *Cancer Res* **75**, 3479–3491 (2015).
154. Kim, O. H. *et al.* Proangiogenic TIE2+/CD31+ macrophages are the predominant population of tumor-associated macrophages infiltrating metastatic lymph nodes. *Mol Cells* **36**, 432–438 (2013).
155. Chen, Y. *et al.* Tumor-associated macrophages: An accomplice in solid tumor progression. *J Biomed Sci* **26**, (2019).
156. Yeo, E. J. *et al.* Myeloid wnt7b mediates the angiogenic switch and metastasis in breast cancer. *Cancer Res* **74**, 2962–2973 (2014).
157. Palazon, A. *et al.* An HIF-1 α /VEGF-A Axis in Cytotoxic T Cells Regulates Tumor Progression. *Cancer Cell* **32**, 669–683.e5 (2017).
158. Kadowaki, I. *et al.* Accelerated lymphangiogenesis in malignant lymphoma: Possible role of VEGF-A and VEGF-C. *Br J Haematol* **130**, 869–877 (2005).
159. De Maria, A., Bozzano, F., Cantoni, C. & Moretta, L. Revisiting human natural killer cell subset function revealed cytolytic CD56dimCD16+ NK cells as rapid producers of abundant IFN- γ on activation. *Proceedings of the National Academy of Sciences* **108**, 728–732 (2011).
160. Kärre, K. NK cells, MHC class I molecules and the missing self. *Scand J Immunol* **55**, 221–228 (2002).
161. Vivier, E. *et al.* Innate or adaptive immunity? The example of natural killer cells. *Science* (1979) **331**, 44–49 (2011).
162. Paul, S. & Lal, G. The molecular mechanism of natural killer cells function and its importance in cancer immunotherapy. *Front Immunol* **8**, (2017).
163. Kumar, S. Natural killer cell cytotoxicity and its regulation by inhibitory receptors. *Immunology* **154**, 383–393 (2018).
164. Sivori, S. *et al.* Inhibitory Receptors and Checkpoints in Human NK Cells, Implications for the Immunotherapy of Cancer. *Front Immunol* **11**, (2020).
165. Dębska-Zielkowska, J. *et al.* Kir receptors as key regulators of nk cells activity in health and disease. *Cells* **10**, (2021).
166. Slamon, D. *et al.* Adjuvant Trastuzumab in HER2-Positive Breast Cancer. *New England Journal of Medicine* **14**, 1273–83 (2011).
167. Maloney, D. G. *et al.* IDEC-C2B8 (Rituximab) Anti-CD20 Monoclonal Antibody Therapy in Patients With Relapsed Low-Grade Non-Hodgkin's Lymphoma. *Blood* **90**, 2189–2195 (1997).
168. Mendelsohn, J. & Baselga, J. Status of Epidermal Growth Factor Receptor Antagonists in the Biology and Treatment of Cancer. *Journal of Clinical Oncology* **21**, 2787–2799 (2003).

169. Shah, M. H. *et al.* Phase I study of IMGN901, a CD56-targeting antibody-drug conjugate, in patients with CD56-positive solid tumors. *Invest New Drugs* **34**, 290–299 (2016).
170. Gordon, M. S. *et al.* Phase I Safety and Pharmacokinetic Study of Recombinant Human Anti-Vascular Endothelial Growth Factor in Patients With Advanced Cancer. *Journal of Clinical Oncology* **19**, (2001).
171. Fu, Z., Li, S., Han, S., Shi, C. & Zhang, Y. Antibody drug conjugate: the “biological missile” for targeted cancer therapy. *Signal Transduct Target Ther* **7**, (2022).
172. Diamantis, N. & Banerji, U. Antibody-drug conjugates - An emerging class of cancer treatment. *Br J Cancer* **114**, 362–367 (2016).
173. Peters, C. & Brown, S. Antibody-drug conjugates as novel anti-cancer chemotherapeutics. *Biosci Rep* **35**, (2015).
174. Issell, B. F. & Crooke, S. T. Maytansine. *Cancer Treat Rev* **5**, 199–207 (1978).
175. Kupchan, S. M. *et al.* Maytansine, a novel antileukemic ansa macrolide from *Maytenus ovatus*. *J Am Chem Soc* **94**, 1354–1356 (1972).
176. Sieber, S. M. *et al.* Experimental studies with maytansine--a new antitumor agent. *Bibl Haematol* **43**, 495–500 (1975).
177. Bhattacharyya, A. & Wolff, J. Maytansine binding to the vinblastine sites of tubulin. *FEBS Lett* **75**, 159–162 (1977).
178. Krop, I. E. *et al.* Phase I study of trastuzumab-DM1, an HER2 antibody-drug conjugate, given every 3 weeks to patients with HER2-positive metastatic breast cancer. *Journal of Clinical Oncology* **28**, 2698–2704 (2010).
179. Geller, J. I. *et al.* ADVL1522: A phase 2 study of lorvotuzumab mertansine (IMGN901) in children with relapsed or refractory wilms tumor, rhabdomyosarcoma, neuroblastoma, pleuropulmonary blastoma, malignant peripheral nerve sheath tumor, or synovial sarcoma—A Children’s Oncology Group study. *Cancer* **126**, 5303–5310 (2020).
180. Woll, P. J. *et al.* Efficacy results from a phase I study of lorvotuzumab mertansine (IMGN901) in patients with CD56-positive solid tumors. *Journal of Clinical Oncology* **29**, (2011).
181. Staudacher, A. H. & Brown, M. P. Antibody drug conjugates and bystander killing: is antigen-dependent internalisation required. *Br J Cancer* **117**, 1736–1742 (2017).
182. Han, Y., Liu, D. & Li, L. PD-1/PD-L1 pathway: current researches in cancer. *Am J Cancer Res* **10**, 727–742 (2020).
183. Alsaab, H. O. *et al.* PD-1 and PD-L1 checkpoint signaling inhibition for cancer immunotherapy: mechanism, combinations, and clinical outcome. *Front Pharmacol* **8**, (2017).
184. Pardoll, D. M. The blockade of immune checkpoints in cancer immunotherapy. *Nat Rev Cancer* **12**, 252–264 (2012).
185. Lee, H. T., Lee, S. H. & Heo, Y. S. Molecular interactions of antibody drugs targeting PD-1, PD-L1, and CTLA-4 in immuno-oncology. *Molecules* **24**, (2019).
186. Buchbinder, E. I. & Desai, A. CTLA-4 and PD-1 pathways similarities, differences, and implications of their inhibition. *American Journal of Clinical Oncology: Cancer Clinical Trials* **39**, 98–106 (2016).
187. Rotte, A. Combination of CTLA-4 and PD-1 blockers for treatment of cancer. *Journal of Experimental and Clinical Cancer Research* **38**, (2019).
188. Rohaan, M. W. *et al.* Tumor-Infiltrating Lymphocyte Therapy or Ipilimumab in Advanced Melanoma. *New England Journal of Medicine* **387**, 2113–2125 (2022).
189. Völkel, T., Korn, T., Bach, M., Mü, R. & Kontermann, R. E. *Optimized Linker Sequences for the Expression of Monomeric and Dimeric Bispecific Single-Chain Diabodies*. *Protein Engineering* vol. 14 (2001).

190. Shah, N. N. & Fry, T. J. Mechanisms of resistance to CAR T cell therapy. *Nat Rev Clin Oncol* **16**, 372–385 (2019).
191. Gorovits, B. & Koren, E. Immunogenicity of Chimeric Antigen Receptor T-Cell Therapeutics. *BioDrugs* **33**, 275–284 (2019).
192. Klee, G. G. Human anti-mouse antibodies. *Arch Pathol Lab Med* **124**, 921–923 (2000).
193. Gruber, R. The human antimouse immunoglobulin response and the anti-idiotypic network have no influence on clinical outcome in patients with minimal residual colorectal cancer treated with monoclonal antibody CO17-1A. *Cancer Res* **60**, 1921–1926 (2000).
194. DeNardo, G. L., Bradt, B. M., Mirick, G. R. & DeNardo, S. J. Human antiglobulin response to foreign antibodies: therapeutic benefit? *Cancer Immunology, Immunotherapy* **52**, 309–316 (2003).
195. Muyldermans, S. Nanobodies: Natural Single-Domain Antibodies. *Annual Reviews of Biochemistry* **82**, 775–797 (2013).
196. Ackaert, C. *et al.* Immunogenicity Risk Profile of Nanobodies. *Front Immunol* **12**, (2021).
197. Rossotti, M. A., Bélanger, K., Henry, K. A. & Tanha, J. Immunogenicity and humanization of single-domain antibodies. *Federation of European Biochemical Societies Journal* **289**, 4304–4327 (2022).
198. Bocker, T. & Karjalainen, K. Signals through T Cell Receptor- ζ Chain Alone Are Insufficient to Prime Resting T Lymphocytes. *Journal of Experimental Medicine* **181**, 1653–1659 (1995).
199. Imai, C. *et al.* Chimeric receptors with 4-1BB signaling capacity provoke potent cytotoxicity against acute lymphoblastic leukemia. *Leukemia* **18**, 676–684 (2004).
200. Maher, J., Brentjens, R. J., Gunset, G., Riviere, I. & Sadelain, M. Human T-lymphocyte cytotoxicity and proliferation directed by a single chimeric TCR ζ /CD28 receptor. *Nat Biotechnol* **20**, 70–75 (2002).
201. Van Der Stegen, S. J. C., Hamieh, M. & Sadelain, M. The pharmacology of second-generation chimeric antigen receptors. *Nat Rev Drug Discov* **14**, 499–509 (2015).
202. Chen, Y. J., Abila, B. & Mostafa Kamel, Y. CAR-T: What Is Next? *Cancers (Basel)* **15**, (2023).
203. Subklewe, M., Von Bergwelt-Baildon, M. & Humpe, A. Chimeric Antigen Receptor T Cells: A Race to Revolutionize Cancer Therapy. *Transfusion Medicine and Hemotherapy* **46**, 15–24 (2019).
204. Li, H., Song, W., Li, Z. & Zhang, M. Preclinical and clinical studies of CAR-NK-cell therapies for malignancies. *Front Immunol* **13**, (2022).
205. Liu, S. *et al.* NK cell-based cancer immunotherapy: from basic biology to clinical development. *J Hematol Oncol* **14**, (2021).
206. Lin, X. *et al.* iPSC-derived CAR-NK cells for cancer immunotherapy. *Biomedicine and Pharmacotherapy* **165**, (2023).
207. Goldenson, B. H., Hor, P. & Kaufman, D. S. iPSC-Derived Natural Killer Cell Therapies - Expansion and Targeting. *Front Immunol* **13**, (2022).
208. Cichocki, F. *et al.* iPSC-derived NK cells maintain high cytotoxicity and enhance in vivo tumor control in concert with T cells and anti-PD-1 therapy. *Sci Transl Med* **12**, (2020).
209. Li, Y., Hermanson, D. L., Moriarity, B. S. & Kaufman, D. S. Human iPSC-Derived Natural Killer Cells Engineered with Chimeric Antigen Receptors Enhance Anti-tumor Activity. *Cell Stem Cell* **23**, 181–192.e5 (2018).
210. You, F. *et al.* A novel CD7 chimeric antigen receptor-modified NK-92MI cell line targeting T-cell acute lymphoblastic leukemia. *Am J Cancer Res* **9**, 64–78 (2019).

211. Sheng, L. *et al.* Cytotoxicity of Donor Natural Killer Cells to Allo-Reactive T Cells Are Related With Acute Graft-vs.-Host-Disease Following Allogeneic Stem Cell Transplantation. *Front Immunol* **11**, (2020).
212. Olson, J. A. *et al.* NK cells mediate reduction of GVHD by inhibiting activated, alloreactive T cells while retaining GVT effects. *Blood* **115**, 4293–4301 (2010).
213. Asai, O. *et al.* Suppression of Graft-Versus-Host Disease and Amplification of Graft-Versus-Tumor Effects by Activated Natural Killer Cells after Allogeneic Bone Marrow Transplantation. *J Clin Invest* **101**, 1835–1842 (1998).
214. Simonetta, F., Alvarez, M. & Negrin, R. S. Natural killer cells in graft-versus-host-disease after allogeneic hematopoietic cell transplantation. *Front Immunol* **8**, (2017).
215. Ruggeri, L. *et al.* Effectiveness of Donor Natural Killer Cell Alloreactivity in Mismatched Hematopoietic Transplants. *Science* (1979) **295**, 2097–2100 (2002).
216. Zama, L. *et al.* Understanding the Synergy of NKP46 and Co-Activating Signals in Various NK Cell Subpopulations: Paving the Way for More Successful NK-Cell-Based Immunotherapy. *Cells* **9**, (2020).
217. Zhang, L., Meng, Y., Feng, X. & Han, Z. CAR-NK cells for cancer immunotherapy: from bench to bedside. *Biomark Res* **10**, (2022).
218. Bauer, S. *et al.* Activation of NK Cells and T Cells by NKG2D, a Receptor for Stress-Inducible MICA. *Science* (1979) **285**, 727–729 (1999).
219. Fuertes, M. B., Domaica, C. I. & Zwirner, N. W. Leveraging NKG2D Ligands in Immuno-Oncology. *Front Immunol* **12**, (2021).
220. Zingoni, A. *et al.* NKG2D and its ligands: ‘One for all, all for one’. *Front Immunol* **9**, (2018).
221. Raullet, D. H., Gasser, S., Gowen, B. G., Deng, W. & Jung, H. Regulation of ligands for the NKG2D activating receptor. *Annu Rev Immunol* **31**, 413–441 (2013).
222. Boivin, W. A., Cooper, D. M., Hiebert, P. R. & Granville, D. J. Intracellular versus extracellular granzyme B in immunity and disease: Challenging the dogma. *Laboratory Investigation* **89**, 1195–1220 (2009).
223. Ewen, C. L., Kane, K. P. & Bleackley, R. C. A quarter century of granzymes. *Cell Death Differ* **19**, 28–35 (2012).
224. Agaoglu, S., Hargreaves, A., De Sousa, P., De Waele, P. & Gilham, D. The high expression of NKG2D ligands on tumor and the lack of surface expression on healthy tissues provides a strong rationale to support NKG2D-based therapeutic approaches for cancer. *Annals of Oncology* **29**, viii420 (2018).
225. McGilvray, R. W. *et al.* NKG2D ligand expression in human colorectal cancer reveals associations with prognosis and evidence for immunoediting. *Clinical Cancer Research* **15**, 6993–7002 (2009).
226. Li, K. *et al.* Clinical significance of the NKG2D ligands, MICA/B and ULBP2 in ovarian cancer: high expression of ULBP2 is an indicator of poor prognosis. *Cancer Immunology, Immunotherapy* **58**, 641–652 (2009).
227. Cho, H. *et al.* MICA/B and ULBP1 NKG2D ligands are independent predictors of good prognosis in cervical cancer. *BMC Cancer* **14**, (2014).
228. de Kruif, E. M. *et al.* NKG2D ligand tumor expression and association with clinical outcome in early breast cancer patients: an observational study. *BMC Cancer* **12**, (2012).
229. Chen, J., Xu, H. & Zhu, X. X. Abnormal expression levels of sMICA and NKG2D are correlated with poor prognosis in pancreatic cancer. *Ther Clin Risk Manag* **12**, 11–18 (2015).
230. Vetter, C. S. *et al.* Expression of Stress-induced MHC Class I Related Chain Molecules on Human Melanoma. *J Invest Dermatol* **118**, 600–605 (2002).

231. Tsukagoshi, M. *et al.* Overexpression of natural killer group 2 member D ligands predicts favorable prognosis in cholangiocarcinoma. *Cancer Sci* **107**, 116–122 (2016).
232. Liu, G., Atteridge, C. L., Wang, X., Lundgren, A. D. & Wu, J. D. Cutting Edge: The Membrane Type Matrix Metalloproteinase MMP14 Mediates Constitutive Shedding of MHC Class I Chain-Related Molecule A Independent of A Disintegrin and Metalloproteinases. *The Journal of Immunology* **184**, 3346–3350 (2010).
233. Salih, H. R., Rammensee, H.-G. & Steinle, A. Cutting Edge: Down-Regulation of MICA on Human Tumors by Proteolytic Shedding. *The Journal of Immunology* **169**, 4098–4102 (2002).
234. Kaiser, B. K. *et al.* Disulphide-isomerase-enabled shedding of tumour-associated NKG2D ligands. *Nature* **447**, 482–486 (2007).
235. Xing, S. & Ferrari de Andrade, L. NKG2D and MICA/B shedding: a ‘tag game’ between NK cells and malignant cells. *Clin Transl Immunology* **9**, (2020).
236. Waldhauer, I. *et al.* Tumor-associated MICA is shed by ADAM proteases. *Cancer Res* **68**, 6368–6376 (2008).
237. Vyas, M. *et al.* Soluble NKG2D ligands in the ovarian cancer microenvironment are associated with an adverse clinical outcome and decreased memory effector T cells independent of NKG2D downregulation. *Oncoimmunology* **6**, (2017).
238. Groh, V., Wu, J., Yee, C. & Spies, T. Tumour-derived soluble MIC ligands impair expression of NKG2D and T-cell activation. *Nature* **419**, 734–738 (2002).
239. Klöß, S. *et al.* Increased sMICA and TGFβ1 levels in HNSCC patients impair NKG2D-dependent functionality of activated NK cells. *Oncoimmunology* **4**, (2015).
240. Jinushi, M., Hodi, F. S. & Dranoff, G. Therapy-induced antibodies to MHC class I chain-related protein A antagonize immune suppression and stimulate antitumor cytotoxicity. *Proceedings of the National Academy of Sciences* **103**, 9190–9195 (2006).
241. Hodi, F. S. *et al.* Immunologic and clinical effects of antibody blockade of cytotoxic T lymphocyte-associated antigen 4 in previously vaccinated cancer patients. *Proceedings of the National Academy of Sciences* **105**, 3005–3010 (2008).
242. Badrinath, S. *et al.* A vaccine targeting resistant tumours by dual T cell plus NK cell attack. *Nature* **606**, 992–998 (2022).
243. De Andrade, L. F. *et al.* Antibody-mediated inhibition of MICA and MICB shedding promotes NK cell-driven tumor immunity. *Science* (1979) **359**, 1537–1542 (2018).
244. Wieczorek, M. *et al.* Major histocompatibility complex (MHC) class I and MHC class II proteins: Conformational plasticity in antigen presentation. *Front Immunol* **8**, (2017).
245. Stern, L. J. & Wiley, D. C. Antigenic peptide binding by class I and class II histocompatibility proteins. *Structure* **2**, 245–251 (1994).
246. Engelhard, V. H. Structure of Peptides Associated with Class I and Class II MHC Molecules. *Annu Rev Immunol* **12**, 181–207 (1994).
247. Bjorkman, P. J. & Parham, P. Structure, Function, and diversity of Class I Major Histocompatibility Complex Molecules. *Annual Reviews of Biochemistry* **59**, 253–288 (1990).
248. van der Merwe, P. A. & Davis, S. J. Molecular Interactions Mediating T Cell Antigen Recognition. *Annu Rev Immunol* **21**, 659–684 (2003).
249. Klein, J. & Sato, A. The HLA System. First of two parts. *N Engl J Med* 702–709 (2000) doi:10.1056/NEJM200009073431006.
250. Pamer, E. & Cresswell, P. Mechanisms of MHC Class I-Restricted Antigen Processing. *Annu Rev Immunol* **16**, 323–358 (1998).
251. Pugliese, A. Central and peripheral autoantigen presentation in immune tolerance. *Immunology* **111**, 138–146 (2004).

252. Walters, L. C. *et al.* Pathogen-derived HLA-E bound epitopes reveal broad primary anchor pocket tolerability and conformationally malleable peptide binding. *Nat Commun* **9**, (2018).
253. Walters, L. C., McMichael, A. J. & Gillespie, G. M. Detailed and atypical HLA-E peptide binding motifs revealed by a novel peptide exchange binding assay. *Eur J Immunol* **50**, 2075–2091 (2020).
254. Kraemer, T. *et al.* HLA-E: Presentation of a broader peptide repertoire impacts the cellular immune response - Implications on HSCT outcome. *Stem Cells Int* **2015**, (2015).
255. Ruibal, P. *et al.* Peptide Binding to HLA-E Molecules in Humans, Nonhuman Primates, and Mice Reveals Unique Binding Peptides but Remarkably Conserved Anchor Residues. *The Journal of Immunology* **205**, 2861–2872 (2020).
256. Romagnani, C. *et al.* Identification of HLA-E-specific alloreactive T lymphocytes: A cell subset that undergoes preferential expansion in mixed lymphocyte culture and displays a broad cytolytic activity against allogeneic cells. *Proceedings of the National Academy of Sciences* **99**, 11328–11333 (2002).
257. Braud, V., Jones, E. Y. & McMichael, A. The human major histocompatibility complex class Ib molecule HLA-E binds signal sequence-derived peptides with primary anchor residues at positions 2 and 9. *Eur J Immunol* **27**, 1164–1169 (1997).
258. Michaëlsson, J. *et al.* A signal peptide derived from hsp60 binds HLA-E and interferes with CD94/NKG2A recognition. *Journal of Experimental Medicine* **196**, 1403–1414 (2002).
259. Pietra, G., Romagnani, C., Moretta, L. & Mingiri, M. C. HLA-E and HLA-E-Bound Peptides: Recognition by Subsets of NK and T Cells. *Current Pharmaceutical Design* **15**, 3336–3344 (2009).
260. Braud, V. M., Allan, D. S. J., Wilson, D. & McMichael, A. J. TAP- and tapasin-dependent HLA-E surface expression correlates with the binding of an MHC class I leader peptide. *Current Biology* **8**, 1–10 (1997).
261. Ishido, S., Wang, C., Lee, B.-S., Cohen, G. B. & Jung, J. U. Downregulation of Major Histocompatibility Complex Class I Molecules by Kaposi's Sarcoma-Associated Herpesvirus K3 and K5 Proteins. *J Virol* **74**, 5300–5309 (2000).
262. Gainey, M. D., Rivenbark, J. G., Cho, H., Yang, L. & Yokoyama, W. M. Viral MHC class I inhibition evades CD8⁺ T-cell effector responses in vivo but not CD8⁺ T-cell priming. *Proc Natl Acad Sci U S A* **109**, (2012).
263. Cohen, G. B. *et al.* The Selective Downregulation of Class I Major Histocompatibility Complex Proteins by HIV-1 Protects HIV-Infected Cells from NK Cells. *Immunity* **10**, 661–671 (1999).
264. Petersen, J. L., Morris, C. R. & Solheim, J. C. Virus Evasion of MHC Class I Molecule Presentation. *The Journal of Immunology* **171**, 4473–4478 (2003).
265. Koutsakos, M. *et al.* Downregulation of MHC class I expression by influenza A and B viruses. *Front Immunol* **10**, (2019).
266. Wang, E. C. Y. *et al.* UL40-mediated NK evasion during productive infection with human cytomegalovirus. *Proceedings of the National Academy of Sciences* **99**, (2002).
267. Ulbrecht, M. *et al.* Cutting Edge: The Human Cytomegalovirus UL40 Gene Product Contains a Ligand for HLA-E and Prevents NK Cell-Mediated Lysis. *The Journal of Immunology* **164**, 5019–5022 (2000).
268. Tomasec, P. *et al.* Surface Expression of HLA-E, an Inhibitor of Natural Killer Cells, Enhanced by Human Cytomegalovirus gpUL40. *Science* (1979) **287**, 1031–1033 (2000).
269. Borrego, F., Ulbrecht, M., Weiss, E. H., Coligan, J. E. & Brooks, A. G. Recognition of Human Histocompatibility Leukocyte Antigen (HLA)-E Complexed with HLA Class I Signal Sequence-Derived Peptides by CD94/NKG2 Confers Protection from Natural Killer

- Cell-Mediated Lysis. The Journal of Experimental Medicine* • vol. 187 <http://www.jem.org> (1998).
270. Brooks, A. G. *et al.* Specific Recognition of HLA-E, But Not Classical, HLA Class I Molecules by Soluble CD94/NKG2A and NK Cells. *The Journal of Immunology* **162**, 305–313 (1999).
 271. Huisman, B. D. *et al.* An unbiased characterization of the HLA-E and CD94/NKG2x peptide repertoire reveals 1 peptide ligands that skew NK cell activation 2 3. *BioRxiv* (2022) doi:10.1101/2022.08.03.502719.
 272. Lee, N. I. *et al.* HLA-E is a major ligand for the natural killer inhibitory receptor CD94NKG2A. *Proceedings of the National Academy of Sciences* **95**, 5199–5204 (1998).
 273. Braud, V. M. *et al.* HLA-E binds to natural killer cell receptors CD94/NKG2A, B and C. *Nature* **391**, 795–799 (1998).
 274. lo Monaco, E. *et al.* Human leukocyte antigen E contributes to protect tumor cells from lysis by natural killer cells. *Neoplasia* **13**, 822–830 (2011).
 275. Gooden, M. *et al.* HLA-E expression by gynecological cancers restrains tumor-infiltrating CD8 + T lymphocytes. *Proc Natl Acad Sci U S A* **108**, 10656–10661 (2011).
 276. Ferns, D. M. *et al.* Classical and non-classical HLA class I aberrations in primary cervical squamous- and adenocarcinomas and paired lymph node metastases. *J Immunother Cancer* **4**, (2016).
 277. Van Esch, E. M. G. *et al.* Alterations in classical and nonclassical HLA expression in recurrent and progressive HPV-induced usual vulvar intraepithelial neoplasia and implications for immunotherapy. *Int J Cancer* **135**, 830–842 (2014).
 278. Le Dréan, E. *et al.* Inhibition of antigen-induced T cell response and antibody-induced NK cell cytotoxicity by NKG2A: Association of NKG2A with SHP-1 and SHP-2 protein-tyrosine phosphatases. *Eur J Immunol* **28**, 264–276 (1998).
 279. Wang, X., Xiong, H. & Ning, Z. Implications of NKG2A in immunity and immune-mediated diseases. *Front Immunol* **13**, (2022).
 280. Vega, M. A. & Strominger, J. L. Cell Biology Constitutive endocytosis of HLA class I antigens requires a specific portion of the intracytoplasmic tail that shares structural features with other endocytosed molecules. *Proceedings of the National Academy of Sciences* **86**, 2688–2692 (1989).
 281. He, W. *et al.* Intracellular trafficking of HLA-E and its regulation. *J Exp Med* **220**, (2023).
 282. Barber, C. *et al.* Structure-guided stabilization of pathogen-derived peptide-HLA-E complexes using non-natural amino acids conserves native TCR recognition. *Eur J Immunol* **52**, 618–632 (2022).
 283. Hoare, H. L. *et al.* Subtle Changes in Peptide Conformation Profoundly Affect Recognition of the Non-Classical MHC Class I Molecule HLA-E by the CD94–NKG2 Natural Killer Cell Receptors. *J Mol Biol* **377**, 1297–1303 (2008).
 284. Strong, R. K. *et al.* HLA-E Allelic Variants: Correlating differential expression, peptide affinities, crystal structures, and thermal stabilities. *Journal of Biological Chemistry* **278**, 5082–5090 (2003).
 285. Walters, L. C. *et al.* Primary and secondary functions of HLA-E are determined by stability and conformation of the peptide-bound complexes. *Cell Rep* **39**, (2022).
 286. O’Callaghan, C. A. *et al.* Structural Features Impose Tight Peptide Binding Specificity in the Nonclassical MHC Molecule HLA-E. *Mol Cell* **1**, 531–541 (1998).
 287. Yazdi, M. T. *et al.* The positive prognostic effect of stromal CD8+ tumor-infiltrating T cells is restrained by the expression of HLA-E in non-small cell lung carcinoma. *Oncotarget* **7**, (2015).
 288. Wu, Z. *et al.* HLA-E expression in diffuse glioma: Relationship with clinicopathological features and patient survival. *BMC Neurol* **20**, (2020).

289. Wolpert, F. *et al.* HLA-E contributes to an immune-inhibitory phenotype of glioblastoma stem-like cells. *J Neuroimmunol* **250**, 27–34 (2012).
290. Seliger, B. *et al.* HLA-E expression and its clinical relevance in human renal cell carcinoma. *Oncotarget* **7**, 67360–67372 (2016).
291. Eugène, J. *et al.* The inhibitory receptor CD94/NKG2A on CD8+ tumor-infiltrating lymphocytes in colorectal cancer: a promising new druggable immune checkpoint in the context of HLA-E/ β 2m overexpression. *Modern Pathology* **33**, 468–482 (2020).
292. Bossard, C. *et al.* HLA-E/ β 2 microglobulin overexpression in colorectal cancer is associated with recruitment of inhibitory immune cells and tumor progression. *Int J Cancer* **131**, 855–863 (2012).
293. Levy, E. M. *et al.* Human leukocyte antigen-E protein is overexpressed in primary human colorectal cancer. *Int J Oncol* **32**, 633–641 (2008).
294. Zheng, H. *et al.* Human leukocyte antigen-E alleles and expression in patients with serous ovarian cancer. *Cancer Sci* **106**, 522–528 (2015).
295. Andersson, E. *et al.* Non-classical HLA-class I expression in serous ovarian carcinoma: Correlation with the HLA-genotype, tumor infiltrating immune cells and prognosis. *Oncoimmunology* **5**, (2016).
296. Borst, L. *et al.* NKG2A is a late immune checkpoint on CD8 T cells and marks repeated stimulation and cell division. *Int J Cancer* **150**, 688–704 (2022).
297. Hamid, M. A. *et al.* Enriched HLA-E and CD94/NKG2A interaction limits antitumor CD8+ tumor-infiltrating T lymphocyte responses. *Cancer Immunol Res* **7**, 1293–1306 (2019).
298. Sun, C. *et al.* High NKG2A expression contributes to NK cell exhaustion and predicts a poor prognosis of patients with liver cancer. *Oncoimmunology* **6**, (2017).
299. André, P. *et al.* Anti-NKG2A mAb Is a Checkpoint Inhibitor that Promotes Anti-tumor Immunity by Unleashing Both T and NK Cells. *Cell* **175**, 1731–1743.e13 (2018).
300. Greenberg, A. S. *et al.* A new antigen receptor gene family that undergoes rearrangement and extensive somatic diversification in sharks. *Nature* **374**, (1995).
301. Hamers-Casterman, C. *et al.* Naturally occurring antibodies devoid of light chains. *Nature* **363**, 446–448 (1993).
302. Davies, J. & Riechmann, L. Antibody VH domains as small recognition units. *Biotechnology* **13**, 475–479 (1995).
303. Reiter, Y., Schuck, P., Boyd, L. F. & Plaksin, D. An antibody single-domain phage display library of a native heavy chain variable region: Isolation of functional single-domain VH molecules with a unique interface. *J Mol Biol* **290**, 685–698 (1999).
304. Feng, M. *et al.* Therapeutically targeting glypican-3 via a conformation-specific single-domain antibody in hepatocellular carcinoma. *Proceedings of the National Academy of Sciences* **110**, 1–9 (2013).
305. Li, N., Fu, H., Hewitt, S. M., Dimitrov, D. S. & Ho, M. Therapeutically targeting glypican-2 via single-domain antibody-based chimeric antigen receptors and immunotoxins in neuroblastoma. *Proceedings of the National Academy of Sciences* **114**, E6623–E6631 (2017).
306. Chen, W., Zhu, Z., Feng, Y., Xiao, X. & Dimitrov, D. S. Construction of a large phage-displayed human antibody domain library with a scaffold based on a newly identified highly soluble, stable heavy chain variable domain. *J Mol Biol* **382**, 779–789 (2008).
307. Ward, E. S., Guusow, D., Griffiths, A. D., Jones, P. T. & Winter, G. Binding activities of a repertoire of single immunoglobulin variable domains secreted from Escherichia coli. *Nature* **341**, 544–546 (1989).
308. Holt, L. J., Herring, C., Jespers, L. S., Woolven, B. P. & Tomlinson, I. M. Domain antibodies: proteins for therapy. *Trends Biotechnol* **21**, 484–490 (2003).

309. Tanha, J. *et al.* Optimal Design Features of Camelized Human Single-domain Antibody Libraries. *Journal of Biological Chemistry* **276**, 24774–24780 (2001).
310. Van Der Linden, R. H. J. *et al.* Comparison of physical chemical properties of llama VHH antibody fragments and mouse monoclonal antibodies. *Biochim Biophys Acta* **1431**, 37–46 (1999).
311. Kijanka, M., Dorresteyn, B., Oliveira, S. & Van Bergen En Henegouwen, P. M. P. Nanobody-based cancer therapy of solid tumors. *Nanomedicine* **10**, 161–174 (2015).
312. Fang, T. *et al.* Nanobody immunostaining for correlated light and electron microscopy with preservation of ultrastructure. *Nat Methods* **15**, 1029–1032 (2018).
313. Tijink, B. M. *et al.* Improved tumor targeting of anti-epidermal growth factor receptor Nanobodies through albumin binding: Taking advantage of modular Nanobody technology. *Mol Cancer Ther* **7**, 2288–2297 (2008).
314. Rashidian, M. *et al.* Immuno-PET identifies the myeloid compartment as a key contributor to the outcome of the antitumor response under PD-1 blockade. *Proceedings of the National Academy of Sciences* **116**, 16971–16980 (2019).
315. Altintas, I. *et al.* Nanobody-albumin nanoparticles (NANAPs) for the delivery of a multikinase inhibitor 17864 to EGFR overexpressing tumor cells. *Journal of Controlled Release* **165**, 110–118 (2013).
316. Iezzi, M. E., Policastro, L., Werbach, S., Podhajcer, O. & Canziani, G. A. Single-Domain Antibodies and the Promise of Modular Targeting in Cancer imaging and Treatment. *Front Immunol* **9**, 1–11 (2018).
317. Bannas, P., Hambach, J. & Koch-Nolte, F. Nanobodies and nanobody-based human heavy chain antibodies as antitumor therapeutics. *Front Immunol* **8**, 1–13 (2017).
318. Rahbarizadeh, F., Ahmadvand, D. & Sharifzadeh, Z. Nanobody; an Old Concept and New Vehicle for Immunotargeting. *Immunol Invest* **40**, 299–338 (2011).
319. Wesolowski, J. *et al.* Single domain antibodies: promising experimental and therapeutic tools in infection and immunity. *Med Microbiol Immunol* **198**, 157–174 (2009).
320. Hu, Y., Liu, C. & Muyldermans, S. Nanobody-Based Delivery Systems for Diagnosis and Targeted Tumor Therapy. *Front Immunol* **8**, (2017).
321. De Meyer, T., Muyldermans, S. & Depicker, A. Nanobody-based products as research and diagnostic tools. *Trends Biotechnol* **32**, 263–270 (2014).
322. Chanier, T. & Chames, P. Nanobody Engineering: Toward Next Generation Immunotherapies and Immunoimaging of Cancer. *Antibodies* **8**, (2019).
323. Lecocq, Q. *et al.* Theranostics Theranostics in immuno-oncology using nanobody derivatives. *Theranostics* **9**, 7772–7791 (2019).
324. Ingram, J. R., Schmidt, F. I. & Ploegh, H. L. Exploiting Nanobodies' Singular Traits. *Annu Rev Immunol* **36**, (2018).
325. Woodham, A. W. *et al.* Nanobody-antigen conjugates elicit HPV-specific antitumor immune responses. *Cancer Immunol Res* **6**, 870–880 (2018).
326. Cheloha, R. W. *et al.* Improved GPCR ligands from nanobody tethering. *Nat Commun* **11**, 1–11 (2020).
327. Huang, L. *et al.* SPECT imaging with 99mTc-labeled EGFR-specific nanobody for in vivo monitoring of EGFR expression. *Mol Imaging Biol* **10**, 167–175 (2008).
328. Vaneycken, I. *et al.* Preclinical screening of anti-HER2 nanobodies for molecular imaging of breast cancer. *The FASEB Journal* **25**, 2433–2446 (2011).
329. Jaikhan, N. *et al.* Noninvasive imaging of tumor progression, metastasis, and fibrosis using a nanobody targeting the extracellular matrix. *Proceedings of the National Academy of Sciences* **116**, 14181–14190 (2019).

330. Oda, K., Matsuoka, Y., Funahashi, A. & Kitano, H. A comprehensive pathway map of epidermal growth factor receptor signaling. *Mol Syst Biol* 1–17 (2005) doi:10.1038/msb4100014.
331. Gibson, T. B., Ranganathan, A. & Grothey, A. Randomized Phase III Trial Results of Panitumumab, a Fully Human Anti—Epidermal Growth Factor Receptor Monoclonal Antibody, in Metastatic Colorectal Cancer. *Clin Colorectal Cancer* 6, 29–31 (2006).
332. Roovers, R. C. *et al.* Efficient inhibition of EGFR signalling and of tumour growth by antagonistic anti-EGFR Nanobodies. *Cancer Immunology, Immunotherapy* 56, 303–317 (2007).
333. Gainkam, L. O. T. *et al.* Comparison of the biodistribution and tumor targeting of two 99mTc-labeled anti-EGFR nanobodies in mice, using pinhole SPECT/micro-CT. *Journal of Nuclear Medicine* 49, 788–795 (2008).
334. Roovers, R. C. *et al.* A biparatopic anti-EGFR nanobody efficiently inhibits solid tumour growth. *Int J Cancer* 129, 2013–2024 (2011).
335. Omidfar, K. *et al.* Efficient growth inhibition of EGFR over-expressing tumor cells by an anti-EGFR nanobody. *Mol Biol Rep* 40, 6737–6745 (2013).
336. Kijanka, M. *et al.* Rapid optical imaging of human breast tumour xenografts using anti-HER2 VHHs site-directly conjugated to IRDye 800CW for image-guided surgery. *Eur J Nucl Med Mol Imaging* 40, 1718–1729 (2013).
337. Pruszyński, M. *et al.* Targeting breast carcinoma with radioiodinated anti-HER2 Nanobody. *Nucl Med Biol* 40, 52–59 (2013).
338. Olsson, A.-K., Dimberg, A., Kreuger, J. & Claesson-Welsh, L. VEGF receptor signalling - in control of vascular function. *Nat Rev Mol Cell Biol* 7, 359–371 (2006).
339. Holmes, K., Roberts, O. L., Thomas, A. M. & Cross, M. J. Vascular endothelial growth factor receptor-2: Structure, function, intracellular signalling and therapeutic inhibition. *Cell Signal* 19, 2003–2012 (2007).
340. Behdani, M. *et al.* Generation and characterization of a functional Nanobody against the vascular endothelial growth factor receptor-2; angiogenesis cell receptor. *Mol Immunol* 50, 35–41 (2012).
341. Ma, L. *et al.* Generation and characterization of a human nanobody against VEGFR-2. *Acta Pharmacol Sin* 37, 857–864 (2016).
342. Kazemi-Lomedasht, F. *et al.* Inhibition of angiogenesis in human endothelial cell using VEGF specific nanobody. *Mol Immunol* 65, 58–67 (2015).
343. Kazemi-Lomedasht, F., Muyldermans, S., Habibi-Anbouhi, M. & Behdani, M. Design of a humanized anti vascular endothelial growth factor nanobody and evaluation of its in vitro function. *Iran J Basic Med Sci* 21, 260–266 (2018).
344. Ebrahimizadeh, W., Mousavi Gargari, S. L., Javidan, Z. & Rajabibazl, M. Production of Novel VHH Nanobody Inhibiting Angiogenesis by Targeting Binding Site of VEGF. *Appl Biochem Biotechnol* 176, 1985–1995 (2015).
345. Bottaro, D. P. *et al.* Identification of the hepatocyte growth factor receptor as the c-met proto-oncogene product. *Science (1979)* 251, 802–804 (1991).
346. Gherardi, E., Birchmeier, W., Birchmeier, C. & Vande Woude, G. Targeting MET in cancer: rationale and progress. *Nat Rev Cancer* 12, 89–103 (2012).
347. Boccaccio, C. & Comoglio, P. M. Invasive growth: a MET-driven genetic programme for cancer and stem cells. *Nat Rev Cancer* 6, 637–645 (2006).
348. Wallenius, V. *et al.* Overexpression of the hepatocyte growth factor (HGF) receptor (Met) and presence of a truncated and activated intracellular HGF receptor fragment in locally aggressive/malignant human musculoskeletal tumors. *American Journal of Pathology* 156, 821–829 (2000).

349. Heukers, R. *et al.* Targeting hepatocyte growth factor receptor (Met) positive tumor cells using internalizing nanobody-decorated albumin nanoparticles. *Biomaterials* **35**, 601–610 (2014).
350. Schmidt Slørdahl, T. *et al.* Anti-c-MET Nanobody® - A new potential drug in multiple myeloma treatment. *Eur J Haematol* **91**, 399–410 (2013).
351. Vosjan, M. J. W. D. *et al.* Nanobodies targeting the hepatocyte growth factor: Potential new drugs for molecular cancer therapy. *Mol Cancer Ther* **11**, 1017–1025 (2012).
352. Balkwill, F. Cancer and the chemokine network. *Nat Rev Cancer* **4**, 540–550 (2004).
353. Bradley, M. E. *et al.* Potent and efficacious inhibition of CXCR2 signaling by biparatopic nanobodies combining two distinct modes of action. *Mol Pharmacol* **87**, 251–262 (2015).
354. Jähnichen, S. *et al.* CXCR4 nanobodies (VHH-based single variable domains) potently inhibit chemotaxis and HIV-1 replication and mobilize stem cells. *Proceedings of the National Academy of Sciences* **107**, 20565–20570 (2010).
355. De Wit, R. H. *et al.* CXCR4-specific nanobodies as potential therapeutics for WHIM syndrome. *Journal of Pharmacology and Experimental Therapeutics* **363**, 35–44 (2017).
356. Van Hout, A. *et al.* CXCR4-targeting nanobodies differentially inhibit CXCR4 function and HIV entry. *Biochem Pharmacol* **158**, 402–412 (2018).
357. Maussang, D. *et al.* Llama-derived single variable domains (nanobodies) directed against chemokine receptor CXCR7 reduce head and neck cancer cell growth in vivo. *Journal of Biological Chemistry* **288**, 29562–29572 (2013).
358. Blanchetot, C. *et al.* Neutralizing nanobodies targeting diverse chemokines effectively inhibit chemokine function. *Journal of Biological Chemistry* **288**, 25173–25182 (2013).
359. Burg, J. S. *et al.* Structural basis for chemokine recognition and activation of a viral G protein-coupled receptor John. *Science (1979)* **347**, 1113–1117 (2015).
360. Heukers, R. *et al.* The constitutive activity of the virally encoded chemokine receptor US28 accelerates glioblastoma growth. *Oncogene* **37**, 4110–4121 (2018).
361. De Groof, T. W. M. *et al.* Nanobody-Targeted Photodynamic Therapy Selectively Kills Viral GPCR-Expressing Glioblastoma Cells. *Mol Pharm* **16**, 3145–3156 (2019).
362. Cortez-Retamozo, V. *et al.* Efficient Cancer Therapy with a Nanobody-Based Conjugate. *Cancer Res* **64**, 2853–2857 (2004).
363. Wang, H., Meng, A.-M., Li, S.-H. & Zhou, X.-L. A nanobody targeting carcinoembryonic antigen as a promising molecular probe for non-small cell lung cancer. *Mol Med Rep* **16**, 625–630 (2017).
364. Kaliberov, S. A. *et al.* Adenoviral targeting using genetically incorporated camelid single variable domains. *Laboratory Investigation* **94**, 893–905 (2014).
365. Chatalic, K. L. S. *et al.* A novel ¹¹¹In-labeled anti-prostate-specific membrane antigen nanobody for targeted SPECT/CT imaging of prostate cancer. *Journal of Nuclear Medicine* **56**, 1094–1099 (2015).
366. Evazalipour, M. *et al.* Generation and characterization of nanobodies targeting PSMA for molecular imaging of prostate cancer. *Contrast Media Mol Imaging* **9**, 211–220 (2014).
367. Zare, H. *et al.* Production of nanobodies against prostate-specific membrane antigen (PSMA) recognizing LnCaP cells. *International Journal of Biological Markers* **29**, 169–179 (2014).
368. Fan, X. *et al.* Ultrasonic nanobubbles carrying anti-PSMA nanobody: Construction and application in prostate cancer-targeted imaging. *PLoS One* **10**, 1–13 (2015).
369. Saerens, D. *et al.* Single domain antibodies derived from dromedary lymph node and peripheral blood lymphocytes sensing conformational variants of prostate-specific antigen. *Journal of Biological Chemistry* **279**, 51965–51972 (2004).

370. Movahedi, K. *et al.* Nanobody-based targeting of the macrophage mannose receptor for effective in vivo imaging of tumor-associated macrophages. *Cancer Res* **72**, 4165–4177 (2012).
371. Blykers, A. *et al.* PET imaging of macrophage mannose receptor-expressing macrophages in tumor stroma using ¹⁸F-radiolabeled camelid single-domain antibody fragments. *Journal of Nuclear Medicine* **56**, 1265–1271 (2015).
372. Tang, J. *et al.* Novel CD7-specific nanobody-based immunotoxins potently enhanced apoptosis of CD7-positive malignant cells. *Oncotarget* **7**, 34070–34083 (2016).
373. Yu, Y. *et al.* Humanized CD7 nanobody-based immunotoxins exhibit promising anti-T-cell acute lymphoblastic leukemia potential. *Int J Nanomedicine* **12**, 1969–1983 (2017).
374. Wan, R. *et al.* Screening and antitumor effect of an anti-CTLA-4 nanobody. *Oncol Rep* **39**, 511–518 (2018).
375. Ingram, J. R. *et al.* Anti-CTLA-4 therapy requires an Fc domain for efficacy. *Proceedings of the National Academy of Sciences* **115**, 3912–3917 (2018).
376. Zhang, F. *et al.* Structural basis of a novel PD-L1 nanobody for immune checkpoint blockade. *Cell Discov* **3**, 1–12 (2017).
377. Broos, K. *et al.* Evaluating a single domain antibody targeting human PD-L1 as a nuclear imaging and therapeutic agent. *Cancers (Basel)* **11**, 1–19 (2019).
378. Broos, K. *et al.* Non-invasive assessment of murine PD-L1 levels in syngeneic tumor models by nuclear imaging with nanobody tracers. *Oncotarget* **8**, 41932–41946 (2017).
379. Xing, Y. *et al.* Early phase I study of a ^{99m}Tc-labeled anti-programmed death ligand-1 (PD-L1) single-domain antibody in SPECT/CT assessment of PD-L1 expression in non-small cell lung cancer. *Journal of Nuclear Medicine* **60**, 1213–1220 (2019).
380. Ingram, J. R. *et al.* PD-L1 is an activation-independent marker of brown adipocytes. *Nat Commun* **8**, (2017).
381. Rashidian, M. *et al.* Predicting the response to CTLA-4 blockade by longitudinal noninvasive monitoring of CD8 T cells. *Journal of Experimental Medicine* **214**, 2243–2255 (2017).
382. Rossotti, M. *et al.* Streamlined method for parallel identification of single domain antibodies to membrane receptors on whole cells. *Biochim Biophys Acta* **1850**, 1397–1404 (2015).
383. Rashidian, M. *et al.* Noninvasive imaging of immune responses. *Proceedings of the National Academy of Sciences* **112**, 6146–6151 (2015).
384. Krasniqi, A. *et al.* Theranostic radiolabeled anti-CD20 sdAb for targeted radionuclide therapy of non-hodgkin lymphoma. *Mol Cancer Ther* **16**, 2828–2839 (2017).
385. Fumey, W. *et al.* Nanobodies effectively modulate the enzymatic activity of CD38 and allow specific imaging of CD38+ tumors in mouse models in vivo. *Sci Rep* **7**, 1–13 (2017).
386. Bachran, C. *et al.* The activity of myeloid cell-specific VHH immunotoxins is target-, epitope-, subset- and organ dependent. *Sci Rep* **7**, 2–11 (2017).
387. Van Elssen, C. H. M. J. *et al.* Noninvasive imaging of human immune responses in a human xenograft model of graft-versus-host disease. *Journal of Nuclear Medicine* **58**, 1003–1008 (2017).
388. Rashidian, M. *et al.* Use of ¹⁸F-2-fluorodeoxyglucose to label antibody fragments for immuno-positron emission tomography of pancreatic cancer. *ACS Cent Sci* **1**, 142–147 (2015).
389. Samec, N. *et al.* Glioblastoma-specific anti-TUFM nanobody for in-vitro immunoimaging and cancer stem cell targeting. *Oncotarget* **9**, 17282–17299 (2018).
390. Van Impe, K. *et al.* A nanobody targeting the F-actin capping protein CapG restrains breast cancer metastasis. *Breast Cancer Research* **15**, 1–15 (2013).

391. Araste, F., Ebrahimizadeh, W., Rasooli, I., Rajabibazl, M. & Mousavi Gargari, S. L. A novel VHH nanobody against the active site (the CA domain) of tumor-associated, carbonic anhydrase isoform IX and its usefulness for cancer diagnosis. *Biotechnol Lett* **36**, 21–28 (2014).
392. van Brussel, A. S. A. *et al.* Hypoxia-Targeting Fluorescent Nanobodies for Optical Molecular Imaging of Pre-Invasive Breast Cancer. *Mol Imaging Biol* **18**, 535–544 (2016).
393. Romão, E. *et al.* Identification of nanobodies against the acute myeloid leukemia marker CD33. *Int J Mol Sci* **21**, (2020).
394. Ma, L. *et al.* Preclinical development of a novel CD47 nanobody with less toxicity and enhanced anti-cancer therapeutic potential. *J Nanobiotechnology* **18**, 1–15 (2020).
395. Sockolosky, J. T. *et al.* Durable antitumor responses to CD47 blockade require adaptive immune stimulation. *Proceedings of the National Academy of Sciences* **113**, E2646–E2654 (2016).
396. Koch-Nolte, F. *et al.* Single domain antibodies from llama effectively and specifically block T cell ecto-ADP-ribosyltransferase ART2.2 in vivo. *The FASEB Journal* **21**, 3490–3498 (2007).
397. Ji, X. *et al.* Neutralization of TNF α in tumor with a novel nanobody potentiates paclitaxel-therapy and inhibits metastasis in breast cancer. *Cancer Lett* **386**, 24–34 (2017).
398. Weissleder, R. Molecular imaging in cancer. *Science* (1979) **312**, 1168–1171 (2006).
399. Hong, H., Zhang, Y., Sun, J. & Cai, W. Molecular imaging and therapy of cancer with radiolabeled nanoparticles. *Nano Today* **4**, 399–413 (2009).
400. de Vos, J., Devoogdt, N., Lahoutte, T. & Muyldermans, S. Camelid single-domain antibody-fragment engineering for (pre)clinical in vivo molecular imaging applications: adjusting the bullet to its target. *Expert Opin Biol Ther* **13**, 1149–1160 (2013).
401. Knowles, S. M. & Wu, A. M. Advances in immuno-positron emission tomography: Antibodies for molecular imaging in oncology. *Journal of Clinical Oncology* **30**, 3884–3892 (2012).
402. Vosjan, M. J. W. D. *et al.* Facile labelling of an anti-epidermal growth factor receptor Nanobody with ⁶⁸Ga via a novel bifunctional desferal chelate for immuno-PET. *Eur J Nucl Med Mol Imaging* **38**, 753–763 (2011).
403. Oliveira, S. *et al.* Rapid visualization of human tumor xenografts through optical imaging with a near-infrared fluorescent anti-epidermal growth factor receptor nanobody. *Mol Imaging* **11**, 33–46 (2012).
404. Hernot, S. *et al.* Nanobody-coupled microbubbles as novel molecular tracer. *Journal of Controlled Release* **158**, 346–353 (2012).
405. Berger, A. How does it work? Positron emission tomography. *The British Medical Journal Preprint at* <https://doi.org/10.1136/bmj.326.7404.1449> (2003).
406. Vaidyanathan, G., Bigner, D. D. & Zalutsky, M. R. Fluorine-18-labeled monoclonal antibody fragments: A potential approach for combining radioimmunoscintigraphy and positron emission tomography. *Journal of Nuclear Medicine* **33**, 1535–1541 (1992).
407. Cai, W. *et al.* PET imaging of colorectal cancer in xenograft-bearing mice by use of an ¹⁸F-labeled T84.66 anti-carcinoembryonic antigen diabody. *Journal of Nuclear Medicine* **48**, 304–310 (2007).
408. Xavier, C. *et al.* Synthesis, preclinical validation, dosimetry, and toxicity of ⁶⁸Ga-NOTA-anti-HER2 nanobodies for iPET imaging of HER2 receptor expression in cancer. *Journal of Nuclear Medicine* **54**, 776–784 (2013).
409. Keyaerts, M. *et al.* Phase I study of ⁶⁸Ga-HER2-Nanobody for PET/CT assessment of HER2 expression in breast carcinoma. *Journal of Nuclear Medicine* **57**, 27–33 (2016).

410. Xavier, C. *et al.* Clinical Translation of [68Ga]Ga-NOTA-anti-MMR-sdAb for PET/CT Imaging of Protumorigenic Macrophages. *Mol Imaging Biol* **21**, 898–906 (2019).
411. Banerjee, S. R. & Pomper, M. G. Clinical applications of Gallium-68. *Applied Radiation and Isotopes* **76**, 2–13 (2013).
412. Garcia-Torano, E. & Ibarra, M. R. The half-life of 18F. *Applied Radiation and Isotopes* **68**, 1561–1565 (2010).
413. Xavier, C. *et al.* 18F-nanobody for PET imaging of HER2 overexpressing tumors. *Nucl Med Biol* **43**, 247–252 (2016).
414. Leach, D. R., Krummel, M. F. & Allison, J. P. Enhancement of Antitumor Immunity by CTLA-4 Blockade. *Science* (1979) **271**, 1734–1736 (1996).
415. Lipson, E. J. *et al.* Antagonists of PD-1 and PD-L1 in Cancer Treatment. *Semin Oncol* **42**, 587–600 (2015).
416. Zhang, Y. *et al.* Myeloid cells are required for PD-1/PD-L1 checkpoint activation and the establishment of an immunosuppressive environment in pancreatic cancer. *Gut* **66**, 124–136 (2017).
417. Bocanegra, A. *et al.* PD-L1 expression in systemic immune cell populations as a potential predictive biomarker of responses to PD-L1/PD-1 blockade therapy in lung cancer. *Int J Mol Sci* **20**, 1–13 (2019).
418. Pico De Coaña, Y., Masucci, G., Hansson, J. & Kiessling, R. Myeloid-derived suppressor cells and their role in CTLA-4 blockade therapy. *Cancer Immunology, Immunotherapy* **63**, 977–983 (2014).
419. Dedman, J. R., Gracy, R. W. & Harris, B. G. A method for estimating sequence homology from amino acid compositions. The evolution of *Ascaris* employing aldolase and glyceraldehyde-3-phosphate dehydrogenase. *Comparative Biochemistry and Physiology B, Basic Health* **49**, 715–731 (1974).
420. Fang, T. *et al.* Targeted antigen delivery by an anti-class II MHC VHH elicits focused α UC1(Tn) immunity. *Chem Sci* **8**, 5591–5597 (2017).
421. Vaneycken, I. *et al.* In vitro analysis and in vivo tumor targeting of a humanized, grafted Nanobody in mice using pinhole SPECT/micro-CT. *Journal of Nuclear Medicine* **51**, 1099–1106 (2010).
422. Van Driel, P. B. A. A. *et al.* Intraoperative fluorescence delineation of head and neck cancer with a fluorescent Anti-epidermal growth factor receptor nanobody. *Int J Cancer* **134**, 2663–2673 (2014).
423. Debie, P. *et al.* Improved Debulking of Peritoneal Tumor Implants by Near-Infrared Fluorescent Nanobody Image Guidance in an Experimental Mouse Model. *Mol Imaging Biol* **20**, 361–367 (2018).
424. Bannas, P. *et al.* Molecular imaging of tumors with nanobodies and antibodies: Timing and dosage are crucial factors for improved in vivo detection. *Contrast Media Mol Imaging* **10**, 367–378 (2015).
425. Debie, P. *et al.* Effect of dye and conjugation chemistry on the biodistribution profile of near-infrared-labeled nanobodies as tracers for image-guided surgery. *Mol Pharm* **14**, 1145–1153 (2017).
426. Zhang, J. *et al.* The optimized fabrication of a novel nanobubble for tumor imaging. *Front Pharmacol* **10**, 1–15 (2019).
427. Kogan, P., Gessner, R. C. & Dayton, P. A. Microbubbles in imaging: Applications beyond ultrasound. *Bubble Sci Eng Technol* **2**, 3–8 (2010).
428. Yin, T. *et al.* Nanobubbles for enhanced ultrasound imaging of tumors. *Int J Nanomedicine* **7**, 895–904 (2012).

429. Gainkam, L. O. T. *et al.* Localization, mechanism and reduction of renal retention of technetium-99m labeled epidermal growth factor receptor-specific nanobody in mice. *Contrast Media Mol Imaging* **6**, 85–92 (2011).
430. Zhou, Z., Devoogdt, N., Zalutsky, M. R. & Vaidyanathan, G. An Efficient Method for Labeling Single Domain Antibody Fragments with ¹⁸F Using Tetrazine-Trans-Cyclooctene Ligation and a Renal Brush Border Enzyme-Cleavable Linker. *Bioconjug Chem* **29**, 4090–4103 (2018).
431. Baumeister, S. H., Freeman, G. J., Dranoff, G. & Sharpe, A. H. Coinhibitory Pathways in Immunotherapy for Cancer. *Annu Rev Immunol* **34**, 539–573 (2016).
432. Curran, M. A., Montalvo, W., Yagita, H. & Allison, J. P. PD-1 and CTLA-4 combination blockade expands infiltrating T cells and reduces regulatory T and myeloid cells within B16 melanoma tumors. *Proceedings of the National Academy of Sciences* **107**, 4275–4280 (2010).
433. Ingram, J. R. *et al.* Localized CD47 blockade enhances immunotherapy for murine melanoma. *Proceedings of the National Academy of Sciences* **114**, 2–7 (2017).
434. Peters, C. & Brown, S. Antibody-drug conjugates as novel anti-cancer chemotherapeutics. *Biosci Rep* **35**, (2015).
435. Thomas, A., Teicher, B. A. & Hassan, R. Antibody-drug conjugates for cancer therapy. *Lancet Oncology* **17**, e254–e262 (2016).
436. Fang, T. *et al.* Structurally-defined α MHC-II nanobody-drug conjugates: Therapeutic and imaging platforms for B-cell lymphoma. *Angewandte Chemie International Edition* **55**, 2416–2420 (2016).
437. Helft, J. *et al.* GM-CSF Mouse Bone Marrow Cultures Comprise a Heterogeneous Population of CD11c+MHCII+ Macrophages and Dendritic Cells. *Immunity* **42**, 1197–1211 (2015).
438. Becher, B. *et al.* High-dimensional analysis of the murine myeloid cell system. *Nat Immunol* **15**, 1181–1189 (2014).
439. Knox, S. J. *et al.* Yttrium-90-labeled Anti-CD20 Monoclonal Antibody Therapy of Recurrent B-Cell Lymphoma. *Clinical Cancer Research* **2**, 457–470 (1996).
440. Witzig, T. E. *et al.* Randomized controlled trial of yttrium-90-labeled ibritumomab tiuxetan radioimmunotherapy versus rituximab immunotherapy for patients with relapsed or refractory low-grade, follicular, or transformed B-cell non-Hodgkin's lymphoma. *Journal of Clinical Oncology* **20**, 2453–2463 (2002).
441. Witzig, T. E. *et al.* Phase I/II Trial of IDEC-Y2B8 Radioimmunotherapy for Treatment of Relapsed or Refractory CD20+ B-Cell Non-Hodgkin's Lymphoma. *Journal of Clinical Oncology* **17**, 3793–3803 (1999).
442. Vose, J. M. *et al.* Phase II Trial of ¹³¹Iodine Tositumomab with High-Dose Chemotherapy and Autologous Stem Cell Transplantation for Relapsed Diffuse Large B Cell Lymphoma. *Biology of Blood and Marrow Transplantation* **19**, 123–128 (2013).
443. Jurcic, J. G. *et al.* Targeted α particle immunotherapy for myeloid leukemia. *Blood* **100**, 1233–1239 (2002).
444. Sgouros, G. *et al.* Pharmacokinetics and dosimetry of an α -particle emitter labeled antibody: ²¹³Bi-HuM195 (anti-CD33) in patients with leukemia. *Journal of Nuclear Medicine* **40**, 1935–1946 (1999).
445. Mattes, M. J., Sharkey, R. M., Karacay, H., Czuczman, M. S. & Goldenberg, D. M. Therapy of advanced B-lymphoma xenografts with a combination of ⁹⁰Y-anti-CD22 IgG (epratuzumab) and unlabeled anti-CD20 IgG (veltuzumab). *Clinical Cancer Research* **14**, 6154–6160 (2008).

446. Sharkey, R. M., Press, O. W. & Goldenberg, D. M. A re-examination of radioimmunotherapy in the treatment of non-Hodgkin lymphoma: prospects for dual-targeted antibody/radioantibody therapy. *Blood* **113**, 3891–3895 (2009).
447. Verheijen, R. H. *et al.* Phase III trial of intraperitoneal therapy with yttrium-90-labeled HMFG₁ murine monoclonal antibody in patients with epithelial ovarian cancer after a surgically defined complete remission. *Journal of Clinical Oncology* **24**, 571–578 (2006).
448. Wong, J. Y. C. *et al.* A Phase I Radioimmunotherapy Trial Evaluating 90 Yttrium-labeled Anti-Carcinoembryonic Antigen (CEA) Chimeric T84.66 in Patients with Metastatic CEA-producing Malignancies. *Clinical Cancer Research* **6**, 3855–3863 (2000).
449. Liersch, T. *et al.* Phase II trial of carcinoembryonic antigen radioimmunotherapy with ¹³¹I-labetuzumab after salvage resection of colorectal metastases in the liver: five-year safety and efficacy results. *Journal of Clinical Oncology* **23**, 6763–6770 (2005).
450. Myers, R. *et al.* Toxicology study of repeat intracerebral administration of a measles virus derivative producing carcinoembryonic antigen in rhesus macaques in support of a phase I/II clinical trial for patients with recurrent gliomas. *Hum Gene Ther* **19**, 690–698 (2008).
451. Meredith, R. F. *et al.* Phase II Study with Interferon of Dual ¹³¹I-labeled Monoclonal Antibody Therapy in Patients with Metastatic Colorectal. *Clinical Cancer Research* **2**, 1811–1818 (1996).
452. D'Huyvetter, M. *et al.* Targeted radionuclide therapy with A ¹⁷⁷Lu-labeled anti-HER2 nanobody. *Theranostics* **4**, 708–720 (2014).
453. D'Huyvetter, M. *et al.* ¹³¹I-labeled anti-HER2 camelid sdAb as a theranostic tool in cancer treatment. *Clinical Cancer Research* **23**, 6616–6628 (2017).
454. Stein, R. *et al.* Advantage of a residualizing iodine radiolabel in the therapy of a colon cancer xenograft targeted with an anticarcinoembryonic antigen monoclonal antibody. *Clinical Cancer Research* **11**, 2727–2734 (2005).
455. Pruszyński, M. *et al.* Improved tumor targeting of anti-her2 nanobody through n-succinimidyl 4-guanidinomethyl-3-iodobenzoate radiolabeling. *Journal of Nuclear Medicine* **55**, 650–656 (2014).
456. Torchilin, V. P. Multifunctional nanocarriers. *Adv Drug Deliv Rev* **58**, 1532–1555 (2006).
457. Oliveira, S. *et al.* Downregulation of EGFR by a novel multivalent nanobody-liposome platform. *Journal of Controlled Release* **145**, 165–175 (2010).
458. Talelli, M. *et al.* Nanobody - Shell functionalized thermosensitive core-crosslinked polymeric micelles for active drug targeting. *Journal of Controlled Release* **151**, 183–192 (2011).
459. Liu, Y. *et al.* EGFR-Targeted Nanobody Functionalized Polymeric Micelles Loaded with mTHPC for Selective Photodynamic Therapy. *Mol Pharm* **17**, 1276–1292 (2020).
460. Xu, R. *et al.* Extracellular vesicles in cancer — implications for future improvements in cancer care. *Nat Rev Clin Oncol* **15**, 617–638 (2018).
461. Kooijmans, S. A. A. *et al.* Display of GPI-anchored anti-EGFR nanobodies on extracellular vesicles promotes tumour cell targeting. *J Extracell Vesicles* **5**, 1–11 (2016).
462. Breckpot, K., Aerts, J. L. & Thielemans, K. Lentiviral vectors for cancer immunotherapy: transforming infectious particles into therapeutics. *Gene Ther* **14**, 847–862 (2007).
463. Gennari, F., Lopes, L., Verhoeven, E., Marasco, W. & Collins, M. K. Single-Chain Antibodies That Target Lentiviral Vectors to MHC Class II on Antigen-Presenting Cells. *Hum Gene Ther* **20**, 554–562 (2009).
464. Goyvaerts, C. *et al.* Development of the Nanobody display technology to target lentiviral vectors to antigen-presenting cells. *Gene Ther* **19**, 1133–1140 (2012).
465. Eichhoff, A. M. *et al.* Nanobody-Enhanced Targeting of AAV Gene Therapy Vectors. *Mol Ther Methods Clin Dev* **15**, 211–220 (2019).

466. Duarte, J. N. *et al.* Generation of Immunity against Pathogens via Single-Domain Antibody–Antigen Constructs. *Journal of Immunology* **197**, 4838–4847 (2016).
467. Chinnnasamy, D. *et al.* Gene therapy using genetically modified lymphocytes targeting VEGFR-2 inhibits the growth of vascularized syngenic tumors in mice. *Journal of Clinical Investigation* **120**, 3953–3968 (2010).
468. Davila, M. L. *et al.* Efficacy and Toxicity Management of 19-28z CAR T Cell Therapy. *Sci Transl Med* **6**, (2014).
469. Maude, S. L. *et al.* Chimeric antigen receptor T cells for sustained remissions in leukemia. *New England Journal of Medicine* **371**, 1507–1517 (2014).
470. Lee, D. W. *et al.* T cells expressing CD19 chimeric antigen receptors for acute lymphoblastic leukaemia in children and young adults: a phase 1 dose-escalation trial. *Lancet Oncology* **385**, 517–528 (2015).
471. Gorovits, B. & Koren, E. Immunogenicity of Chimeric Antigen Receptor T-Cell Therapeutics. *BioDrugs* **33**, 275–284 (2019).
472. Albert, S. *et al.* A novel nanobody-based target module for retargeting of T lymphocytes to EGFR-expressing cancer cells via the modular UniCAR platform. *Oncoimmunology* **6**, 1–17 (2017).
473. Albert, S. *et al.* From mono- to bivalent: Improving theranostic properties of target modules for redirection of UniCAR T cells against EGFR-expressing tumor cells in vitro and in vivo. *Oncotarget* **9**, 25597–25616 (2018).
474. Hajari Taheri, F. *et al.* T cell engineered with a novel nanobody-based chimeric antigen receptor against VEGFR2 as a candidate for tumor immunotherapy. *IUBMB Life* **71**, 1259–1267 (2019).
475. De Munter, S. *et al.* Nanobody based dual specific CARs. *Int J Mol Sci* **19**, 1–11 (2018).
476. Xie, Y. J. *et al.* Nanobody-based CAR T cells that target the tumor microenvironment inhibit the growth of solid tumors in immunocompetent mice. *Proceedings of the National Academy of Sciences* **116**, 7624–7631 (2019).
477. Xie, Y. J. *et al.* Improved Antitumor Efficacy of Chimeric Antigen Receptor T Cells that Secrete Single-Domain Antibody Fragments. *Cancer Immunol Res* **8**, 518–530 (2020).
478. Hambach, J. *et al.* Targeting CD38-Expressing Multiple Myeloma and Burkitt Lymphoma Cells In Vitro with Nanobody-Based Chimeric Antigen Receptors (Nb-CARs). *Cells* **9**, 1–14 (2020).
479. Koch-Nolte, F. *et al.* Single domain antibodies from llama effectively and specifically block T cell ecto-ADP-ribosyltransferase ART2.2 in vivo. *The FASEB Journal* **21**, 3490–3498 (2007).
480. Araste, F., Ebrahimizadeh, W., Rasooli, I., Rajabibazl, M. & Mousavi Gargari, S. L. A novel VHH nanobody against the active site (the CA domain) of tumor-associated, carbonic anhydrase isoform IX and its usefulness for cancer diagnosis. *Biotechnol Lett* **36**, 21–28 (2014).
481. van Brussel, A. S. A. *et al.* Hypoxia-Targeting Fluorescent Nanobodies for Optical Molecular Imaging of Pre-Invasive Breast Cancer. *Mol Imaging Biol* **18**, 535–544 (2016).
482. Van Impe, K. *et al.* A nanobody targeting the F-actin capping protein CapG restrains breast cancer metastasis. *Breast Cancer Research* **15**, 1–15 (2013).
483. Rossotti, M. *et al.* Streamlined method for parallel identification of single domain antibodies to membrane receptors on whole cells. *Biochim Biophys Acta* **1850**, 1397–1404 (2015).
484. Woodham, A. W. *et al.* Nanobody–antigen conjugates elicit HPV-specific antitumor immune responses. *Cancer Immunol Res* **6**, 870–880 (2018).
485. Krasniqi, A. *et al.* Theranostic radiolabeled anti-CD20 sdAb for targeted radionuclide therapy of non-hodgkin lymphoma. *Mol Cancer Ther* **16**, 2828–2839 (2017).

486. Romão, E. *et al.* Identification of nanobodies against the acute myeloid leukemia marker CD33. *Int J Mol Sci* **21**, (2020).
487. Li, T. *et al.* Immuno-targeting the multifunctional CD38 using nanobody. *Nature Publishing Group* **6**, 1–11 (2016).
488. Fumey, W. *et al.* Nanobodies effectively modulate the enzymatic activity of CD38 and allow specific imaging of CD38+ tumors in mouse models in vivo. *Sci Rep* **7**, 1–13 (2017).
489. Sockolosky, J. T. *et al.* Durable antitumor responses to CD47 blockade require adaptive immune stimulation. *PNAS* **113**, E2646–54 (2016).
490. Ingram, J. R. *et al.* Localized CD47 blockade enhances immunotherapy for murine melanoma. *PNAS* **114**, 2–7 (2017).
491. Ma, L. *et al.* Preclinical development of a novel CD47 nanobody with less toxicity and enhanced anti-cancer therapeutic potential. *J Nanobiotechnology* **18**, 1–15 (2020).
492. Tang, J. *et al.* Novel CD7-specific nanobody-based immunotoxins potently enhanced apoptosis of CD7-positive malignant cells. *Oncotarget* **7**, 34070–34083 (2016).
493. Yu, Y. *et al.* Humanized CD7 nanobody-based immunotoxins exhibit promising anti-T-cell acute lymphoblastic leukemia potential. *Int J Nanomedicine* **12**, 1969–1983 (2017).
494. Rashidian, M. *et al.* Predicting the response to CTLA-4 blockade by longitudinal noninvasive monitoring of CD8 T cells. *Journal of Experimental Medicine* **214**, 2243–2255 (2017).
495. Cortez-Retamozo, V. *et al.* Efficient Cancer Therapy with a Nanobody-Based Conjugate. *Cancer Res* **64**, 2853–2857 (2004).
496. Kaliberov, S. A. *et al.* Adenoviral targeting using genetically incorporated camelid single variable domains. *Laboratory Investigation* **94**, 893–905 (2014).
497. Wang, H., Meng, A.-M., Li, S.-H. & Zhou, X.-L. A nanobody targeting carcinoembryonic antigen as a promising molecular probe for non-small cell lung cancer. *Mol Med Rep* **16**, 625–630 (2017).
498. Schmidt Slørdahl, T. *et al.* Anti-c-MET Nanobody® - A new potential drug in multiple myeloma treatment. *Eur J Haematol* **91**, 399–410 (2013).
499. Heukers, R. *et al.* Targeting hepatocyte growth factor receptor (Met) positive tumor cells using internalizing nanobody-decorated albumin nanoparticles. *Biomaterials* **35**, 601–610 (2014).
500. Wan, R. *et al.* Screening and antitumor effect of an anti-CTLA-4 nanobody. *Oncol Rep* **39**, 511–518 (2018).
501. Ingram, J. R. *et al.* Anti-CTLA-4 therapy requires an Fc domain for efficacy. *PNAS* **115**, 3912–3917 (2018).
502. Blanchetot, C. *et al.* Neutralizing nanobodies targeting diverse chemokines effectively inhibit chemokine function. *Journal of Biological Chemistry* **288**, 25173–25182 (2013).
503. Bradley, M. E. *et al.* Potent and efficacious inhibition of CXCR2 signaling by biparatopic nanobodies combining two distinct modes of action. *Mol Pharmacol* **87**, 251–262 (2015).
504. Jähnichen, S. *et al.* CXCR4 nanobodies (VHH-based single variable domains) potently inhibit chemotaxis and HIV-1 replication and mobilize stem cells. *PNAS* **107**, 20565–20570 (2010).
505. De Wit, R. H. *et al.* CXCR4-specific nanobodies as potential therapeutics for WHIM syndrome. *Journal of Pharmacology and Experimental Therapeutics* **363**, 35–44 (2017).
506. Van Hout, A. *et al.* CXCR4-targeting nanobodies differentially inhibit CXCR4 function and HIV entry. *Biochem Pharmacol* **158**, 402–412 (2018).
507. Maussang, D. *et al.* Llama-derived single variable domains (nanobodies) directed against chemokine receptor CXCR7 reduce head and neck cancer cell growth in vivo. *Journal of Biological Chemistry* **288**, 29562–29572 (2013).

508. Omidfar, K. *et al.* Production of a novel camel single-domain antibody specific for the type III mutant EGFR. *Tumor Biology* **25**, 296–305 (2004).
509. Roovers, R. C. *et al.* Efficient inhibition of EGFR signalling and of tumour growth by antagonistic anti-EGFR Nanobodies. *Cancer Immunology, Immunotherapy* **56**, 303–317 (2007).
510. Hofman, E. G. *et al.* EGF induces coalescence of different lipid rafts. *J Cell Sci* **121**, 2519–2528 (2008).
511. Huang, L. *et al.* SPECT imaging with 99mTc-labeled EGFR-specific nanobody for in vivo monitoring of EGFR expression. *Mol Imaging Biol* **10**, 167–175 (2008).
512. Tijink, B. M. *et al.* Improved tumor targeting of anti-epidermal growth factor receptor Nanobodies through albumin binding: Taking advantage of modular Nanobody technology. *Mol Cancer Ther* **7**, 2288–2297 (2008).
513. Gainkam, L. O. T. *et al.* Comparison of the biodistribution and tumor targeting of two 99mTc-labeled anti-EGFR nanobodies in mice, using pinhole SPECT/micro-CT. *Journal of Nuclear Medicine* **49**, 788–795 (2008).
514. Roovers, R. C. *et al.* A biparatopic anti-EGFR nanobody efficiently inhibits solid tumour growth. *Int J Cancer* **129**, 2013–2024 (2011).
515. Omidfar, K. *et al.* Efficient growth inhibition of EGFR over-expressing tumor cells by an anti-EGFR nanobody. *Mol Biol Rep* **40**, 6737–6745 (2013).
516. Jalkhiani, N. *et al.* Noninvasive imaging of tumor progression, metastasis, and fibrosis using a nanobody targeting the extracellular matrix. *PNAS* **116**, 14181–14190 (2019).
517. Vaneycken, I. *et al.* Preclinical screening of anti-HER2 nanobodies for molecular imaging of breast cancer. *The FASEB Journal* **25**, 2433–2446 (2011).
518. D'Huyvetter, M. *et al.* Targeted radionuclide therapy with A 177Lu-labeled anti-HER2 nanobody. *Theranostics* **4**, 708–720 (2014).
519. Kijanka, M. *et al.* Rapid optical imaging of human breast tumour xenografts using anti-HER2 VHHs site-directly conjugated to IRDye 800CW for image-guided surgery. *Eur J Nucl Med Mol Imaging* **40**, 1718–1729 (2013).
520. Pruszyński, M. *et al.* Targeting breast carcinoma with radioiodinated anti-HER2 Nanobody. *Nucl Med Biol* **40**, 52–59 (2013).
521. Vosjan, M. J. W. D. *et al.* Nanobodies targeting the hepatocyte growth factor: Potential new drugs for molecular cancer therapy. *Mol Cancer Ther* **11**, 1017–1025 (2012).
522. Bachran, C. *et al.* The activity of myeloid cell-specific VHH immunotoxins is target-, epitope-, subset- and organ dependent. *Sci Rep* **7**, 2–11 (2017).
523. Rashidian, M. *et al.* Use of 18F-2-fluorodeoxyglucose to label antibody fragments for immuno-positron emission tomography of pancreatic cancer. *ACS Cent Sci* **1**, 142–147 (2015).
524. Van Elssen, C. H. M. J. *et al.* Noninvasive imaging of human immune responses in a human xenograft model of graft-versus-host disease. *Journal of Nuclear Medicine* **58**, 1003–1008 (2017).
525. Movahedi, K. *et al.* Nanobody-based targeting of the macrophage mannose receptor for effective in vivo imaging of tumor-associated macrophages. *Cancer Res* **72**, 4165–4177 (2012).
526. Blykers, A. *et al.* PET imaging of macrophage mannose receptor-expressing macrophages in tumor stroma using 18F-radiolabeled camelid single-domain antibody fragments. *Journal of Nuclear Medicine* **56**, 1265–1271 (2015).
527. Zhang, Y. *et al.* Myeloid cells are required for PD-1/PD-L1 checkpoint activation and the establishment of an immunosuppressive environment in pancreatic cancer. *Gut* **66**, 124–136 (2017).

528. Broos, K. *et al.* Non-invasive assessment of murine PD-L1 levels in syngeneic tumor models by nuclear imaging with nanobody tracers. *Oncotarget* **8**, 41932–41946 (2017).
529. Broos, K. *et al.* Evaluating a single domain antibody targeting human PD-L1 as a nuclear imaging and therapeutic agent. *Cancers (Basel)* **11**, 1–19 (2019).
530. Xing, Y. *et al.* Early phase I study of a 99mTc-labeled anti-programmed death ligand-1 (PD-L1) single-domain antibody in SPECT/CT assessment of PD-L1 expression in non-small cell lung cancer. *Journal of Nuclear Medicine* **60**, 1213–1220 (2019).
531. Saerens, D. *et al.* Single domain antibodies derived from dromedary lymph node and peripheral blood lymphocytes sensing conformational variants of prostate-specific antigen. *Journal of Biological Chemistry* **279**, 51965–51972 (2004).
532. Zare, H. *et al.* Production of nanobodies against prostate-specific membrane antigen (PSMA) recognizing LnCaP cells. *International Journal of Biological Markers* **29**, 169–179 (2014).
533. Evazalipour, M. *et al.* Generation and characterization of nanobodies targeting PSMA for molecular imaging of prostate cancer. *Contrast Media Mol Imaging* **9**, 211–220 (2014).
534. Chatalic, K. L. S. *et al.* A novel ¹¹¹In-labeled anti-prostate-specific membrane antigen nanobody for targeted SPECT/CT imaging of prostate cancer. *Journal of Nuclear Medicine* **56**, 1094–1099 (2015).
535. Fan, X. *et al.* Ultrasonic nanobubbles carrying anti-PSMA nanobody: Construction and application in prostate cancer-targeted imaging. *PLoS One* **10**, 1–13 (2015).
536. Ji, X. *et al.* Neutralization of TNF α in tumor with a novel nanobody potentiates paclitaxel-therapy and inhibits metastasis in breast cancer. *Cancer Lett* **386**, 24–34 (2017).
537. Samec, N. *et al.* Glioblastoma-specific anti-TUFM nanobody for in-vitro immunoimaging and cancer stem cell targeting. *Oncotarget* **9**, 17282–17299 (2018).
538. Behdani, M. *et al.* Generation and characterization of a functional Nanobody against the vascular endothelial growth factor receptor-2; angiogenesis cell receptor. *Mol Immunol* **50**, 35–41 (2012).
539. Kazemi-Lomedasht, F. *et al.* Inhibition of angiogenesis in human endothelial cell using VEGF specific nanobody. *Mol Immunol* **65**, 58–67 (2015).
540. Kazemi-Lomedasht, F., Muyldermans, S., Habibi-Anbouhi, M. & Behdani, M. Design of a humanized anti vascular endothelial growth factor nanobody and evaluation of its in vitro function. *Iran J Basic Med Sci* **21**, 260–266 (2018).
541. Ma, L. *et al.* Generation and characterization of a human nanobody against VEGFR-2. *Acta Pharmacol Sin* **37**, 857–864 (2016).
542. Ebrahimizadeh, W., Mousavi Gargari, S. L., Javidan, Z. & Rajabibazl, M. Production of Novel VHH Nanobody Inhibiting Angiogenesis by Targeting Binding Site of VEGF. *Appl Biochem Biotechnol* **176**, 1985–1995 (2015).
543. Heukers, R. *et al.* The constitutive activity of the virally encoded chemokine receptor US28 accelerates glioblastoma growth. *Oncogene* **37**, 4110–4121 (2018).
544. De Groof, T. W. M. *et al.* Nanobody-Targeted Photodynamic Therapy Selectively Kills Viral GPCR-Expressing Glioblastoma Cells. *Mol Pharm* **16**, 3145–3156 (2019).
545. Burg, J. S. *et al.* Structural basis for chemokine recognition and activation of a viral G protein-coupled receptor John. *Science (1979)* **347**, 1113–1117 (2015).
546. Rajabzadeh, A., Ahmadvand, D., Salmani, M. K., Rahbarizadeh, F. & Hamidieh, A. A. A VHH-based anti-MUC1 chimeric antigen receptor for specific retargeting of human primary T cells to MUC1-positive cancer cells. *Cell J* **22**, 502–513 (2021).
547. Hajari Taheri, F. *et al.* T cell engineered with a novel nanobody-based chimeric antigen receptor against VEGFR2 as a candidate for tumor immunotherapy. *IUBMB Life* **71**, 1259–1267 (2019).

548. Jamnani, F. R. *et al.* T cells expressing VHH-directed oligoclonal chimeric HER2 antigen receptors: Towards tumor-directed oligoclonal T cell therapy. *Biochimica et Biophysica Acta (BBA) - General Subjects* **1840**, 378–386 (2014).
549. Rahbarizadeh, F., Ahmadvand, D. & Moghimi, S. CAR T-cell bioengineering: Single variable domain of heavy chain antibody targeted CARs. *Adv Drug Deliv Rev* **141**, 41–46 (2019).
550. Bao, C. *et al.* The application of nanobody in CAR-T therapy. *Biomolecules* **11**, 1–18 (2021).
551. Zajc, C. U. *et al.* Driving CARs with alternative navigation tools – the potential of engineered binding scaffolds. *FEBS Journal* **288**, 2103–2118 (2021).
552. Pardon, E. *et al.* A general protocol for the generation of Nanobodies for structural biology. *Nat Protoc* **9**, 674–693 (2014).
553. Jeong, H. J., Abhiraman, G. C., Story, C. M., Ingram, J. R. & Dougan, S. K. Generation of Caz+-independent sortase A mutants with enhanced activity for protein and cell surface labeling. *PLoS One* **12**, (2017).
554. Beatty, J. D., Beatty, B. G. & Vlahos, W. G. Measurement of monoclonal antibody affinity by non-competitive enzyme immunoassay. *J Immunol Methods* **100**, 173–179 (1987).
555. Truong, T. T. T., Huynh, V. Q., Vo, N. T. & Nguyen, H. D. Studying the characteristics of nanobody CDR regions based on sequence analysis in combination with 3D structures. *Journal of Genetic Engineering and Biotechnology* **20**, (2022).
556. Klarenbeek, A. *et al.* Camelid Ig V genes reveal significant human homology not seen in therapeutic target genes, providing for a powerful therapeutic antibody platform. *MABS* **7**, 693–706 (2015).
557. Klussmeier, A. *et al.* High-Throughput MICA/B Genotyping of Over Two Million Samples: Workflow and Allele Frequencies. *Front Immunol* **11**, (2020).
558. Fang, T. *et al.* Structurally Defined α MHC-II Nanobody-Drug Conjugates: A Therapeutic and Imaging System for B-Cell Lymphoma. *Angewandte Chemie - International Edition* **55**, 2416–2420 (2016).
559. Hervier, B. *et al.* Increased Concentrations of Circulating Soluble MHC Class I-Related Chain A (sMICA) and sMICB and Modulation of Plasma Membrane MICA Expression: Potential Mechanisms and Correlation With Natural Killer Cell Activity in Systemic Lupus Erythematosus. *Front Immunol* **12**, (2021).
560. Li, J. J. *et al.* Prognostic value of soluble MICA levels in the serum of patients with advanced hepatocellular carcinoma. *Chin J Cancer* **32**, 141–148 (2013).
561. Arai, J. *et al.* Baseline soluble MICA levels act as a predictive biomarker for the efficacy of regorafenib treatment in colorectal cancer. *BMC Cancer* **22**, (2022).
562. Henry Dunand, C. J. & Wilson, P. C. Restricted, canonical, stereotyped and convergent immunoglobulin responses. *Philos Trans R Soc Lond B Biol Sci* **370**, (2015).
563. Tian, C. *et al.* Genome-wide association and HLA region fine-mapping studies identify susceptibility loci for multiple common infections. *Nat Commun* **8**, (2017).
564. Tsuji, I. *et al.* Somatic Hypermutation and Framework Mutations of Variable Region Contribute to Anti-Zika Virus-Specific Monoclonal Antibody Binding and Function. *J Virol* **96**, (2022).
565. Klein, F. *et al.* Somatic mutations of the immunoglobulin framework are generally required for broad and potent HIV-1 neutralization. *Cell* **153**, 126–138 (2013).
566. Briney, B. S., Willis, J. R. & Crowe, J. E. Location and length distribution of somatic hypermutation-associated DNA insertions and deletions reveals regions of antibody structural plasticity. *Genes Immun* **13**, 523–529 (2012).
567. Wilson, P. C. *et al.* Somatic Hypermutation Introduces Insertions and Deletions into Immunoglobulin V Genes. *Journal of Experimental Medicine* **187**, 59–70 (1998).

568. Bemark, M. & Neuberger, M. S. By-products of immunoglobulin somatic hypermutation. *Genes Chromosomes Cancer* **38**, 32–39 (2003).
569. Koskela, S. *et al.* MICA and MICB allele assortment in Finland. *HLA Immune Response Genetics* **102**, 52–61 (2023).
570. Fuentes-Antrás, J., Genta, S., Vijenthira, A. & Siu, L. L. Antibody–drug conjugates: in search of partners of choice. *Trends Cancer* **9**, 339–354 (2023).
571. Fu, Y. & Ho, M. DNA damaging agent-based antibody–drug conjugates for cancer therapy. *Antib Ther* **1**, 43–53 (2018).
572. Fuentes-Antrás, J., Genta, S., Vijenthira, A. & Siu, L. L. Antibody–drug conjugates: in search of partners of choice. *Trends Cancer* **9**, 339–354 (2023).
573. Milenic, D. E., Brady, E. D. & Brechbiel, M. W. Antibody-targeted radiation cancer therapy. *Nat Rev Drug Discov* **3**, 488–498 (2004).
574. Lin, M., Paolillo, V., Le, D. B., Macapinlac, H. & Ravizzini, G. C. Monoclonal antibody based radiopharmaceuticals for imaging and therapy. *Curr Probl Cancer* **45**, (2021).
575. Verhaar, E. R. *et al.* MICA-specific nanobodies for diagnosis and immunotherapy of MICA+ tumors. *Front Immunol* **15**, (2024).
576. Verhaar, E. R., Woodham, A. W. & Ploegh, H. L. Nanobodies in cancer. *Semin Immunol* **52**, (2021).
577. Pleiner, T., Bates, M. & Görlich, D. A toolbox of anti-mouse and anti-rabbit IgG secondary nanobodies. *Journal of Cell Biology* **217**, 1143–1154 (2018).
578. Zhong, P. *et al.* CRGD-installed docetaxel-loaded mertansine prodrug micelles: Redox-triggered ratiometric dual drug release and targeted synergistic treatment of B16F10 melanoma. *Nanotechnology* **28**, (2017).
579. Sievers, N. M., Dörrie, J. & Schaft, N. CARs: Beyond t cells and t cell-derived signaling domains. *Int J Mol Sci* **21**, (2020).
580. Guedan, S., Calderon, H., Posey, A. D. & Maus, M. V. Engineering and Design of Chimeric Antigen Receptors. *Mol Ther Methods Clin Dev* **12**, 145–156 (2019).
581. Jayaraman, J. *et al.* CAR-T design: Elements and their synergistic function. *EBioMedicine* **58**, (2020).
582. Ajina, A. & Maher, J. Strategies to address chimeric antigen receptor tonic signaling. *Mol Cancer Ther* **17**, 1795–1815 (2018).
583. Gil, D. & Schrum, A. G. Strategies to stabilize compact folding and minimize aggregation of antibody-based fragments. *Advances in Bioscience and Biotechnology* **04**, 73–84 (2013).
584. Wörn, A. & Plückthun, A. Stability engineering of antibody single-chain Fv fragments. *J Mol Biol* **305**, 989–1010 (2001).
585. Martin, T. *et al.* Ciltacabtagene Autoleucel, an Anti-B-cell Maturation Antigen Chimeric Antigen Receptor T-Cell Therapy, for Relapsed/Refractory Multiple Myeloma: CARTITUDE-1 2-Year Follow-Up. *Journal of Clinical Oncology* **41**, 1265–1274 (2022).
586. Raje, N. *et al.* Anti-BCMA CAR T-Cell Therapy bb2121 in Relapsed or Refractory Multiple Myeloma. *New England Journal of Medicine* **380**, 1726–1737 (2019).
587. Chen, Y. J., Abila, B. & Mostafa Kamel, Y. CAR-T: What Is Next? *Cancers (Basel)* **15**, (2023).
588. Oelsner, S. *et al.* Continuously expanding CAR NK-92 cells display selective cytotoxicity against B-cell leukemia and lymphoma. *Cytotherapy* **19**, 235–249 (2017).
589. You, F. *et al.* A novel CD7 chimeric antigen receptor-modified NK-92MI cell line targeting T-cell acute lymphoblastic leukemia. *Am J Cancer Res* **9**, 64–78 (2019).
590. Imai, C., Iwamoto, S. & Campana, D. Genetic modification of primary natural killer cells overcomes inhibitory signals and induces specific killing of leukemic cells. *Blood* **106**, 376–383 (2005).

591. Muller, T. *et al.* Expression of a CD20-specific chimeric antigen receptor enhances cytotoxic activity of NK cells and overcomes NK-resistance of lymphoma and leukemia cells. *Cancer Immunology, Immunotherapy* **57**, 411–423 (2007).
592. Boissel, L. *et al.* Retargeting NK-92 cells by means of CD19- and CD20-specific chimeric antigen receptors compares favorably with antibody-dependent cellular cytotoxicity. *Oncoimmunology* **2**, e26527 (2013).
593. Boissel, L., Betancur, M., Wels, W. S., Tuncer, H. & Klingemann, H. Transfection with mRNA for CD19 specific chimeric antigen receptor restores NK cell mediated killing of CLL cells. *Leuk Res* **33**, 1255–1259 (2009).
594. Li, L. *et al.* Expression of chimeric antigen receptors in natural killer cells with a regulatory-compliant non-viral method. *Cancer Gene Ther* **17**, 147–154 (2010).
595. Shimasaki, N. *et al.* A clinically adaptable method to enhance the cytotoxicity of natural killer cells against B-cell malignancies. *Cytotherapy* **14**, 830–840 (2012).
596. Battula, V. L. *et al.* Ganglioside GD2 identifies breast cancer stem cells and promotes tumorigenesis. *Journal of Clinical Investigation* **122**, 2066–2078 (2012).
597. Altvater, B. *et al.* 2B4 (CD244) signaling by recombinant antigen-specific chimeric receptors costimulates natural killer cell activation to leukemia and neuroblastoma cells. *Clinical Cancer Research* **15**, 4857–4866 (2009).
598. Esser, R. *et al.* NK cells engineered to express a GD 2-specific antigen receptor display built-in ADCC-like activity against tumour cells of neuroectodermal origin. *J Cell Mol Med* **16**, 569–581 (2012).
599. Zhang, C. *et al.* ErbB2/HER2-Specific NK Cells for Targeted Therapy of Glioblastoma. *J Natl Cancer Inst* **108**, (2016).
600. Morgan, R. A. *et al.* Case report of a serious adverse event following the administration of t cells transduced with a chimeric antigen receptor recognizing ERBB2. *Molecular Therapy* **18**, 843–851 (2010).
601. Wouters, Y. *et al.* VHHs as tools for therapeutic protein delivery to the central nervous system. *Fluids Barriers CNS* **19**, (2022).
602. Chekol Abebe, E., Yibeltal Shiferaw, M., Tadele Admasu, F. & Asmamaw Dejenie, T. Ciltacabtagene autoleucel: The second anti-BCMA CAR T-cell therapeutic armamentarium of relapsed or refractory multiple myeloma. *Front Immunol* **13**, (2022).
603. Zhang, X. *et al.* Cytokine Release Syndrome After Modified CAR-NK Therapy in an Advanced Non-small Cell Lung Cancer Patient: A Case Report. *Cell Transplant* **31**, (2022).
604. Groh, V. *et al.* Cell stress-regulated human major histocompatibility complex class I gene expressed in gastrointestinal epithelium. *Immunology* **93**, 12445–12450 (1996).
605. Ghadially, H. *et al.* MHC class i chain-related protein A and B (MICA and MICB) are predominantly expressed intracellularly in tumour and normal tissue. *Br J Cancer* **116**, 1208–1217 (2017).
606. Kim, Y., Born, C., Bléry, M. & Steinle, A. MICAgen Mice Recapitulate the Highly Restricted but Activation-Inducible Expression of the Paradigmatic Human NKG2D Ligand MICA. *Front Immunol* **11**, (2020).
607. Tam, Y. K., Martinson, J. A., Doligosa, K. & Klingemann, H.-G. Ex vivo expansion of the highly cytotoxic human natural killer-92 cell-line under current good manufacturing practice conditions for clinical adoptive cellular immunotherapy. *Cytotherapy* **5**, 259–272 (2003).
608. Yeap, W. H. *et al.* CD16 is indispensable for antibodydependent cellular cytotoxicity by human monocytes. *Sci Rep* **6**, (2016).
609. Sondel, P. M. & Alderson, K. L. Clinical cancer therapy by NK cells via antibody-dependent cell-mediated cytotoxicity. *J Biomed Biotechnol* **2011**, (2011).

610. Zhu, H. *et al.* Pluripotent stem cell-derived NK cells with high-affinity noncleavable CD16a mediate improved antitumor activity. *Blood* **135**, 399–410 (2020).
611. Christodoulou, I. *et al.* Engineering CAR-NK cells to secrete IL-15 sustains their anti-AML functionality but is associated with systemic toxicities. *J Immunother Cancer* **9**, (2021).
612. Xu, D. L. *et al.* A Novel Sushi-IL15-PD1 CAR-NK92 Cell Line With Enhanced and PD-L1 Targeted Cytotoxicity Against Pancreatic Cancer Cells. *Front Oncol* **12**, (2022).
613. López-Cantillo, G., Urueña, C., Camacho, B. A. & Ramírez-Segura, C. CAR-T Cell Performance: How to Improve Their Persistence? *Front Immunol* **13**, (2022).
614. Zhang, J. *et al.* Generation of anti-GD2 CAR macrophages from human pluripotent stem cells for cancer immunotherapies. *Stem Cell Reports* **18**, 585–596 (2023).
615. Su, S. *et al.* Induced CAR-Macrophages as a Novel Therapeutic Cell Type for Cancer Immune Cell Therapies. *Cells* **11**, (2022).
616. Sloas, C., Gill, S. & Klichinsky, M. Engineered CAR-Macrophages as Adoptive Immunotherapies for Solid Tumors. *Front Immunol* **12**, (2021).
617. Klichinsky, M. *et al.* Human chimeric antigen receptor macrophages for cancer immunotherapy. *Nat Biotechnol* **38**, 947–953 (2020).
618. Wang, S. *et al.* CAR-macrophage: An extensive immune enhancer to fight cancer. *EBioMedicine* **76**, 103873 (2022).
619. Pierini, S. *et al.* Chimeric antigen receptor macrophages (CAR-M) sensitize solid tumors to anti-PD1 immunotherapy. in *Journal for ImmunoTherapy of Cancer* A390–A390 (BMJ, 2022). doi:10.1136/jitc-2022-sitc2022.0371.
620. Verhaar, E. R., van Keizerswaard, W. J. C., Knoflook, A., Balligand, T. & Ploegh, H. L. Nanobody-based CAR NK cells for possible immunotherapy of MICA+ tumors. *PNAS nexus* **3**, pga184 (2024).
621. Naviaux, R. K., Costanzi, E., Haas, M. & Verma, I. M. The pCL Vector System: Rapid Production of Helper-Free, High-Titer, Recombinant Retroviruses. *J Virol* **70**, 5701–5705 (1996).
622. Xie, G. *et al.* CAR-NK cells: A promising cellular immunotherapy for cancer. *EBioMedicine* **59**, (2020).
623. Hensel, J. A., Khattar, V., Ashton, R. & Ponnazhagan, S. Characterization of immune cell subtypes in three commonly used mouse strains reveals gender and strain-specific variations. *Laboratory Investigation* **99**, 93–106 (2019).
624. Kim, Y. *et al.* Optimized conditions for gene transduction into primary immune cells using viral vectors. *Sci Rep* **13**, (2023).
625. Dufait, I. *et al.* Retroviral and Lentiviral Vectors for the Induction of Immunological Tolerance. *Scientifica (Cairo)* **2012**, 1–14 (2012).
626. Pishesha, N., Harmand, T. J. & Ploegh, H. L. A guide to antigen processing and presentation. *Nat Rev Immunol* **22**, 751–764 (2022).
627. Ravindranath, M. H., Pham, T., El-Awar, N., Kaneku, H. & Terasaki, P. I. Anti-HLA-E mAb 3D12 mimics MEM-E/02 in binding to HLA-B and HLA-C alleles: Web-tools validate the immunogenic epitopes of HLA-E recognized by the antibodies. *Mol Immunol* **48**, 423–430 (2011).
628. McMaster, M. *et al.* HLA-G Isoforms Produced by Placental Cytotrophoblasts and Found in Amniotic Fluid Are Due to Unusual Glycosylation. *The Journal of Immunology* **160**, 5922–5928 (1998).
629. Stam, N. J., Spits, H. & Ploegh, H. L. Monoclonal antibodies raised against denatured HLA-B locus heavy chains permit biochemical characterization of certain HLA-C locus products. *The Journal of Immunology* **137**, 2299–2306 (1986).

630. Seitz, C., Uchanska-Ziegler, B., Zank, A. & Ziegler, A. The monoclonal antibody HCA2 recognises a broadly shared epitope on selected classical as well as several non-classical HLA class I molecules. *Mol Immunol* **35**, 819–827 (1998).
631. Barnstable, C. J. *et al.* Production of monoclonal antibodies to group A erythrocytes, HLA and other human cell surface antigens-new tools for genetic analysis. *Cell* **14**, 9–20 (1978).
632. Stam, N. J., Vroom, Th. M., Peters, P. J., Pastoors, E. B. & Ploegh, H. L. HLA-A- and HLA-B-specific monoclonal antibodies reactive with free heavy chains in Western blots, in formalin-fixed, paraffin-embedded tissue sections and in cryo-immuno-electron microscopy. *Int Immunol* **2**, 113–125 (1990).
633. Grimsley, C. *et al.* Definitive high resolution typing of HLA-E allelic polymorphisms: Identifying potential errors in existing allele data. *Tissue Antigens* **60**, 306–312 (2002).
634. Geraghty, D. E., Stockschleider, M., Ishitani, A. & Hansen, J. A. Polymorphism at the HLA-E locus predates most HLA-A and -B polymorphism. *Hum Immunol* **33**, 174–184 (1992).
635. Guimaraes, C. P. *et al.* Site-specific C-terminal and internal loop labeling of proteins using sortase-mediated reactions. *Nat Protoc* **8**, 1787–1799 (2013).
636. French, D., Fischberg, E., Buhl, S. & Scharff, M. D. The production of more useful monoclonal antibodies I. Modifications of the basic technology. *Immunol Today* **7**, 344–346 (1986).
637. Zhao, Y., Long, M. J. C., Wang, Y., Zhang, S. & Aye, Y. Ube2V2 Is a Rosetta Stone Bridging Redox and Ubiquitin Codes, Coordinating DNA Damage Responses. *ACS Cent Sci* **4**, 246–259 (2018).
638. Tsang, M., Gantchev, J., Ghazawi, F. M. & Litvinov, I. V. Protocol for adhesion and immunostaining of lymphocytes and other non-adherent cells in culture. *Biotechniques* **63**, 230–233 (2017).
639. Salomé, B. *et al.* NKG2A and HLA-E define an alternative immune checkpoint axis in bladder cancer. *Cancer Cell* **40**, 1027–1043.e9 (2022).
640. Kwon, S. *et al.* Targeted Delivery of Cyclotides via Conjugation to a Nanobody. *ACS Chem Biol* **13**, 2973–2980 (2018).
641. Ovchinnikov, V., Louveau, J. E., Barton, J. P., Karplus, M. & Chakraborty, A. K. Role of framework mutations and antibody flexibility in the evolution of broadly neutralizing antibodies. *Elife* (2018) doi:10.7554/eLife.33038.001.
642. Verma, S. *et al.* Trastuzumab Emtansine for HER2-Positive Advanced Breast Cancer. *New England Journal of Medicine* **367**, 1783–1791 (2012).
643. Matulonis, U. A. *et al.* Efficacy and Safety of Mirvetuximab Soravtansine in Patients With Platinum-Resistant Ovarian Cancer With High Folate Receptor Alpha Expression: Results From the SORAYA Study. *Journal of Clinical Oncology* **41**, 2436–2445 (2023).
644. Bouchard, H., Viskov, C. & Garcia-Echeverria, C. Antibody-drug conjugates - A new wave of cancer drugs. *Bioorg Med Chem Lett* **24**, 5357–5363 (2014).
645. Khantasup, K., Chantima, W., Sangma, C., Poornputsa, K. & Dharakul, T. Design and generation of humanized single-chain Fv derived from mouse hybridoma for potential targeting application. *Monoclon Antib Immunodiagn Immunother* **34**, 404–417 (2015).
646. Bell, M. & Gottschalk, S. Engineered Cytokine Signaling to Improve CAR T Cell Effector Function. *Front Immunol* **12**, (2021).
647. Pei, K. *et al.* A Comparison Study of Anti-CLL1 CART Cells Equipped with Different Co-Stimulatory Domains in the Treatment of Children with Refractory/Relapsed Acute Myeloid Leukemia. *Blood* **138**, 824–824 (2021).
648. Kagoya, Y. *et al.* A novel chimeric antigen receptor containing a JAK–STAT signaling domain mediates superior antitumor effects. *Nat Med* **24**, 352–359 (2018).

649. Boucher, J. C. *et al.* CD28 costimulatory domain-targeted mutations enhance chimeric antigen receptor T-cell function. *Cancer Immunol Res* **9**, 62–74 (2021).
650. Feucht, J. *et al.* Calibration of CAR activation potential directs alternative T cell fates and therapeutic potency. *Nat Med* **25**, 82–88 (2019).
651. Llames, S., García-Pérez, E., Meana, Á., Larcher, F. & Del Río, M. Feeder Layer Cell Actions and Applications. *Tissue Eng Part B Rev* **21**, 345–353 (2015).
652. Borst, L., van der Burg, S. H. & van Hall, T. The NKG2A-HLA-E axis as a novel checkpoint in the tumor microenvironment. *Clinical Cancer Research* **26**, 5549–5556 (2021).
653. Ravindranath, M. H., Pham, T., El-Awar, N., Kaneku, H. & Terasaki, P. I. Anti-HLA-E mAb 3D12 mimics MEM-E/o2 in binding to HLA-B and HLA-C alleles: Web-tools validate the immunogenic epitopes of HLA-E recognized by the antibodies. *Mol Immunol* **48**, 423–430 (2011).

Targeting MHC-I Related Proteins for Cancer Diagnosis and Therapy - Elisha Verhaar

